THERMAL DECOMPOSITION OF AQUEOUS GLYCERINE MIXTURES, ETHYL ACETATE, DIETHYL CARBONATE, AND ETHANOL AT HIGH TEMPERATURES IN A FILM BOILING REACTOR

A Dissertation

Presented to the Faculty of the Graduate School

of Cornell University

In Partial Fulfillment of the Requirements for the Degree of

Doctor of Philosophy

by

Wei-Chih Kuo

August 2014

© 2014 Wei-Chih Kuo

THERMAL DECOMPOSITION OF AQUEOUS GLYCERINE MIXTURES, ETHYL ACETATE, DIETHYL CARBONATE, AND ETHANOL AT HIGH TEMPERATURES IN A FILM BOILING REACTOR

Wei-Chih Kuo, Ph. D.

Cornell University 2014

This study employs film boiling as a means to thermally decompose organic gas in a relatively low temperature liquid pool. Film boiling is a multiphase heat transfer mode characterized by a vapor film surrounding a heated surface immersed in a pool of subcooled liquid. Due to the relatively low thermal conductivity of gases compared to liquids, the vapor film acts as an insulating layer between the surface and liquid with potential to support a large temperature drop that can promote chemical conversion of the vapors flowing in the film. The vapor thus serves as a reactant which decomposes in a reactor configuration that is essentially self-assembled.

Decomposition by film boiling of the following organic liquids is discussed: aqueous glycerine ($C_3H_5(OH)_3$) mixtures, ethyl acetate ($CH_3COOC_2H_5$), diethyl carbonate (($CH_3CH_2O)_2CO$), and ethanol ($C_2H_5(OH)$). Ethyl acetate and diethyl carbonate decompose in a unimolecular process. Thermal decomposition of aqueous glycerine mixtures is more complicated. Ethanol, which is a product of diethyl carbonate decomposition, can thermally decompose in several routes which are discussed.

The experimental results presented suggest that aqueous glycerol mixtures decompose by film boiling primarily into synthesis gas (a mixture of hydrogen (H_2) and carbon monoxide (CO)), which can be used as an alternative fuel. Ethyl acetate and diethyl carbonate decompose by a unimolecular process as expected.

BIOGRAPHICAL SKETCH

Wei-Chih Kuo was born in Taipei City, Taiwan in 1983. He received B.S. in Mechanical Engineering from National Cheng Kung University in 2005. With a particular interest in solid mechanics, he pursued graduate studies in Institute of Applied Mechanics in National Taiwan University advised by Professor Tsung-Tsong Wu, and received his M.S. in 2007. After finishing the compulsory military service in 2008, he worked as a research assistant in National Taiwan University. In 2010, motivated by the thermal sciences especially in boiling phenomenon, he joined the Ph.D. program in Sibley School of Mechanical and Aerospace Engineering in Cornell University under the supervision of Professor C. Thomas Avedisian. The project focused on utilizing film boiling as a chemical reactor to convert heavy organic molecules to light fractions at high temperatures, and several reactants were investigated to examine their decomposition kinetics.

ACKNOWLEDGMENTS

Many thanks to many people helped me to achieve this challenging accomplishment. First and foremost, I would like to express my deepest gratitude to my special committee member chair, Professor C. Thomas Avedisian, who offered continuing support and constant encouragement in the pursuit of this study and in the preparation of this dissertation. Special thanks go to Dr. Wing Tsang at National Institute of Standards and Technology (NIST) for bringing up the idea of reactants and the discussion on chemical kinetics. I thank my special committee members, Professor Ashim K. Datta and Professor K. Max Zhang, who gave me invaluable comments and warm encouragements. Also, I would like to thank National Science Foundation (NSF) for their financial support under the grant numbers 0933521 and 1336657. The grant provided tuitions and stipends for four years as well as funds for the research. This project can never be possible without these generous supports.

Thanks should also go to the specialists who provided technical supports on this study. I would like to thank Dr. Xia Zeng of Human Ecology Department at Cornell University for his assistance with the GC/MS analysis of liquid samples. Dr. Ivan Keresztes' insight on the GC/MS analysis is also gratefully acknowledged. Mr. Malcolm Thomas who performed EDX and SEM analysis is much appreciated.

I thank all the students at Cornell who worked with me: Robert Chen, Eric Ching, Iris Choi, Daniel Zagnoli, and Adam Lowery. They provided great assistance on the project. I am thankful to the Thermal Sciences Lab colleagues: Dr. Sung Ryel Choi, Dr. Yu-Cheng Liu, John Evangelista, Jeremy Horwitz, Isaac Lee, Anthony Savas, Koffi Trenou, Jeff Roh, James Young, Daniel Kim, and Yuhao Xu. Your accompanying in this lab provided me refreshments during tough times.

The final and deepest acknowledgment credits to my parents, Chang-Ping Kuo and Li-Chu Lin. My achievement would never been possible without their supports and endless love. I am thankful to my brother, Wei-Jen Kuo, for his encouragement and always telling me the bloody truth. Special thanks also go to my girlfriend, Ju-Yun Cheng, who always comforts me while I was down.

My achievement can never been done without all your help. Thank you all, I appreciate from the bottom of my heart.

TABLE OF CONTENTS

LIST OF FIGURES

LIST OF TABLES

NOMENCLATURE

A	pre-exponential factor, s^{-1}
A_i	coefficient of the trend line
A_c	cross-section area, m^2
A_s	surface area, m^2
a_i	coefficient of the calibration curve, mL/min-V^2
B_i	coefficient of the trend line, K
b_i	coefficient of the calibration curve, mL/min-V^1
C_i	coefficient of the trend line in
C_{pi}	product concentration of species i, M
C_R	reactant concentration, M
c_i	coefficient of the calibration curve, mL/min
d_o	outer diameter of heater tube, m
d_i	inner diameter of heater tube, m
E_a	activation energy, cal/mole
G_T^o	Gibbs function at the standard-state pressure and T, J/mole-K
g	gravity, m/s^2
h_{fg}	heat of vaporization, kJ/kg
H_c	heat of combustion, kJ/kg
I	current, A
K	reaction rate, 1/s
K_c	equilibrium constant based on molar concentrations
K_p	equilibrium constant based on partial pressures
L	tube length, m
n	temperature exponent

N	number of product gas species
$\dot{N}$	molar flow rate of a mixture gas, mole/s
$\dot{n}_i$	molar flow rate of the individual non-condensable gases, mole/s
P	pressure, atm
q	power, W
q''	heat flux, kW/m^2
q''_{CHF}	critical heat flux, kW/m^2
q''_{Leid}	Leidenfrost point heat flux, kW/m^2
q''_2	unstable heat flux, kW/m^2
Q_{in}	power supplied to the heater tube, W
R	radius of the heater tube, m
r	resistance, Ω
R'	characteristic length for horizontal cylinders
$\bar{R}$	gas constant, cal/mole-K
$\dot{S}_i$	calibration relation of a single gas, mL/min
t	time, s
T	temperature, K
T_b	normal boiling temperature, K
T_w	tube wall temperature, K
T_{melt}	melting temperature, K
T_{bulk}	bulk liquid temperature, K
T_1	CHF temperature, K
T_2	unstable temperature, K
T_3	post CHF temperature, K
T_4	highest measured temperature, K
$T_{threshold}$	threshold temperature, K

T_{rxn}	reaction temperature, K
V	flow meter output, V
$\dot{V}$	volumetric flow rate of a mixture gas, mL/min
y_i	molar fraction of a single gas in the product gas stream

Greek letters

δ	vapor film thickness, m
ε	the threshold value
ν'	stoichiometric coefficient of a reactant in a chemical reaction
ν''	stoichiometric coefficient of a product in a chemical reaction
ρ	electrical resistivity, μΩ-m
ρ_l	liquid density, kg/m^3
ρ_v	gas density, kg/m^3
σ	surface tension, N/m

CHAPTER 1

INTRODUCTION

1.1 Background and Motivation

Thermal decomposition, or pyrolysis, is the chemical conversion process by which a molecule will decompose by purely thermal means. The importance of thermal decomposition stands on the fact that fuel oxidation is influenced by decomposition kinetics (Marinov 1999). Furthermore, thermal decomposition is typically an endothermic process, which offers an interesting potential for cooling by using it as a heat sink. These aspects have triggered significant interests to develop decomposition kinetics of hydrocarbons that are relevant to fueling ground transportation systems.

When applied thermal decomposition to a fluid, that is a liquid at the standard atmosphere, the liquid must be pre-vaporized before entering the high temperature reaction zone. This is typically accomplished in a process separate from the reactor; the liquid is vaporized and the gas phase reactant is then transported to the high temperature zone of the chemical reactor. Several concepts have been developed that cater to decompose liquids. For example, flow reactors (Li et al 2001) and jet-stirred reactors (Battin-Leclerc et al 2013) as shown in Figure 1.1. A separate vaporization process is required for these reactors.

A different concept to combine the vaporization and thermal decomposition processes derives from the classic Leidenfrost phenomena (Lienhard 1981). Chandra and Avedisian (1991) vaporized droplets that impinge on a hot surface as a means to develop a gaseous reactant such that the droplets are levitated above the surface (e.g.

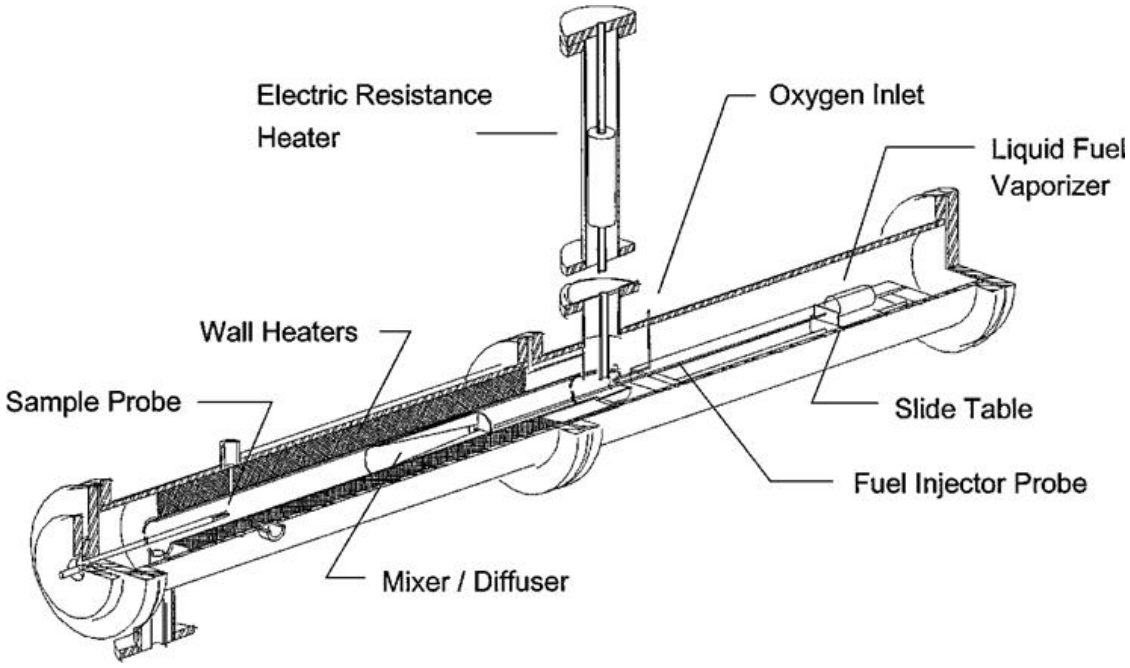

(a)

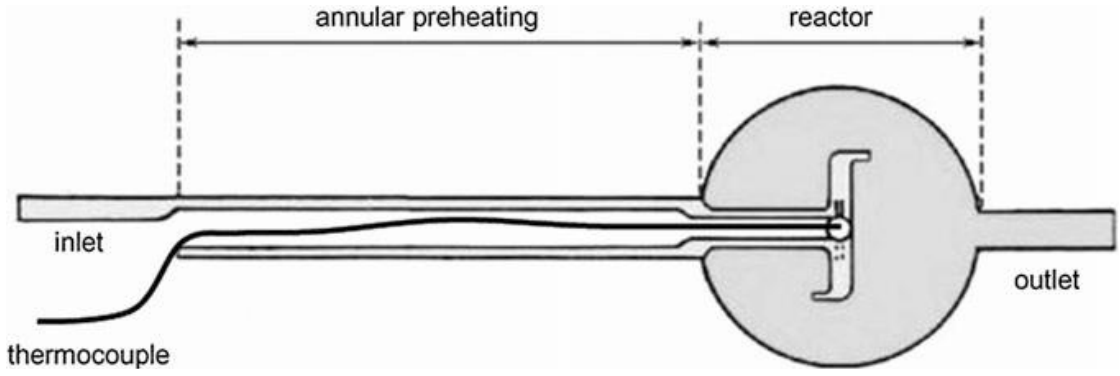

(b)

Figure 1.1: Schematics of (a) flow reactor (Li et al 2001) and (b) jet-stirred reactor (Battin-Leclerc et al 2013).

the Leidenforst phenomena). The vapor underneath the droplet may react homogeneously in the vapor film that separates the liquid from the solid, and the vapors may flow into a porous catalytic substrate (Avedisian and Koplik 1987, Chandra and Avedisian 1992), or heterogeneously react on the surface of the pores (Salge et al 2006). This latter process also forms the basis of a droplet impingement reactor concept described by Varady (2010).

In the pool film boiling process, which is described by a stable vapor blanket surrounding the heater surface (Lienhard 1981), it provides a continuous reactant supply to the high temperature zone (e.g. the vapor film) that has the potential to thermally decompose organic liquids. The idea that organic molecules could thermally decompose when in film boiling derive from the very high surface temperatures, which is a characteristic of film boiling heat transfer.

To apply film boiling as a chemical reactor, the operational domain needs to be firstly defined by a so called "boiling curve," which provides the relation between the input heat flux and the heater temperature. Figure 1.2 illustrates a schematic diagram of the boiling curve. Three regions are indicated on the figure: nucleate boiling (A-B), transition boiling (B-C), and film boiling (C-D).

In the nucleate boiling regime (A-B), numerous bubbles are released from the heater surface. As temperature increases in this regime, more nucleation sites become active and increased bubble formation causes bubble interference and coalescence. The maximum heat flux (point B) in the nucleate boiling regime is the critical heat flux (CHF). At this point, all the bubbles coalesce and a vapor film is formed, making it difficult to continuously wet the heater surface.

In the transition boiling regime (B-C), which is also called unstable film boiling or partial film boiling, bubbles start to coalesce and a vapor blanket begins to cover the surface. The fraction of the vapor film covers the surface increases with

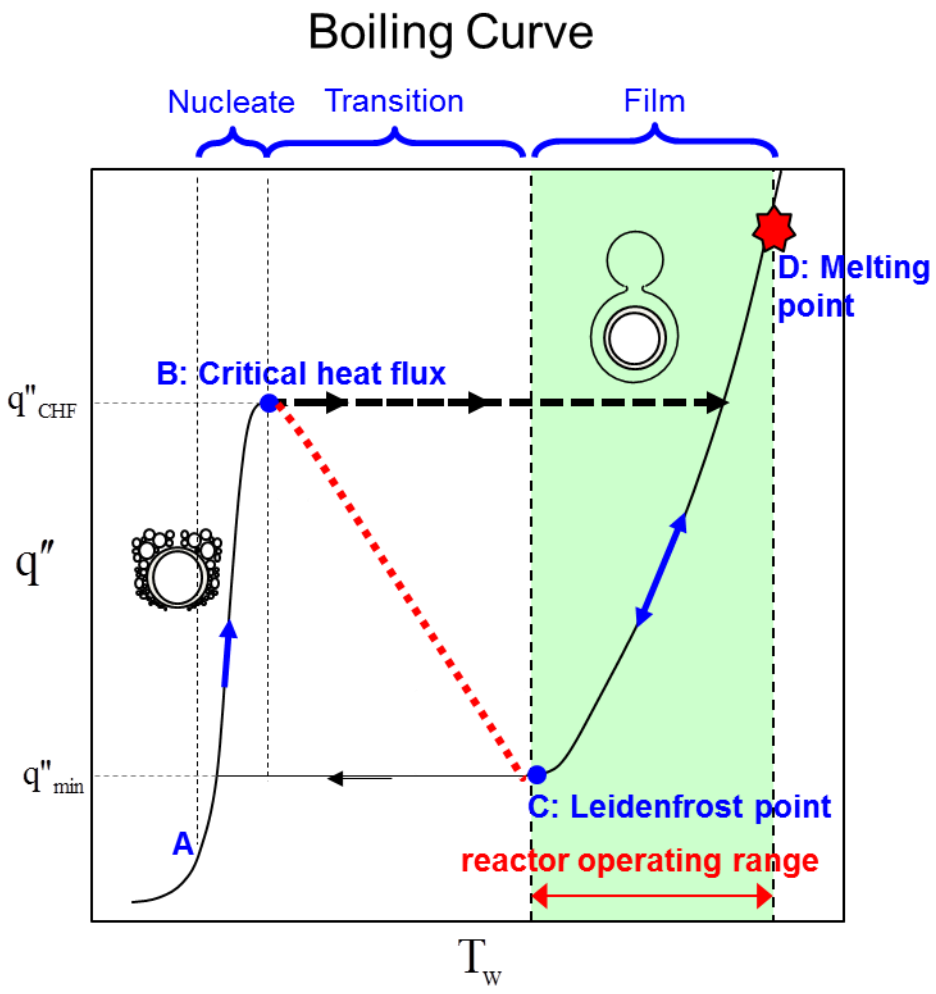

Figure 1.2: A schematic of boiling curve demonstrating the operational domain (green area) of the film boiling reactor. The lower end of the reactor is the Leidenfrost point while the upper is limited by the melting point of the heater material.

increasing temperature. In this regime, the heat flux decreases with increasing temperature is because the thermal conductivity of the vapor is much less compared with the liquid. The vapor film can be viewed as an insulating layer that confines the supplied energy.

In the film boiling regime (C-D), the heater surface is completely covered by a vapor blanket. The point C refers to the minimum heat flux to maintain film boiling, which is also called the Leidenfrost point. Any temperature or heat flux below this point in the film boiling regime will lead to destabilize of the vapor film. The highest temperature in the film boiling regime is limited by the melting point of the heater material (D). The film boiling regime is the operational domain of the chemical reactor. Due to the low thermal conductivity of the vapor film which insulates the heater tube, a high tube temperature is expected, and the thermal decomposition, or pyrolysis, could potentially occur within the vapor film.

Above description assumes that the surface temperature is an independent controllable parameter. However, many applications involve controlling the power input to the heater, which is the y-axis of the boiling curve. Consider starting with point A, and gradually increase the power to reach CHF (point B). Any increase in power at CHF will lead to a sharp temperature jump, causing it to transition from CHF to film boiling. The temperature jump may exceed the melting point of the heater, which leads to burnout. Thus, the point D is often referred as the burnout point or boiling crisis. Similarly, by decreasing the power in the film boiling regime, any power lower than the Leidenfrost point will collapse film boiling, and transition it back to nucleate boiling. Thus, the transition boiling regime (B-C) is not accessible for the power controlled method.

1.2 Physics of Film Boiling and Chemical Conversion

Figure 1.3 depicts the morphology of nucleate and film boiling: (a) and (d) show the pictures of nucleate and film boiling; (b) and (e) depict the schematics of two boiling modes; and (c) and (f) illustrate the temperature distributions perpendicular to the heater surface. In nucleate boiling (A-B in Figure 1.2), bubbles transport energy efficiently from the heater and they create significant turbulent mixing near the heater surface that enhances heat transfer. In this regime, heater temperatures typically sustains superheats of only few degrees above the boiling point of the liquid as suggested in the temperature plot in Figure 1.3 (c). In film boiling (C-D in Figure 1.2), the relatively low thermal conductivity of the vapor film serves as an insulator and can lead to high solid temperatures at which film boiling is established. If the melting point is above the heater temperature, a large temperature drop can arise from the heater surface to the vapor/liquid interface, as illustrated in Figure 1.3 (f). In film boiling, the heater temperature is high enough that is possibly to overcome the activation energy barrier, which would lead to chemical conversion around the heater.

It should be noted that as the heater temperature is above the Leidenfrost point, film boiling can be established; however, the temperature of the heater may not be high enough to thermally decompose reactants. That is, the temperature higher than the Leidenfrost point guarantees film boiling (e.g. chemical reactor) to be successfully achieved. Whether decomposition occurs or not depends on the chemical kinetic of the reactant investigated.

Film boiling is easily considered for the configuration of a horizontal tube. Figure 1.4 is an expected cross-section view of a vapor film surrounding the heated tube. A horizontal tube is immersed in a pool of reactant and heated by joule heating. As the boiling mode around the tube is film boiling, a stable vapor film blankets the heater tube. Liquid reactant vaporizes at the vapor/liquid interface to enter the vapor

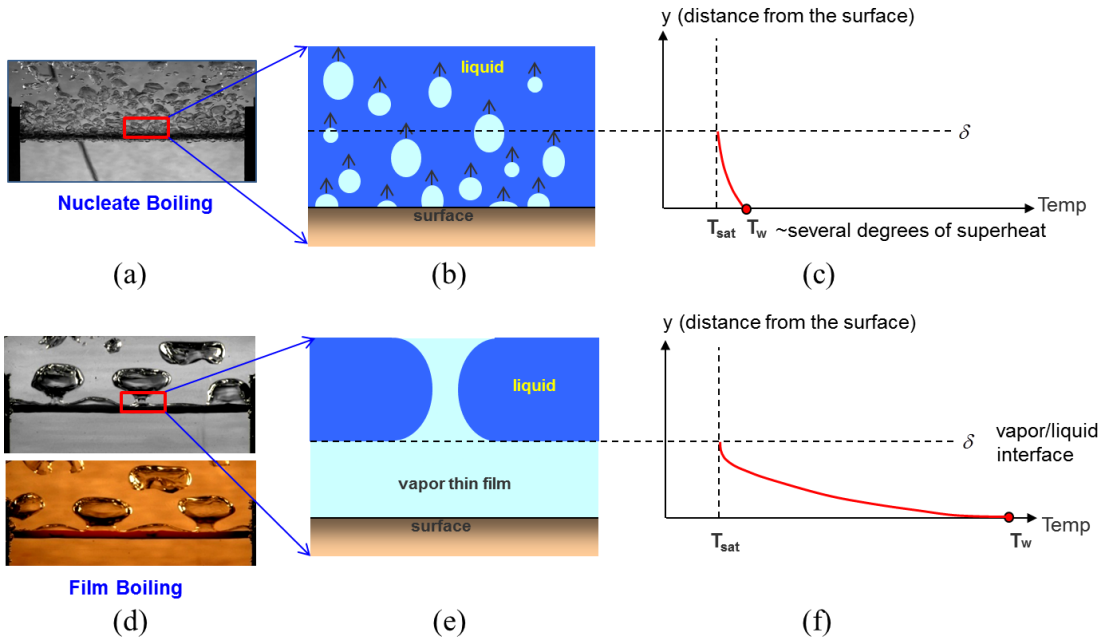

Figure 1.3: Pictures of nucleate (a) and film boiling (d); schematic diagrams (b and e) of two boiling modes; and the corresponding temperature distributions (c and f). the vapor film in film boiling can support a large temperature drop due to its relatively low thermal conductivity.

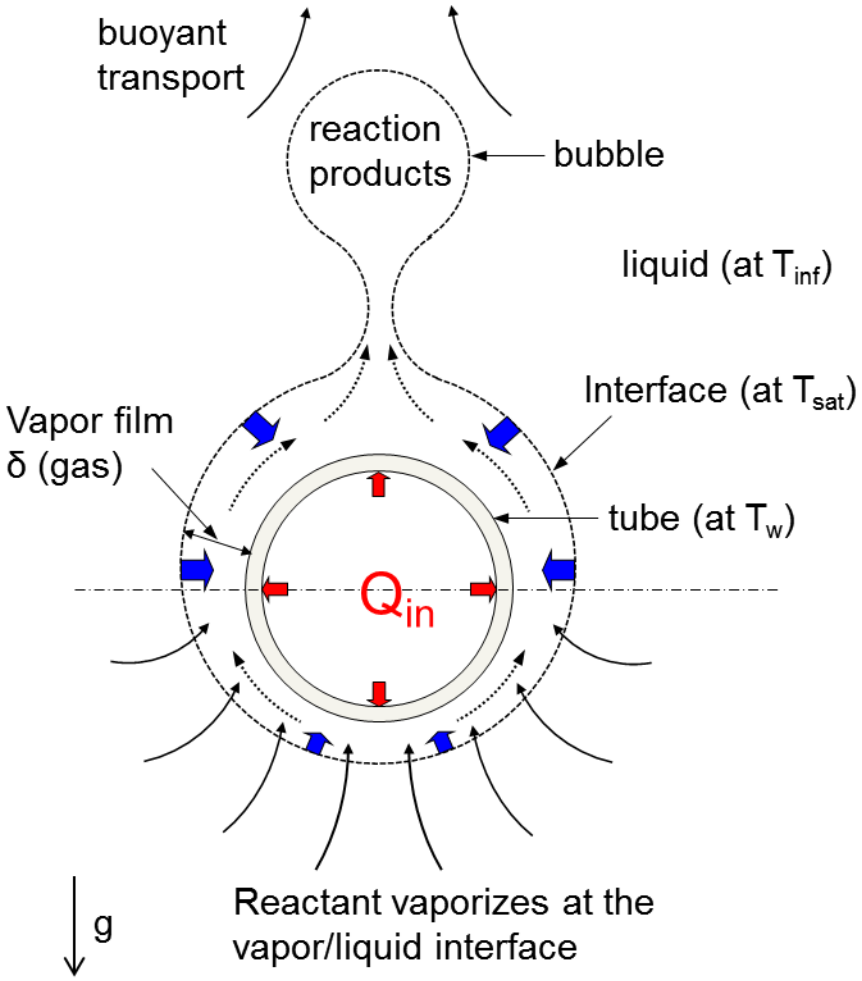

Figure 1.4: A cross-sectional schematic diagram shows a heated tube surrounded by film boiling. The liquid reactant vaporizes, thermally decomposes, and products are transported in a self-assembled manner.

film. As the reactant vapor flows by the high temperature heater by the action of buoyancy, reactions may occur at rates appropriate to the gas temperature. Products from the chemical conversion can also be transported upward by buoyancy, and released as bubbles percolate through the liquid pool. Several advantages of using film boiling to promote chemical reactions include the following.

a) The reactor is self-assembled. By immersing the heater surface in a pool of reactant and increasing the heater temperature so high, the heat transfer mode surrounding the heater will ultimately transition to film boiling. The virtue of the reactor is, therefore, its simplicity.

b) The reaction products can be transported by buoyancy, if no forced flow is imposed. The density difference between liquid and gas reactants facilitates the reactant and product transport.

c) A high temperature environment is not required in the film boiling process. As film boiling is maintained, only the heater tube needs to achieve a high temperature while the bulk liquid can be maintained at its boiling point, which is relatively low compared with the tube temperature.

d) Bring reactor to the reactant. This reactor is portable and easy to operate.

At the same time, it is important to note several potential disadvantages.

a) The reactor can be destroyed during operation. Film boiling has the characteristic of high surface temperature. If the temperature is above the melting point of the metal, the heater will melt.

b) Lack of the precise parameter control. The only parameter that we can control in the experiment is the tube temperature. For example, we cannot increase the reactor volume (vapor film thickness) while fixing the temperature as a constant, and vice versa.

c) The temperature at which chemical conversion is occurring is not a constant because of a large temperature drop that occurs across the vapor. This subject is addressed in this thesis whereas a suitable reaction temperature is defined.

1.3 Literature Review of Film Boiling with Reactions

1.3.1 Experimental Study

Early studies of film boiling with chemical reactions (Higgins 1955; Rebsamen et al 1952; Lustman 1955; Crooks et al 1962) were motivated by nuclear reactor safety and the thermal runaway scenarios. Interactions between molten metal and water can lead to film boiling, steam explosions, and violent reactions (Corradini and Joseph 1991; Kranert and Kottowski 1991). The reaction is as follows (Epstein et al 1984).

$$M + nH_2O \rightarrow MO_n + nH_2 \qquad (1.1)$$

where M is metal. For example, zirconium was often considered since one of the main uses of zirconium alloys is in the nuclear technology, as the cladding of fuel rods in nuclear reactors, especially water reactors. In the loss of coolant scenario, zirconium rapidly reacts with water steam at high temperature. Oxidation of zirconium by water is accompanied by release of hydrogen gas (Lustman 1955).

$$Zr + 2H_2O \rightarrow ZrO_2 + 2H_2 \qquad (1.2)$$

Several studies investigated lithium reaction with water (Herzog and Corradini 1989; Kranert and Kottowski 1990; Anderson et al 2001).

$$Li + 2H_2O \rightarrow LiOH + 1/2\, H_2 \quad (1.3)$$

or $$2Li + H_2O \rightarrow Li_2O + H_2 \quad (1.4)$$

Most of them only provided phenomenological understanding of the chemical reaction and operated in a poor controlled environment. Since film boiling is often related to the nuclear safety scenarios, the concept of manipulating it as a chemical reactor is limited.

Satterfield and Audibert (1966) were one of the first examined the thermal decomposition hydrogen peroxide by using a horizontal silver tube as the catalyst.

$$2H_2O_2 \rightarrow 2H_2O + O_2 \quad (1.5)$$

The coupling of the heat transfer with a mass transfer and chemical reaction process were discussed. Okuyama and Iida (1994) applied film boiling to study catalytic decomposition of methanol (CH_3OH). They showed that film boiling can be used as a means to decompose organic liquid in a controllable manner. Zukov et al (2003) used a platinum wire to attain film boiling and study thermal decomposition of various organic liquids. Choi et al (2011) and Evangelista et al (2012) studied catalytic reaction and thermal decomposition of methanol and aqueous ethylene glycol ($C_2H_4(OH)_2$). The results suggested a unimolecular decomposition of methanol was observed from the product gas analysis while secondary reactions occurring within the vapor film for ethylene glycol. Carbon formation on the heater was confirmed by the energy dispersive X-ray spectroscopy (EDX).

Another category of applying film boiling with chemical reaction is to use it as a means to grow graphite or carbon layers on heated substrates (Bruneton et al 1997; Rovillain 2001; Okuno et al 2002; Zhang et al 2002a 2002b; Delhaes 2002; Delhaes et al 2005). Different organic molecules (C_6H_6, C_6H_{12}, C_6H_5Cl, $C_6H_5CH_3$) were used as

carbon precursors and the carbon properties were examined (Rovillain 2001). Carbon nanotubes (CNT) was able to be deposited on the heater surface with appropriate catalyst (iron film) coated on the substrate surface. Without coating the catalyst, the deposit is merely carbon as the by-product of the thermal decomposition. Delhaes et al (2005) used film boiling as a fast densification process to fabricate C/C composite material.

1.3.2 Numerical Study

Kirillov and Ogarkov (1979) first built a mathematical model for film boiling of a liquid on a vertical catalyst surface. The effect of the parameters of the mathematical description on the process was investigated. Epstein et al (1984) provided a rigorous model (steady-state stagnation flow theory) on water reacting with at the zirconium surface, and metal oxide and hydrogen are the products from the reaction. Urban et al (2006) provided a rigorous model of catalytic decomposition of methanol that assumed one step Arrhenius process by using the rate expression from Okuyama and Iida (1994). Temperature was found to be the most important parameter that influences the product, with the tube diameter as a secondary effect. Avedisian et al (2008) incorporated the radiation effect within Urban's (2006) model, and the results suggested that the surface emission is significant as the tube temperature is above 1000 K, which results in a thicker vapor film and higher product yield. Lee (2010) refined Urban's study (2006) to include bulk liquid motion and sub-cooling effect in the model. The results suggested that sub-cooling has a large effect on product yields, while other factors involving liquid motion, either along the interface or normal to the interface, have a negligible effect.

Thus far, using film boiling as a chemical reactor has been only experimentally realized for limited organic chemicals. This study is intended to extend the knowledge to different molecules such as aqueous glycerine mixtures, ethyl acetate, diethyl carbonate, and ethanol.

1.4 Liquids Examined

Four chemicals were examined in this study. Each has both industrial importance and a fundamental value that is suitable for conversion by film boiling. The chemicals are the following: aqueous glycerine ($C_3H_5(OH)_3$) mixtures, ethyl acetate (EA, $CH_3COOC_2H_5$), diethyl carbonate (DEC, $(CH_3CH_2O)_2CO$), and ethanol (EtOH, $C_2H_5(OH)$). Table 1.1 lists representative properties. Table 1.2 is a summary of important temperatures from the experiments, and Figure 1.5 shows these temperatures (T_1 to T_4) on the boiling curve. Table 1.3 shows a summary of the critical heat flux, unstable heat flux, and minimum heat flux (Leidenfrost point). It should be noted the unstable heat flux (q''_2) is much higher than the predicted minimum heat flux (q''_{Leid}), which suggests that the measured boiling curve in the film boiling regime could probably reach an ever lower temperature.

Crude glycerine generated from the biodiesel production process usually contains water because of the impurity of the reactant (Quispe et al 2013). Both ethyl acetate and diethyl carbonate have a unimolecular decomposition process and simple products. One of the products in the diethyl carbonate decomposition, ethanol, is used as the reactant to conduct the thermal decomposition reaction.

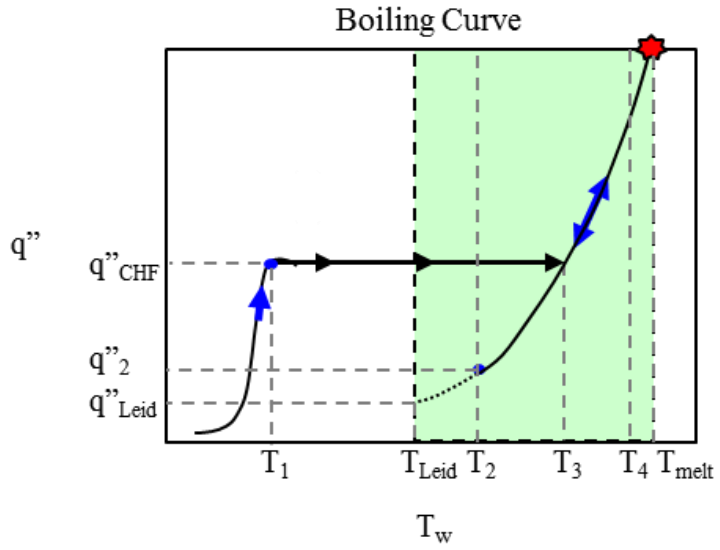

Figure 1.5: Illustration of temperatures measured (T_1, T_2, T_3, and T_4) during the experiment.

Table 1.1: Selected properties of species studied in the standard atmosphere and boiling point.

Chemical	Formula	MW (kmole/kg)	T_b (K)	h_{fg} (kJ/kg)	ρ_l (kg/m^3)	ρ_v (kg/m^3)	σ (N/m)
Glycerine	$C_3H_5(OH)_3$	92.094[1]	563[1]	652[1]	1060[3]	1.99[2]	0.0370[3]
Water	H_2O	18.015[1]	373[1]	2257[1]	958[1]	0.59[2]	0.0589[1]
Ethyl Acetate	$CH_3COOC_2H_5$	88.107[1]	350[1]	366[1]	826[1]	3.06[2]	0.0173[1]
Diethyl carbonate	$(CH_3CH_2O)_2CO$	118.131[1]	399[1]	300[1]	848[4]	3.60[2]	0.0152[5]
Ethanol	$C_2H_5(OH)$	46.068[1]	352[1]	838[1]	735[1]	1.60[2]	0.0156[1]

MW, T_b, h_{fg}, ρ_l, ρ_v, and σ stand for the molecular weight, normal boiling point, heat of vaporization, liquid density, vapor density, and surface tension, respectively.

[1]CRC Handbook of Chemistry and Physics.

[2]Calculated by the ideal gas law.

[3]Physical Properties of Glycerine and Its Solutions.

[4]Yang et al 2006.

[5]Zhao et al 2010.

Table 1.2: A summary important temperatures for all liquids investigated.

	Tube Temperature (T_w)				Reaction Temperature (T_2 to T_4)	
	T_1 (K)	T_2 (K)	T_3 (K)	T_4 (K)	T_{rxn} (K) $\varepsilon = 0.10$	T_{rxn} (K) $\varepsilon = 0.01$
G97/W3[1]	561	1319	—[2]	1521	1243- 1423	1183-1347
G94/W6	524	1268	—	1547	1197-1445	1142-1367
G90/W10	501	1276	—	1535	1205-1434	1149-1357
G80/W20	449	1282	—	1534	1210-1433	1154-1357
EA	382	711	935	1470	687-1378	667-1308
DEC	424	713	943	1462	670-1344	669-1274
EtOH	375	627	1135	1468	614-1286	603-1234

[1]G/W indicates glycerine/water mass fraction.

[2]Quenching method used.

Table 1.3: A summary of critical heat flux, unstable heat flux, and minimum heat flux (Leidenfrost point).

	Critical Heat Flux			Unstable Heat Flux		Leidenfrost Point
	T_{bulk} (K)	Measured q''_{CHF} (kW/m^2)	Predicted[3] q''_{CHF} (kW/m^2)	T_{bulk} (K)	Measured q''_2 (kW/m^2)	Predicted[5] q''_{Leid} (kW/m^2)
G97/W3[1]	444 [20][2]	1354	562-1224[4]	451 [13]	695	12-16[6]
G94/W6	414 [18]	1189	562-1224	423 [9]	605	12-16
G90/W10	402 [10]	1077	562-1224	411 [1]	562	12-16
G80/W20	388 [5]	963	562-1224	394 [1]	522	12-16
EA	348 [2]	262	282	349 [1]	145	7
DEC	398 [1]	222	244	395 [4]	151	6
EtOH	352 [0]	372	448	351 [1]	129	9

[1]G/W indicates glycerine/water mass fraction.

[2]Subcooling [T_{sat}-T_{bulk}] is given in brackets.

[3]Lienhard and Lienhard (2012).

[4]562 and 1224 kW/m^2 represent predicted critical heat flux of pure glycerine and water.

[5]Lienhard and Dhir (1980).

[6]12 and 16 kW/m^2 represent predicted Leidenfrost point critical heat flux of pure glycerine and water.

The prediction of G/W mixtures are given in the range because the mixture properties (e.g. h_{fg} and σ) are not accessible at its boiling points.

1.4.1Aqueous Glycerine Mixtures

The importance of glycerine is that it is a major product from biodiesel formation by the transesterification process (Ma and Hanna 1999, Van Kasteren and Nisworob 2007). Figure 1.6 shows the process of the transesterification reaction, in which the triglyceride could come from vegetable oils such as rape seed, almond oil, and sunflower oils (van Kasteren and Nisworob 2007). Glycerine has enormous practical industrial applications such as food, drugs, toothpaste, cosmetics, and lacquers. However, so much glycerine is being produced now in biodiesel production processes that there is currently a worldwide glut of it (Nilles 2006), and something has to be done with it.

Two possibilities are to burn it directly as a fuel or convert it to something else. Several studies (Metzger 2007; Bohon et al 2011; Queiro´s et al 2013; Steinmetz et al 2013) focused on the combustion of crude glycerine. However, some difficulties were reported (Metzger 2007; Bohon et al 2011) as following. (a) Glycerine has a low heat of combustion (around 16 MJ/kg compared with gasoline, 47 MJ/kg), which makes it difficult to maintain a stable flame in a conventional burner. (b) The self-ignition temperature of glycerine is high (approximately 643 K compared with gasoline, 553 K, and kerosene, 483 K). (c) Burning glycerol can form produce toxic products such as acrolein (CH_2CHCHO). (d) Its high viscosity at room temperature makes it difficult to atomize with conventional atomizers. (e) Its salt content will cause corrosion issues in burner injectors and in post combustion systems.

McNeil et al (2012) burned pure glycerine in engines and noted the virtue of burning it because it is low-toxic, non-odorous, non-volatile, water-soluble and classified as neither a flammable nor a combustible liquid. Emission from glycerine combustion is even less than diesel combustion while the power output is similar to

burning diesel fuels. However, two major issues still remain. Glycerine has to be heated to reduce it viscosity and combustion is unstable as the inlet air temperature is not high enough. Since burning glycerine would cause many issues, a different approach, which is to thermally decompose glycerine, is proposed.

$$C_3H_5(OH)_3 \rightarrow 4H_2 + 3CO \qquad (1.6)$$

Through the decomposition of glyceine, synthesis gas (or syn-gas, which is a combination of hydrogen (H_2) and carbon monoxide (CO)) will be produced as the products (Stein and Antal 1983; Valliyappan et al 2007; Skoulou et al 2012), which can be utilized as fuels (Hagos et al 2014) in a gas turbine engine (Oliveira et al 2010; Ghenai 2010) or duel fuel diesel engine (Sahoo et al 2011, 2012).

Thermal decomposition of aqueous glycerine mixtures at elevated temperatures (> 1200K) is interesting since the previous only studied the glycerine conversion at lower temperatures (< 1200 K) (Stein and Antal 1983; Valliyappan et al 2007; Adhikari et al 2008; Corma et al 2008; Buffoni et al 2009; Fernández et al 2009; Rennard et al 2009; Pompeo et al 2010). The details of the glyceriene decomposition will be discussed in Chapter 3.

1.4.2 Ethyl Acetate

Ethyl acetate is a colorless compound with a characteristic fruity smell. It is often used in coatings, inks, adhesives, glues, nail polish removers, decaffeinating tea and coffee, and cigarettes.

The complexity of the molecules or reactions examined by film boiling will make it a challenge to infer the reaction pathways from measurement of the exhaust gas composition. Ethyl acetate was identified to have several attributes that make it

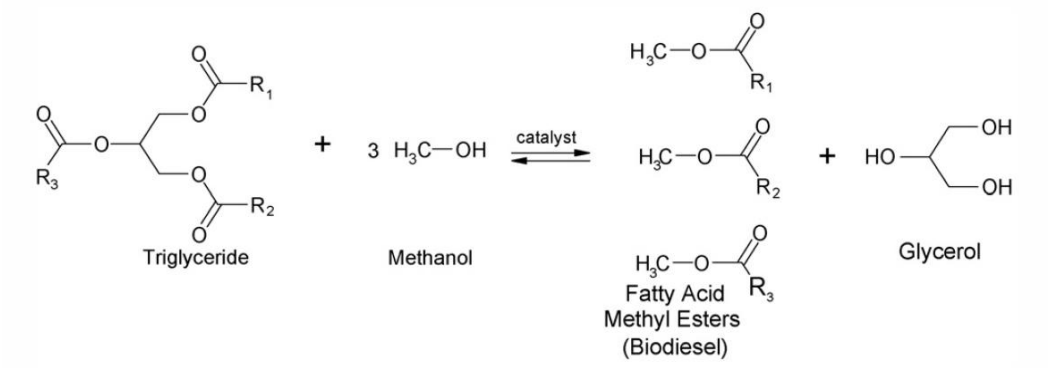

Figure 1.6: Transesterification reaction of tri-glyceride and methanol to fatty acid methyl esters (biodiesel) and glycerine (van Kasteren and Nisworob 2007).

attractive for studying its decomposition by film boiling: (a) Conversion is only by a unimolecular process as following (Blades 1954; Blades and Gilderson 1960; Scheer et al 1963; Gutman et al 1977; Tsang et al 1978; Eberhardt et al 1982; Saito et al 1990).

$$CH_3COOC_2H_5 \rightarrow CH_3COOH + C_2H_4 \qquad (1.7)$$

(b) The products contain only two species, which makes it easy to identify assumed decomposition reaction. (c) The rate constant for decomposition is known (Blades 1954; Blades and Gilderson 1960; Scheer et al 1963; Gutman et al 1977; Tsang et al 1978), which will make the data useful for comparing with a suitable model of film boiling. The details of the ethyl acetate decomposition will be discussed in Chapter 4.

1.4.3 Diethyl Carbonate and Ethanol

Diethyl carbonate has attracted much attention because it has been widely used in electrochemistry (Aurbach et al 1995; Lee et al 2002; Varlamova and Yurina 2006; Kanamura et al 2005) and fuel additives (Roh, et al 2002; Bruno et al 2009). Ethanol is a very important renewable energy source, which can be used as a neat fuel, an oxygenate additive, or a fuel extender in gasoline (Park et al 2002; Wu et al 2011). It is mostly blended with gasoline to increase the octane number and reduce smog emissions. The thermal decomposition of ethanol under combustion process is also important since it will affect the combustion process.

These two chemicals are grouped together because ethanol is a product of diethyl carbonate in a unimolecular decomposition.

$$(CH_3CH_2O)_2CO \rightarrow C_2H_4 + CO_2 + C_2H_5OH \qquad (1.8)$$

The generated products are ethylene, carbon dioxide, and ethanol with known rate constants (Gordon and Norris 1965, Bigley and Wren 1971, Cross et al 1976, Taylor 1983, Herzler et al 1997, Notario et al 2005). The decomposition products contain

three species, which makes it easy to identify assumed decomposition reaction. Ethanol can potentially thermally decompose along with diethyl carbonate conversion. Thus, thermal decomposition of ethanol will also be examined in this study. The details will be discussed in Chapter 5.

1.5 Objectives

The purpose of this study is to extend the knowledge of chemical conversion by film boiling to different organic molecules such as aqueous glycerine mixtures, ethyl acetate, diethyl carbonate, and ethanol. The objectives are the following.

a) Determine the operational domain of each chemical by measuring the boiling curves.
b) Identify the production rate and product species, and infer possible reaction routes for the chemicals investigated.
c) Determine a suitable reaction temperature within the vapor film as the representative temperature for the thermal state and chemical reaction.
d) Use the film boiling reactor as a means to perform thermal decomposition at high temperatures.

CHAPTER 2

EXPERIMENT OVERVIEW

2.1 Film Boiling Platform

An experimental platform was developed to maintain film boiling. The design is based on the work of Choi (2010) and Evangelista (2010). Its capabilities are as follows.

a) Power control: the power supplied to the heater is a control valuable. Temperature control is an alternative; however, it is difficult to achieve because of the nature of the boiling curve as discussed in Chapter 1.
b) Temperature measurement: temperatures of the tube and the liquid must be measured.
c) Product yield rate monitoring: flow meters are required to record the exhaust gas flow rate by chemical conversion.
d) Condensable species removal: condensable products and vaporized reactant need to be removed from the product gas stream to prevent clogging in the flow meter.
e) Chemical analysis of product gas stream and liquid pool.
f) Data acquisition (DAQ), and LabVIEW control of the experiment.

Figure 2.1 is a schematic of the film boiling reactor platform. A horizontal cylinder is selected as the heater geometry because it could include the scalability of product yields with diameter. Theoretical modeling of film boiling with chemical reaction has considered the horizontal tube geometry, which is well suited for analysis (Urban et al 2006; Avedisian et al 2008). The apparatus is designed around three broad capacities: 1) a chamber to house the tube that supports film boiling; 2) a

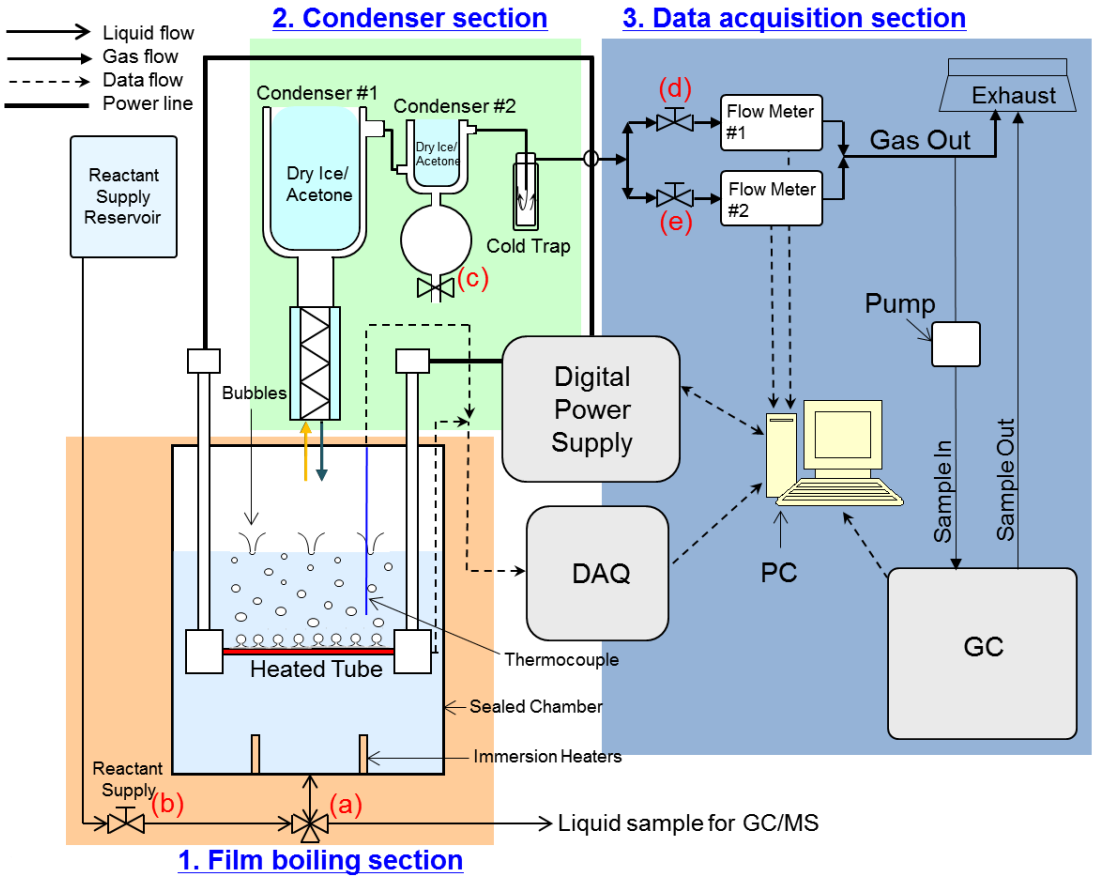

Figure 2.1: A schematic of experiment apparatus consists of three sections: 1) film boiling section; 2) condenser section; 3) data acquisition section (Choi 2010; Evangelista 2010). Five valves ((a) to (e)) are also labeled as shown.

condenser arrangement for removing condensable gases from the product stream; and 3) a data acquisition arrangement that will digitally record experiment variables such as power, temperatures, flow rates, and chemical species. Detailed discussions on these three sections are the following.

1) Film boiling section

The heater tube (Inconel 600, MicroGroup, 600F10093X010SL, melting point of 1686 K) used to support the vapor film consisted of Inconel 600 immersed in the reactant liquid pool in a glass chamber (Glass Cross Pipe DN 150 L 250, Goel Scientific Glass Works Pvt. Ltd.). The diameter and the height of the chamber are 150 mm and 250 mm, respectively. The volume of the chamber is 4.4 L; when conducting the experiment, 3.5 L (h = 200 mm) of reactant will be required.

Two thermocouples (KMQXL-010G-18, Omega) mounted in the tube through a ceramic inserted (ORX-132116, Omega), recorded the average tube temperature as shown in Figure 2.2. The inserted length from the left side of the tube is 22.2 mm while it is 25.2 mm from the right side. The dimensions of the heater tube as well as the locations of mounted thermocouples are shown in Figure 2.2 (a). The configurations of thermocouple positions used are titled T.C.-A and T.C.-B. T.C.-A is the configuration of four thermocouple positions whereas T.C.-B represents two thermocouple positions.

Figure 2.2 (b) shows a representative temperature distribution as a function of position with three different heat flux settings. The temperature distribution for the T.C.-A that uses four thermocouples is symmetric and uniform apart from a small drop in temperature near the ends of the heater tube due to heat losses to the copper clamps. In the T.C.-B configuration which uses two thermocouples, T.C.-B1 is closer to the end compared to T.C.-B2, the reading of T.C.-B1 is slightly lower than T.C.-B2, which can be seen in Figure 2.2 (b). Both two configurations result in eventually the same

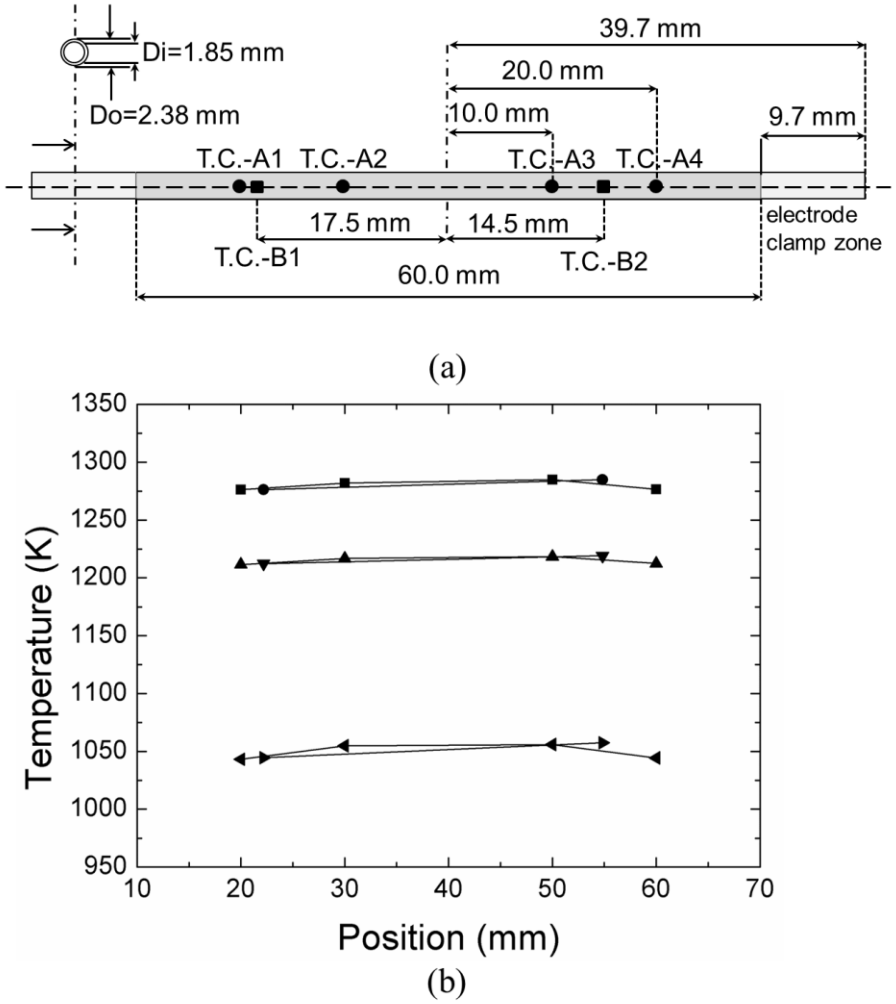

Figure 2.2: (a) Heater tube dimensions with different configurations of thermocouple positions: T.C-A and T.C.-B. (b) Temperature distribution of T.C-A and T.C.-B along the tube with three heat flux settings. (■: 569.3 kW/m², T_{avg} = 1280.0 K; ●: 572.3 kW/m², T_{avg} =1280.6 K; ▲: 470.1 kW/m², T_{avg} =1214.8 K; ▼: 479.4 kW/m², T_{avg} =1215.7 K; ◄: 339.5 kW/m², T_{avg} =1049.6 K; ►: 336.1 kW/m², T_{avg} =1051.0 K)

temperature distribution of the tube, regardless of heat flux settings. To reduce the cost of the experiment without loss of accuracy, we have changed from four thermocouples to two thermocouples.

Figure 2.3 shows a picture of the nickel alloy heater tube, the ceramic tube, and copper clamps. The heater tube dimension is as follows: length: 79.38 mm; OD: 2.38 mm; D: 1.85 mm, and the ceramic tube specification is listed as below: length: 82.55 mm; OD: 1.59 mm; ID: 0.79 mm. Note that the length of the ceramic tube has to be longer than that of the Inconel tube to provide electrical shielding of the thermocouples (see Figure B.2). The thermocouple reading will fluctuate if it is in contact with in the Inconel heater tube or copper buses as power is supplied. The ceramic insert that also provides support for the tube as it is heated to within several hundred degrees of its melting point.

Four immersion heaters (300W, Wattco) are used to maintain the reactant liquid at its boiling point, and one additional thermocouple (KMQXL-040E-12, Omega) monitors the bulk liquid temperature in real time. The maximum temperature that this film boiling section can withhold is 473 K, which is limited by the O-ring and the sealant used. If the temperature of the reactant liquid is above this limit, the seal will break and result in the leak of the chamber. The bulk liquid is sampled from the bottom of the chamber for the chemical analysis.

2) Condenser section

The condenser module is designed to remove condensable products and the vaporized reactant from the product gas stream. This unit ensures that that flow will be entirely due to the reaction products. The product gas flow signifies that any reaction is occurring. If the liquid enters the flow meter, the condensed liquid will clog the sensor and lead to flow meter malfunction.

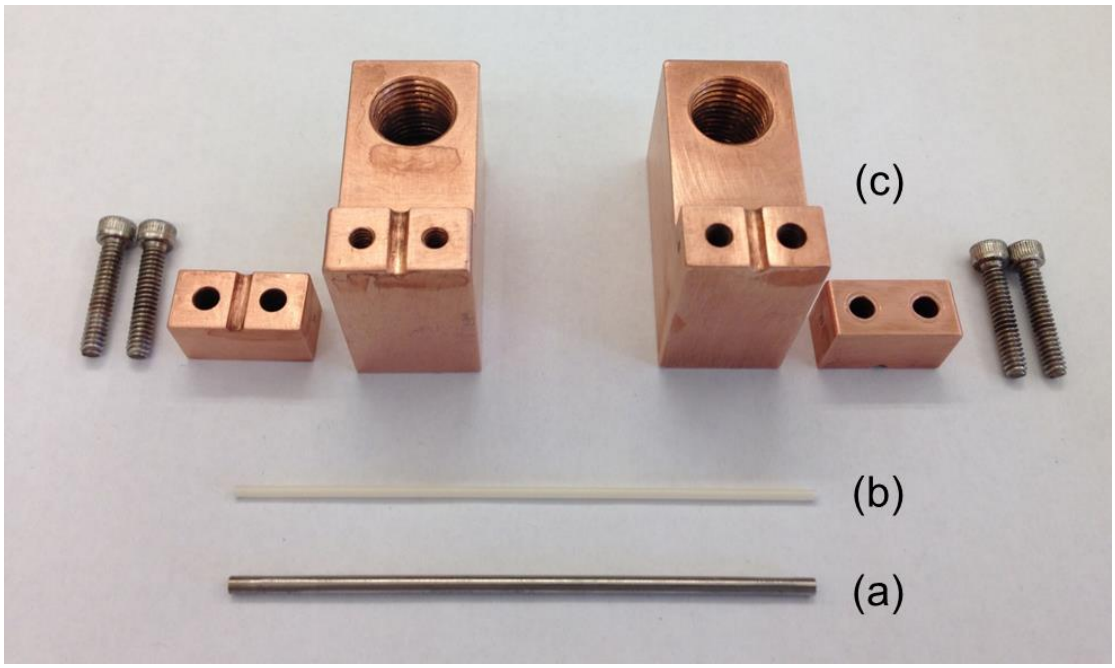

Figure 2.3: A picture showing disassembled electrode clamps: (a) Inconel heater tube; (b) ceramic tube; (c) copper clamps.

The condenser module is composed of three components: condenser #1 (Z164038, Sigma-Aldrich), condenser #2 (Z422347, Sigma-Aldrich), and a cold trap (Z256870, Sigma-Aldrich), as illustrated in Figure 2.1 (see Figure B.5 for the picture). Condensers #1 and #2 are filled with dry ice and acetone mixtures which bring the temperature down to 195 K while the cold trap is immersed in a ice and water mixture that maintains the temperature at 273 K. Condensable products are successfully removed from the product gas stream by the condenser section. The detailed heat exchanger analysis can be found in the previous study (Choi 2010).

In this study, the condensable products are refluxed to the liquid pool, and the bulk liquid concentration will, therefore, change depending on the reactor volume and the reaction rate. The bulk liquid will be sampled and analyzed at the end of the experiment to determine its concentration.

3) Data acquisition section

The data acquisition section includes two flow meters (FMA A-2309 and FMA 4310, Omega Engineering), a digital power supply (6681A, Agilent), a personal computer (Compaq dc5000, HP), and a gas chromatograph (GC600P00012801, Gow-Mac Instrument Company). Two flow meters with different accuracies and detection ranges are mounted in parallel to easily switch the flow as necessary to the meter with the higher precision. Detection of flow rates indicates that noncondensable products are forming by the thermal decomposition of the reactant.

A LabVIEW program (LabVIEW V8.0, National Instruments) is utilized to control the power supplied to the heater tube, to record the tube temperature and the flow meter outputs, and to control GC analysis in real time. The detailed experiment procedure and data processing are discussed in Appendices D and E. Calibration

curves are required to convert the digital flow meter output (voltage) to flow rate (mL/min) which is discussed in the Appendix D.3.

The power control method is used in the course of experiments due to its simplicity, as discussed in Chapter 1. As measuring the boiling curve, the transition boiling region will be by-passed due to this method. A more detailed description of the experimental apparatus can be found elsewhere (Choi 2010; Evangelista 2010).

2.2 Visualization of the film boiling process

Besides recording power, temperature, and flow rate, and performing chemical analysis, images of film boiling are also recorded for the experiments to observe the bubble dynamics.

As described in Chapter 1, by controlling power as an independent input parameter, the heat transfer mode would experience from CHF to film boiling (c.f. Figure 1.2). Figure 2.4 (DEC) and Figure 2.5 (EtOH) are collections of photographs showing the transition process. The reactor (film boiling) is essentially self-assembled. The arrows mark the position of the vapor film as film boiling is established. The time between each frame is one second. The length of the tube is 60 mm, the outer diameter is 2.38 mm, and the inner diameter is 1.85 mm. As seen in Figure 2.4, the film starts forming on the right side and propagates to the left with an average velocity of 3.5 mm/s. At the same time, the tube temperature jumps from 424 K to 943 K. It is noted that we also observed the starting film boiling to be on the left side, as well as in the middle of the tube.

We speculate that the initiation of film boiling depends on the surface morphology of the heater tube. Since the surface condition of each tube is not identical, the starting position could be random. For EtOH, the tube temperature

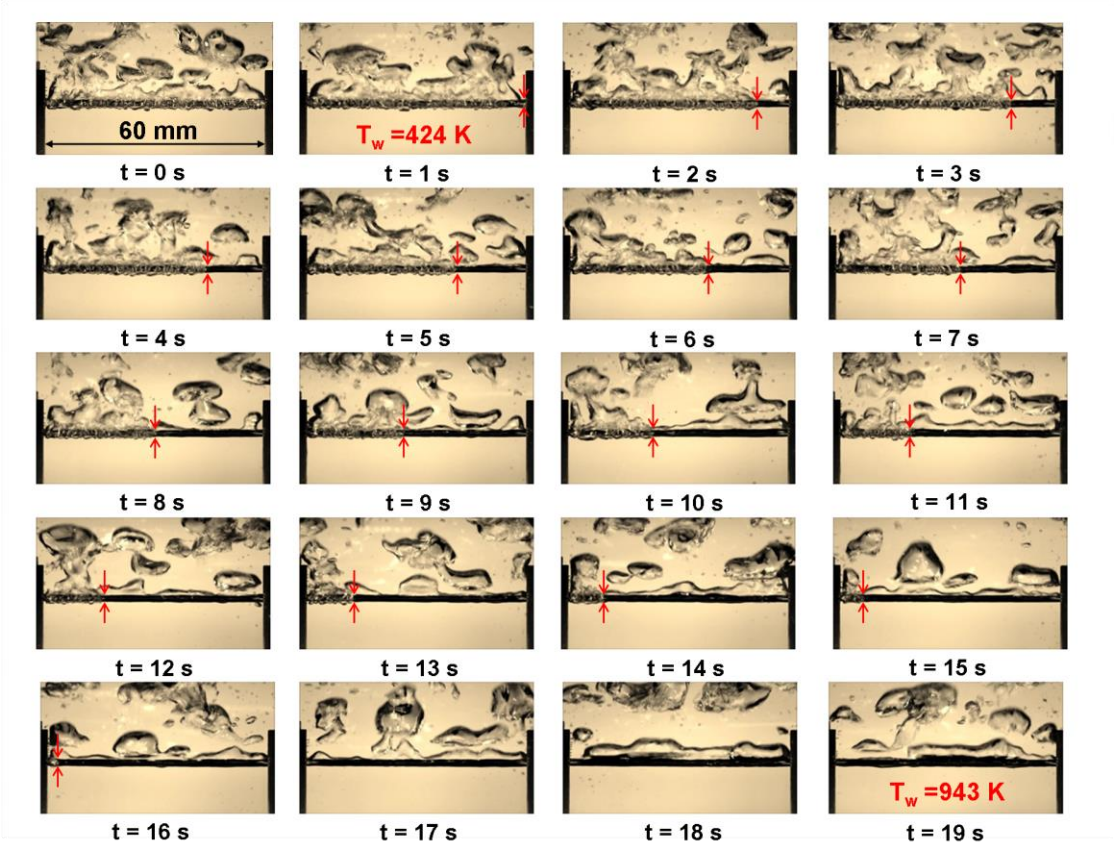

Figure 2.4: Transition from nucleate boiling (at CHF) to film boiling of DEC (T_{bulk} = 400 K). The time interval between each frame is 1 second and the arrow shows the transition front. The averaged film boiling front speed is 3.5 mm/s.

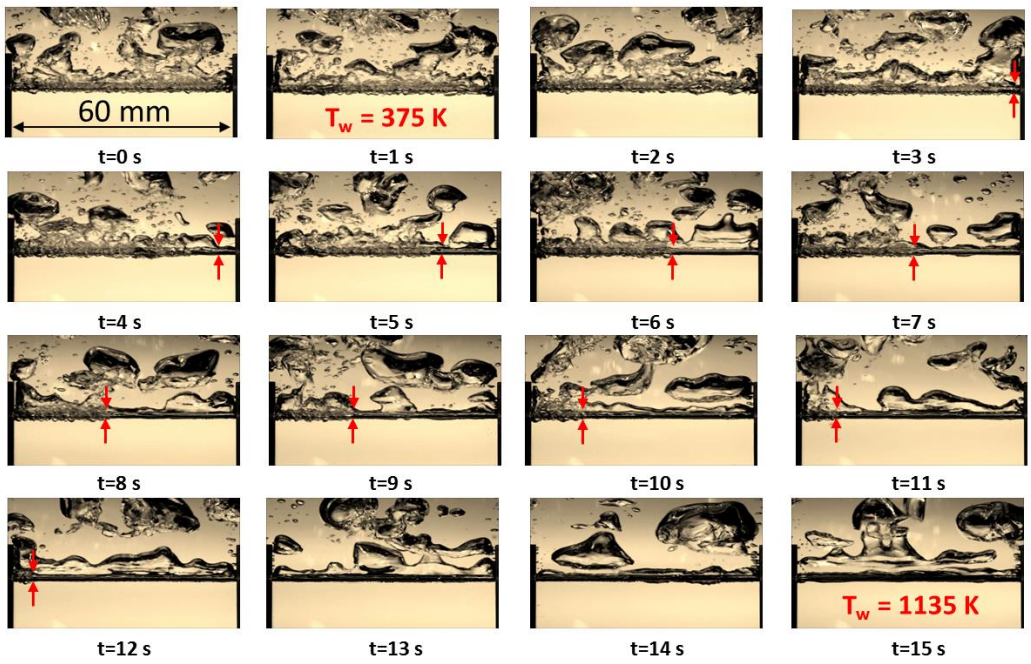

Figure 2.5: Transition from nucleate boiling (at CHF) to film boiling of EtOH (T_{bulk} = 351 K). The time interval between each frame is 1 second and the arrow shows the transition front. The average film boiling front propagating speed is 5.7 mm/s.

increased to 1135 K from 375 K after film boiling was formed (Figure 2.5), and the average velocity of the vapor film front is 5.7 mm/s. As can be observed in Figure 2.4 and Figure 2.5, the bubble morphology in film boiling is smoother than in nucleate boiling.

Figure 2.6 shows two film boiling pictures of a 90/10 (glycerine/water, mass fraction) aqueous glycerine mixture with a tube temperature of 1288 K. The mushroom shaped bubbles are fairly typical of film boiling for non-reactive conditions (Lienhard 1981) and are observed here for the reactive case as well. These bubbles are the carrier of the products as film boiling is a self-assembled reactor.

Figure 2.7 shows a front view of film boiling of ethyl acetate at different times for ostensibly the same thermal condition of an average tube temperature of 1443 K. Mushroom-shaped bubble morphologies are evident. The configurations are highly stochastic and continually vary over time as the bubbles form and depart from the top of the tube. The bubbles contain the reaction products and unreacted vapors.

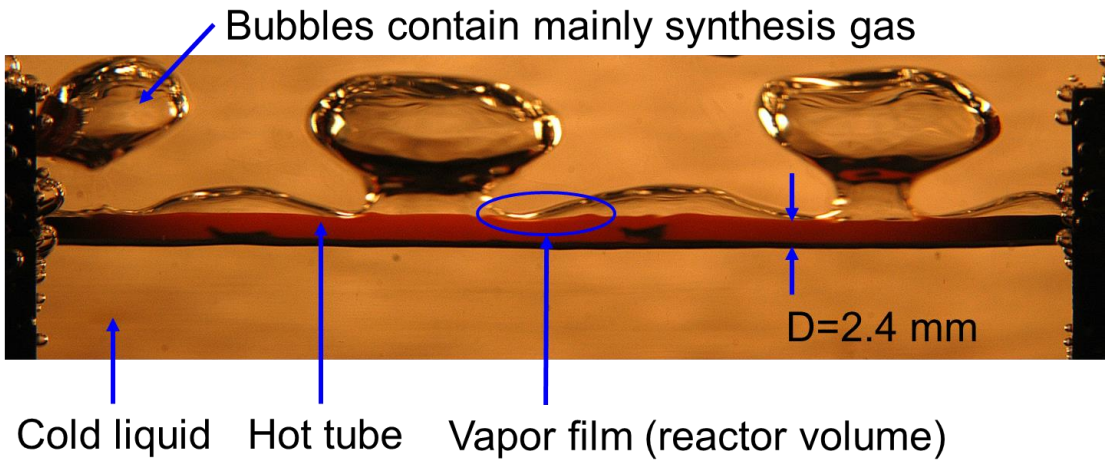

(a)

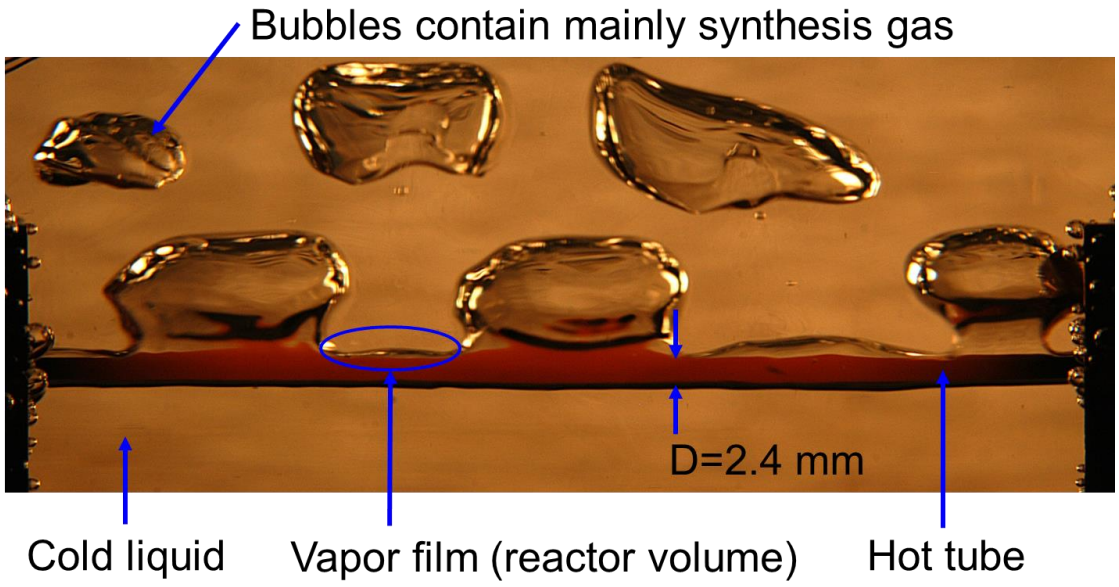

(b)

Figure 2.6: Pictures showing film boiling of aqueous glycerine mixtures (90/10) at two different instants ((a) and (b)). The tube temperature is 1288 K and the bulk liquid temperature is at 410 K.

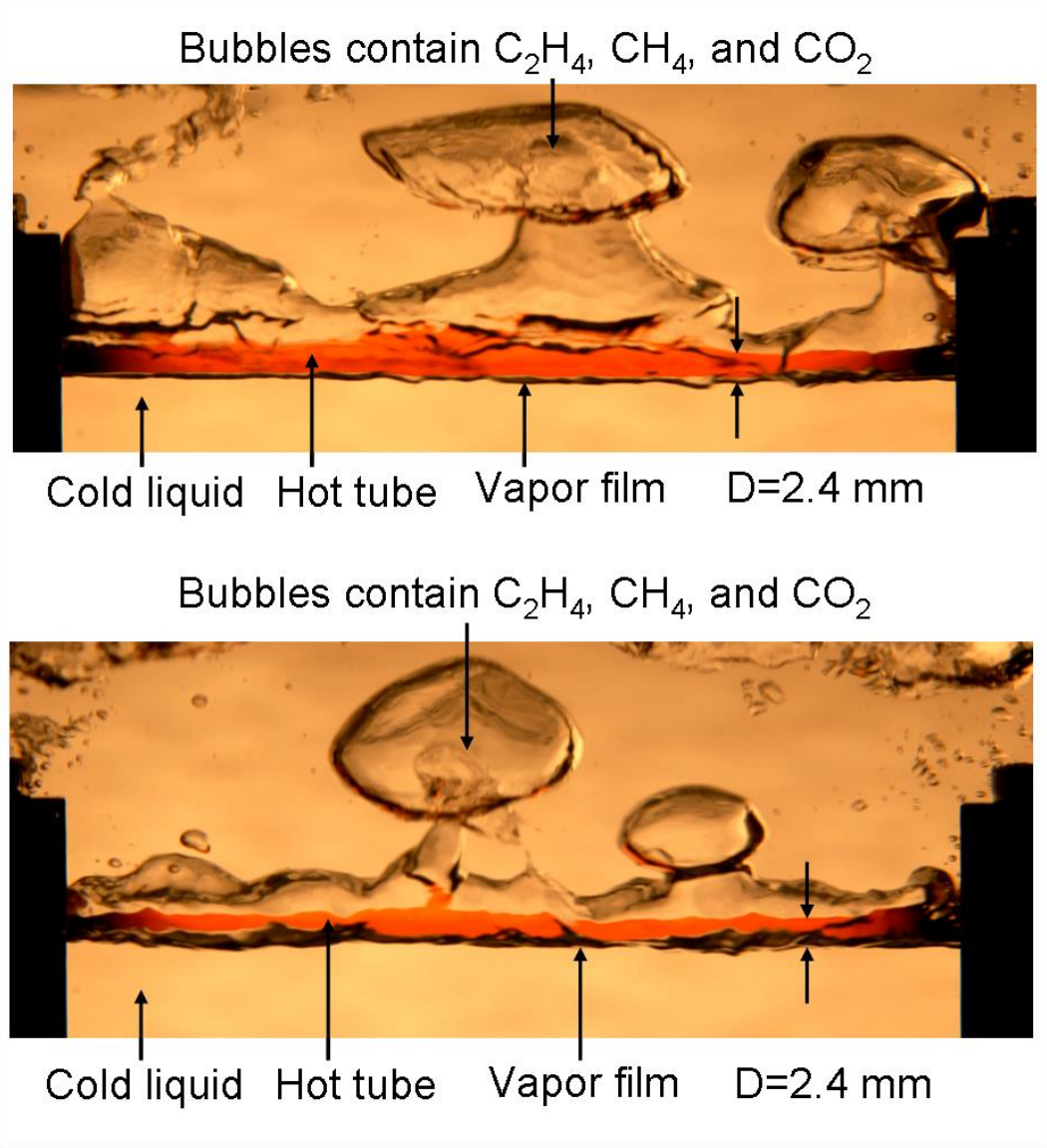

Figure 2.7: Flash photographs of film boiling surrounding the tube at two different times. The liquid is EA at the boiling point of 350 K and the averaged tube temperature is 1443 K. The mushroom type bubble is the characteristic of film boiling.

CHAPTER 3

AQUEOUS GLYCERINE MIXTURES

3.1 Introduction

Previous work (Stein and Antal 1983; Valliyappan et al 2007; Skoulou et al 2012) has shown that glycerine ($C_3H_5(OH)_3$) can be converted to synthesis gas (or syn-gas, a combination of hydrogen (H_2) and carbon monoxide (CO)) through the reaction.

$$C_3H_5(OH)_3 \rightarrow 4H_2 + 3CO \qquad (3.1)$$

The virtue here is that syngas can be burned directly in a gas turbine (Oliveira et al 2010; Ghenai 2010) or duel fuel diesel engine (Sahoo et al 2011, 2012). It can also be converted to methane (CH_4), which itself can be burned (Ghenai 2010), via Fischer–Tropsch process.

$$CO + 3H_2 \rightleftarrows CH_4 + \mathbf{H_2O} \qquad (3.2)$$

[1] [2]

Through the thermal decomposition, glycreine can be converted into valuable fuels.

As described in Chapter 2, the highest temperature that the film boiling chamber can withstand is about 470 K, which is 90 degrees lower than the boiling point of glyceirne (563 K). If the temperature exceeds 470 K, the containment seals will fail. To avoid this possibility, water (H_2O) was added to glycerine to lower the liquid boiling point. Figure 3.1 (a) is the vapor liquid equilibrium diagram of aqueous glycerine mixtures (Chen and Thomson 1970). It shows that adding a small amount of water lowers significantly the boiling point of the mixture. Concurrently, the water content in the vapor film will be enriched due to preferential vaporization. Figure 3.1

[1] The bold type species indicate condensable products in the current apparatus used.
[2] The forward and backward arrows are determined by the equilibrium constant (see Appendix E).

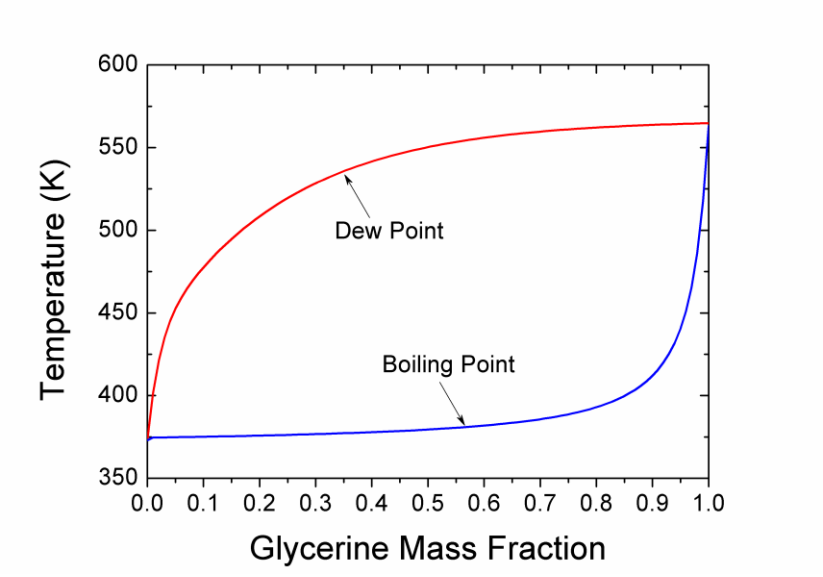

(a)

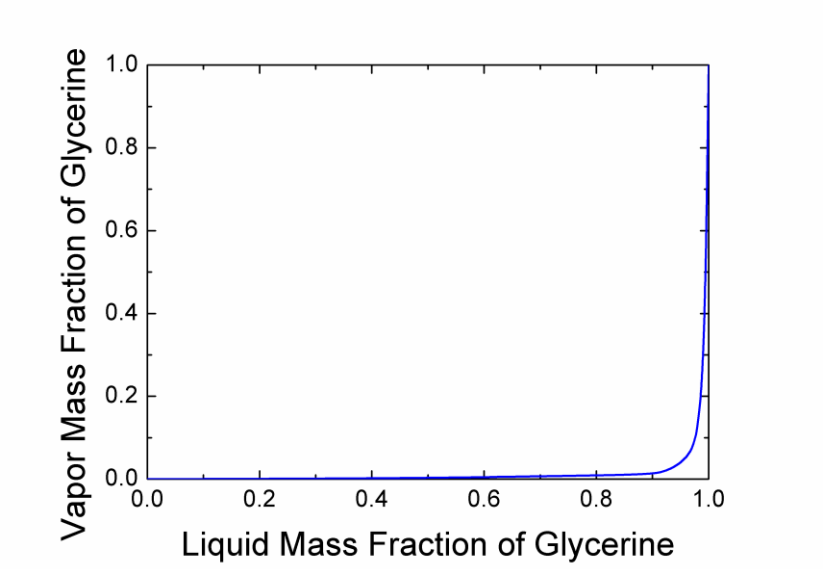

(b)

Figure 3.1: (a) Vapor liquid equilibrium diagram of aqueous glycerine mixtures at normal pressure. (b) Vapor fractions for indicated liquid fractions in the aqueous glycerine mixture (Chen and Thompson 1970). Vapor film is enriched with water addition.

(b) shows the expected vapor fractions that result from dilution of glycerine by water. With the presence of water in the vapor film, the steam reforming of glycerine (Buffoni et al 2009; Pompeo et al 2010; Wang et al 2010; Skoulou et al 2012) and water gas shift reactions could also occur in the vapor film and concurrently, with formation of syngas (Eq. (3.1))

$$C_3H_5(OH)_3 + 3H_2O \rightarrow 7H_2 + 3CO_2 \quad (3.3)$$

$$CO + \mathbf{H_2O} \rightleftarrows H_2 + CO_2 \quad (3.4)$$

Four aqueous glyceirne mixtures are studied (mass fraction of glycerine): 97/3, 94/6, 90/10, with saturation temperature (Figure 3.1 (a)) approximately 464 K, 432 K, 412 K, and 393 K, respectively.

In this study, we will use the experimental results to determine the dominant reaction for glycerine conversion by measuring the boiling curve, product flow rate, and performing chemical species analysis of all mixtures.

3.2 Results and Discussion

3.2.1 Boiling Curve

The boiling curves of aqueous glycerine mixtures (97/3, 94/6, 90/10, and 80/20) are shown in Figure 3.2. Data shown in the film boiling regime includes three runs while it includes one run for the nucleate boiling regime. Film boiling for all mixtures is attained by the quenching method (see Appendix C) so that T_3 is not labeled.

In the nucleate boiling regime (below CHF), the heat fluxes are strongly influenced by the water fraction at a given average tube temperature due to mixture effects on liquid properties (e.g., surface tension, liquid density, viscosity, and heat of vaporization). However, composition effects are comparatively weak in the film boiling regime. Heat is transferred across the vapor film, and the rate is determined by

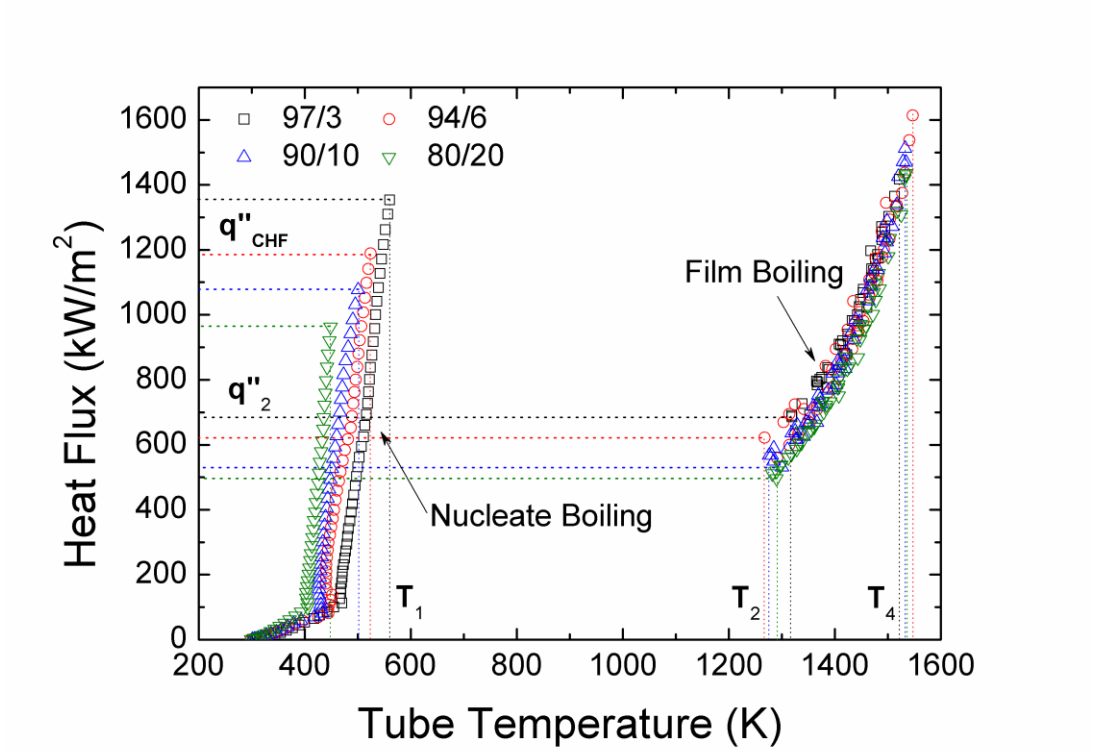

Figure 3.2: Boiling curves of four aqueous glycerine mixtures (97/3, 94/6, 90/10, and 80/20). Transition boiling is not accessible due to the power-controlled method employed.

the thermal conductivity and vapor film thickness that gases flow within it. For vapor film is comprised predominately of water (Figure 3.1 (b)) so that the thermal conductivity will be similar among the different liquid mixtures investigated.

The measured CHF for four mixtures (97/3, 94/6, 90/10, and 80/20) are 1354 kW/m^2 (at 561 K), 1189 kW/m^2 (at 524 K), 1077 kW/m^2 (at 501 K), and 963 kW/m^2 (at 449 K), which is summarized in Table 1.3. Figure 3.3 shows that the CHF varies with glycerine fractions. The progressive increase of CHF as the glycerine fraction increases suggests an even higher CHF for pure glycerine, which is not accessible in our experimental apparatus as discussed in Chapter 2. From the previous study (Rao and Andrews 1978), it shows that the CHF of pure glycerine and water are approximately 2000 kW/m^2 and 1500 kW/m^2, which would suggest a similar trend: the CHF of an aqueous glycerine mixture increases with increasing glycerine fractions.

It should be noted that the CHF of water from Rao and Andrews (1978) is close to the prediction (1224 kW/m^2) by Lienhard and Lienhard (2012) (Eq. (9.12) and (9.18), $q''_{CHF} = \left(0.89 + 2.27e^{-3.44\sqrt{R'}}\right)\cdot\left(0.131\rho_v^{1/2}h_{fg}\sqrt[4]{g(\rho_l-\rho_v)\sigma}\right), R' = R\sqrt{g(\rho_l-\rho_v)/\sigma}$). However, the estimation of pure glycerine (562 kW/m^2) is different from the extrapolation (1700 kW/m^2). It may suggest that the viscosity would need to be considered in the estimation.

The gap in the data from the nucleate to the film boiling regimes of the boiling curve (i.e., the transition boiling regime) is (as previously noted in Chapter 1) a result of the fact that input power is the control variable. The transition boiling portion of the boiling curve is not accessible when power is the control variable.

In the film boiling regime which is attained by the quenching method (Appendix C), the highest tube temperature that can be sustained is limited by the

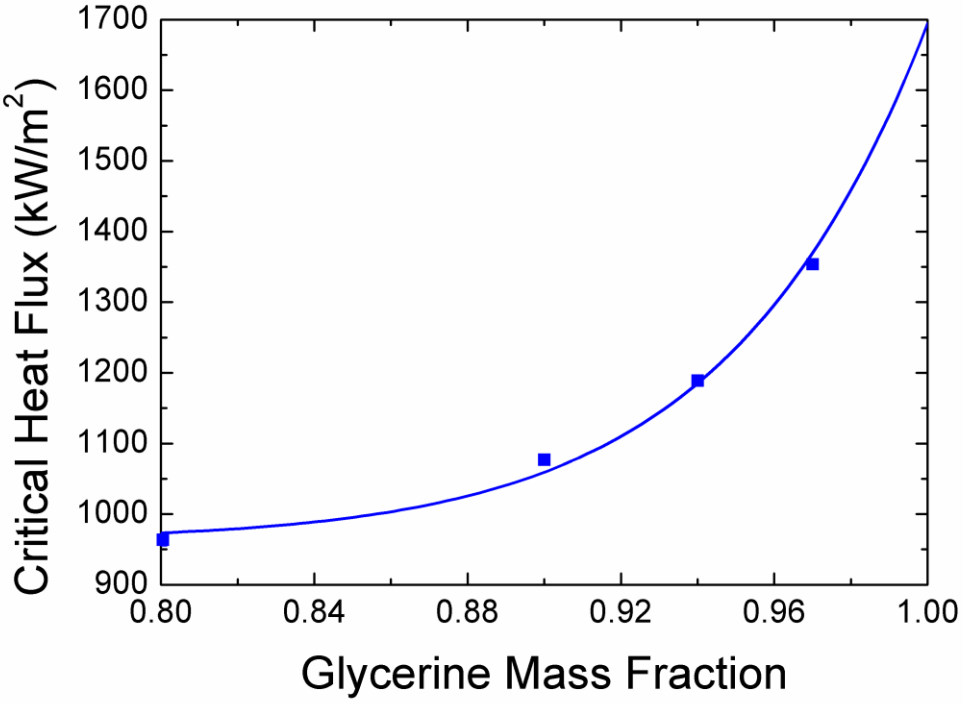

Figure 3.3: Measured critical heat flux with different glycerine fractions and its trend line. The critical heat flux increases with increasing glycerine fraction from 0.80 to 0.97.

Inconel 600 melting point (1686 K) while the lower end is bounded by the point which film boiling starts to collapse (q''_2). The measured unstable film boiling temperatures (T_2) for four mixtures are labeled in Figure 3.2 and summarized in Table 1.3.

Figure 3.4 shows the unstable heat flux varies with glycerine fractions. Similar to the CHF in Figure 3.3, the unstable heat flux to maintain film boiling also increases with increasing glycerine fractions. The measured unstable heat fluxes for four mixtures are not even in the range of Leidenfrost heat flux prediction for pure water and glycreine: 16 and 12 kW/m^2 by Lienhard and Dhir (1980) ($q''_{Leid} = 0.06 \times \rho_v h_{fg} \left(\sqrt[4]{g(\rho_l - \rho_v)\sigma / (\rho_l + \rho_v)^2} \right) \times \left[R'^2 \left(2R'^2 + 1 \right) \right]^{-1/4}$). The possible reason could be that the power is increased as film boiling collapses. There might be an even lower range of boiling curve in the film boiling regime that is not measured in this study.

The density of the bulk liquid was measured before and after a 94/6 mixture experiment. After three hours of operation, the density dropped from 1243 to 1241 kg/m^3, which is a negligible difference. It may suggest that water is condensed and refluxed to the liquid pool which altered the bulk liquid concentration, yet the amount is very small.

3.2.2 Product Yield Rate

Figure 3.5 shows the variation of total exhaust gas flow rate as a function of average tube temperature for the indicated concentrations (note the discussion in Appendix A on the reaction temperature). A logarithmic scale plot is inserted to better illustrate the flow rates at the highest water concentration (80/20) where the flow rates are comparatively low. Solid lines suggest the trends of the data. The horizontal dotted line in the inserted plot represents the detection limit (20 mL/min) of the flow meter (FMA-A2309) used in measurement. Measurements

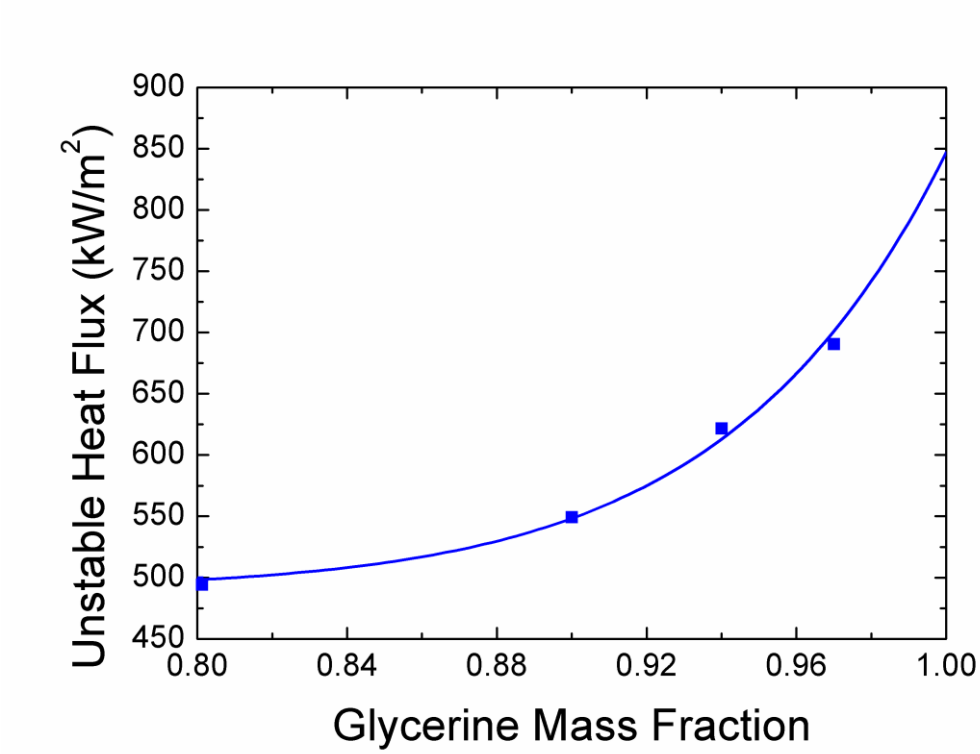

Figure 3.4: Measured unstable flux (q''_2) with different glycerine fractions and the trend line. The unstable heat flux increases with increasing glycerine fractions.

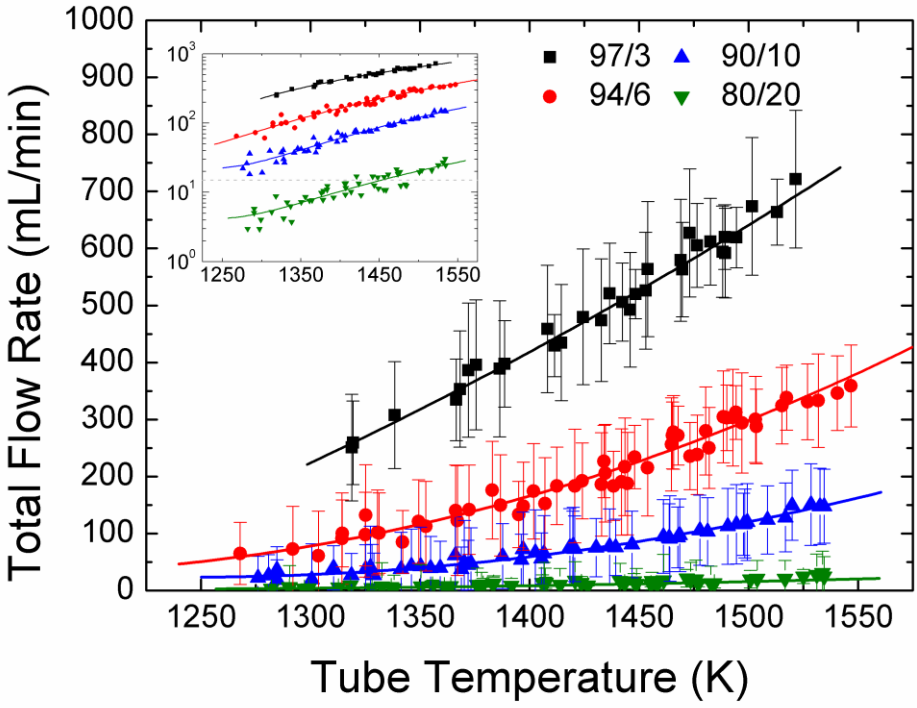

Figure 3.5: Measured total flow rate and suggested trend lines from thermal decomposition of aqueous glycerine mixtures with a logarithm scale plot inserted. The flow yield rate increases with increasing glycerine fractions and temperatures.

below the detection limit are not reliable since they might include uncertainties. For the 80/20 mixture, the product yield rate is close to the detection limit of the current flow meter (FMA-A2309). The product yield rate of glycerine fractions lower than 80/20 cannot be detected without replacing a lower detection limit flow meter.

From Figure 3.5, it is seen that the total flow rate increases with increasing temperature for all concentrations. For a fix the tube temperature, the product yield rate increases with increasing glycerine fraction since more reactant is preferential vaporized to the vapor film.

The extrapolation of the measured product yields to pure glycerine (not accessible with the current apparatus used) shown in Figure 3.6 suggests the potential for a substantial increase in the product yield rate over the lowest water dilution examined (97/3), by a factor of two. Decreasing the water concentration increases the product yields because of the increase of glycerine fraction in the vapor film (c.f. Figure 3.1). The vapor film is thereby enriched with glycerine and the product gas flow rate increases as a result of more production of the non-condensable products.

Among all gas products detected, hydrogen and carbon monoxide have the highest concentration for all mixtures.

As shown in Figure 3.7, six product species are detected from the GC analysis: hydrogen (H_2), carbon monoxide (CO), methane (CH_4), carbon dioxide (CO_2), ethylene (C_2H_4), and ethane (C_2H_6). These species are likely produced according to reactions (3.1) to (3.4), while ethylene and ethane may be formed by

$$C_3H_5(OH)_3 \rightarrow C_2H_4 + CO + 2\mathbf{H_2O} \qquad (3.5)$$

$$C_2H_4 + H_2 \rightleftarrows C_2H_6 \qquad (3.6)$$

Ratio of hydrogen to carbon monoxide (H_2:CO) for all mixtures is plotted in Figure 3.8. The 97/3 mixture is quite close to the expected (stoichiometric) ratio from Eq. (3.1): 4:3 (note the dotted horizontal line in the figure). By increasing the water

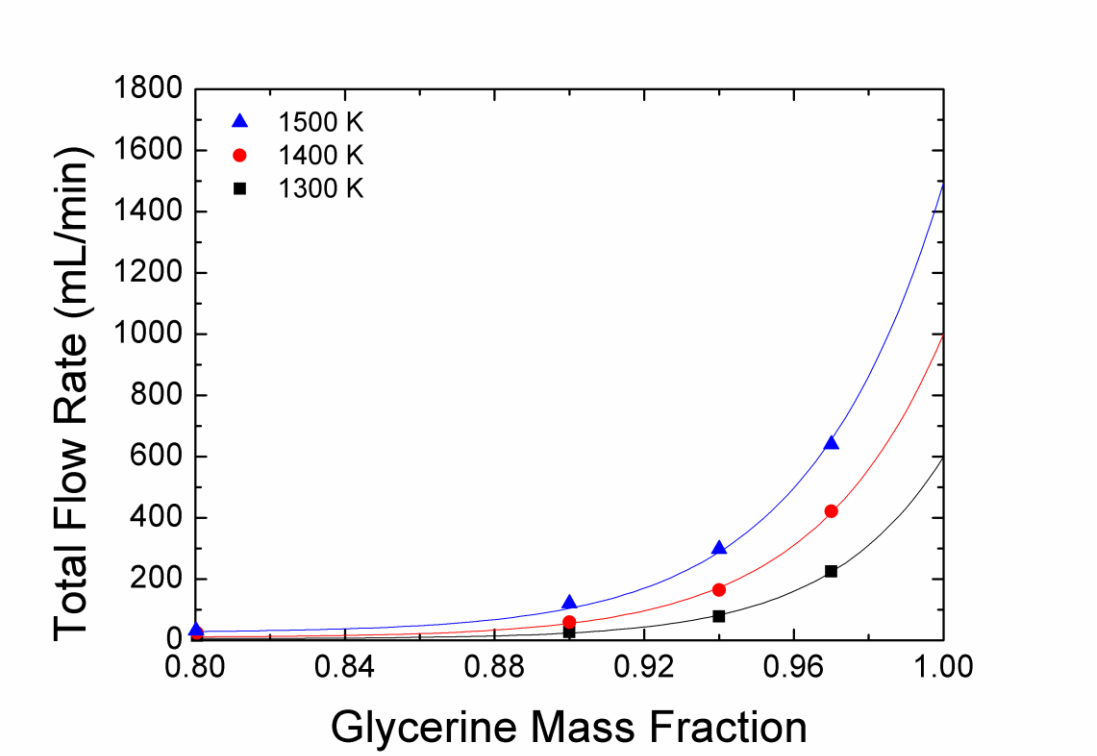

Figure 3.6: Total flow rate from thermal decomposition of aqueous glycerine mixtures. Three specific temperatures are selected to demonstrate the potential of pure glycerine experiment.

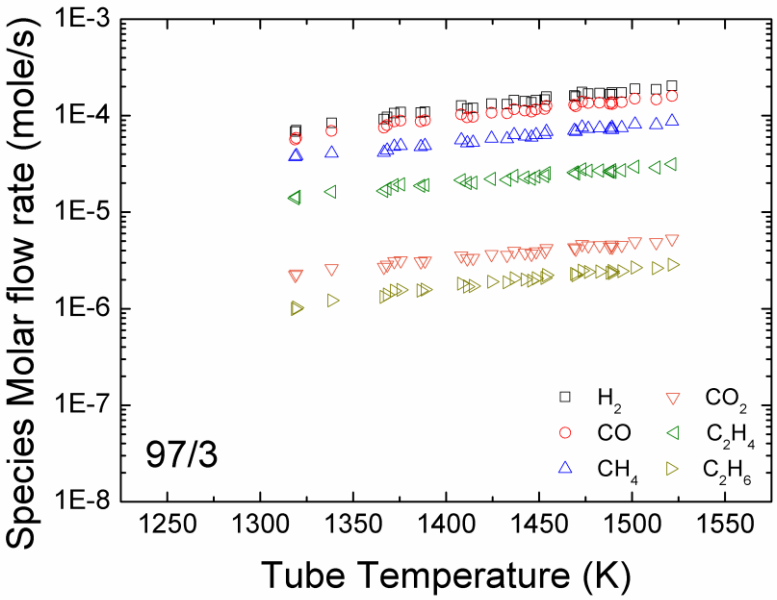
Species Molar flow rate (mole/s)
1E-3
1E-4
1E-5
1E-6
1E-7
1E-8
1250
1300
1350
1400
1450
1500
1550
Tube Temperature (K)
97/3
H2
CO
CH4
CO2
C2H4
C2H6

(a)

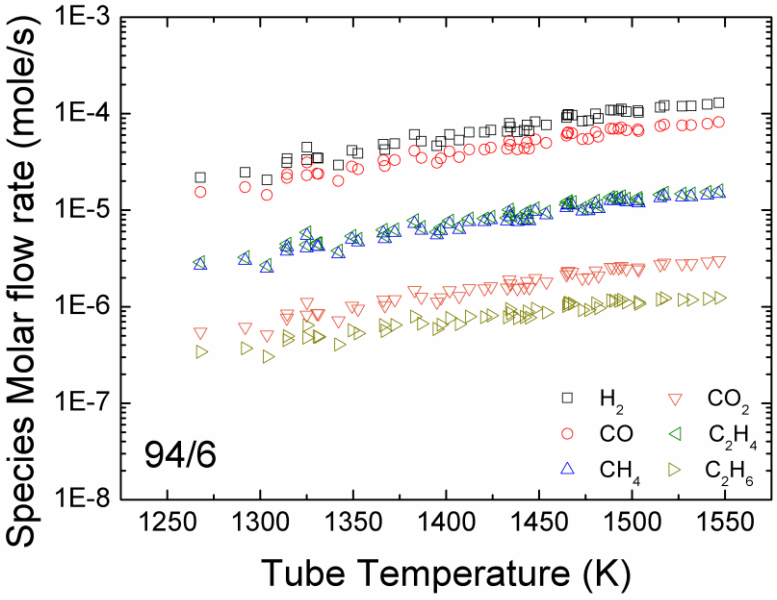
Species Molar flow rate (mole/s)
1E-3
1E-4
1E-5
1E-6
1E-7
1E-8
1250
1300
1350
1400
1450
1500
1550
Tube Temperature (K)
94/6
H2
CO
CH4
CO2
C2H4
C2H6

(b)

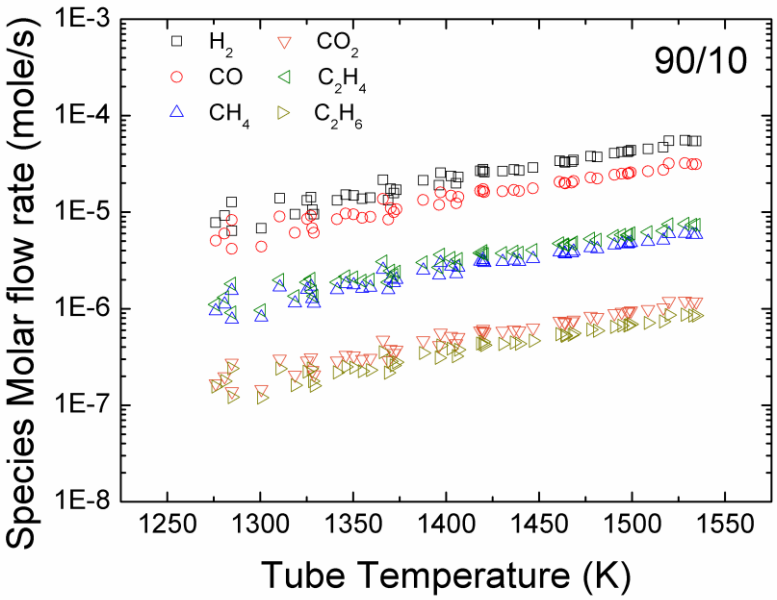

(c)

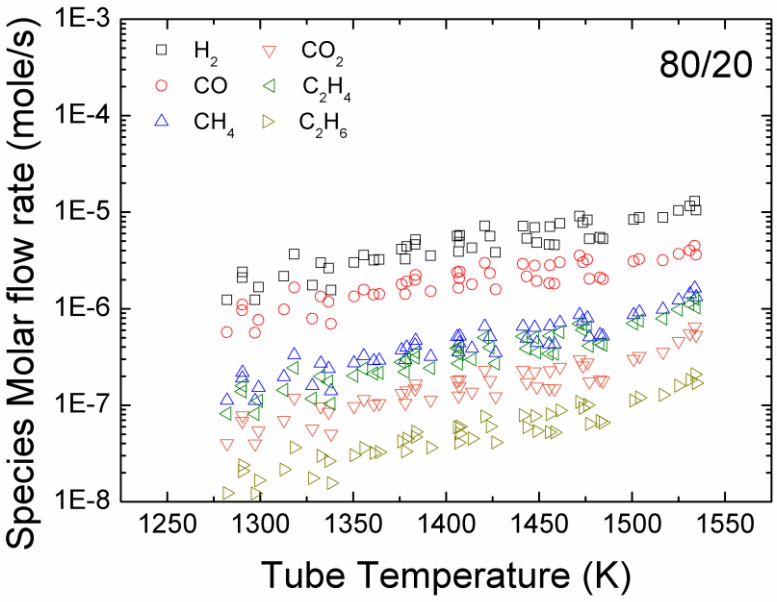

(d)

Figure 3.7: Species molar flow rate of aqueous glycerine decomposition: (a) 97/3; (b) 94/6; (c) 90/10; (d) 80/20. Six species are detected in the product gas stream and the molar flow rate increases with increasing tube temperatures.

fraction in glycerine, the H_2:CO ratio increases since more hydrogen atoms are reacted and generated hydrogen gas.

Figure 3.7 shows that both carbon dioxide and ethane have the lowest concentrations regardless of mixture fractions. This suggests that any reaction with these two species would be minor in comparison: (3.3), (3.4), and (3.6). The remaining reactions ((3.1), (3.2), and (3.5)) would seem to be more important since the product concentrations are relatively high. As for carbon monoxide and hydrogen reacting to form methane, Eq. (3.2) seems likely. For the 97/3 mixture (Figure 3.7 (a)), the water fraction is relative low (compared with 80/20), which would favor the forward reaction of (3.2), and result in a relatively higher methane concentration in the product gas stream. For the 80/20 mixture, a higher water fraction (compared with 97/3) favors reaction (3.2) in the backward direction, which results in lowering the methane concentration, and increasing the H_2:CO ratio which is consistent with Figure 3.8. Regarding reaction (3.5), it generates ethylene, carbon monoxide, and water, which are not at negligible level.

For the 94/6 mixture experiment, the bulk liquid is sampled after three hours of operation and analyzed by GC/MS with a derivatization process (see Appendix C.4). The results show essentially no condensable organic species in the liquid above the detection limit. The plausible condensable organic products (Rennard et al 2009) from glycerine decomposition are listed in Table 3.1, but none could be detected. With increasing temperature, most of the condensable products are water (>97%). Hence, we believe that the liquid pool contains either glycerine or water. The lowest reaction temperature reported is 1142 K, which is higher than 1073 K (Valliyappan 2004). The higher temperature could potentially thermal decompose condensable organic products into lighter fractions.

3.3 Conclusion

The conclusions of this effort are the following.

1) The thermal decomposition of aqueous glycerine mixtures has been realized by film boiling without additional efforts to vaporize and transport the reactant.
2) Decomposition of glycerine/water mixtures yields primarily synthesis gas as the main product, which is an alternative fuel.
3) The product yield rate increases with increasing glycerine fraction and tube temperature, showing the potential of the pure glyceriene decomposition experiment.
4) The water fraction in the aqueous glycerine mixtures affects the boiling curve in the nucleate boiling regime but not the film boiling regime.
5) The trend of mixture CHF is consistent with the previous study (Rao and Andrew 2012) while the measured unstable heat flux is not even in the range of the minimum heat flux prediction (Lienhard and Dhir 1980).
7) The high tube temperature created by film boiling further decomposes condensable organics products, which results in the liquid pool containing either glycerine or water.

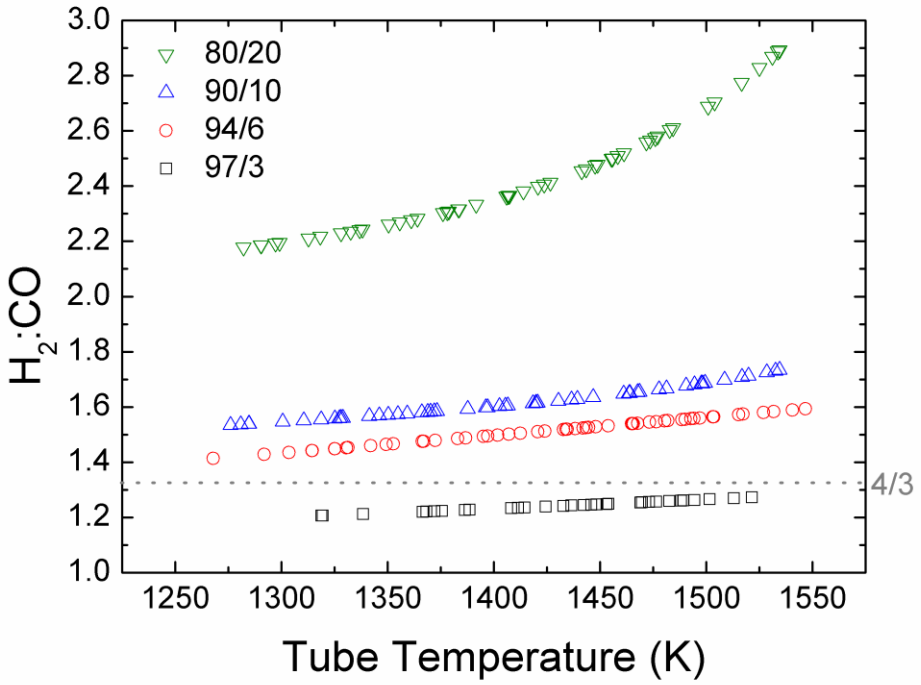

Figure 3.8: H_2:CO ratio as a function of temperature and concentration. The dotted line indicates the stoichiometric ratio of the reaction (3.1). The H_2:CO ratio increasing with increasing water dilution in the glycerine mixture.

Table 3.1: Detection limits of possible condensable organic products.

Chemicals	Formula	Detection limit (vol %)
Methanol	CH_3OH	0.10%
Ethanol	C_2H_5OH	1%
Formic acid	HCOOH	1%
Acetic acid	CH_3COOH	1%
Lactic Acid	$CH_3CH(OH)COOH$	1%
Acrolein	CH_2CHCHO	20%

CHAPTER 4

ETHYL ACETATE

4.1 Introduction

The objective is to study thermal decomposition of ethyl acetate ($CH_3COOC_2H_5$, EA) by measuring its boiling curve and product yield rate, as well as performing chemical analysis of the product gas stream and liquid sample.

Pyrolysis of EA is expected to be a unimolecular process with two main products forming: acetic acid (CH_3COOH, AA) and ethylene (C_2H_4),

$$CH_3COOC_2H_5 \rightarrow \mathbf{CH_3COOH} + C_2H_4 \qquad (4.1)$$

with known rate constants (Blades 1954; Blades and Gilderson 1960; Scheer et al 1963; Beadle et al 1972; Gutman et al 1977; Tsang et al 1978; Eberhardt et al 1982; Saito et al 1990). Note that AA is labeled in bold showing that it is condensable in the apparatus; it is also soluble in EA. The experimental design described in Chapter 2 has no special provision to prevent refluxing (e.g., by dripping) of condensable species into the chamber. As a result, the liquid pool will be transformed over time from a single component reactant (EA) to a miscible mixture containing mainly EA, AA, and other condensable and soluble products.

For an EA/AA mixture, AA will preferentially vaporize to enter the vapor film and it too can thermally decompose depending on the vapor temperature. The decomposition of AA proceeds as,

$$CH_3COOH \rightarrow CO_2 + CH_4 \qquad (4.2)$$

with rate constants developed by Bamford and Dewar (1949), Blake and Jackson (1968), Blake and Jackson (1969), Mackie and Doolan (1984), Duan and Page (1995), and Nguyen et al (1995).

The extent to which it could be known if reaction (4.2) contributes to the overall decomposition process depends in part on detecting carbon dioxide (CO_2) and methane (CH_4) in the product stream. Considering equations (4.1) and (4.2) as describing the overall conversion process, complete conversion of EA is schematically indicated as

$$CH_3COOC_2H_5 \xrightarrow{CH_3COOH} CO_2 + CH_4 + C_2H_4 \qquad (4.3)$$

with AA being an intermediary.

It should be noted that the concentration of acetic acid in the bulk liquid is dependent in part on the physical size (i.e., volume) of the chamber and the EA conversion rate. For an arbitrarily large containment volume or low conversion rate, the concentration of AA in the liquid and, thus, in the vapor film would of course be small. Furthermore, if the condensate were flushed through the system and prevented from returning to the liquid pool (i.e., a different experimental design than described in Chapter 2), the reactant liquid would remain as a pure component regardless of the number of condensable species formed by decomposition. The influence of concentration of dissolved products on performance should therefore be viewed somewhat in the context of the experimental design.

To illustrate the effect of a changing liquid composition due to the effect discussed above, Figure 4.1 shows the measured evolution of liquid concentration from GC/MS measurements at the indicated times for a fixed tube temperature of 1313 K over a four hour period. 10 mL of bulk liquid is withdrawn hourly. The concentration change due to sampling process (i.e. volume change) is examined to be small. The increase of AA concentration is evident, which is due to refluxing. The specific molar concentrations shown are dependent on the volume of the liquid containment and the conversion rate of EA; while for the data shown in Figure 4.1 is

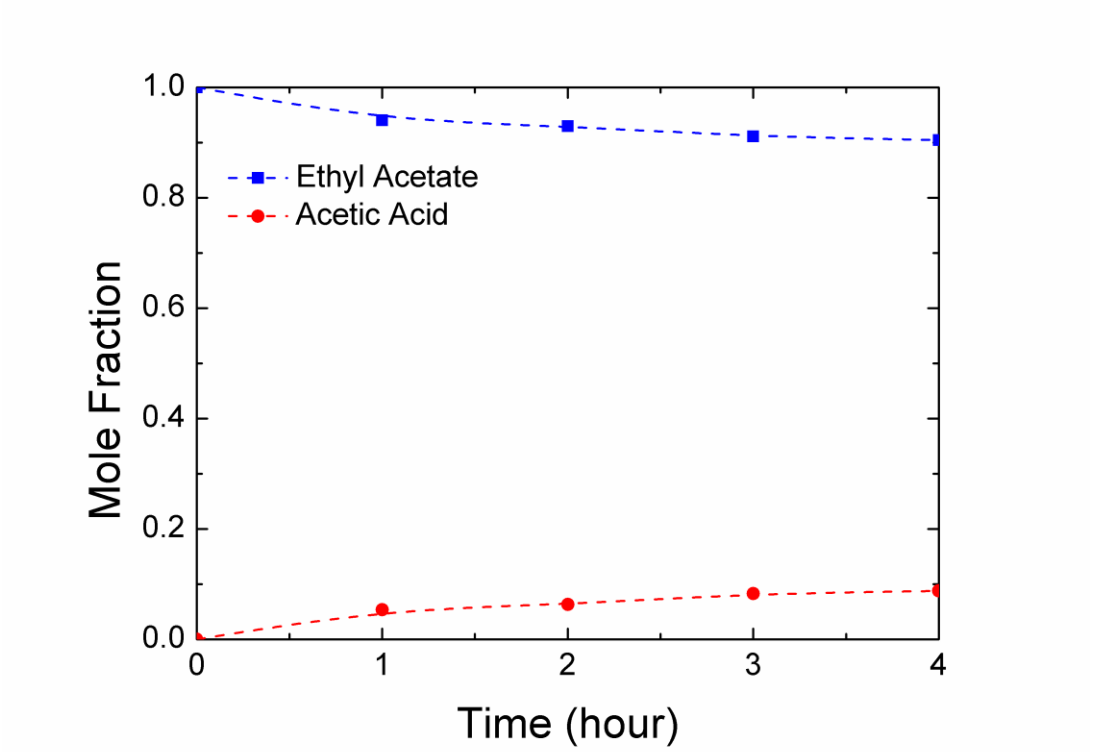

Figure 4.1: Measured bulk liquid concentrations as a function of time for EA and AA at T_w = 1313 K over a four hour interval. The bulk liquid transitions from a pure EA to a mixture mainly composed of EA (0.9) and AA (0.1).

approximately 4 L. With AA in the liquid, there is potential for its conversion along with EA.

The fractional amount of soluble products in the vapor film is determined by the phase equilibrium behavior of the mixture. Considering a binary EA/AA mixture, Figure 4.2 (a) shows the bubble point curve at atmospheric pressure and Figure 4.2 (b) illustrates the variation of vapor mole fraction in equilibrium with the indicated liquid composition in solution (Garner et al 1954). The liquid mole fraction of the binary mixture is not the same the vapor mole fraction sue to the preferential vaporization.

In reality, there may are more condensable species. Table 4.1 illustrates the suite of chemicals for a tube wall temperature of 1313 K along with the normal boiling points of the species. It is clear that the dominant condensable product species is AA. From Table 4.1, it can be observed that the liquid mole fraction of AA is 0.0876 after a four hour operation, which would result in the AA vapor mole fraction to be 0.02 (c.f. Figure 4.2 (b)). This concentration is relatively small compared with EA.

4.2 Results and Discussion

4.2.1 Boiling Curve

The operational parameters of a reactor based on film boiling are defined by the boiling curve, which displays the relationship between the applied heat flux and the wall temperature as discussed in Chapter 1. Figure 4.3 shows the measured boiling curve of EA. Four separate experimental runs are shown that illustrate the repeatability of the measurements; each data point in the figure represent an averaged temperature over a five-minute constant power duration (see Appendix D.1).

The boiling curve was developed with the tube initially submerged in the liquid pool, and the power then increased in steps. The nucleate boiling portion terminated at

Table 4.1: Liquid composition (mole fraction) at the indicated times for T_w=1313 K.

Chemical	Formula	T_b [K]	1 hr	2 hr	3 hr	4 hr
Ethene	C_2H_4	169.4	0.0003	0.0003	0.0003	0.0003
Acetaldehyde	CH_3CHO	293.9	0.0005	0.0005	0.0005	0.0005
Ethanol	C_2H_5OH	351.5	0.0002	0.0004	0.0003	0.0003
Acetone	$(CH_3)_2CO$	329.3	0.0004	0.0003	0.0003	0.0003
3-Penten-1-yne	C_5H_6	317.2	0.0000	0.0001	0.0001	0.0001
Ethyl acetate	*$CH_3COOC_2H_5$*	*350.2*	*0.9405*	*0.9296*	*0.9108*	*0.9045*
Acetic acid	*CH_3COOH*	*391.2*	*0.0533*	*0.0631*	*0.0825*	*0.0876*
Propanoic acid	CH_3CH_2COOH	414.0	0.0011	0.0015	0.0012	0.0012
Butane, 1-ethoxy-	$C_6H_{14}O$	364.7	0.0006	0.0010	0.0008	0.0012
Acetic acid, anhydride	$(CH_3CO)_2O$	412.0	0.0027	0.0022	0.0027	0.0032
Heptane, 2-methyl-	C_8H_{18}	390.7	0.0005	0.0009	0.0005	0.0008

The significance of the itlatic characters in this table is that these two chemicals are the main constituents of the bulk liquid.

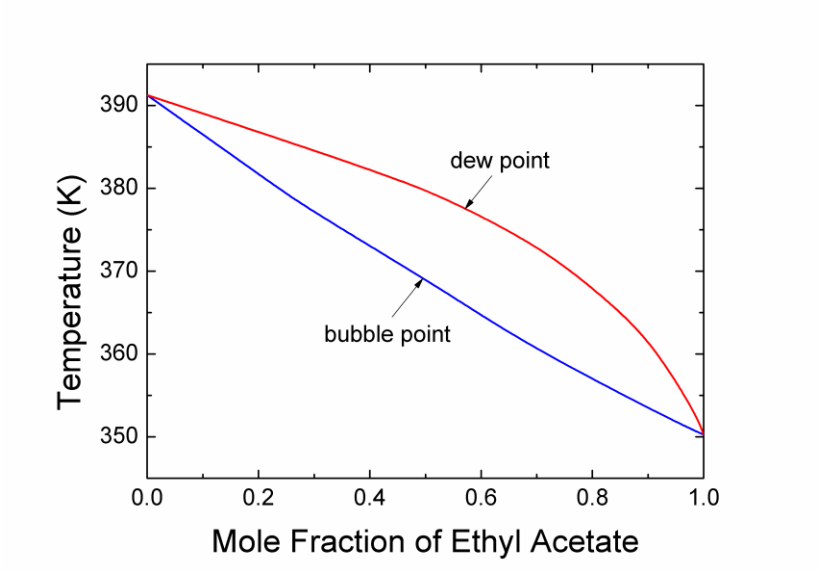

(a)

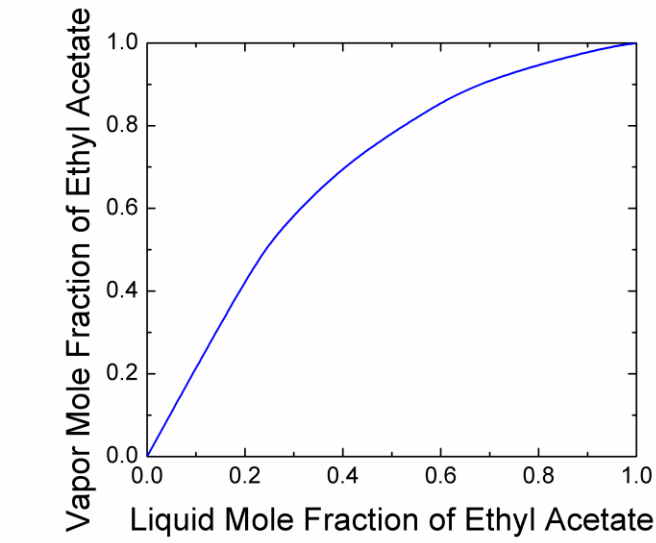

(b)

Figure 4.2: (a) Variation of bubble and dew point temperatures with mole fraction of EA at normal atmospheric pressure in an EA/AA mixture. (b) Vapor mole fractions for indicated liquid mole fractions in a binary EA/AA mixture (Garner et al 1954).

the CHF which was measured as approximately 253 kW/m^2 at T_w = 381 K. This value is within the range of predictions given by Lienhard and Lienhard (2012) as corrected for the heater size, $q''_{CHF} = \left(0.89 + 2.27e^{-3.44\sqrt{R'}}\right) \times \left(0.131\rho_v^{1/2} h_{fg} \sqrt[4]{g(\rho_l - \rho_v)\sigma}\right)$ (Eqs. (9.12) and (9.15)) where $R' = R\sqrt{g(\rho_l - \rho_v)/\sigma}$ (Eq. (9.18)) which gives q''_{CHF} = 282 kW/m^2 using the properties listed in Table 1.1.

Above the CHF, a wall temperature excursion occurs to transition the heat transfer mode to film boiling. For EA, the temperature jumped to about 940 K (note the arrows in Figure 4.3). Because this temperature is well below Inconel's melting point, film boiling could easily be established on the tube when beginning with a submerged rod and heating it without danger of melt-down on the transition from CHF to film boiling. Once in film boiling, the average tube surface temperature is systematically adjusted to traverse the film boiling states, with the low end being 145 kW/m^2 at 711 K (unstable film boiling starts). Below this temperature, the bubbling instability of the transition region is not conducive to promoting pyrolysis, and the temperature in this regime is too low for significant product yields to be expected. The practical range for the experiments reported here for EA is between 711 K to about 1450 K.

The estimated minimum heat flux in the film boiling regime (q''_{Leid}) is 7 kW/m^2 by Lienhard and Dhir (1980) using the formula $q''_{Leid} = 0.06 \times \rho_v h_{fg} \left(\sqrt[4]{g(\rho_l - \rho_v)\sigma/(\rho_l + \rho_v)^2}\right) \times \left[R'^2\left(2R'^2 + 1\right)\right]^{-1/4}$ and the properties in Table 1.1. There is a significant difference between the prediction and the measurement (145 kW/m^2). The reason for this difference could be the unstable heat flux measured in the experiment is the beginning of destabilization but not the actual Leidenfrost point. The transition boiling portion of the boiling curve is not accessible, hence the gap in data between 381 K and 711 K.

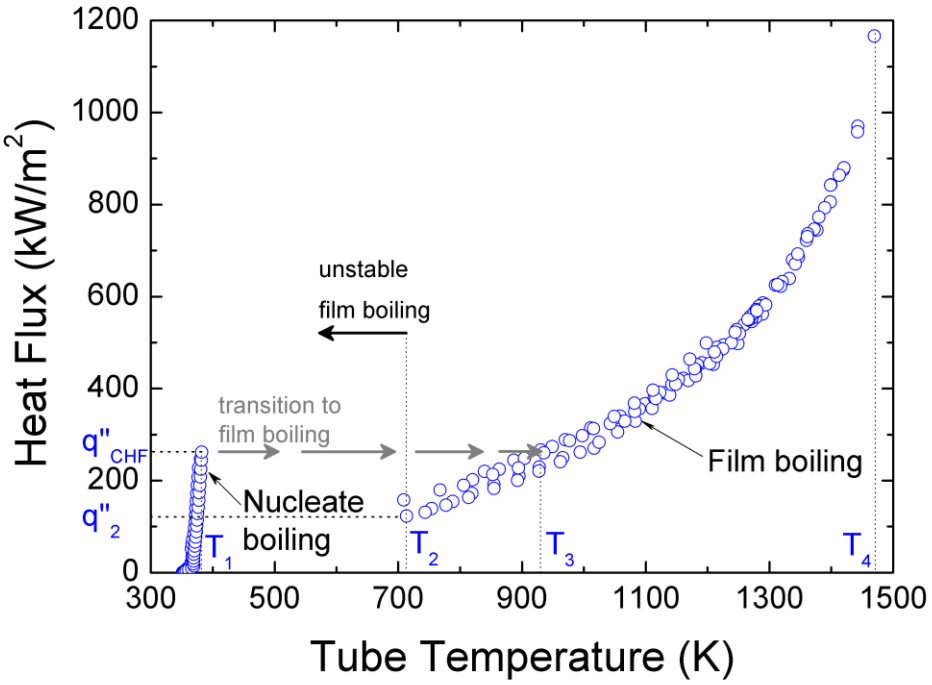

Figure 4.3: Measured boiling curve of EA. Thermal decomposition is confined to the film boiling domain. The arrows indicate the temperature excursion that occurs on transitioning from the critical heat flux (CHF at T_1) to the film boiling regime (T_3). T_2 to T_4 is the operation domain of the reactor.

4.2.2 Product Yield Rate

The boiling curve shown in Figure 4.3 offers no substantive clue of reactions in the vapor film. The exhaust gas flow rate and chemical analysis of the gas stream provides the direct evidence of a particular decomposition route (e.g., Eqs (4.1) and (4.2)).

Figure 4.4 shows the variation of exhaust gas flow rate of EA with average tube surface temperature measured by two flow meters. The flow rates were obtained from the flow meter voltage output by converting raw voltage signals to flow rate with the aid of a calibration. The simplicity of EA decomposition (4.3) facilitated this conversion as the only non-condensable product gases in the exhaust stream are ethylene, methane, and carbon dioxide while AA is condensed and returned to the liquid pool. A voltage-to-flow-rate conversion is only needed for these three gases, which is discussed in Appendix D.

The tube wall temperature is used as a representative value for the reaction conditions in presenting the data. Other temperatures can also be used to represent the reaction condition. This matter is discussed in Appendix A where a reaction temperature is proposed.

The conversion rates for the decomposition reactions discussed in section 4.1 are expected to follow Arrhenius equation ($K = A\exp(-E_a/\bar{R}T)$. Since the highest gas temperature is at the tube surface, the conversion rate is highest at T_w, and it drops exponentially as the gas temperature is less than the wall temperature. The inset to Figure 4.4 shows the sharp decline in the exhaust gas flow rate that is consistent with the strong dependence of the reaction rate on temperature. The solid line denotes the precision limit of the FMA-A2309 flow meter (e.g., 44mL/min) while the dashed line is the limit for the FMA-4310 flow meter (e.g., 9 mL/min). Below these levels, the

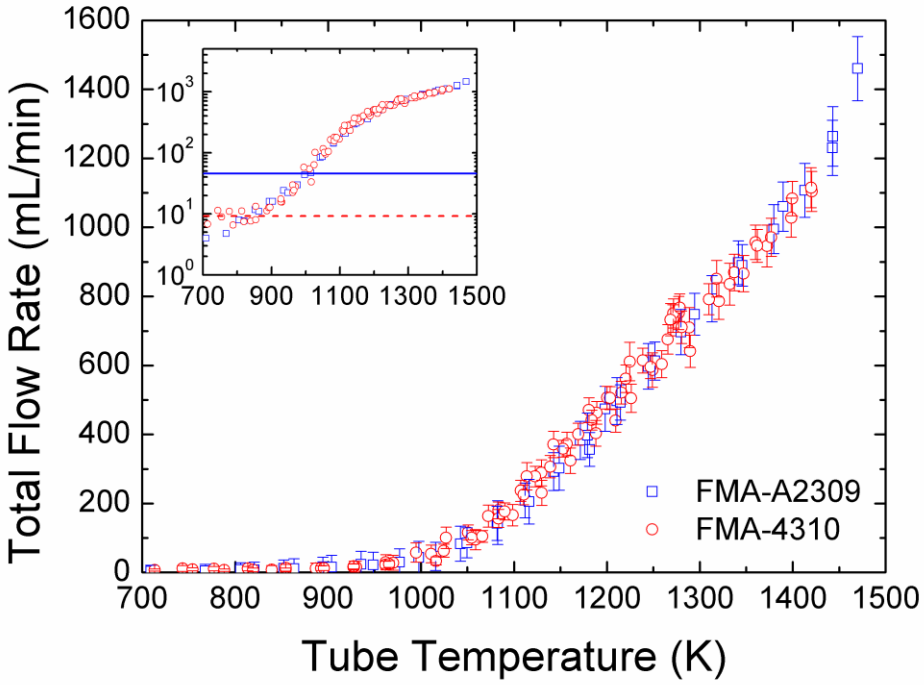

Figure 4.4: Product yields as a function of tube temperature. Inset shows the same data on a logarithmic scale to magnify the flow rate at lower temperatures. The solid line (44 mL/min) and dashed line (9 mL/min) indicate the detection limit of flow meter FMA-A2309 and FMA-4310.

measurements are not reliable. In overlapping ranges the two flow meters gave virtually identical flow rates.

Three gases were detected in the exhaust stream: ethylene, methane and carbon dioxide. Figure 4.5 shows the measured fractional amounts of these species as the tube temperature is varied. Ethylene dominates the gas concentration up to about 1300 K indicating that reaction (4.1) is the main conversion process even though AA is in the vapor. At higher temperatures, carbon dioxide and methane concentrations increase indicating the potential importance of AA decomposition reaction (4.2) in the overall conversion process. The increase in carbon dioxide and methane concentrations and the concomitant slight reduction of ethylene with temperature shown in Figure 4.5 tracks with the increase of dissolved AA in EA due to refluxing noted.

While reactions (4.1) and (4.2) are believed to be the primary route for EA decomposition by film boiling, GC/MS analysis of the liquid identified many more condensable products. Over a four hour experiment, the species detected hourly in the liquid pool at specific value of T_w = 1313 K are listed in Table 4.1. Considering the low level of these additional species, reactions (4.1) and (4.2) are most likely the primary decomposition routes for ethyl acetate by film boiling.

Since reactions (4.1) and (4.2) are unimolecular decomposition reactions, the law of mass action leads to the rate of formation of product species as $dC_{pi}/dt = KC_R$ (Willams 1965). Unfortunately, this equation cannot be integrated because the molar concentration of EA and AA in the exhaust gas was not measured in the experiment, as these species were condensed and allowed to reflux into the liquid pool. However, the reaction rates provide a further clue on which of reactions (4.1) and (4.2) is likely to be dominant. From the available rate constants (Blades 1954, Blades and Gilderson 1960, Scheer et al 1963, Gutman et al 1977, Tsang et al 1978, Bamford and Dewar

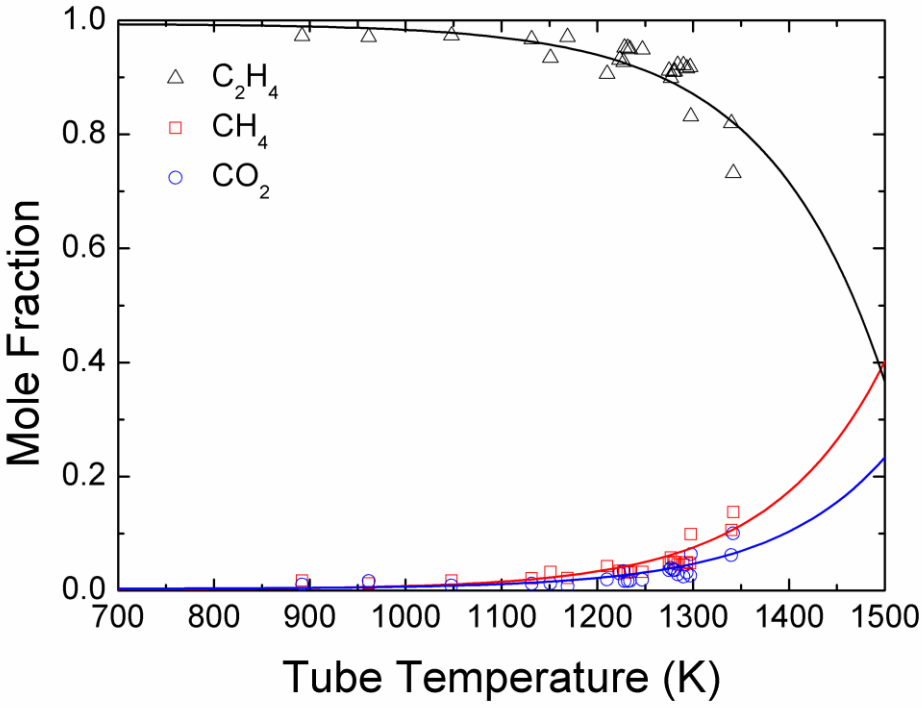

Figure 4.5: Measured product gas compositions as a function of tube temperature. Three species are detected, and solid lines shown are the trend lines.

1949, Blake and Jackson 1968, Blake and Jackson 1969, Mackie and Doolan 1984, Duan and Page 1995, Nguyen et al 1995), we can say with reasonable certainty that AA decomposition (Eq. (4.2)) should proceed at a slower rate than EA as both species are transported around the tube in the vapor film.

Figure 4.6 shows the species molar flow rate of the individual non-condensable product gases in the exhaust stream. At low temperatures, the ethylene molar flow rate (produced from reaction (4.1)) is several orders of magnitude higher than methane and carbon dioxide (reaction (4.2)) in keeping with the higher rate constant and lower activation energy of EA decomposition relative to AA. This large difference is maintained for almost the entire temperature range investigated, except at the highest temperatures where the molar rates appear to converge. This trend is consistent with Figure 4.5 which also shows negligible concentrations of the products of AA decomposition at low tube temperatures and increasing concentrations of the AA products at high temperatures. The concentration of methane and carbon dioxide tracks together throughout the temperature range as shown in Figure 4.6. This trend is consistent with Eq. (4.2) which shows that the molar concentrations (and hence the molar flow rates of these two species) should be equal.

A final point to note regarding decomposition of organic molecules by film boiling is the potential for surface (catalytic) effects in the conversion process and the formation of a carbonaceous layer on the tube. The fact that the highest temperature in the vapor film occurs at the tube surface, with a steep drop in temperature to the liquid/vapor interface, and that the tube material itself (being a nickel alloy in the present experiments) could be catalytic suggest this possibility.

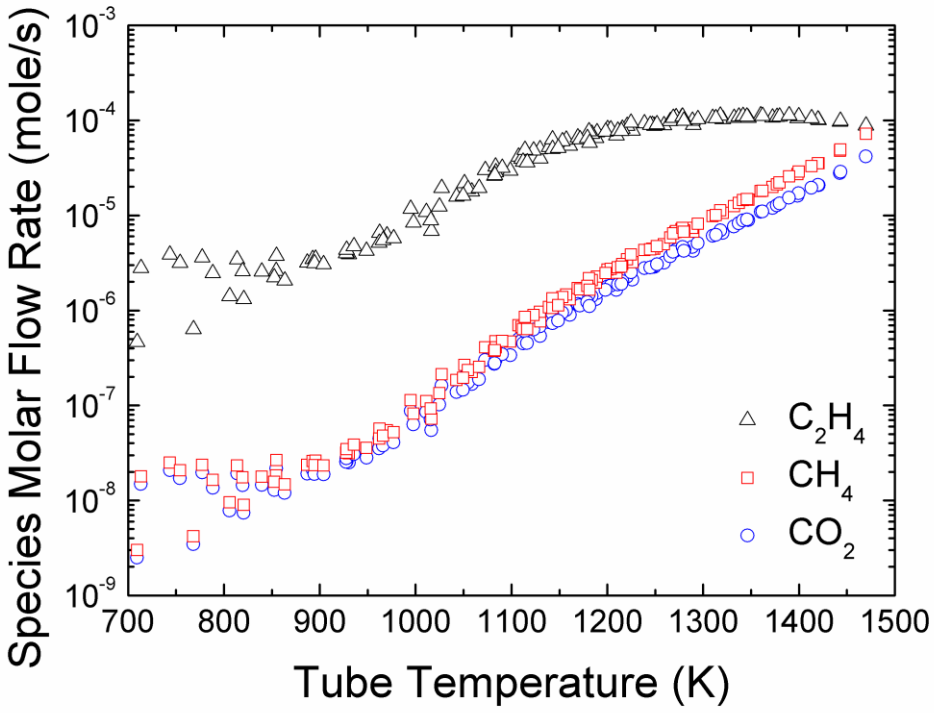

Figure 4.6: Molar flow rate of the individual non-condensable product gases from EA decomposition. The highest flow rate is ethylene, which suggested that EA decomposition reaction is the main reaction occurring in the vapor film.

4.3 Conclusion

The conclusions of this effort to study EA decomposition by film boiling are the following:

1) Thermal decomposition of EA by film boiling resulted in formation of AA and ethylene in proportions consistent with a unimolecular decomposition process.
2) The estimated CHF is close to the prediction while the estimated minimum heat flux (Leidenfrost point) much lower than the unstable heat flux measured.
3) For the experimental design of the present study in which AA was allowed to reflux to the liquid pool, AA further decomposed (along with EA) to form methane and carbon dioxide, with product concentrations increasing with tube surface temperature.
4) Over the temperature range investigated the concentrations of dissolved species other than acetic acid was small, indicating that EA and AA dominated the conversion process.
5) Development of a carbon film on the tube surface was noted which was considered to mitigate the potential for surface catalytic reactions on the bare Inconel support.

CHAPTER 5

DIETHYL CARBONATE AND ETHANOL

5.1 Introduction

The objective of this study is to utilize film boiling as a reactor to study the thermal decomposition of diethyl carbonate ($(CH_3CH_2O)_2CO$, DEC) and ethanol (C_2H_5OH, EtOH) by measuring the boiling curve and exhaust gas flow rate, and performing chemical analysis of the product gas stream and liquid sample.

DEC and EtOH are grouped together because one (EtOH) is a product of another (DEC) in a unimolecular decomposition with known rate constants (Gordon and Norris 1965; Bigley and Wren 1971; Cross et al 1976; Taylor 1983; Herzler et al 1997; Notario et al 2005).

$$(CH_3CH_2O)_2CO \rightarrow C_2H_4 + CO_2 + \mathbf{C_2H_5OH} \qquad (5.1)$$

Products in bold are condensable species. The generated products are ethylene (C_2H_4), carbon dioxide (CO_2), and EtOH.

The experimental design (Chapter 2) allows the condensable species to return to the liquid pool. Refluxed ethanol will therefore preferentially vaporize at the vapor/liquid interface and itself thermally decompose along with DEC. To confirm whether additional species (other than ethylene, carbon dioxide, and EtOH) are formed from ethanol decomposition, thermal decomposition of pure ethanol is also examined.

Ethanol can thermally decompose via several routes (Morris 1931, Gotzoll 1985, Li et al 2001, Park et al 2002, Li et al 2004, Vaidya and Rodrigues 2006),

$$C_2H_5(OH) \rightarrow C_2H_4 + \mathbf{H_2O} \qquad (5.2)$$

$$C_2H_5(OH) \rightarrow \mathbf{CH_3CHO} + H_2 \qquad (5.3)$$

$$C_2H_5(OH) \rightarrow CH_4 + CO + H_2 \qquad (5.4)$$

$$C_2H_5(OH) \rightarrow CH_4 + \mathbf{CH_2O} \quad (5.5)$$

With the presence of water (H_2O), steam reforming of EtOH could also occur (Galvita et al 2001, Llorca et al 2001, Deluga et al 2004) within the vapor film, which generates hydrogen.

$$C_2H_5(OH) + 3H_2O \rightarrow 2CO_2 + 6H_2 \quad (5.6)$$

From the chemical analysis of the product gas stream and liquid sample, we are able to confirm which of the above reaction occurs, or suggest additional reactions.

Figure 5.1 (a) is a vapor-liquid-equilibrium diagram of a binary mixture comprised of DEC and EtOH (Rodriguez et al 2003). The vapor mole fraction is not equal to the liquid mole fraction because of the preferential vaporization. Figure 5.1 (b) shows how much DEC is expected in the vapor for a given liquid composition.

5.2 Results and Discussion

5.2.1 Boiling Curve of DEC

Figure 5.2 depicts the boiling curve of DEC. Data for three individual experiments show good repeatability. In the nucleate boiling regime, the average tube temperature is several degrees higher than the boiling point of the liquid. The measured CHF is 221 kW/m^2 (at 424 K), which is close to the prediction (Eqs. (9.12) (9.15) and (9.18), $q''_{CHF} = \left(0.89 + 2.27e^{-3.44\sqrt{R^*}}\right) \cdot \left(0.131\rho_v^{1/2} h_{fg} \sqrt[4]{g(\rho_l - \rho_v)\sigma}\right)$, Lienhard and Lienhard 2012), 244 kW/m^2. It should be noted that no reaction occurs in the nucleate boiling regime because the exhaust gas flow rate is essentially zero.

The immersion method is used to attain film boiling as discussed in Appendix C. As exceeding CHF, a large temperature jump occurs (519 K for DEC) and film

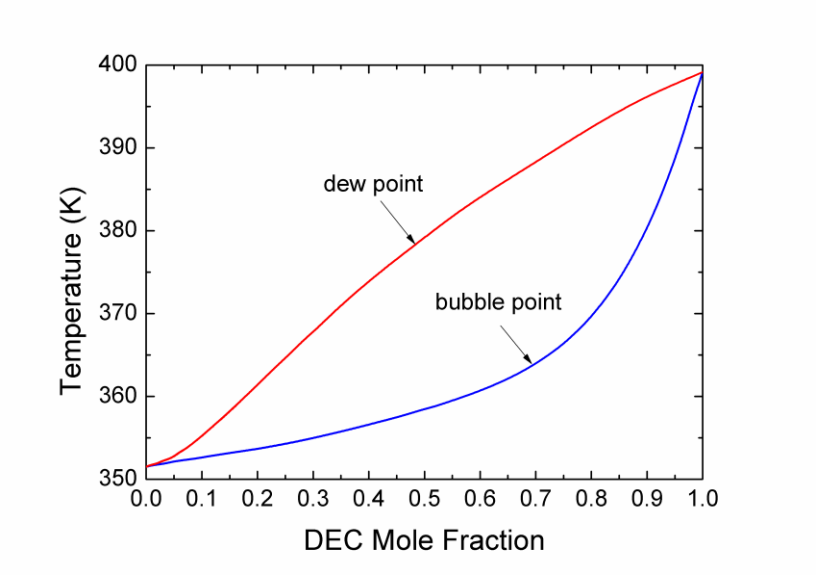

(a)

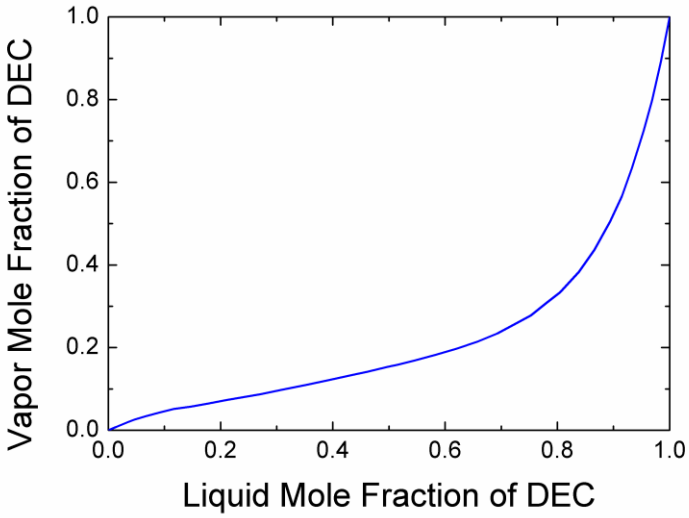

(b)

Figure 5.1: (a) Vapor-liquid-equilibrium diagram of a binary mixture: DEC and EtOH. (b) Vapor mole fractions for indicated liquid mole fractions in the binary DEC/EtOH mixture (Rodriguez et al 2003).

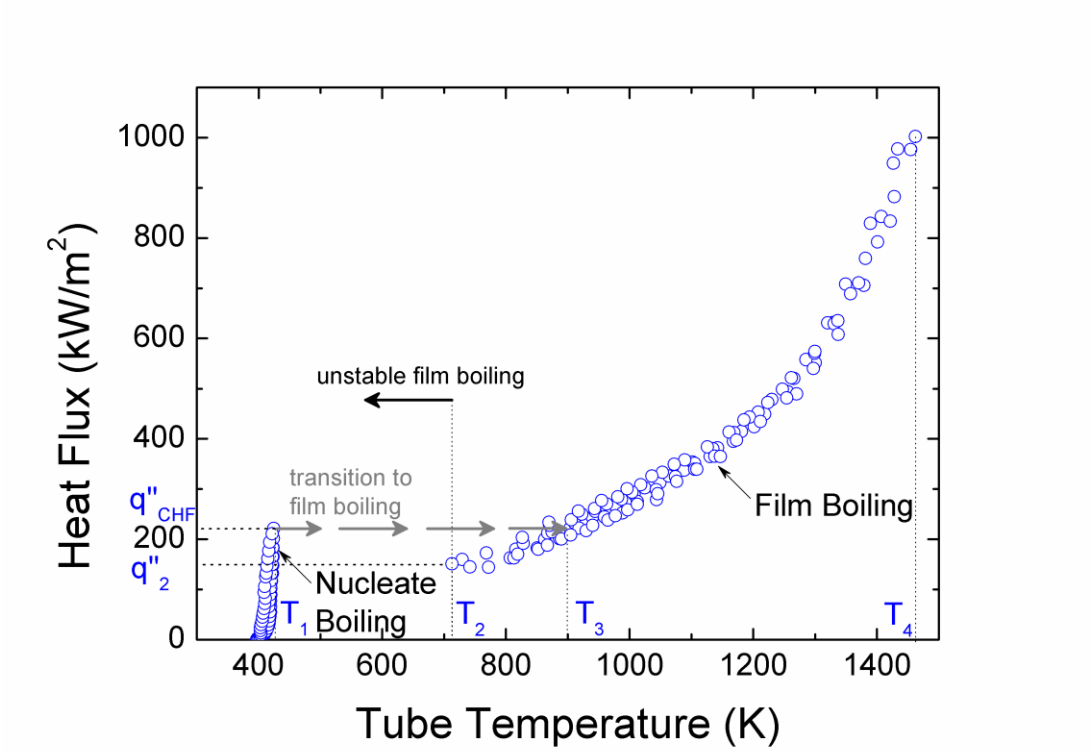

Figure 5.2: Boiling curve of DEC. Thermal decomposition is confined to the stable film boiling regime (T_2 to T_4). The arrow indicates the temperature jump from CHF (T_1) to film boiling (T_3).

boiling is established (c.f. Figure 2.4). The measured unstable film boiling temperature is 151 kW/m^2 at 713 K, which shows a significant difference from the prediction, 6 kW/m^2, from Lienhard and Dhir (1980) $q''_{Leid} = 0.06 \times \rho_v h_{fg} \left(\sqrt[4]{g(\rho_l - \rho_v)\sigma / (\rho_l + \rho_v)^2} \right) \times \left[R'^2 \left(2R'^2 + 1 \right) \right]^{-1/4}$). The measurement may suggest that there is a lower range in the film boiling regime that is not measured in this study. The practical temperature range in Figure 5.2 for the chemical reactor is between 713 K and 1462 K.

5.2.2 Product Yields of Diethyl Carbonate

Figure 5.3 shows measured total exhaust flow rates with average tube temperatures (note the discussion in Appendix A on the reaction temperature). Blue circles represent the data acquired from flow meter FMA-A2309 with lower resolution while the red triangles show the data from the flow meter FMA-4310 with higher resolution. Their resolutions are shown as horizontal lines (44 mL/min for FMA-A2309 and 9 mL/min for FMA-2310) in the logarithm insert. Two flow meter give visually identical measurements in the overlapping region.

As shown in Figure 5.3, an appreciable exhaust gas flow rates is measured above 900 K. Between 713 and 900 K, a stable vapor film is maintained though the tube temperature is apparently too low for reactions at a significant rate. As the tube temperature is increased above 900 K, exhaust product yield rates are detectable and increase with increasing temperatures, which agrees with the Arrhenius equation.

Figure 5.4 shows the variation of individual molar flow rates of non-condensable product species with average tube temperature. Two main products are ethylene and carbon dioxide, with overlapping concentrations for most of the

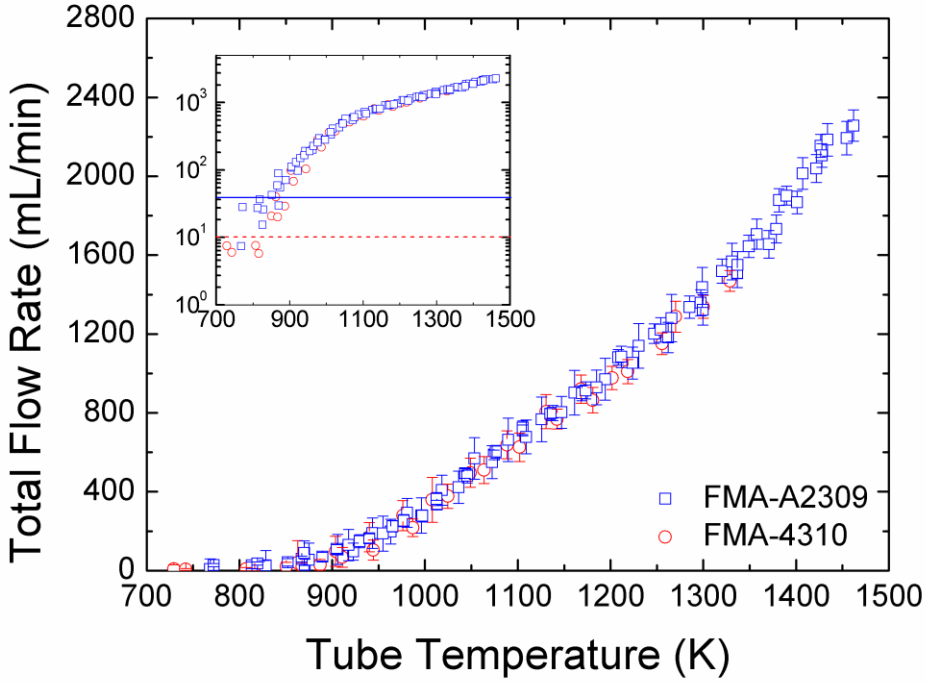

Figure 5.3: Exhaust gas flow rate of DEC thermal decomposition. Two flow meters are used to monitor the flow rate and their detection limits are shown as horizontal lines in the inserted logarithm plot. The product yield rate increases with increasing temperatures which is consistent with Arrhenius equation.

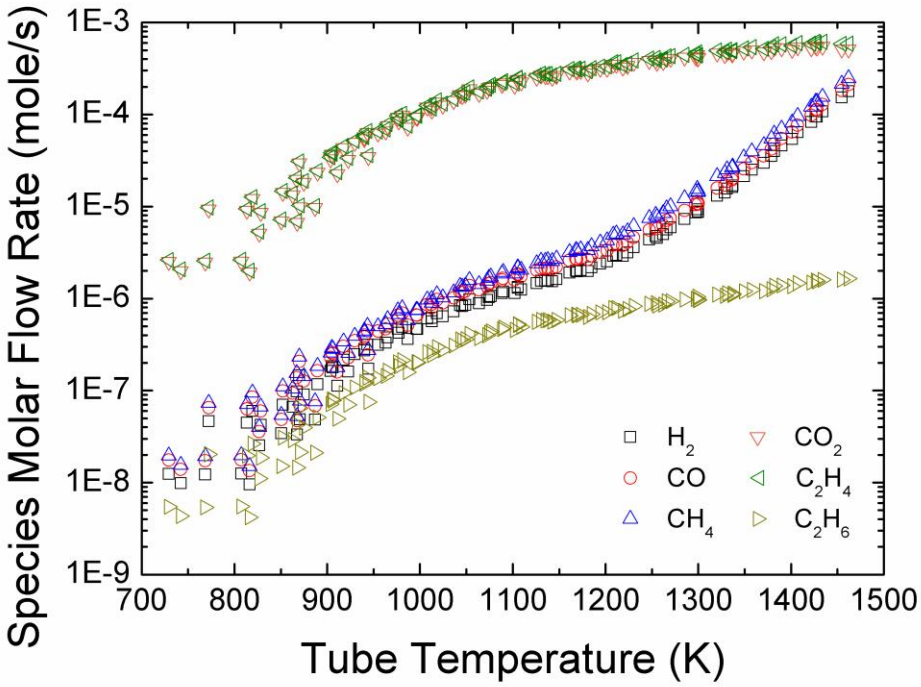

Figure 5.4: Individual species molar flow rate of DEC decomposition. The molar flow ate of ethylene and carbon dioxide is close to a one to one ratio which suggests that the main reaction occurring in the vapor film is DEC thermal decomposition. EtOH is not detectable since it is condensed and dripped back to the liquid pool.

temperature range shown. This fact shows a near 1:1 ratio, which is consistent with Eq. (5.1). Other products are also detected such as hydrogen, carbon monoxide, methane, and ethane. However, their concentrations are relatively low compared to ethylene and carbon dioxide. Ethanol is not detected in the product gas stream since it is condensed and refluxed to the liquid pool. The appearance of carbon monoxide (CO), methane (CH_4), and hydrogen (H_2) arise because of preferential vaporization of ethanol that subsequently decomposes through reactions (5.3) to (5.5). Ethanol can also thermally decompose through reaction (5.2) to produce ethylene and water. As shown in Figure 5.4, ethylene and carbon dioxide follow a near 1:1 ratio, which suggest the ethylene generated from reaction (5.2) is not significant. Ethane could be formed through the ethylene decomposition and recombination reaction.

$$3C_2H_4 \rightarrow 2C+C_2H_6 \qquad (5.7)$$

It should be noted from Figure 5.4 that ethylene, carbon dioxide, and ethane follow a similar trend while ethane production slower. This suggests that ethane formation has some dependence on the DEC decomposition. Besides ethylene and carbon dioxide, rest of the non-condensable products is speculated to be generated relating to ethanol decomposition (reactions (5.2) to (5.7)). Table 5.1 lists the condensable liquid products that are refluxed and dissolved in the liquid pool for the tube temperature maintaining at 1198 K for four hours. The liquid is sampled at the end of the experiment to exclude the volume change that may alter the liquid concentration. It is evident that EtOH is the main condensable product during the DEC experiment. Water, acetaldehyde, and formaldehyde are also detected but at much lower fractions.

According to reaction (5.1), only ethylene, carbon dioxide, and EtOH should be produced by DEC decomposition. The other products in Figure 5.4 (noncondensable and condensable) must, then, from EtOH decomposition. The

Table 5.1: Mole fraction of products detected through GC/MS analysis in the liquid pool during the diethyl carbonate decomposition over a four-hour time interval. The temperature is maintained at 1198 K. The volume change due to reaction is 406 mL (liquid level drops 23 mm).

Chemical	Formula	T_b [K]	Mole Fraction
Diethyl carbonate	*$(CH_3CH_2O)_2CO$*	*400*	*0.8437*
Ethanol	*C_2H_5OH*	*351*	*0.1432*
Water	H_2O	373	0.0051
Acetaldehyde	CH_3CHO	293	0.0078
Formaldehyde	CH_2O	254	0.0002

The significance of the italic characters is that these two chemicals are the main constituents of the bulk liquid.

thermal decomposition of ethanol is conducted to better understand how these species are formed.

5.2.3 Boiling Curve of Ethanol

The procedure used to construct the boiling curve (i.e., the immersion method) for DEC is replicated to establish the boiling curve for ethanol. Figure 5.5 shows the EtOH boiling curve for four separate runs of experiments.

Using properties in Table 1.1, the estimation CHF of EtOH is 448 kW/m^2 (Eqs. (9.12), (9.15) and (9.18), $q''_{CHF} = \left(0.89 + 2.27e^{-3.44\sqrt{R^*}}\right) \cdot \left(0.131\rho_v^{1/2} h_{fg} \sqrt[4]{g(\rho_l - \rho_v)\sigma}\right)$, in Lienhard and Lienhard 2012) while the measured CHF is 372 kW/m^2 at 375 K, which is close to the prediction. At the CHF, any power increment will lead to a large temperature jump (760 K for EtOH) as transitioning from nucleate boiling (375 K) to film boiling (at 1135 K).

In the film boiling regime, the measured unstable point is 129 kW/m^2 at 627 K while the predicted critical heat flux is 9 kW/m^2 from Lienhard and Dhir (1980), Similar to previous discussions, it may suggest that the actual Leidenfrost point is lower than measured. The practical temperature range for film boiling serving as a reactor is between 627 K and 1460 K.

5.2.4 Product Yield Rate of ethanol

Figure 5.6 shows the total flow rate of non-condensable products from ethanol decomposition. Similar to Figure 5.3, two flow meters are used to measure the product yield rate, and their detection limits are labeled as horizontal lines in the

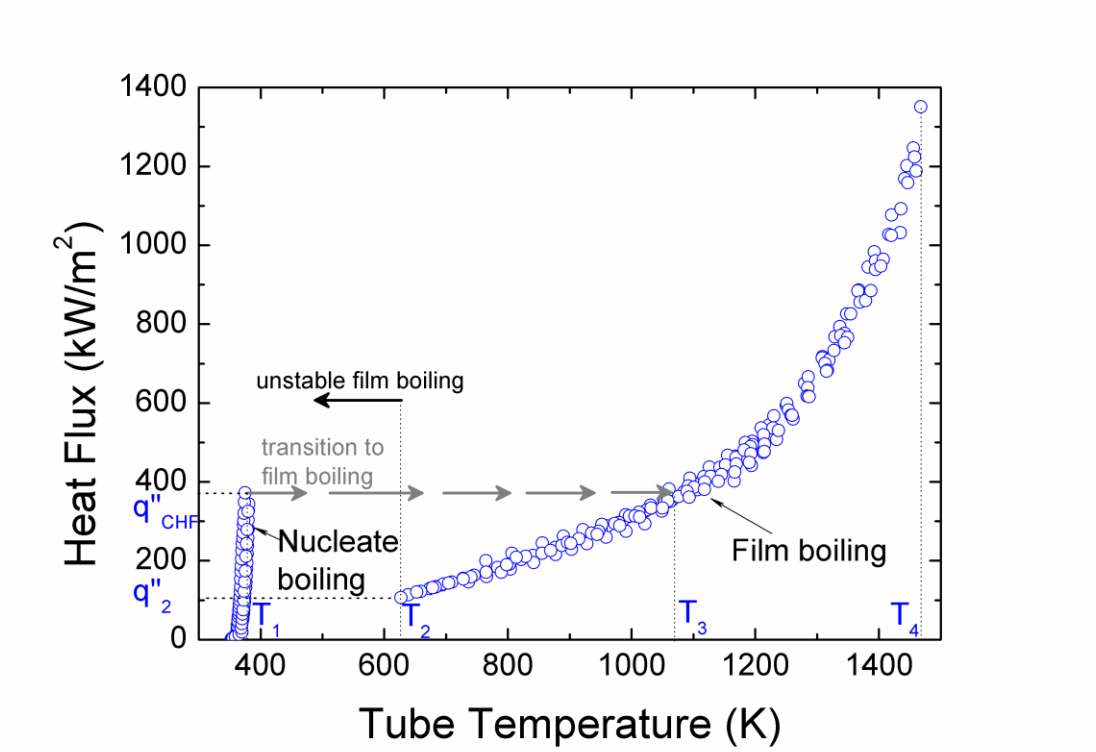

Figure 5.5: Boiling curve of EtOH. Four runs of experiments are included in this plot. The immersion method is used to attain film boiling from T_1 to T_3 and the process can be seen from Figure 2.5.

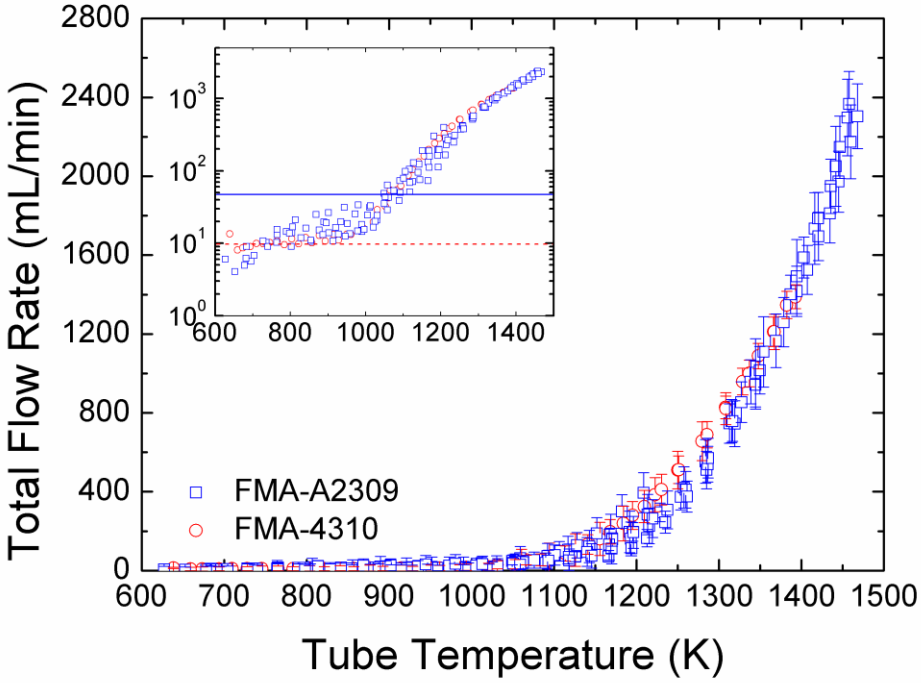

Figure 5.6: Total exhaust gas total flow rate of EtOH decomposition. Two flow meters with different resolutions are used in the measurement, and the detection limits are shown as horizontal lines in the inserted plot.

inserted logarithm plot. Flow rate measured under the detection limits are not reliable since it might include uncertainties. As can be seen, appreciable decomposition rates do not occur until the tube temperature is above 1100 K. As the tube temperature is below 1100 K, the temperature is not high enough to break the bonds of constituents of ethanol. The product yield rate increases with increasing temperature as the temperature is above 1100 K.

Figure 5.7 shows the individual species molar flow rate of the non-condensable products; six species are detected: hydrogen, ethylene, carbon monoxide, methane, carbon dioxide, and ethane. Methane, carbon monoxide, ethylene and hydrogen are believed to have largely formed through reactions (5.2) through (5.5). Given the fact that water is a product of reaction (5.5), it will be condensed and preferential vaporized to the vapor film, which facilitates reaction (5.6) to occur in the vapor film as the source of carbon dioxide formation. In addition, ethane is observed and believed to form from reaction (5.7). It should be noted that ethane and carbon dioxide are at the lowest concentration in the product gas stream in Figure 5.7.

The condensable products are sampled and analyzed by the GC/MS. Table 5.2 lists the detected products as film boiling is maintained at 1206 K for four hours. Besides ethanol, water, acetaldehyde, formaldehyde, ethyl acetate, and acetaldehyde diethyl acetal are detected as condensable products. Acetaldehyde and water are the main condensable products, which are generated from reactions (5.2) and (5.3). Formaldehyde is produced from reaction (5.5); however, since the concentration of formaldehyde is small, the methane formed from reaction (5.5) only has limited contribution to the species molar flow rate in Figure 5.7. Ethyl acetate and acetaldehyde diethyl acetal can be formed from the following reactions.

$$2CH_3CHO \rightarrow \mathbf{CH_3COOC_2H_5} \quad (5.8)$$

$$CH_3CHO + 2C_2H_5OH \leftarrow \mathbf{H_2O} + \mathbf{CH_3CH(OC_2H_5)_2} \quad (5.9)$$

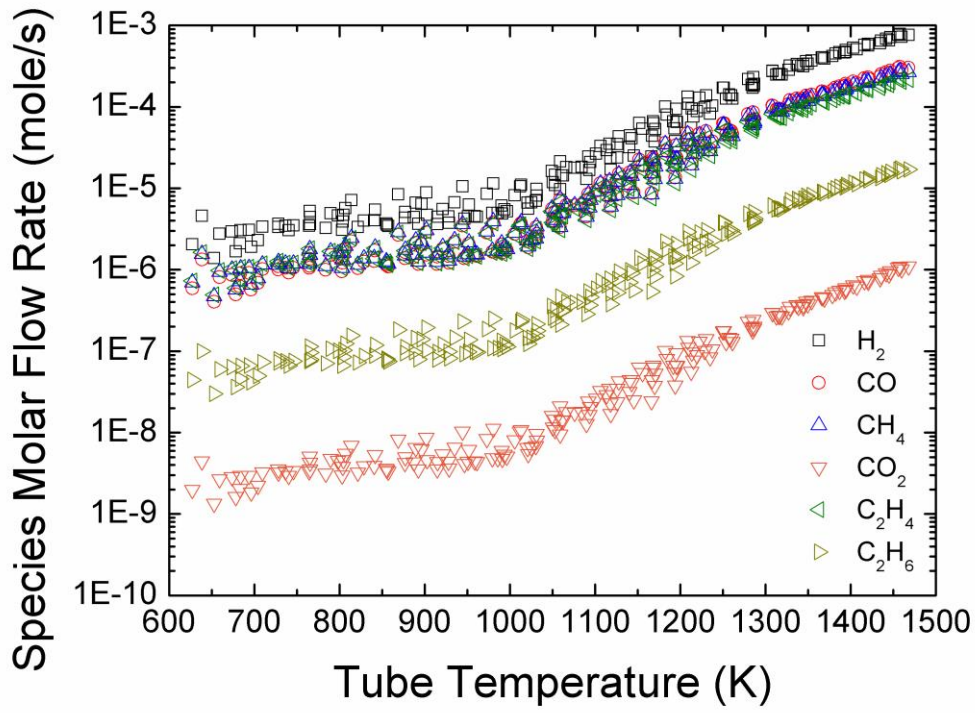

Figure 5.7: Species molar flow rate of non-condensable products from EtOH decomposition. Carbon dioxide and ethane are found at low concentrations in the product gas stream, which suggests that the reactions involving these two species are considered as minor reactions.

Table 5.2: Mole fraction of products detected through GC/MS analysis in the liquid pool during the ethanol decomposition after four hours. The temperature is maintained at 1206 K. The volume change due to reaction is 35 mL (liquid level drops 2 mm).

Chemical	Formula	T_b [K]	Mole Fraction
Ethanol	*C_2H_5OH*	*351*	*0.9498*
Acetaldehyde	*CH_3CHO*	*373*	*0.0375*
Water	H_2O	293	0.0099
Formaldehyde	CH_2O	254	0.0013
Ethyl Acetate	$CH_3COOC_2H_5$	350	0.0005
Acetaldehyde Diethyl Acetal	$CH_3CH(OC_2H_5)_2$	375.7	0.0011

The significance of the italic characters is that these two chemicals are the main constituents of the bulk liquid.

The concentration of formaldehyde, ethyl acetate and acetaldehyde diethyl acetal are low as shown in Table 5.2, which suggests that they are not the primary conversion routes in the ethanol decomposition. Though the equilibrium constant for Eq. (5.9) is less than one, it is believed to be the reaction that generates acetaldehyde diethyl acetal, yet the reactions rate is low. Overall, what can be inferred is that the primary reaction routes for ethanol decomposition are reactions (5.2), (5.3), and (5.4) as these reactions yield the higher product concentrations.

While comparing the ethanol decomposition results (e.g. Figure 5.7) with the ethanol decomposition along with DEC decomposition (e.g. Figure 5.4), it is observed that the relative concentration of hydrogen, carbon monoxide, and methane are different. In Figure 5.7, hydrogen has the highest concentration while carbon monoxide and methane follows almost a one to one ratio. However, in Figure 5.4, the concentration of these three gases is: methane > carbon monoxide > hydrogen. It suggests that methane formation (5.10) and water-gas shift reaction (5.11) are occurring within the vapor film for the DEC decomposition reaction.

$$3H_2 + CO \rightleftarrows CH_4 + \mathbf{H_2O} \qquad (5.10)$$

$$H_2 + CO_2 \rightleftarrows CO + \mathbf{H_2O} \qquad (5.11)$$

Above two forward reactions consume hydrogen to generate methane and carbon monoxide, which leads to a higher exhaust gas flow rate of methane and carbon monoxide compared with hydrogen. However, these two reactions are not prominent since the water concentration in ethanol decomposition result (e.g. Table 5.2) is higher than that in the DEC decomposition result (Table 5.1). The higher concentration of water would force reactions (5.10) and (5.11) to remain backward direction, which generates more hydrogen, as can be seem in Figure 5.7. Reactions (5.10) and (5.11) would therefore serve as complimentary reactions for the ethanol decomposition and adjust the molar flow rate of the primary reactions products. All the remaining

reactions are secondary reactions, as their products form at a much slower rate by or exist in a much smaller concentration by comparison.

A final note is that if the DEC decomposition proceeds to an infinite time with the current apparatus, the ultimate condensable product will be water since the condensable products will preferentially vaporize to the vapor film and thermally decompose to its own products. However, the temperature for thermal decomposition of water (about 2700 K, Srinivasan and Michael 2006) is much higher than the maximum temperature that the current apparatus can achieve.

5.3 Conclusion

The conclusions of this study are the following:

1) The thermal decomposition of DEC by film boiling is consistent with a unimolecular process (Eq. (5.1)).
2) Refluxed EtOH preferentially vaporizes and itself decomposes into methane, carbon monoxide, and hydrogen along with DEC decomposition.
3) Thermal decomposition of EtOH is performed to confirm the additional products formed during DEC decomposition process are produced from EtOH decomposition.
4) Methane formation and water-gas shift reactions serve as complimentary reactions in the EtOH decomposition.
5) As for both DEC and EtOH, the estimated CHF is close to the prediction while the predicted Leidenfrost point is much lower than unstable film boiling starts.

CHAPTER 6

CARBON FORMATION

Thermal decomposition of organic chemicals usually produces carbon deposition on the wall of the chamber. Previous studies (Bruneton et al 1997; Rovillain 2001; Okuno et al 2002; Zhang et al 2002a 2002b; Delhaes 2002; Delhaes et al 2005) have applied film boiling as a means to grow carbon layers on the heated surface. Carbon formed during film boiling is the basis of an industrial process for synthesizing carbon composites from porous substrate preforms (e.g., cyclohexane (C_6H_{12}) is a common feedstock for this purpose (Bruneton et al 1997; Rovillain et al 2001). Formation of a thin carbon layer was noted in a previous study of aqueous ethylene glycol mixtures (Evangelista et al 2012) ethanol (Stralen and Cole (1979)), and for all chemicals investigated, a carbon layer is observed on the heater tube after an experiment.

Some of the product gases detected in the present experiments are involved with reactions that can produce carbonaceous materials, which are listed as follows (Valliyappan 2004):

$$CH_4 \rightarrow 2H_2 + C_{(s)} \tag{6.1}$$

$$2CO \rightleftarrows CO_2 + C_{(s)} \tag{6.2}$$

$$C_2H_4 \rightarrow 2H_2 + 2C_{(s)} \tag{6.3}$$

$$C_2H_6 \rightarrow 3H_2 + 2C_{(s)} \tag{6.4}$$

Which one, if any, of these reactions could be responsible for carbon formation is a complicated question. From the measured species molar flow rates (Figure 3.7, Figure 4.6, Figure 5.4, and Figure 5.7), the lowest species concentration in the product gas stream suggests that could be the source for the carbon formation (reactions (6.1) to (6.4)).

Chemisorption of radicals at active sites on the solid surface can promote nucleation of solid aggregates that grow to form pyrolytic carbon layers. If such sites are not present, or only in a low concentration, the radicals will react with stable species in the gas phase and either produce soot precursors or participate in steps that lead to such additional species, though we have no evidence of homogeneous production of soot for the conditions of the present investigation. Once formed on a metal surface, a thin carbon layer could insulate the underlying metal from the gases flowing around it so that the potential for surface reactions catalyzed by the underlying metal may be diminished.

Figure 6.1 is a picture showing an Inconel heater tube before (upper tube) and after (lower tube) a four hour DEC experiment. As observed, a black layer is formed during the experiment, and the weight of the tube increases from 1.108 g to 1.115 g. To verify if this black layer is composed of carbon only, an energy-dispersive X-ray spectroscopy (EDX) analysis is performed.

EDX is an analytical technique used for the elemental analysis or chemical characterization of a sample. A high-energy electron beam is used to stimulate the emission of characteristic X-rays from a specimen. By analyzing the X-ray spectrum, the chemical species of a specimen can be determined. Figure 6.2 shows the EDX analysis of the Inconel tube (a) and black layer (b). In Figure 6.2 (a), it is found that the bare tube contains nickel, chromium, and iron as the major constituents, which is in good agreements with the Inconel 600 alloy composition (Special Metals Corp 2008). Figure 6.2 (b) shows that the black layer contains carbon only. The surface morphology taken by the scanning electron microscope (SEM) is shown in the inserted pictures of Figure 6.2 (a) and (b). As can be seen, the heater surface changes from a smooth to a much more roughened configuration. During the experiment, a carbon layer gradually covers the heater tube; however, there shows no significant

product yield rates change, which suggests that the chemical conversion occurring in the vapor film is homogeneous reaction.

Figure 6.1: A picture showing the Inconel 600 tube before (upper tube) and after (lower) doing an experiment. The black carbon layer is formed during the film boiling experiment. The tube diameter is 2.38 mm and the length is 80 mm.

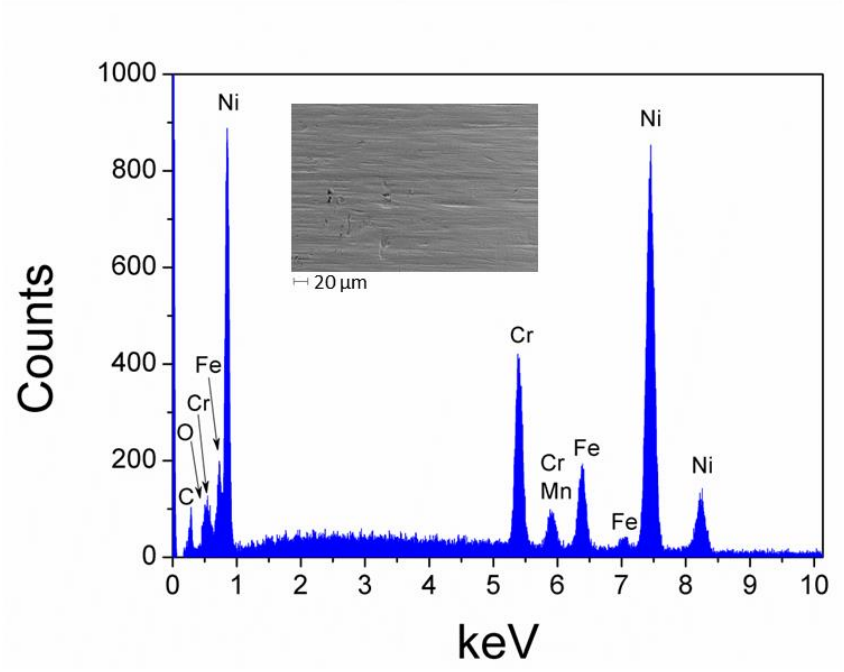

(a)

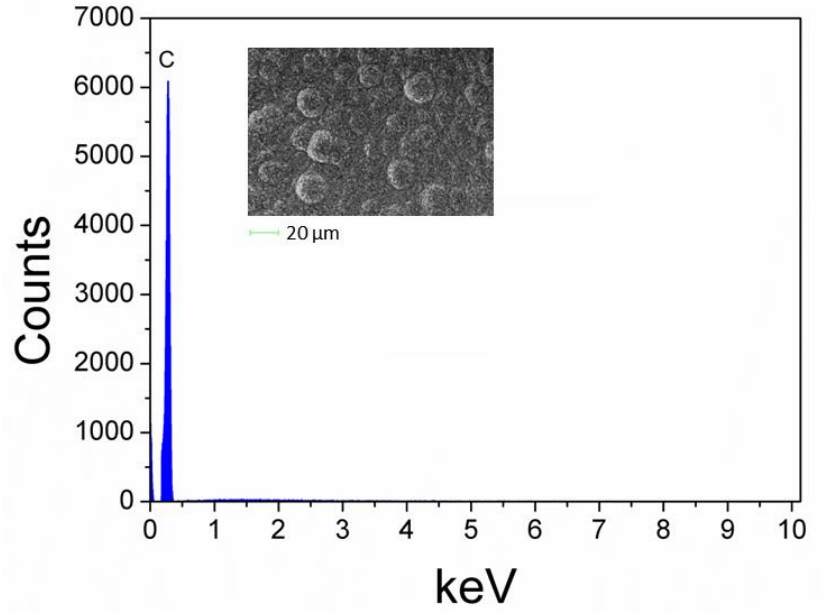

(b)

Figure 6.2: EDX analysis of (a) the bare tube and (b) the deposited black layer from diethyl carbonate decomposition with the SEM images inserted. The deposited are found to contain only carbon.

CHAPTER 7

CONCLUDING REMARKS

We have demonstrated utilizing film boiling as a chemical reactor to promote thermal decomposition (pyrolysis) of aqueous glycerine mixtures, ethyl acetate, diethyl carbonate, and ethanol. The remarkable consistency of the results presented suggests value for film boiling to not only promote chemical change of an organic liquid, but also to use the results to understand the decomposition kinetics involved. The concluding remarks are the following:

1) The boiling curves of aqueous glycerine mixtures, ethyl acetate, diethyl carbonate, and ethanol have been systematically studied. The trends of boiling curve in the film boiling regime are similar, yet the product yields strongly depend on the reactant.
2) The critical heat flux estimations are in good agreements with the measurements for ethyl acetate, diethyl carbonate, and ethanol while the extrapolation of aqueous glycerine results to pure glycerine shows a significant difference. It may suggest that the model would need to include the viscosity since glyceriene is more viscous than rest of the liquids examined.
3) The minimum heat flux (Leidenfrost point) prediction is at least one order less than the measured unstable heat flux. It may suggest that our measurement on the unstable heat flux is not the lower end of the boiling curve in the film boiling regime.
4) The aqueous glycerine results show that film boiling can convert glycerine (the waste generated during biodiesel production) into syngas (an alternative fuel) at high temperatures (> 1200 K) in a particular simple process. The effect of water

dilution reflects mainly on the product yield rate directly but not on the operational domain of the reactor.

5) Ethyl acetate and diethyl carbonate serve as the model reactant owing to its unimolecular decomposition route. A simple and known rate constant reaction can be written to present the chemical conversion in the film boiling reactor. The experimental results agree well with the expected unimolecular conversion and can be used to test the model efficacy in the future.
6) Ethanol is a condensable product from diethyl carbonate decomposition. It refluxes back to the liquid pool, preferential vaporizes at the vapor/liquid interface, and thermally decomposes along with diethyl carbonate vapor. The ethanol result confirms the additional products detected in diethyl carbonate experiment come from ethanol decomposition.
7) The refluxing effect in the current experimental apparatus suggests that if the experiment can run to an infinite time, the ultimate product of diethyl carbonate decomposition would be water.
8) A carbonaceous layer is formed on the heater tube for all molecules examined. The EDX analysis confirms the composition of carbonaceous layer contains carbon only. Results show no significant product yield rates change during the experiment, which suggests that the chemical conversion occurring in the vapor film is homogeneous reaction.
9) The tube temperature cannot sufficiently describe the reaction temperature since there is a large temperature drop across the vapor film. Therefore, a suitable reaction temperature is proposed.

APPENDIX A

REACTION TEMPERATURE

Two extreme temperatures within the vapor film are the saturation temperature of the liquid (T_{sat}) and the temperature of the tube wall (T_w). An issue with the film boiling reactor is that there is a temperature gradient within the vapor film so that the reaction temperature (T_{rxn}) is not specified. The wall temperature is a poor representation of the thermal state of the reaction, and thus we need to define a reaction temperature.

To determine the reaction temperature within the vapor film, the working assumption is that temperature distribution along the gradient is linear (Avedisian et al 2008) between two extremes. Figure A.1 shows the schematic of the linear temperature distribution within the vapor film. The temperature at the tube wall (y=0) is the highest, and it decreases linearly across the vapor film. The lowest temperature is the saturations temperature (T_{sat}), which is at the vapor/liquid interface ($y = \delta$).

The linear temperature profile facilitates averaging the temperature from two ends (wall temperature and saturation temperature) directly. However, it might be too conservative in estimation (Avedisian et al 2008). The reaction should occur at the high temperature zone close to the wall in the vapor film. Here we define a threshold temperature ($T_{threshold}$, see Figure A.1) in which the temperature between the threshold and wall are considered to promote significant reaction rates. The reaction temperature can be defined as the average between the wall and threshold temperatures from the linear assumption as shown below.

$$T_{rxn} = \frac{T_{wall} + T_{threshold}}{2} \qquad \text{(A.1)}$$

The threshold temperature for glycerine, ethyl acetate, and diethyl carbonate decomposition reactions (Van Bennekom et al 2011; Tsang et al 1978; Herzler et al 1997; Park et al 2002) can be found through the following formula,

$$\varepsilon = \frac{K_{threshold}}{K_{wall}} = \frac{A\exp(-E_a / \bar{R}T_{threshold})}{A\exp(-E_a / \bar{R}T_{wall})} \tag{A.2}$$

while it is written in the following form for ethanol decomposition (Sivaramakrishnan et al 2010; Park et al 2002),

$$\varepsilon = \frac{K_{threshold}}{K_{wall}} = \frac{AT_{threshold}^{n}\exp(-E_a / \bar{R}T_{threshold})}{AT_{wall}^{n}\exp(-E_a / \bar{R}T_{wall})} \tag{A.3}$$

where ε is defined as the threshold value for the significant reactions to occur. Two threshold values (ε = 0.10 and 0.01) are examined.

Figure A.2 illustrates a schematic diagram of the threshold value as wall temperature is 1500 K. As shown, the treshold temperature at ε = 0.01 is lower than that of ε = 0.10 since lower threshold value is achieved by the lower temperature (Eq. A.2).

From the linear temperature distribution, the ratio of the threshold thickness ($\delta_{threshold}$) over the vapor film thickness (δ) can be determined as follows.

$$\frac{\delta_{threshold}}{\delta} = \frac{T_{wall} - T_{threshold}}{T_{wall} - T_{sat}} \tag{A.4}$$

It should be noted that the reactions are considered to be significant within the threshold thickness.

Figure A.3, Figure A.5, Figure A.7, Figure A.9, and Figure A.11 depict the reaction temperature as a function of wall temperature for reactions (3.1), (4.1), (5.1), (5.2) and (5.3). A reaction temperature is found by averaging the wall temperature and the threshold temperature at the threshold value specified. Figure A.4, Figure A.6, Figure A.8, Figure A.10, and Figure A.12 illustrate the ratio of the threshold layer

thickness with respect to the tube temperature for different reactions (3.1), (4.1), (5.1), (5.2) and (5.3).

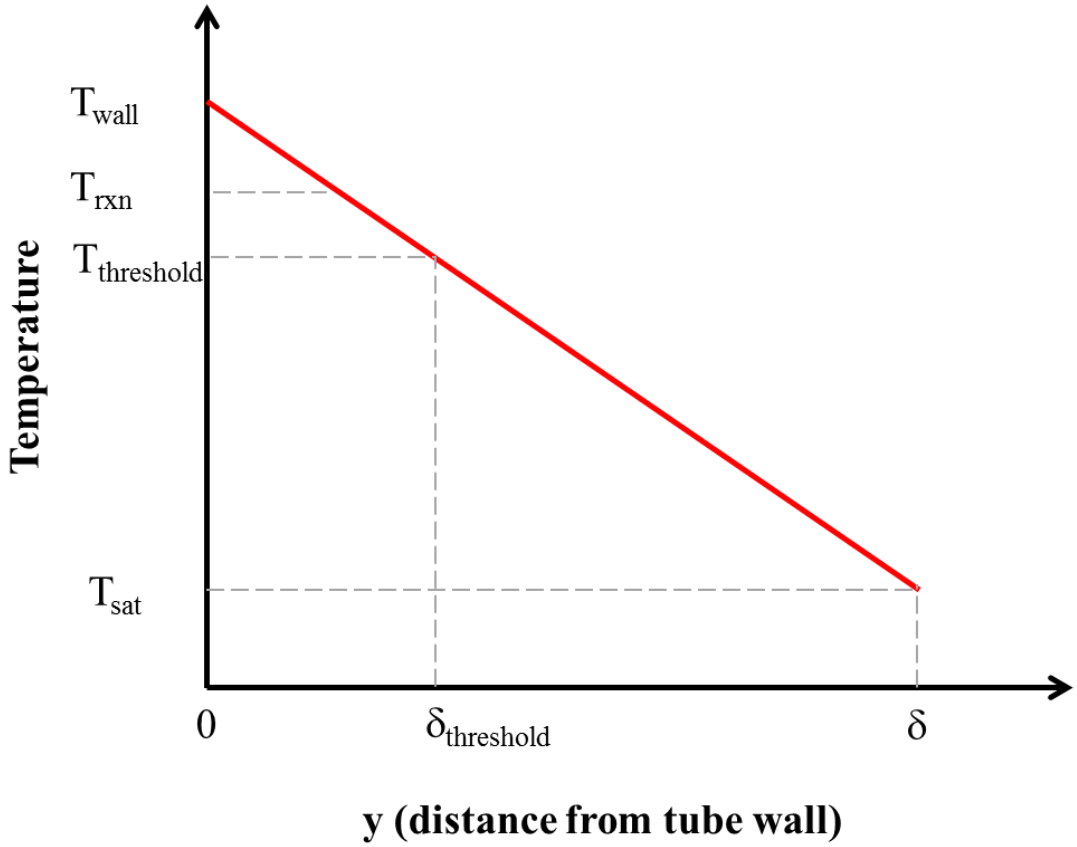

Figure A.1: A schematic diagram illustrating the linear temperature distribution from tube wall to the vapor/liquid interface (Avedisian et al 2008). The reaction temperature is defined as the average between wall the threshold temperature.

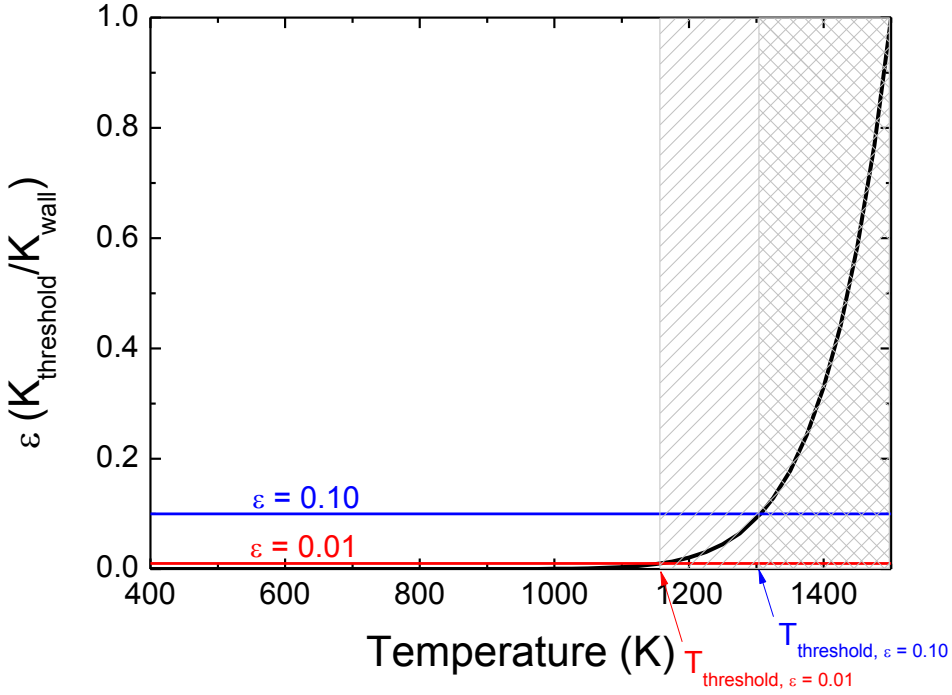

Figure A.2: A schematic diagram showing the two threshold temperature at T_w = 1500 K.

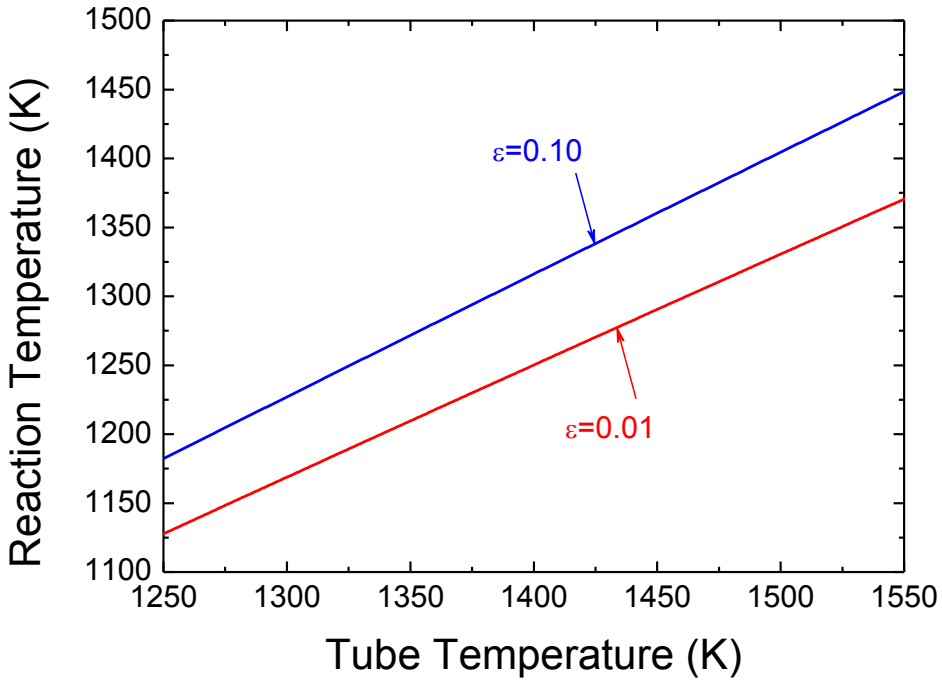

Figure A.3: Reaction temperature vs. tube temperature for glycerine decomposition. The Arrhenius equation, $k = A\exp(-E_a/RT)$, is used for the reaction rate calculation, where E_a = 47.04 [kcal/mole], and R= 1.987×10^{-3} [kcal/K-mole] (Van Bennekom et al 2011).

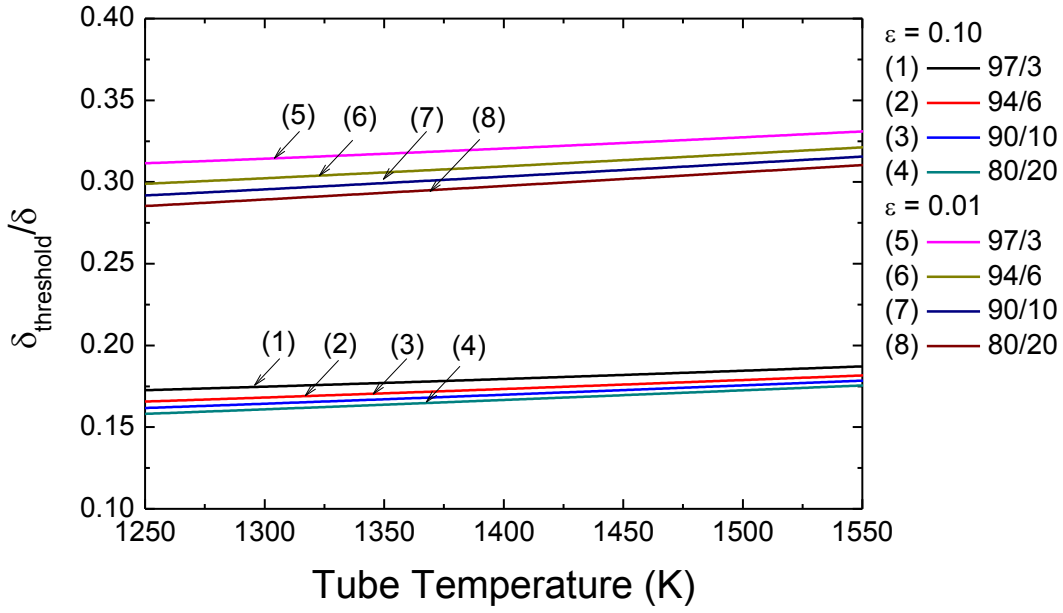

Figure A.4: Ratio of the threshold thickness vs. tube temperature of glycerine decomposition.

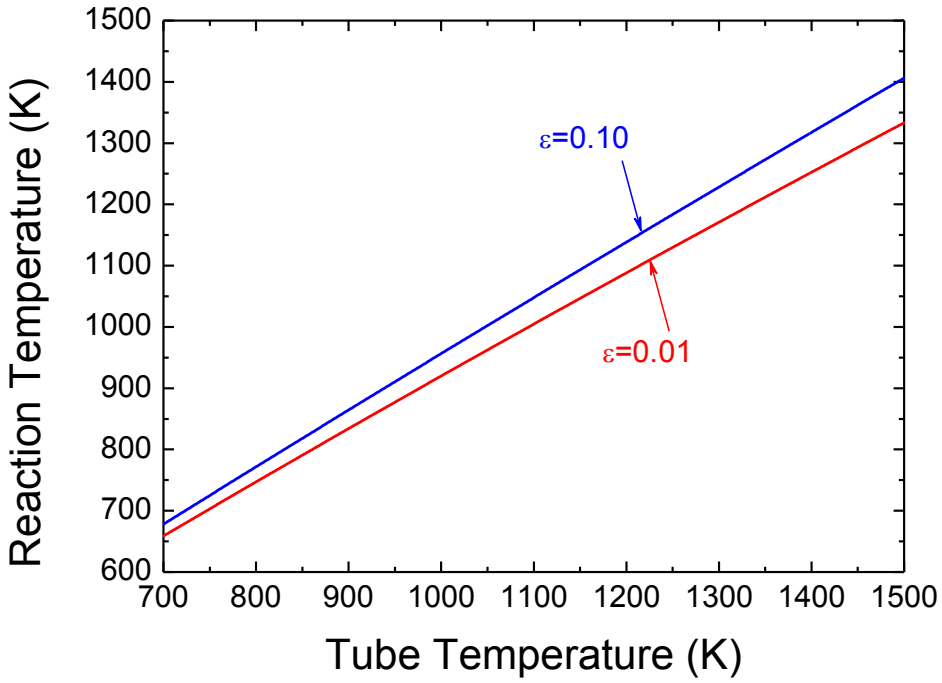

Figure A.5: Reaction temperature vs. tube temperature for ethyl acetate decomposition (Eq. (4.1)). The Arrhenius equation, $k = A\exp(-E_a/RT)$, is used for the reaction rate calculation, where A = $10\times10^{12.59}$ [s^{-1}], E_a = 48.00 [kcal/mole], and R= 1.987×10^{-3} [kcal/K-mole] (Tsang et al 1978).

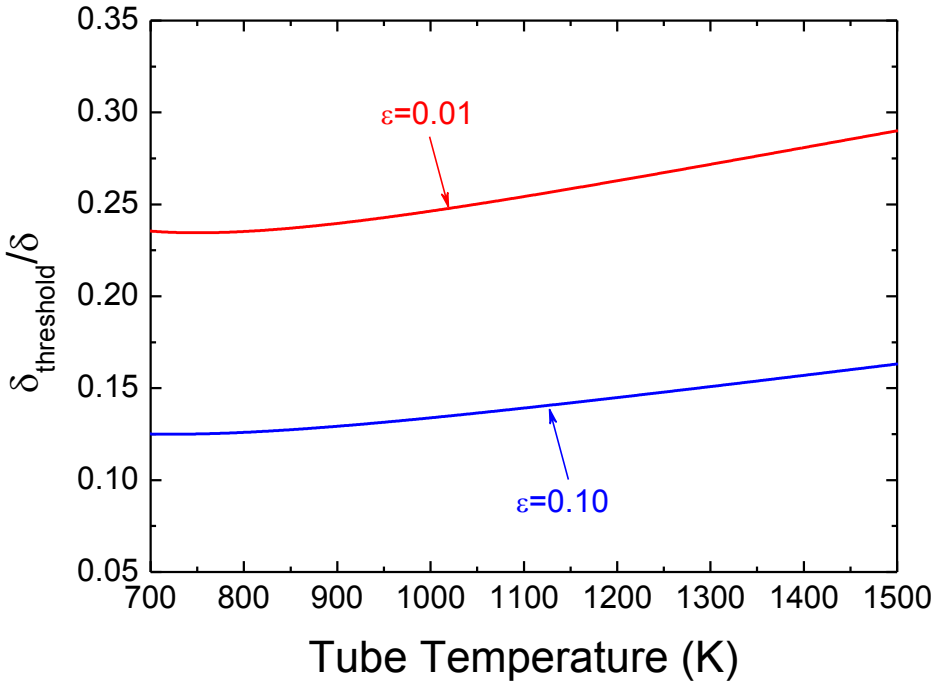

Figure A.6: Ratio of the threshold thickness vs. tube temperature of ethyl acetate decomposition (Eq. (4.1)).

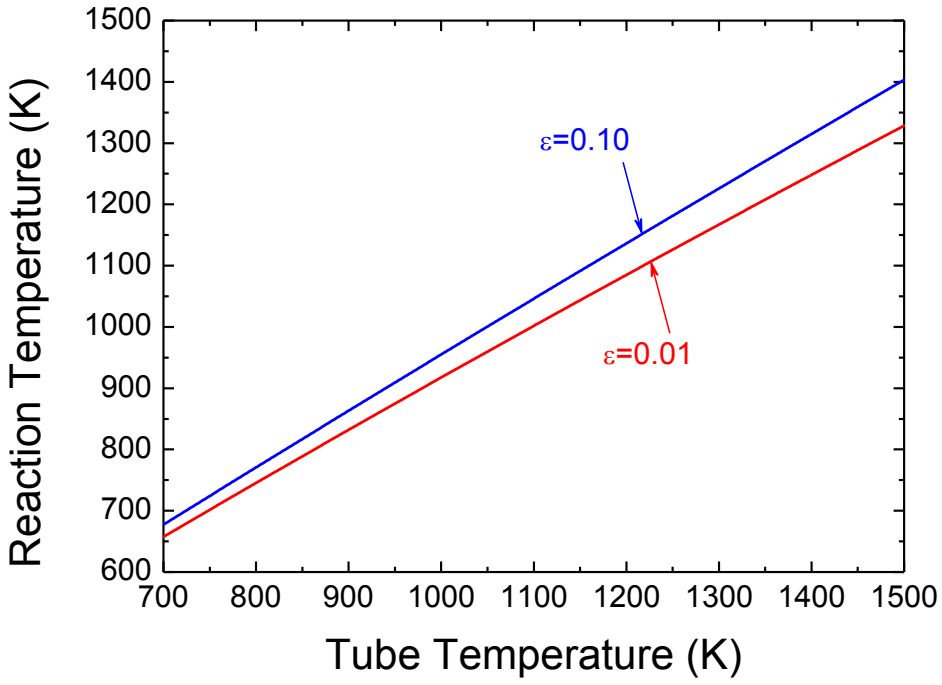

Figure A.7: Reaction temperature vs. tube temperature for diethyl carbonate decomposition (Eq. (5.1)). The Arrhenius equation, $k = A\exp(-E_a/RT)$, is used for the reaction rate calculation, where A = 1.1×10^{13} [s^{-1}], E_a = 46.28 [kcal/mole], and R= 1.987×10^{-3} [kcal/K-mole] (Herzler et al 1997).

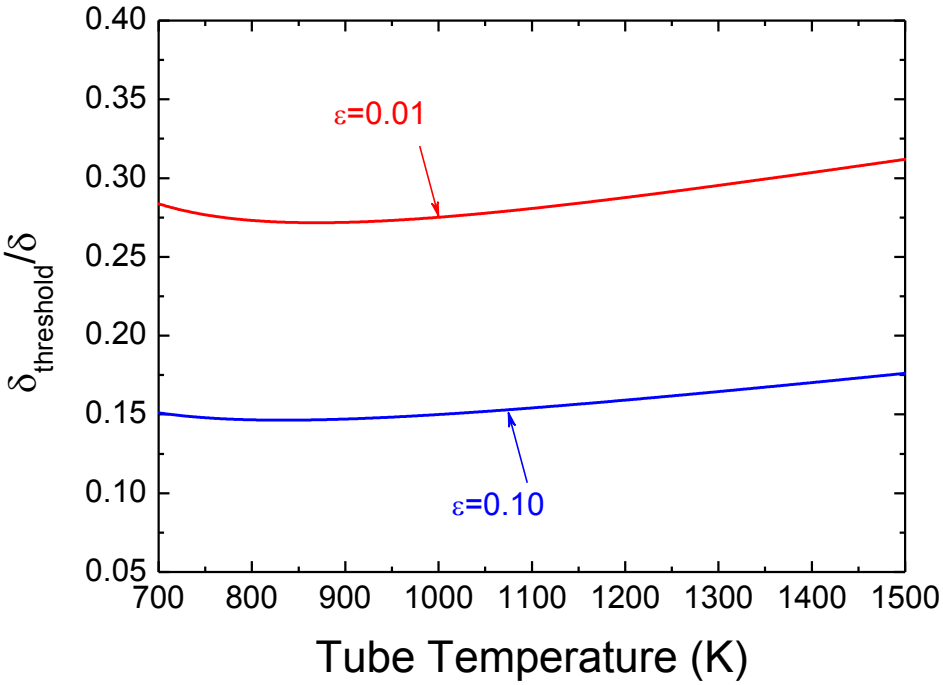

Figure A.8: Ratio of the threshold thickness vs. tube temperature of diethyl carbonate decomposition (Eq. (5.1)).

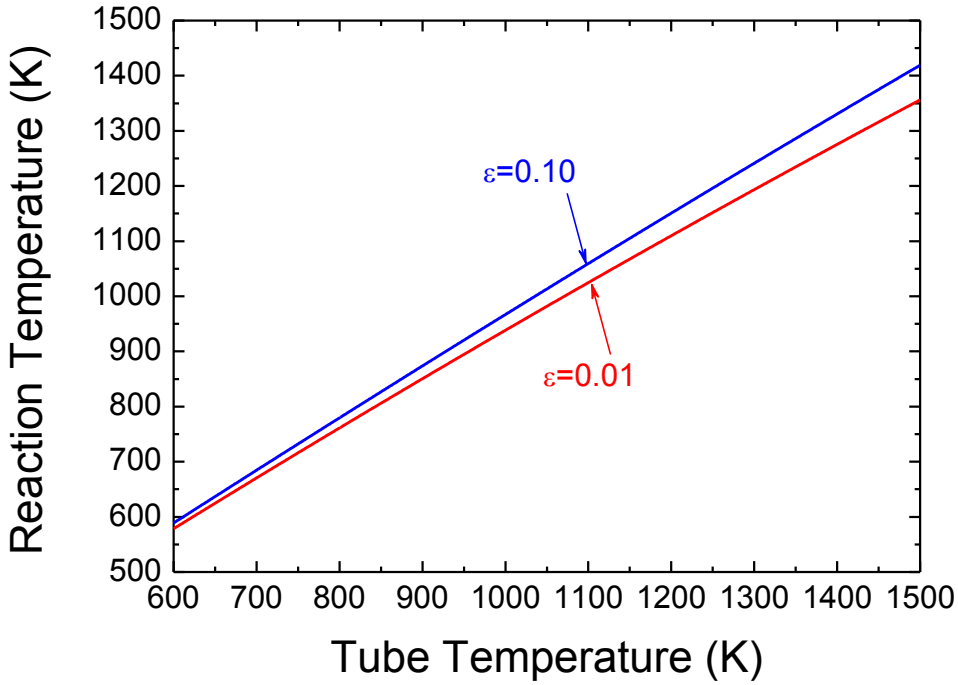

Figure A.9: Reaction temperature vs. tube temperature for ethanol decomposition (Eq. (5.2)). The Arrhenius equation, $k = AT^n \exp(-E_a/RT)$, is used for the reaction rate calculation, where A = 5.23×10^{43} [s^{-1}], E_a = 81.5 [kcal/mole], R= 1.987×10^{-3} [kcal/K-mole], and n is -8.9 (Sivaramakrishnan et al 2010).

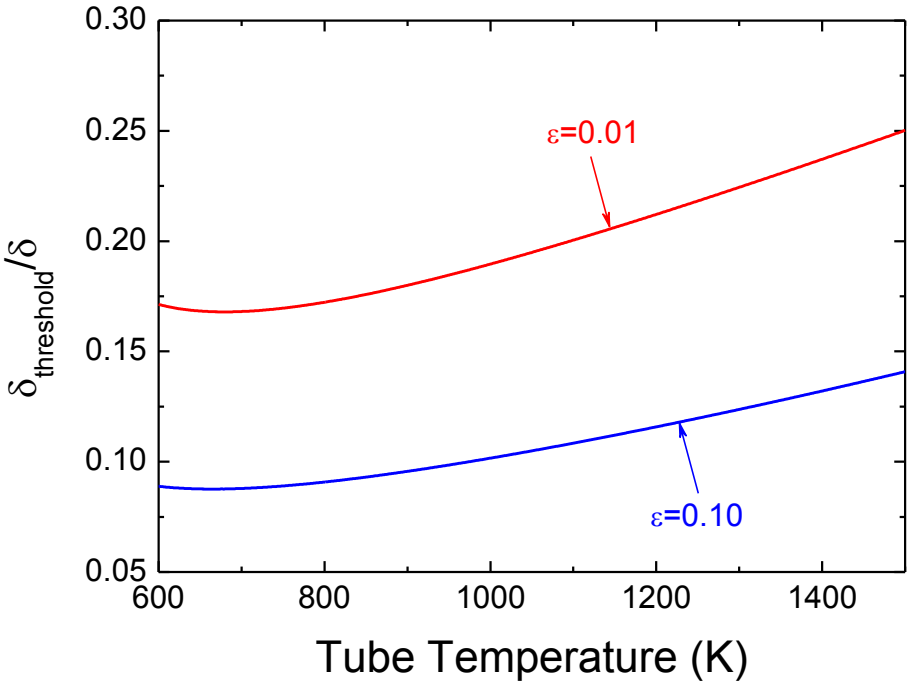

Figure A.10: Ratio of the threshold thickness vs. tube temperature of ethanol decomposition (Eq. (5.2)).

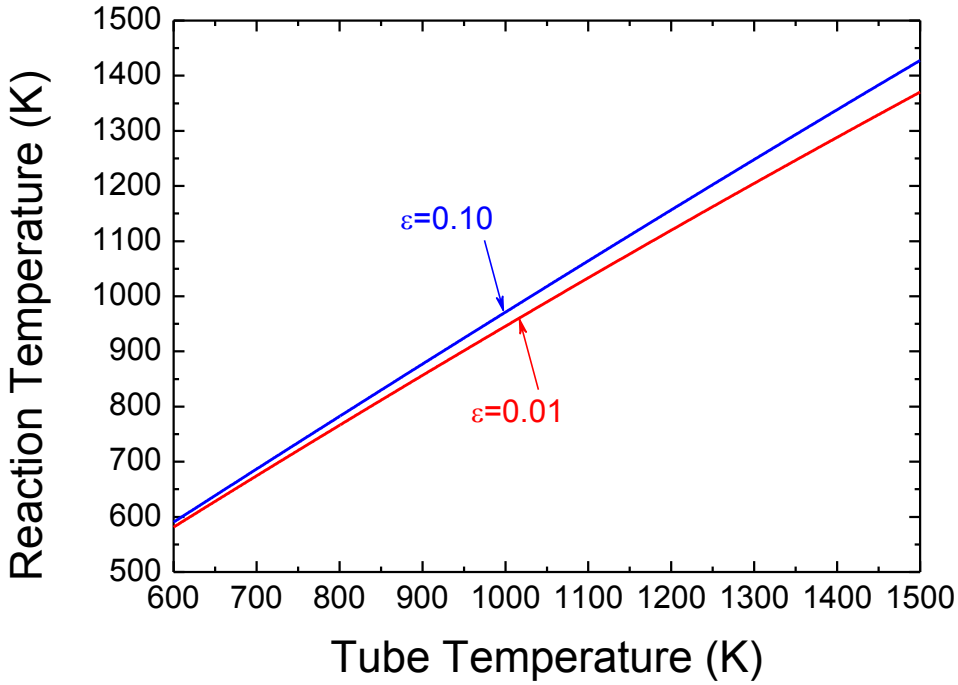

Figure A.11: Reaction temperature vs. tube temperature for ethanol decomposition (Eq. (5.3)). The Arrhenius equation, $k = AT^n \exp(-E_a/RT)$, is used for the reaction rate calculation [24], where A = 1.18×10^{49} [s^{-1}], E_a = 96.1 [kcal/mole], R= 1.987×10^{-3} [kcal/K-mole], and n is -11.3 (Park et al 2002).

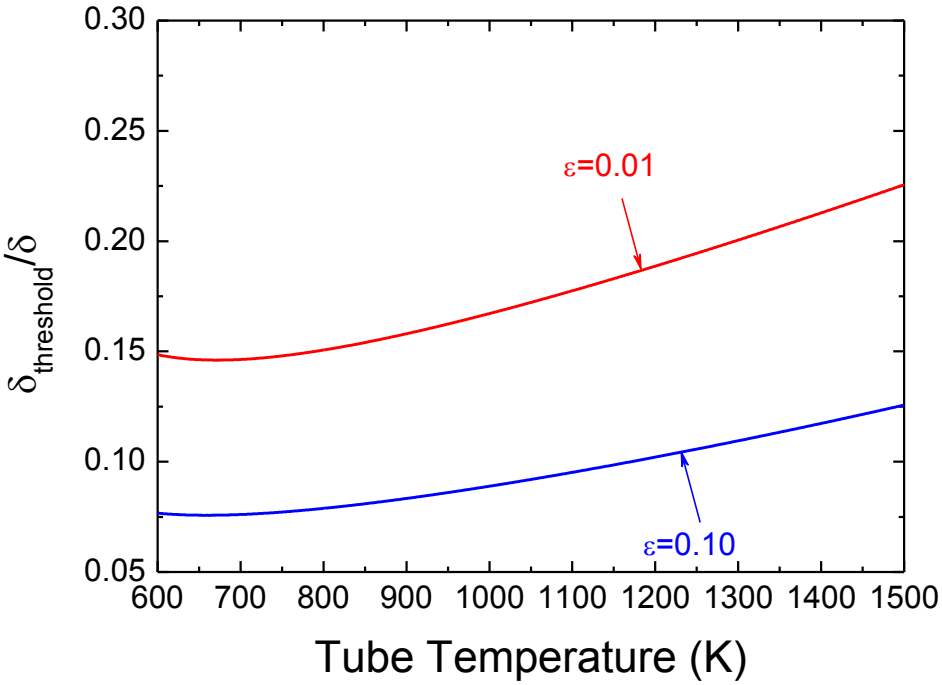

Figure A.12: Ratio of the threshold thickness vs. tube temperature of ethanol decomposition (Eq. (5.3)).

APPENDIX B

EXPERIMENT PREPARATION

This section describes the detailed experiment preparation processes.

B.1 Thermocouple and Heater Tube Assembly

Figure B.1 shows the top plate configuration and all the components. A 127 mm piece of Teflon tubing (Z515337-1PAK, Sigma-Aldrich) is inserted through the top plate (see Figure B.1(a)), and the tube fittings tightened. Two thermocouples (Omega, KMQXL-010G-18) are inserted through the Teflon tubing and placed in the heater tube. The length from the left hand side of the tube is 22.2 mm while it is 25.2 mm from the right hand side, as can be seen in Figure 2.2 (a). It should be noted that the thermocouple cannot be in contact with the heater tube or the copper buses otherwise the fluctuation will occur.

Figure B.2 shows the mounting arrangement of the tube to the clamps. A coat of heat resistant sealant (RTV 736, DOW Corning) is applied at both ends of the heater tube to secure the ceramic tube and thermocouples at desired locations. A coat of sealant (RTV 108, Momentive) is applied at the junction of the thermocouple wire and the yellow connector to strengthen the connection, as it is fragile over the course of experiments.

B.1.1 Clamps Assembly

Figure B.2 shows the clamp assembly. Note that the clamps have an “A” or “B” stamped on one side, and ensure the top and bottom clamps have the same character, facing in the same direction. Tighten the bottom clamps into the copper

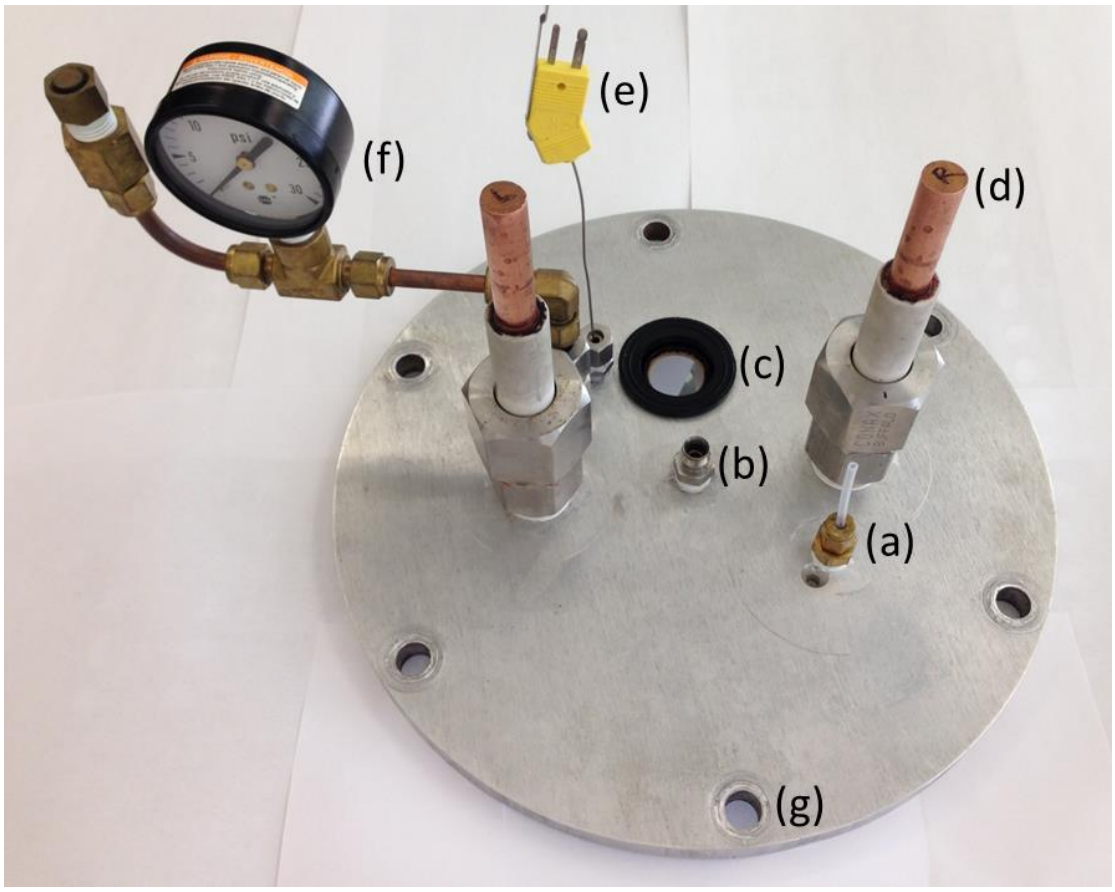

Figure B.1: Top plate configuration: (a) Teflon tubing for thermocouple insertion; (b) connection for the nitrogen gas inflow; (c) product gas outflow (to the condenser #1); (d) electrode copper bus; (e) thermocouple for measuring the bulk liquid temperature; (f) pressure gauge; (g) holes for the bolts to tighten the top plate and the glass chamber.

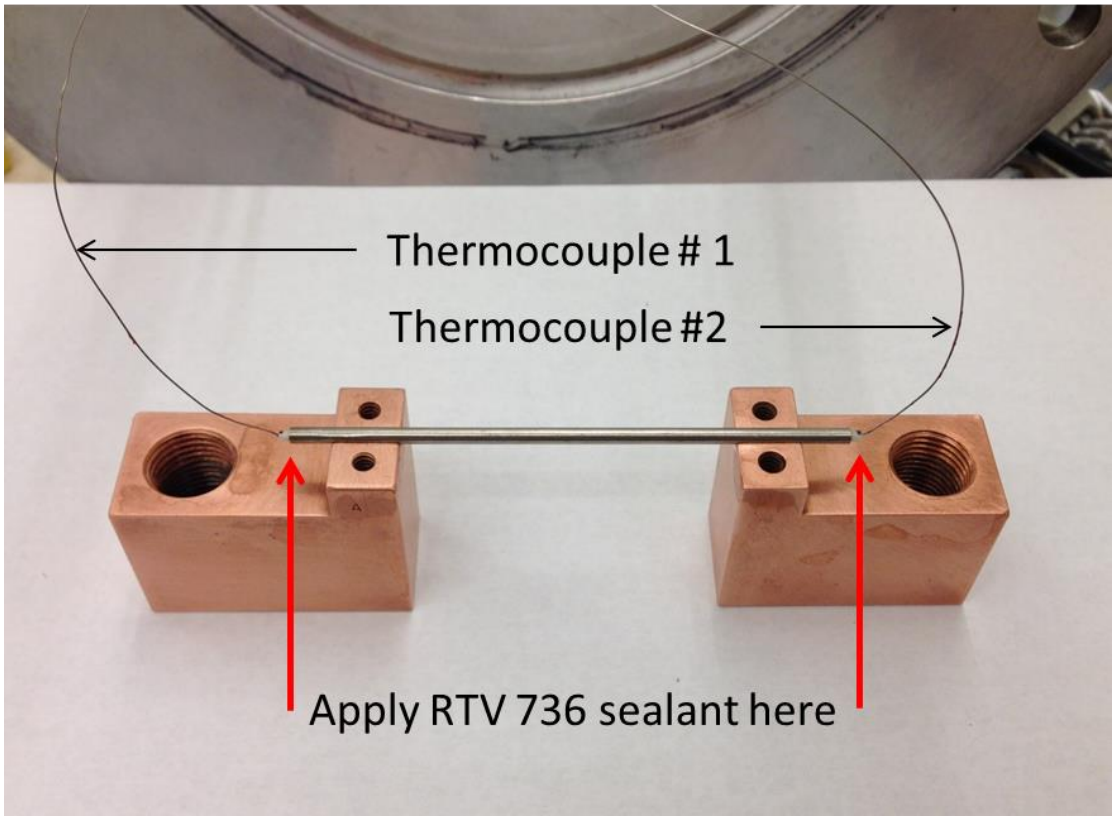

Figure B.2: Assembly of thermocouples into the heater tube. Note that the ceramic tube is longer than the Inconel tube to prevent thermocouple reading fluctuation.

buses, and then loosen the connection between copper buses and the top plate to facilitate the adjustment of the position. Cautiously raise and place the heater into the machined grooves of the bottom clamps. Ensure the tube is at the center of the grooves and two clamps are at the same level. Make any adjustment as needed. Then, tighten the connection of copper buses. Fasten the clamp A by top clamps and the hex screws to hand-tight. Perform an identical process to clamp B. Next, use an allen wrench to fasten the hex screws in a diagonal order, and ensure even pressure is applied to achieve optimum thermal and electrical contact between the heater tube and clamps. Be extremely cautious that the tube may bend and the ceramic tube inserted will crack if you fastening the hex screws too tight. Apply the finger-tight torque with an allen wrench. Adjust the thermocouples so that they are not in contact with electrode buses.

Apply a coat of heat resistant sealant (RTV 736, DOW Corning) on both ends of the heater/clamps assembly to prevent liquid penetrating inside the heater tube. Also, apply a coat of sealant (RTV 108, Momentive) to the top and bottom of the Teflon tube to prevent escape of product gases. Figure B.3 shows the heater and clamp assembly attached to the top plate as above steps are done.

B.1.2 Chamber Assembly

Before mounting the top plate onto the glass chamber, place an O-ring (2-362 VP101-80, Sealing devices) in the groove at the bottom side of the top plate. Mount the top plate on the center of the glass chamber. The markers at the top plate and the glass chamber can help you the alignment. Then, tighten six hex bolts while ensuring the top plate remains at the center of the glass chamber. Use the torque wrench to apply appropriate torque: 4.5 N-m. Be cautious that applying too much torque will

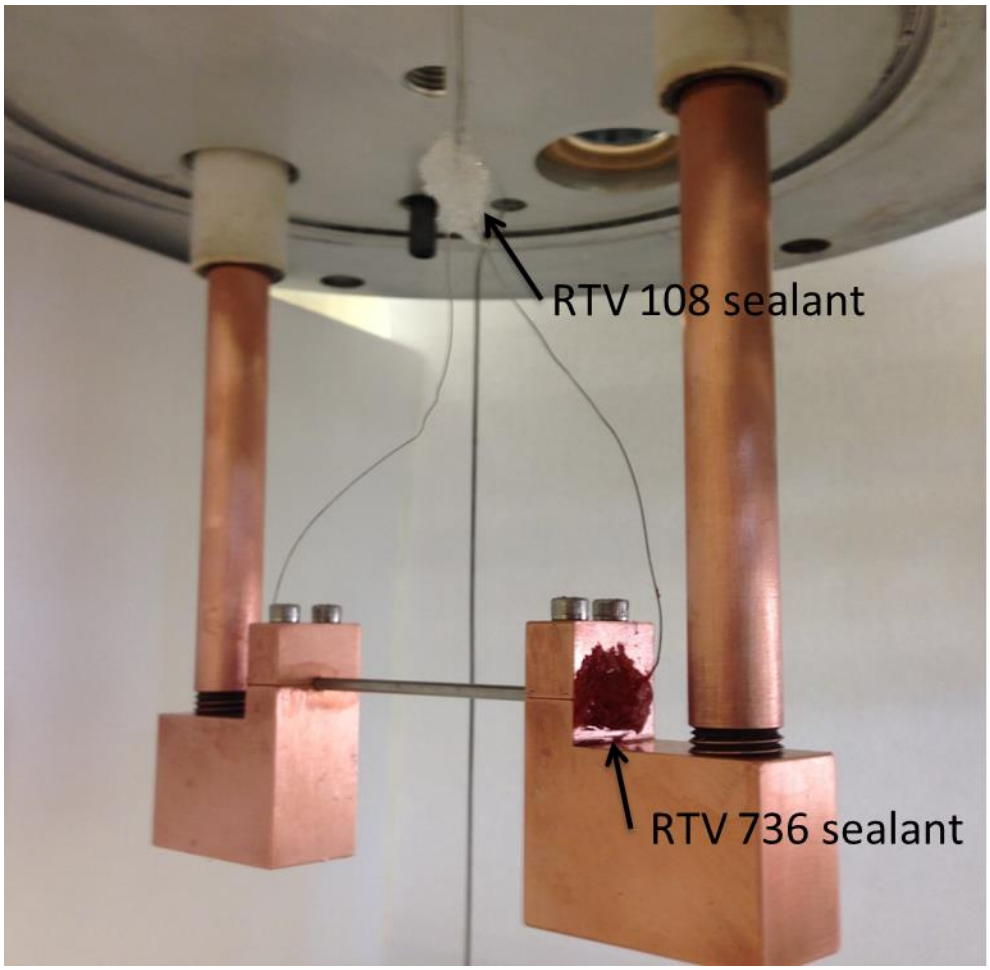

Figure B.3: Heater tube and clamps assembly. The sealants have to be applied to the end of heater tube and Teflon insert.

crack the glass chamber. The value of the torque is specified by the manufacturer of the glass chamber (Goel Scientific Glass Works Ltd.). Then, place the glass chamber with top plate (film boiling reactor module) into the fume hood.

After placing the film boiling reactor module in the fume hood, connect all the necessary connections. See Figure B.4 for details. Align and fasten the chemical inflow/outflow tube (a). Align and fasten electrode terminals to the copper buses (b). Connect the immersion heater power terminals (c). Ensure that a positive (red) and negative (black) are connected to a single immersion heater, and there are four immersion heaters in total. Use an electrical tape to wrap the connection to prevent short circuit. Connect all the numbered thermocouples (d) (two thermocouples for measuring the tube temperature and one thermocouple for measuring the bulk liquid temperature). Use the vacuum sealant (high vacuum grease, Dow Corning) to connect condenser #1 on the top of the glass chamber (e). Connect the nitrogen gas line (f) and fasten the fitting tightly to prevent leakage.

On the left side of the fume hood, connect the condenser #2, cold trap, and flow meters in series. Figure B.5 shows the final assembly which illustrates the configuration of all components. The flow path of the product gas is: condenser #1 → condenser #2 → cold trap → flow meter → exhaust or GC analysis.

B.2 Leak Check

A leak check is necessary to ensure the accuracy in the flow rate measurement. Figure B.6 illustrates the five valves that must be closed for the check. Valve (a) is a three way valve connected to the bottom of the film boiling chamber (inflow/outflow tube). Turning to direction (1) allows the reactant liquid to drain while turning to direction (2) connects the glass chamber and the bulk liquid reservoir. Besides

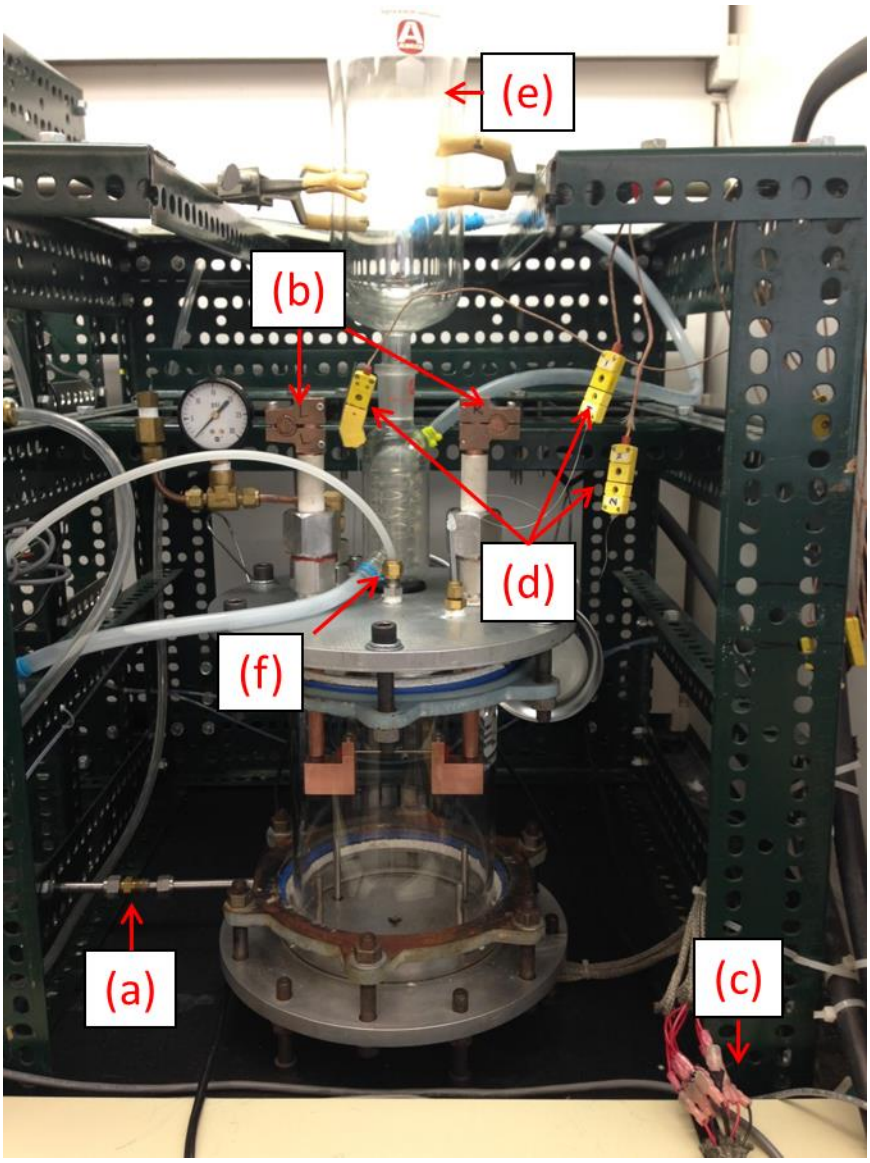

Figure B.4: The chamber mounted in the fume hood. (a) reactant inflow/outflow tube; (b) electrode terminals; (c) immersion heater connections; (d) thermocouple connections; (e) condenser #1; (f) compressed nitrogen gas line.

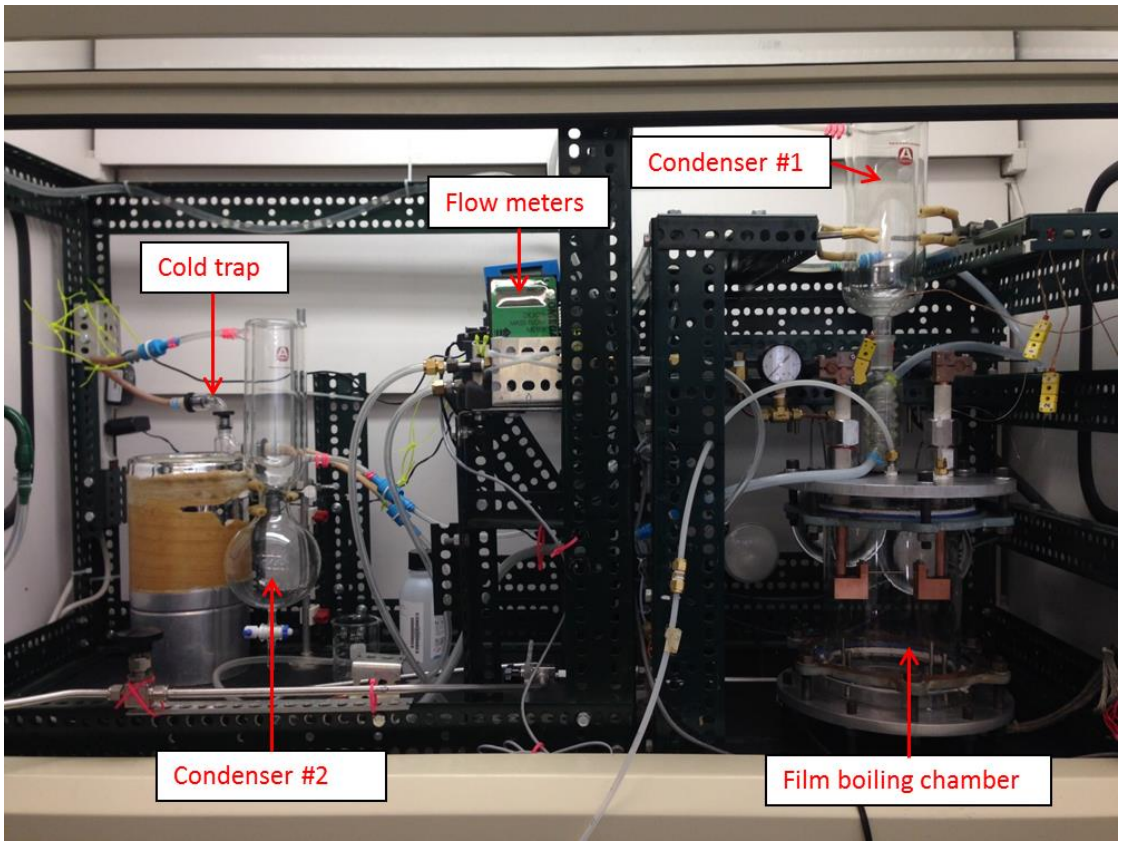

Figure B.5: The configuration of all components after assembly in the fume hood. This picture includes the sections (1) and (2) in Figure 2.1.

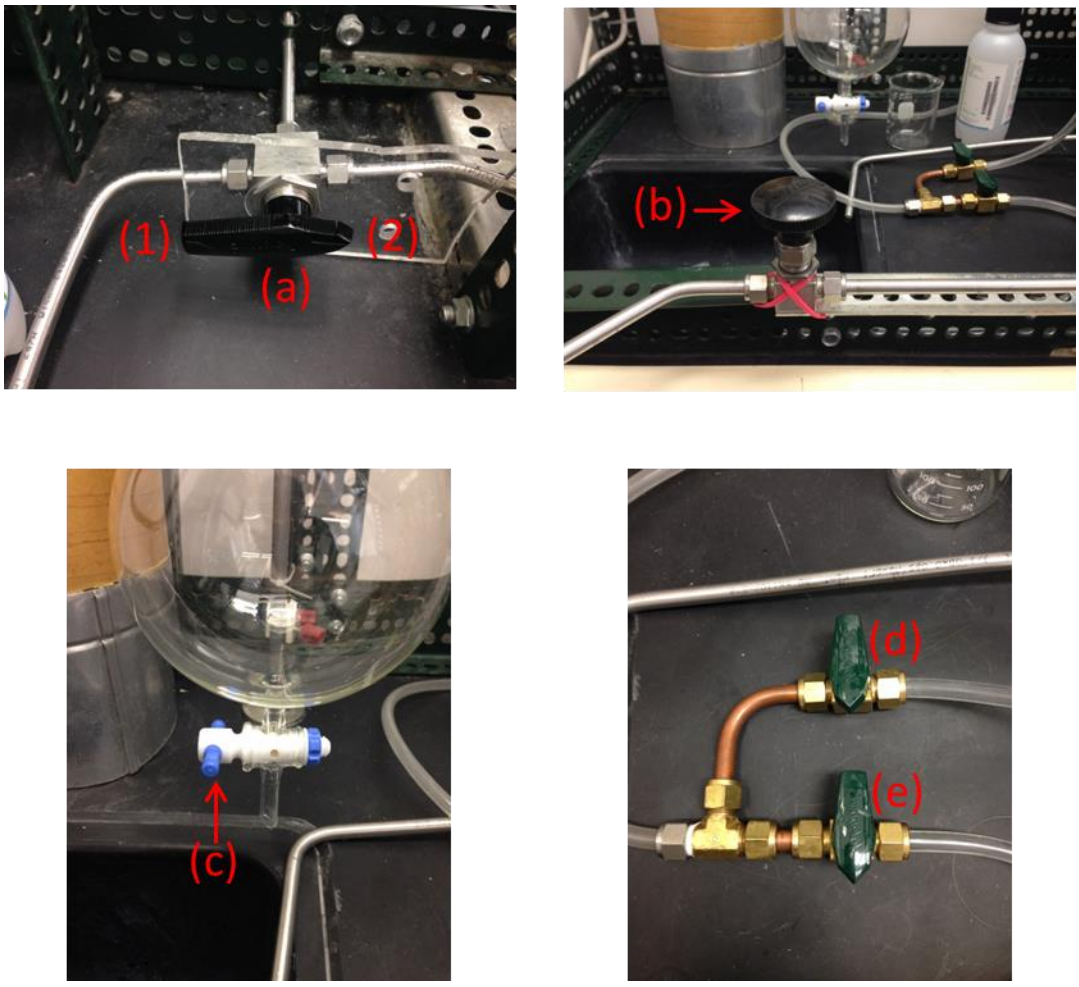

Figure B.6: Five valves (a to e) that need to remain closed while preforming the leak test.

draining the reactant liquid or taking liquid samples, this valve should always remain at direction (2). Valve (b) is open only when the reactant is flowing from the liquid reservoir to the glass chamber (See Figure 2.1). Valve (c) is located at the bottom of the condenser #2. Valves (d) and (e) are connected to two flow meters. The selection of which flow meter to use depends on the total product yield rate. Detailed information of flow meter and calibration curves is given in the Appendix D.

After checking all the valves, nitrogen gas is used to slightly pressurize the chamber to no higher than 5 PSI, and the pressure observed over a 30 minute period to see if there is any significant pressure reduction. A Snoop (Swagelok) leak detector is useful to locate leaks. Locations where leaks have assumed include the following.

a) Sealant (RTV 108, Momentive) applied on the Teflon tubing on the top plate of the chamber (remove the sealant and reapply the sealant again).
b) O-rings between the top/bottom plates and the glass chamber (disassemble the chamber and replace the O-ring).
c) Product gas outflow seal on the top plate (replace the seal (KD-22, BUCHI) and apply the sealant (high vacuum grease, Dow Corning) evenly).
d) Rubber tubing: the rubber tubes might crack and cause the leak (check the rubber tubes before every experiment and replace them if necessary.)
e) Swagelok fittings (tighten them if the leak occurs).

If the pressure remains constant over this period, the leakage check is successful.

B.3 Thermocouple and Power Supply Test

This section describes the testing process to ensure the power supply circuit and thermocouples are functioning well. Two LabVIEW programs need to be used:

power.vi and simplegraphwithpower2_NEW.vi, which are located in the desktop for the experiment (See Figure B.7). These two programs are located in the folder of C:\EXPERIMENTS\ in the computer. The testing procedure is detailed as follows.

a) Switch on the DAQ, power supply, and flow meters.
b) Double click the program power.vi. Figure B.8 (a) shows the interface of power.vi.
c) Click the drop-down box to change the I/O to GPIB0::5::INSTR, and hit Run.
d) After seeing the voltage and current reading, click stop. This step is to ensure the connection between the power supply and the desktop is functioning well.
e) Double click simplegraphwithpower2_NEW.vi. Figure B.8 (b) shows its interface.
f) Enter the numbers as following.

   CUTOFF-TEMP: **1300**

   Divide Voltage by: **1.2**

   Set Current: **580**

   These three numbers need to be entered before running this program for the safety consideration. To avoid burnout of the Inconel heater tube (melting point 1413 ℃), the maximum tube temperature is set to be **1300** ℃. If any thermocouple reaches this value, the voltage will be divided by **1.2** to lower the tube temperature. Maximum current is set to be **580** A according to the power supply specification.
g) Click run. The thermocouple readings, power supplied to the tube, and flow meter outputs will be shown on the program interface and recorded.
h) Turn on the output state and set the voltage to be 0.1 V. The thermocouple output will gradually increase because of resistive heating of the heater tube. If a huge fluctuation of the thermocouple reading is observed, it indicates that the

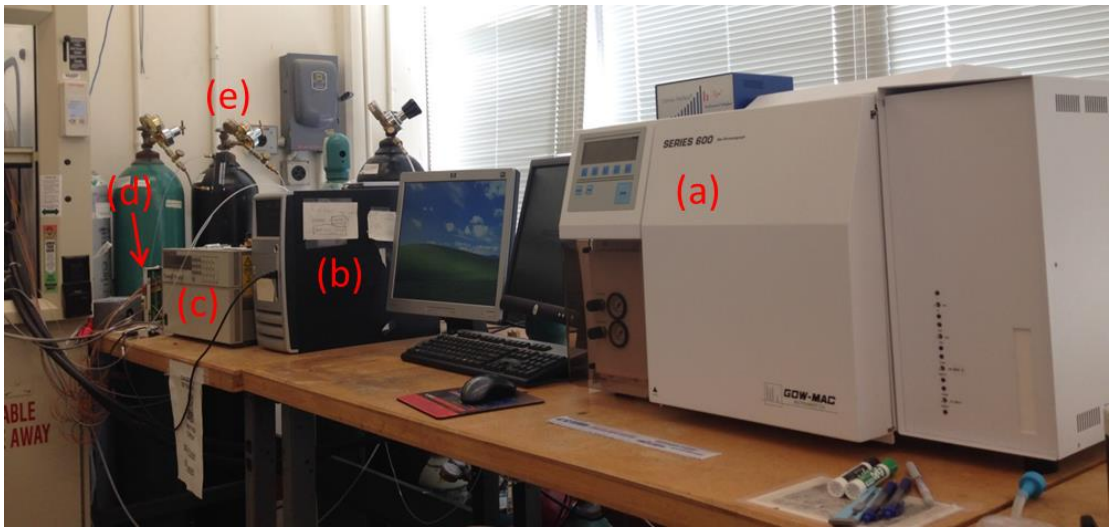

Figure B.7: Data acquisition tools: (a) gas-chromatography (Gow-Mac, GC Series-600 with TCD); (b) personal computer (HP, dc5000); (c) digital power supply (Agilent 6681A); (d) data acquisition hardware (NI, SCXI-1000); (e) gas cylinders (Airgas).

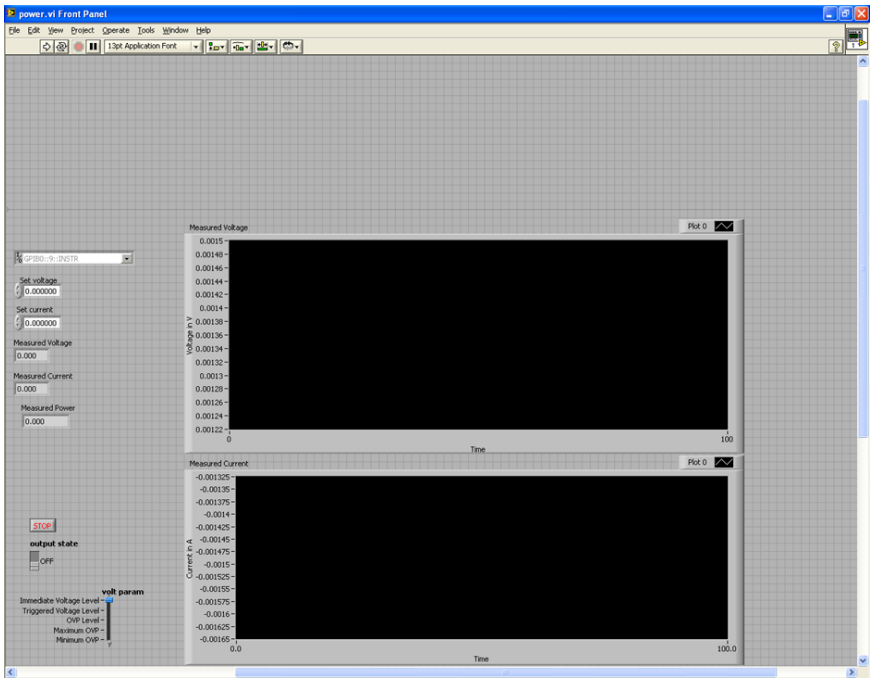

(a)

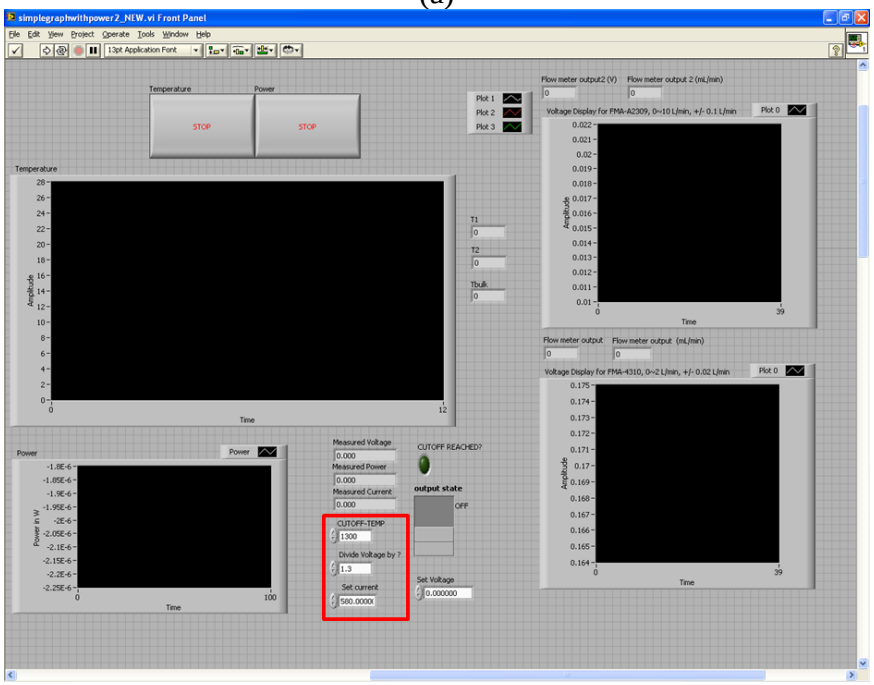

(b)

Figure B.8: (a) LabView interface of program power.vi; (b) LabView interface of program simplegraphwithpower2_NEW.vi.

thermocouple metal is in contact with the power supply circuit. Please disassemble everything to start all over again.

i) If the temperature increases without fluctuation, turn off the output state from the interface and stop the LabVIEW program. The thermocouple and power supply test is then finished.

j) Wrap the glass chamber with fiberglass insulation.

k) Set up the camera for pictures taking during the experiment if desire (see next section).

The experimental apparatus is now ready.

B.4 Photography Setting

Aside from the experimental sections, visual recordings of the film boiling process are captured by a digital camera (Nikon, D5100) accompanied with an advanced lens (Micro-NIKKOR, 55mm f/2.8). The movie mode (HD resolution: 1980×1080, 30 fps) is utilized during the recording process with the aperture and ISO number setting at f/8 and 1600. The shutter speed is set as 1/4000 as taking pictures. Five halogen lamps (PHILIPS EcoVantage, 1750 lumens), in which three positioned at the back of the chamber and two positioned in the front, are used as the light source to enhance the video brightness. A high density polyethylene (HDPE) white sheet with a thickness of 1.6 mm is placed between the back halogen lamps and the glass chamber to provide a backdrop. A tripod is used to fix the camera, and the distance between the chamber surface and the front end of lens is approximately 100 mm.

After the movie has been recorded, the software “VLC media player” is utilized to extract static pictures from the movie. A series of pictures showing the transition from nucleate boiling (CHF) to film boiling is shown in section 2.2 for DEC

and EtOH. Snap shots of film boiling with an aqueous glycerine mixture (90/10) and ethyl acetate are also shown with indicated conditions.

APPENDIX C

EXPERIMENT PROCEDURES

This section describes the experimental procedures including how to achieve and maintain film boiling, and carry out the GC sampling process.

The following supplies must be acquired before proceeding further.

a) reactant prepared or mixed: 4 Liters (pour the prepared reactant liquid into the bulk liquid reservoir).
b) dry ice: 15 Lbs, and acetone: 1 Liter (mix dry ice and acetone in the in the condensers #1 and #2).
c) ice cubes: 16 Lbs (immerse the cold trap in a bucket full ice cube and water).
d) ensure adequate compressed nitrogen gas for both safety feed to the chamber and GC actuator gas.
e) ensure adequate compressed helium gas for GC carrier gas.

The vendors of above supplies can be found in Appendix G.

C.1 Experiment Procedure for Developing Film Boiling

There are two methods for creating film boiling: immersion method and quenching method. As for the immersion method, the tube is initially immersed in the reactant (the distance between the tube and the free liquid interface is 50 mm) with its temperature initially set to its boiling point. The power supplied to the tube is then gradually increased so that the heat transfer transitions from single phase convection, nucleate boiling, CHF, and ultimately to film boiling. Figure 1.2 illustrates this boiling mode transition. In Figure 1.2, the immersion method begins with point A. As the power increased, it reaches point B (CHF), and follows with a horizontal arrow as

shown in the figure to achieve film boiling. Following are the steps of the immersion method.

a) Pour the reactant into the bulk liquid reservoir, and connect the liquid reservoir to the pump. Open the reservoir valve (see Figure C.1).
b) Open valve (b) and (d). Remain valve (a) in the direction (2) (see Figure B.6).
c) Switch on the pump to allow reactant flow into the glass chamber. Wait until the liquid level in the chamber is 50 mm above the tube.
d) Switch off the pump, and close the liquid reservoir valve and valve (b) (see Figure C.1 and Figure B.6).
e) Switch on the immersion heaters, DAQ, power supply, flow meters, and GC machine.
f) Run the "thermocouple and power supply test" (See Appendix B.3). Follow steps a) to g).
g) Increase the variable autotransformer output of immersion heater to 80%. Wait until the bulk liquid temperature reaches its boiling point.
h) Switch on the power supply from the LabVIEW interface, and increase the input voltage to 0.1 V.
i) Wait for 5 minutes to achieve steady-state, then increase the voltage by 0.1 V.
j) Repeat step i) to record data that could be used to measure the boiling curve in the nucleate boiling region.
k) As the boiling mode reaches CHF, any increment of power will lead to bubble coalescence to establish film boiling. This transition is illustrated in Figure 1.2, from point B to move horizontally. Table 1.2 lists the CHF and temperatures for the liquids examined in the study.

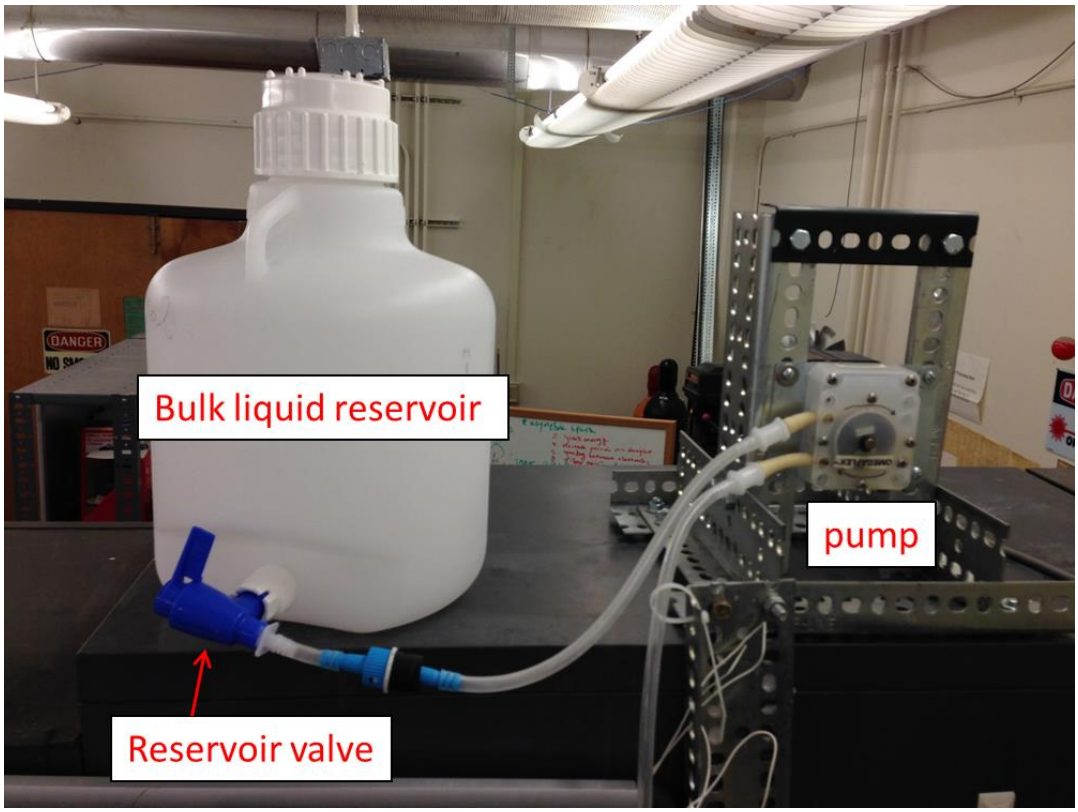

Figure C.1: The set-up of bulk liquid reservoir, valve, and pump.

As performing the quenching method, the boiling curve in the nucleate boiling is automatically recorded. Appendix D shows the data processing procedures to generate the boiling curve.

When the heat transfer mode transitions from CHF to film boiling, the tube may reach the melting point and burnout. For the liquid investigated in this study, all of the aqueous glycerine mixtures (97/3, 64/6, 90/10, and 80/20) exhibited this problem. In such situation, another approach to attaining film boiling without melting the tube is used, developed by Choi (2010) and Evangelista (2010). We review that method here. Figure C.2 shows a schematic diagram of the quenching method. In this approach, the tube is not immersed initially but rather positioned above the liquid. The procedure is as follows.

a) Pour the reactant into the bulk liquid reservoir, and connect the liquid reservoir to the pump. Open the reservoir valve (see Figure C.1).
b) Open valve (b) and (d). Remain valve (a) in the direction (2) (Figure B.6).
c) Switch on the pump to allow reactant flow into the glass chamber. Wait until the liquid level in the chamber is 15 mm below the heater tube.
d) Switch off the pump, and close the liquid reservoir valve and valve (b) (see Figure C.1 and Figure B.6).
e) Switch on the immersion heaters, DAQ, power supply, flow meters, and GC machine.
f) Run the “thermocouple and power supply test” programs separately. Follow steps a) to g).
g) Increase the variable autotransformer output of immersion heater to 80%. Wait until the bulk liquid temperature reaches its boiling point.

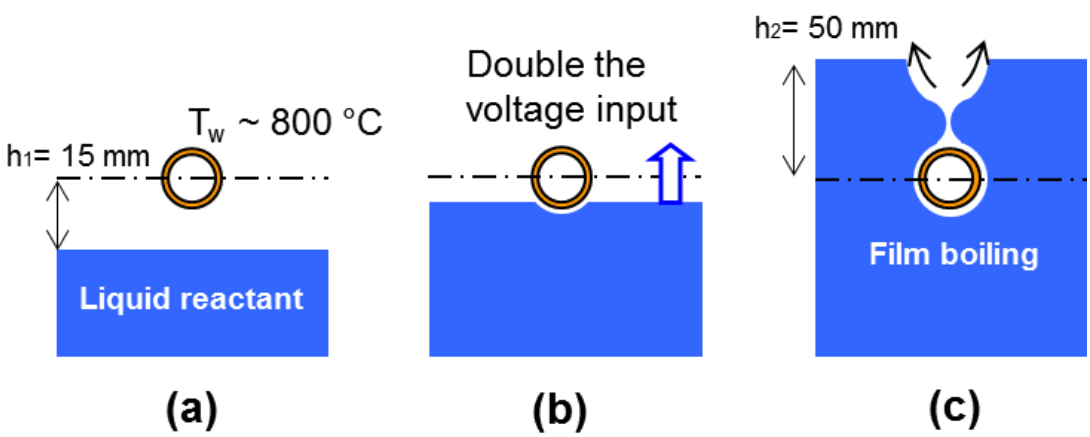

Figure C.2: A schematic of the quenching method (Choi 2010). (a) Heat the heater tube to 1000 ℃ in a nitrogen environment. (b) Allow the reactant to flow into the chamber, and as the liquid level is about to touch the bottom the heater tube, double the voltage input. (c) Film boiling is attained and maintained (Choi 2010).

h) As the bulk liquid temperature is at the saturation temperature, allow nitrogen gas to flow through the chamber for safety considerations at a flow rate approximately at 100 mL/min.

i) Gradually increase the voltage to the tube (increase the voltage by 0.1 V for every 5 minutes until the heater tube temperature approaches 1000 ℃).

j) Open the liquid reservoir valve and valve (b), and switch on the pump to gradually increase the liquid level in the chamber.

k) As the liquid is about to touch the bottom of the heater tube, double the input voltage. Carefully adjust the voltage supplied to the heater tube (if the tube temperature drops, increase the voltage further; if the temperature increases close to the melting point, decrease the voltage; the end goal is to reach a fully submerged state without solid/liquid contact.

l) Turn off the pump as the liquid level is 50 mm above the heater tube, and close the liquid reservoir valve and valve (b).

m) Stop the nitrogen flow, and wait until the bulk liquid temperature rises to the boiling point.

Among four liquids investigated (aqueous glycerine water mixtures, ethyl acetate, diethyl carbonate, and ethanol) in this study, the immersion method is applicable to ethyl acetate, diethyl carbonate, and ethanol while it leads to burnout the heater tube for aqueous glycerine mixtures. Table 1.1 lists the selected properties of these liquids. The surface tension of glycerine and water are about two to three times higher than rest of the liquids. It may suggest that the surface tension is the key parameter to determine which method to use to create film boiling. If the surface tension is at the range of 0.02 N/m, the immersion method would be applicable; the quenching method is favorable as the surface tension is above 0.06 N/m.

The tube will burnout as its temperature exceeding the melting point. In this study, the tube material is Inconel 600 with the melting point of 1354-1413 ℃. An alternative is to change the heater tube material to a higher melting point. Platinum is a good candidate since its melting point is 1735 ℃.

C.2 Experiment Procedures for Measuring Boiling Curve

As film boiling is developed, the input voltage is gradually adjusted to measure the boiling curve in the film boiling regime. The steps are listed as follows.

a) Increase the input voltage by 0.1 V, and wait for 5 minutes to achieve the steady-state.

b) Repeat step a) until the tube temperature reaches 1250 ℃. The highest temperature that the LabVIEW program allowed is 1300 ℃, which is limited by the melting point of the Inconel tube (1354-1413 ℃).

c) Now decrease the voltage by 0.1 V, and wait steady-state conditions to move down the boiling curve, which is from point D to C in Figure 1.2.

d) Repeat step c) until the film boiling reaches the unstable point, which is the minimum temperature to maintain stable film boiling around the heater tube. If the temperature is below this point, the vapor film will collapse. As you see film boiling collapse, increase the voltage by 0.1 V immediately until film boiling is re-established.

e) Repeat steps a) to d) to move up and down, and to ensure enough data points (temperature and heat flux) are recorded between the unstable point and the upper limit of the heater tube temperature in the film boiling regime.

See section 10.4 for the process of terminating power to the experiment apparatus.

C.3 Gas Chromatography (GC) Operation

This section lists the steps involved with operating the GC machine and its software to monitor and record exhaust gas composition.

a) Turn on the GC from the back of the machine.

b) Open the valve of the actuator gas (nitrogen) and carrier gas (helium). Adjust the pressure and the flow rate of these two gases as following so that the actuator gas (nitrogen) pressure is 30-40 PSI, and the carrier gas (helium) pressure is 50 PSI at 30 mL/min.

c) On the GC machine screen, select "Power on".

d) On the GC machine screen, select "Edit → Retrieve → QCTEST1 → Return."

e) Open the software "Chrom Perfect" from the computer desktop (note Figure C.3).

f) Select "Data Acquisition" from the software interface.

g) On the GC machine screen, select "Action → Heat on → Home."

h) Check GC status (on the GC machine screen). After it shows "Ready," go to "Control → Filament On → Return" to turn on the filament in the thermal conductivity detector (TCD).

i) Ensure that the three-way valve at the back of the GC machine (see Figure C.4) allows the product gas to flow into the GC.

j) Turn on the mini-pump (Figure C.5), located above the digital power supply, and adjust the flow rate to approximately 30 mL/min.

k) Referring to the Chrome Perfect software data acquisition interface (see Figure C.6), under "control," click "Claimed" to "Release" (see Figure C.6).

Figure C.3: The Chrom Perfect software interface

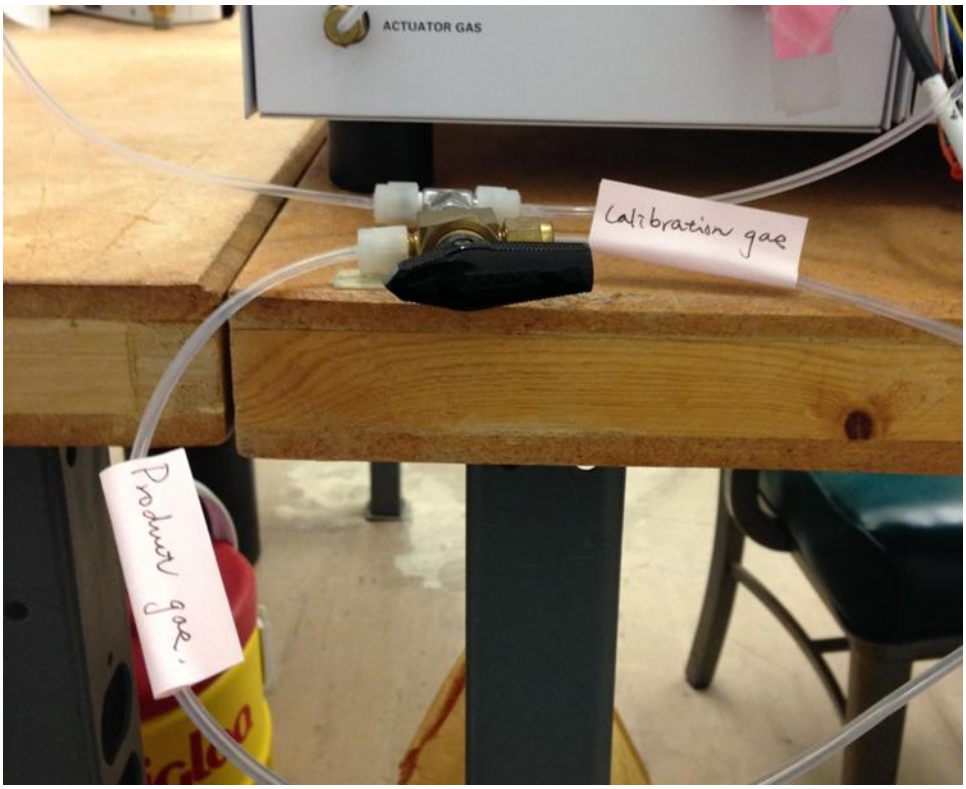

Figure C.4: A three–way valve controls either product gas or calibration gas flowing into the GC machine.

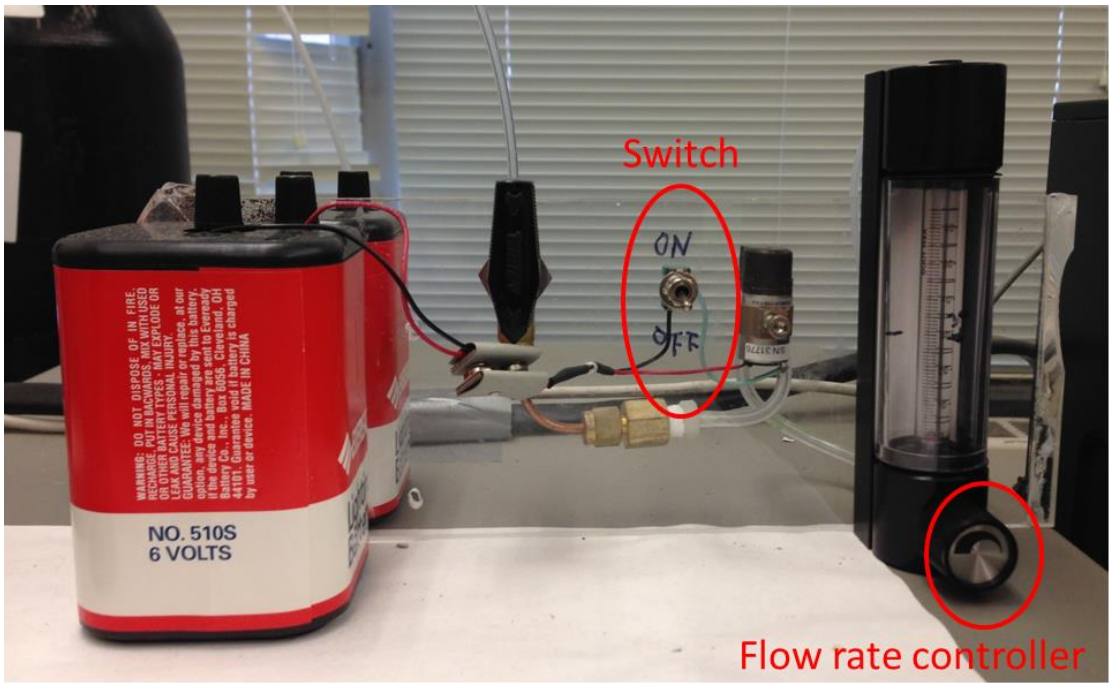

Figure C.5: The mini-pump set-up. The flow rate needs to be maintained at 30 mL/min for GC sampling.

l) In the tool bar, under “View,” click “Instrument Control” (see Figure C.6), and change “Run Time” to 15 minutes to ensure the product gas to flow through the TCD. The gas sample flows through the first column in the first 5 minutes and from 5 to 15 minutes, it flows through the second column.

m) Click “Start Run” (shown as gray in Figure C.6) to start the GC measurement.

n) Record the GC output for a ranged averaged tube temperature as this data will allow showing the relation between product gas composition and tube temperatures.

C.4 Liquid Sampling

The bulk liquid is sampled at the end of the experiment. As sampling the liquid, turn valve (a) in the direction (1) (see Figure B.6) to drain the liquid. Note that some liquid residuals may remain in the tube so that allow the liquid to drain around 10 mL, and then take the liquid sample. It should be noted that taking the liquid sample during the experiment is proved to change the bulk liquid concentration because of the volume change, yet the effect is minimal.

As for the aqueous glycerine experiments, a derivatization process (ASTM D6584, EN 14105) is used to transform the polarity of chemicals from polar to non-polar to accomplish the analysis. A reagent (MSTFA (N-Methyl-N-trimethylsilyltrifluoroacetamide)) that replaces the polar functional group (H radical in a hydroxyl group) with the trimethylsilyl (TMS) group makes the molecule non-polar. Pyridine and decane are added as the buffer and solvent separately. Please see ASTM D6584 and EN 14105 in the reference for a more detailed process.

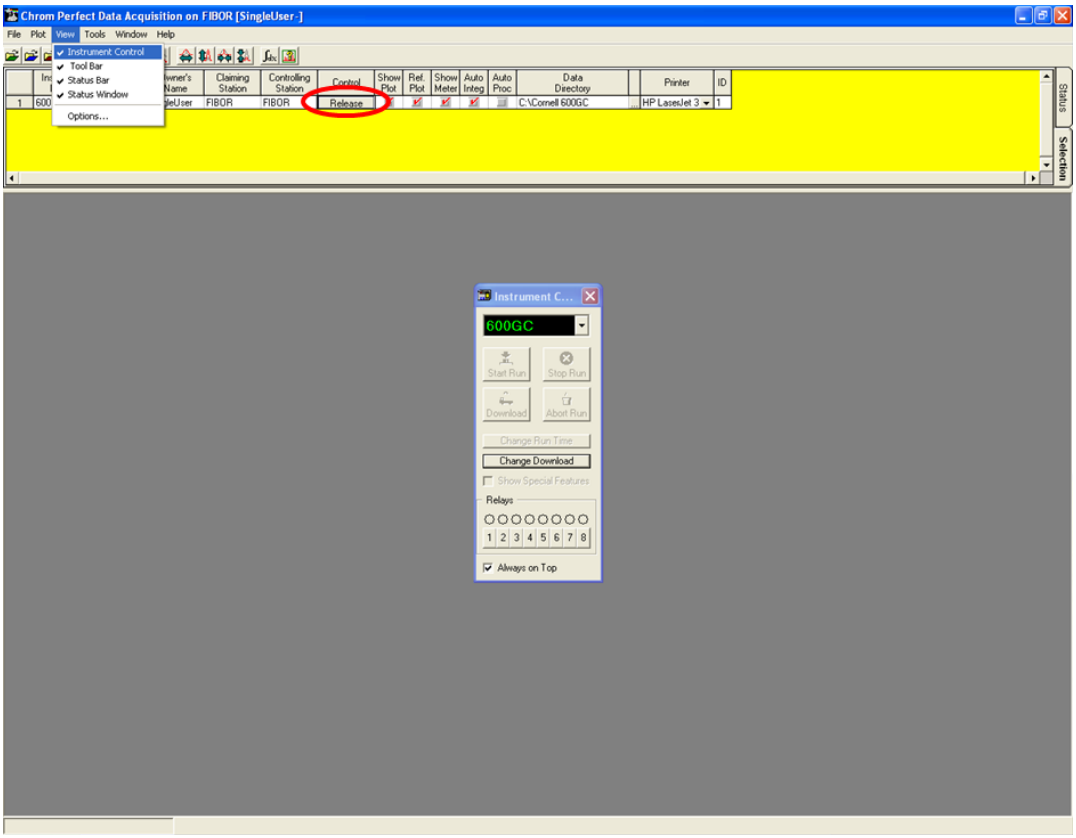

Figure C.6: Data acquisition interface of the Chrom Perfect software.

C.5 End the Experiment

To terminate operation, the followings are carried out.

a) Turn off the "Output Status" of power supply from LabVIEW interface, as show in Figure B.8 (b), and click "Stop" in LabVIEW interface.

b) Turn off the power supply.

c) Turn off the DAQ.

d) Adjust the power output of immersion heaters to 0%, and then shut it down.

e) Turn off the flow meters.

f) Shut down GC from the GC screen: Action → Shut Down. Wait for the column and detector temperatures to drop to the room temperature. Close the valve of the actuator (nitrogen) and carrier (helium) gases. Turn the GC off from the back of the machine.

g) Wait until the reactant cools down (overnight). Disassemble the apparatus and clean all components by using acetone and water.

APPENDIX D

DATA PROCESSING

This section describes the data processing steps for tube and liquid pool temperature, heat flux, flow rate, calibration curve development, and exhaust gas analysis.

D.1 Temperature and Flow Rate

Raw data are recorded as a function of time during an experiment. Each condition is maintained for 5 minutes to wait for steady-state. Figure D.1 illustrates the steady-state condition. A fixed power (514 kW/m^2) is supplied through the heater tube for 50 minutes. The averaged tube temperature over a 50 minute duration is 1206 K, which is the same as the averaged temperature over the first 5 minute duration, except a negligible difference in the standard deviation.

Seven files will be generated for each experiment (C:\EXPERIMENTS\):

a) time.lvm
b) temperatures.lvm
c) green flowrate.lvm
d) blue flowrate.lvm
e) voltage.lvm
f) current.lvm
g) power.lvm

The time increments for temperatures and flow rates are different from the power data. Time, temperatures, and flow rates are recorded approximately every 0.01 seconds (100 Hz) while the power data (voltage, current, power) are saved approximately every 0.13 (7.7 Hz) seconds. The difference comes from the sampling

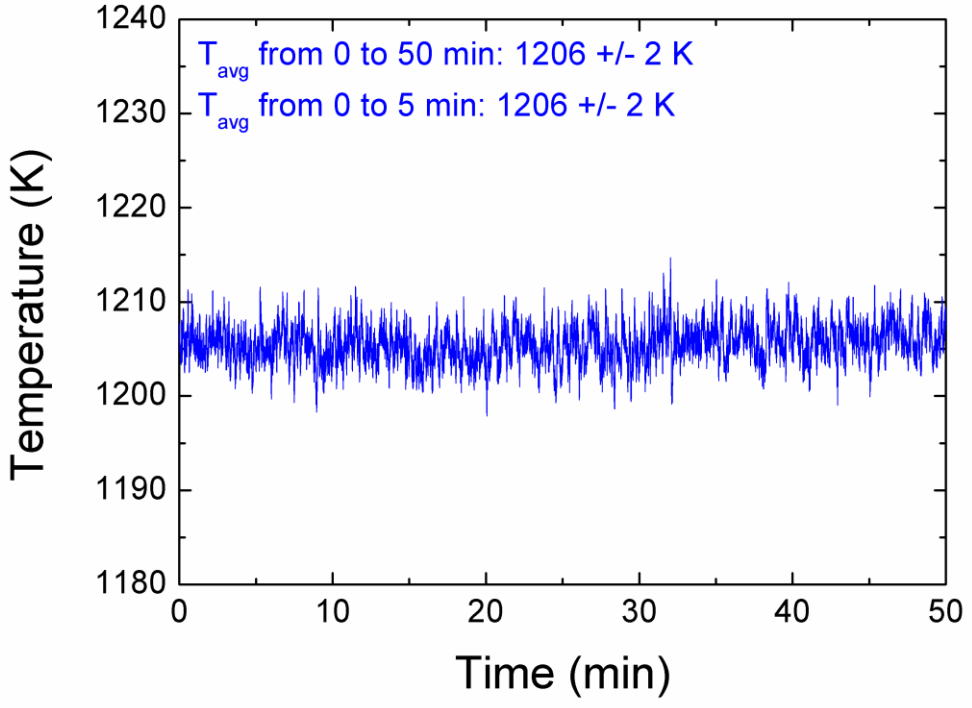

Figure D.1: Proof of the steady-state condition. The average temperatures of 50 minutes and 5 minutes are the same with a corresponding heat flux of 514 kW/m^2.

rate of the data acquisition tool. The National Instruments (NI) temperature and flow rate acquisition provides sampling rate of 100 Hz. The Agilent USB-GPIB provides a sampling rate of 7.7 Hz.

Data files are opened in "Notepad," pasted into the software "Origin Pro 8.0" for plotting and averaging processes. Two separate sheets are suggested to use because of the different time increments noted above. In the first sheet, the raw data from "time.lvm", "temperatures.lvm", "green flowrate.lvm", and "blue flowrate.lvm" are imported. The power data ("voltage.lvm", "current.lvm", and "power.lvm") are imported to in the second sheet.

In the first sheet, temperature and flow rate are plotted as a function of time in separate figures. The x-axis may be expanded to a 10 minute (600 seconds) duration, as can be seen in the raw data for temperature and flow rate as shown in Figure D.2. In Figure D.2 (a), the average tube surface temperature is found to be 1252 +/- 1 K for the corresponding input power of 528 kW/m^2. The temperature and heat flux combination constitutes one point on the boiling curve. Since the temperature fluctuation is very low, we did not label error bars of temperature in our experimental results. Figure D.2 (b) shows the corresponding flow rate measurement at the same condition. The average flow rate is found to be 601 +/- 41 mL/min. The fluctuations are believed to originate from the dry/ice acetone condensers. As dry ice sublimates from solid to gas phase, bubbles are generated in the condenser which results in the flow rate fluctuation. A standard deviation for these fluctuations is determined, and the figures show them.

The Origin Pro software is used to average the raw data by using an internal feature: "Statistics" → "Descriptive Statistics" → "Statistics on Columns." The result will be displayed in a new sheet with corresponding "Mean," "Standard Deviation,"

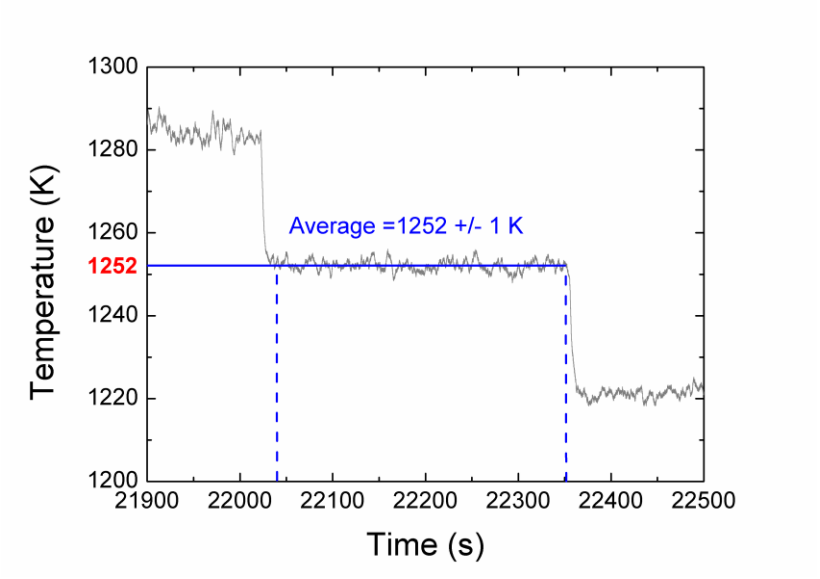

(a)

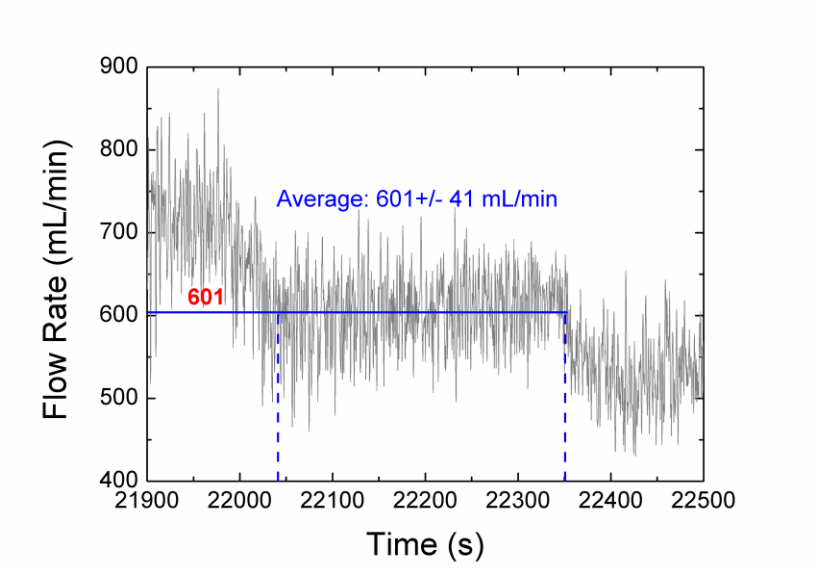

(b)

Figure D.2: Expanded raw data of (a) tube temperature at location T.C.-B1 and (b) exhaust gas flow rate for a heat flux of 528 kW/m^2. Average values and standard deviations are indicated over the sampling interval, which is 5 minutes.

"Sum," "Minimum," "Median," and "Maximum." An Excel file may be created to store the "Mean" and "Standard Deviation" of temperatures and flow meter outputs.

D.2 Boiling Curve Calculation

The input power generated is

$$q = I^2 r \tag{E.1}$$

The resistance of the Inconel tube can be expressed as

$$r = \frac{\rho L}{A_c} = \frac{\rho L}{\frac{\pi}{4}\left(d_o^2 - d_i^2\right)} \tag{E.2}$$

where $\rho = 0.4763 + (5.27\times10^{-3})T - (1.95\times10^{-5})T^2 + (3.56\times10^{-8})T^3 - (3.23\times10^{-11})T^4$ $+(1.35\times10^{-14})T^5 - (1.89\times10^{-18})T^6$ (μΩ-m) (Special Metals Corp 2008).

The total energy generated can be expressed as

$$q = \frac{4\rho L I^2}{\pi(d_o^2 - d_i^2)} \tag{E.3}$$

The input energy is dissipated in the radial and axial direction. A correction for axial losses was previously examined by Evangelista (2010) where it was shown to be small. The heat flux in the radial direction can be expressed as

$$q'' = \frac{q}{A_s} = \frac{q}{\pi d_o L} = \frac{4\rho I^2}{\pi^2 d_o (d_o^2 - d_i^2)} \tag{E.4}$$

The boiling curve can be developed from the measured tube temperature and current. From the previous studies (Choi 2010; Evangelista 2010), it has been proved that the temperature drop from the center of the tube to the outer surface is negligible. Therefore, the temperature reading recorded by the thermocouples inside the heat tube can be viewed as a reasonable measurement of the tube surface temperature.

D.3 Calibration Curve Development

The two digital flow meters in parallel (Figure 2.1) are used during an experiment, depending on the product yield rate range. Flow meter 1 (Omega Engineering, FMA-A2309) has a higher detection range (0 – 10,000 mL/min) but a lower resolution (± 100 mL/min) while flow meter 2 (Omega Engineering, FMA-4310) has a lower detection limit (0 – 2,000 mL/min) but a higher resolution (± 20 mL/min). Both flow meters have a linear output signal over 0 – 5 VDC. The default settings of both flow meters are designed for measuring the nitrogen gas. The 0 – 5 VDC output can be linearly converted to 0 – 10,000 mL/min (flow meter 1) or 0 – 2,000 mL/min (flow meter 2). Since nitrogen gas is not a product in our experiments, as a result, calibration curves (the relationship between flow meter output signal (V) and flow rate (mL/min)) must be needed for gas species expected to be formed during an experiment.

Figure D.3 shows the flow meter arrangement for the calibration process. An absolute flow rate calibration for a given gas species is found using a flow meter (MesaLabs, Bios DryCal Definer 220) to provide an absolute scale of the flow rate. The Definer 220 uses a physical method to measure flow rate: a piston inside the flow meter is pushed by the flow imposed with displacement providing a measure of flow rate. The measured flow rate is independent of the actual gas species. The response time of the Definer 220 is slow compared with digital flow meters especially at lower flow rates so that the digital flow meters are used during an experiment.

The calibration curves are determined as follows.

a) Connect the "gas in" (Figure D.3) to the gas cylinder used to create the calibration curve while keeping the remaining valves closed; the gas could be hydrogen, carbon monoxide, methane, ethylene, or carbon dioxide. These gases are selected since they are the products from the thermal decomposition of reactants examined.

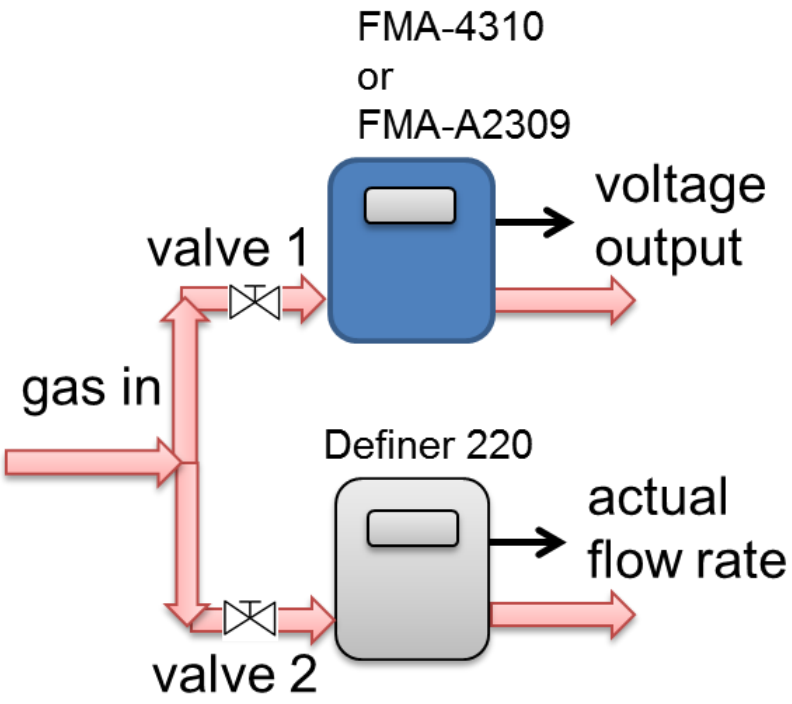

Figure D.3: A schematic of the calibration curve development configuration.

b) Open valve 2 with a constant flow rate, and allow the gas to also flow through the Definer 220 (do this for about three runs).

c) Now, close valve 2 and open valve 1.

d) Record the voltage outputs (V) from the digital flow meters (FMA-A2309 or FMA-4310), and repeat steps b) and c) with different flow rates.

e) The absolute flow rate can be plotted with different voltage outputs.

f) Fit the data with a curve. The calibration curves of the flow meters are shown in Figure D.4 and Figure D.5. A second order polynomial was used to fit the data.

$$\dot{S} = A_0 + A_1 V + A_2 V^2 \qquad \text{(E.5)}$$

The coefficients (A_0, A_1, and A_2) are listed in Table D.1 and Table D.2 for given gas species.

D.4 Chemical Species Analysis of Noncondensable Products

The procedure for product gas analysis using the gas chromatography (Gow-Mac, GC600P00012801) is as follows.

a) Switch the three way valve behind the GC machine to "calibration gas" (see Figure C.4). Run the GC machine with the calibration gas.

b) Open the software "Chrom Perfect," and choose "File Editor."

c) Under the tool bar, choose "File" → "Create New File."

d) Select "Calibration File." (see Figure D.6 (a)).

e) A plain calibration file will be created, as shown in Figure D.6 (b).

f) In this file, enter the peak information: component name, retention time (min), window width (min), level 1 amount, and level 1 response for all peaks shown in calibration gas.

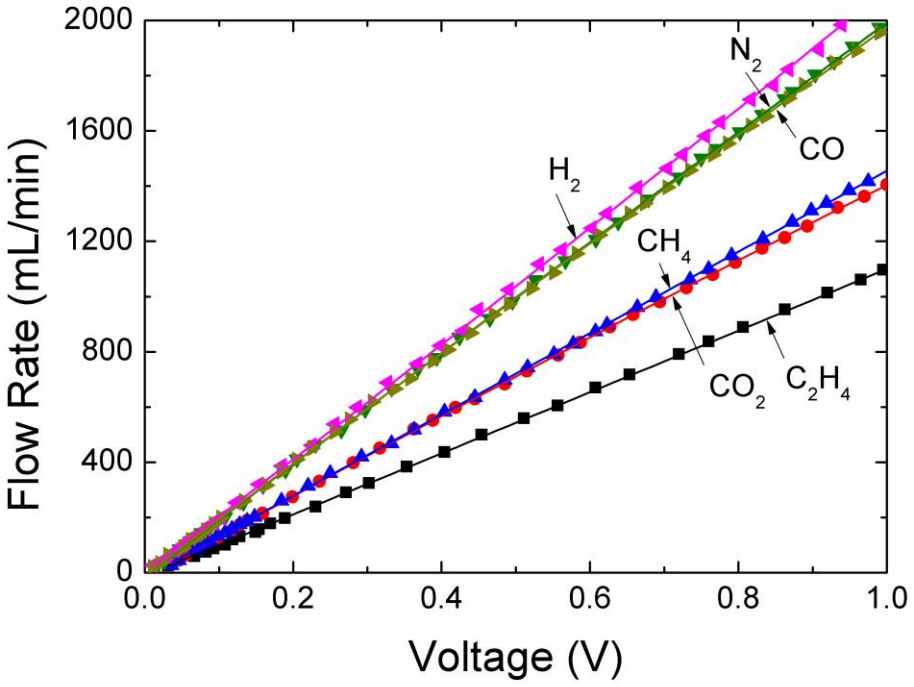

Figure D.4: The calibration curve of the digital flow meter FMA-A2309.

Table D.1: Coefficients of the calibration curves of the digital flow meter FMA-A2309. The calibration curve is fitted by a second order polynomial $\dot{S} = A_0 + A_1 V + A_2 V^2$

	C_2H_4	CO_2	CH_4	N_2	H_2	CO
A_0	0.98	-1.37	0.44	-1.14	4.42	8.14
A_1	227.96	279.79	288.62	383.84	392.35	380.67
A_2	7.84	8.49	8.15	12.69	6.03	13.39

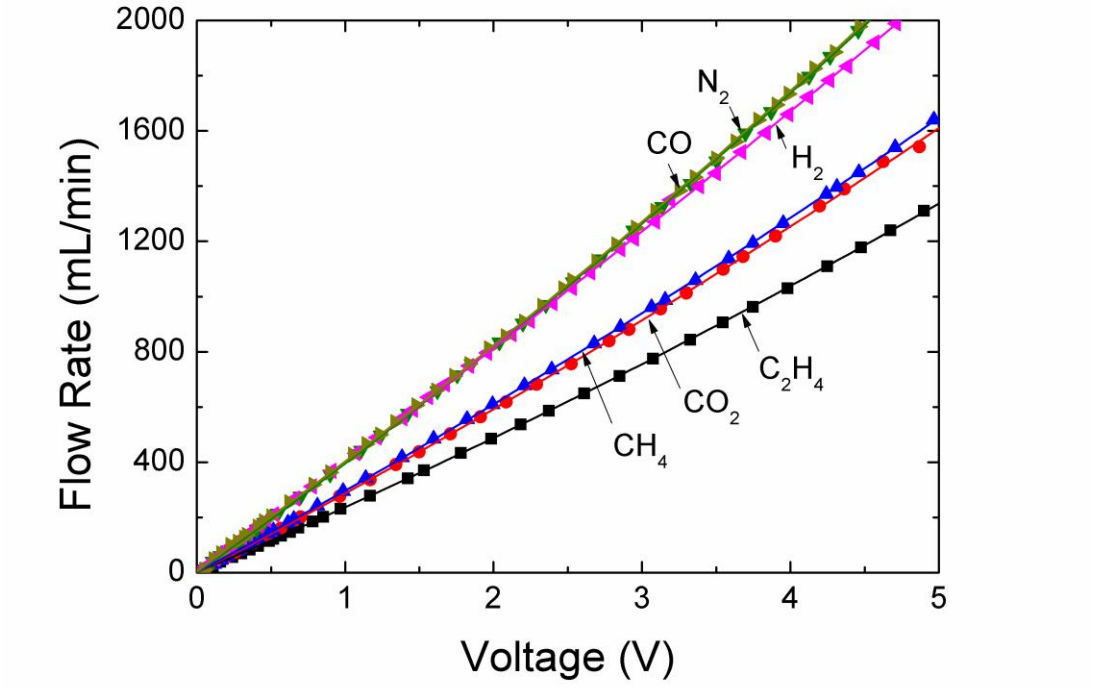

Figure D.5: The calibration curve of the digital flow meter FMA-4310.

Table D.2: Coefficients of the calibration curves of the digital flow meter FMA-4310. The calibration curve is fitted by a second order polynomial $\dot{S} = A_0 + A_1 V + A_2 V^2$

	C_2H_4	CO_2	CH_4	N_2	H_2	CO
A_0	-9.99	-19.41	-16.55	-11.35	0.51	-8.44
A_1	1101.51	1495.65	1475.84	2027.05	2027.36	2023.77
A_2	8.01	-72.17	-3.48	-23.27	90.03	-39.25

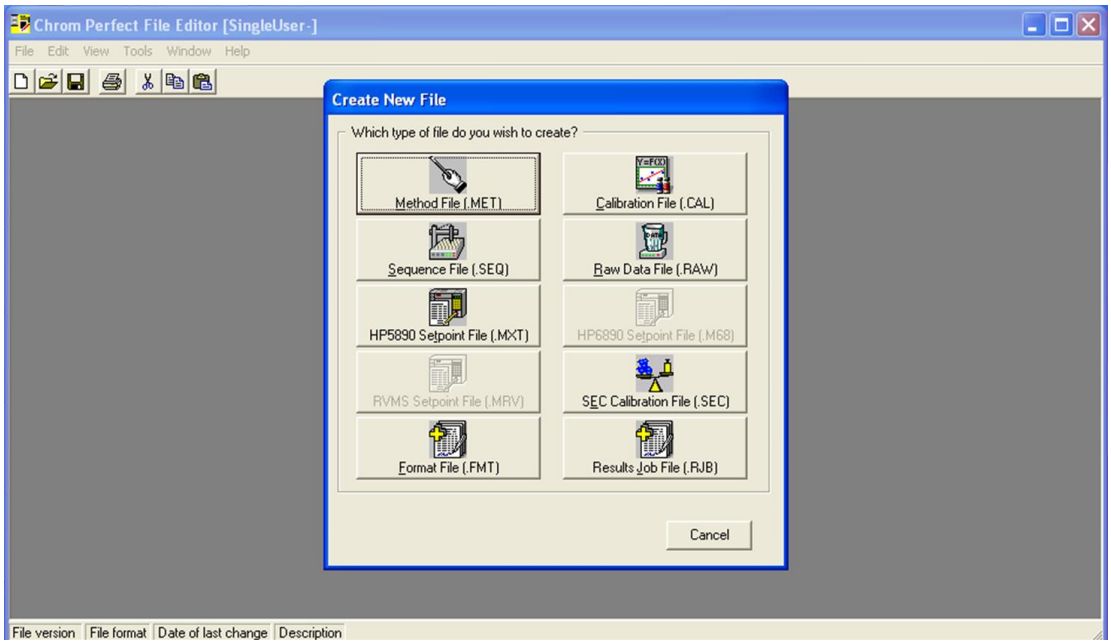

(a)

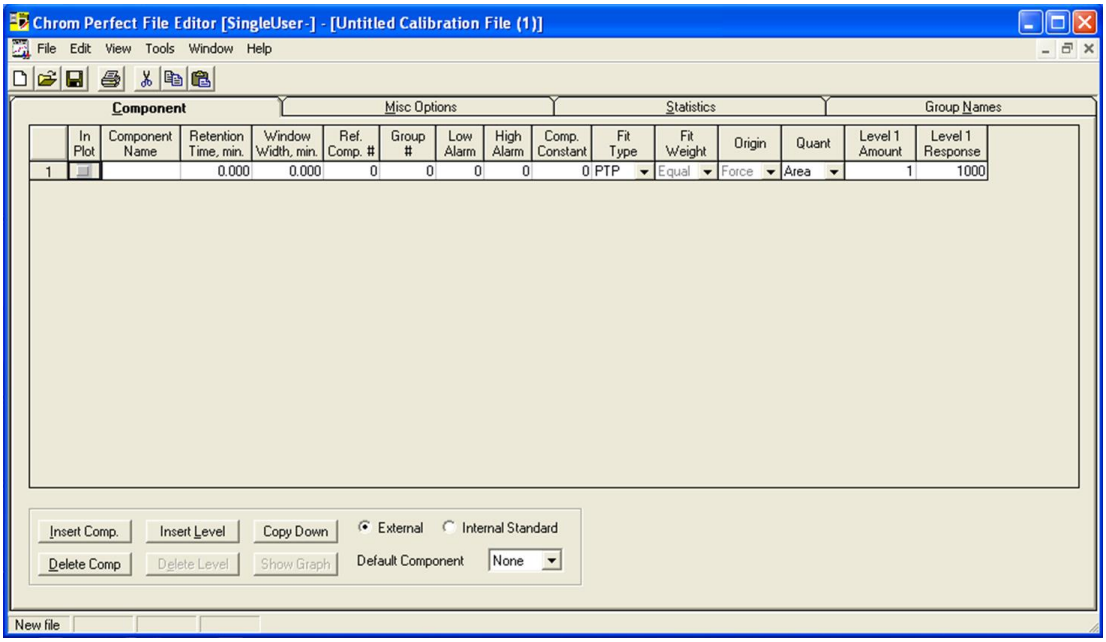

(b)

Figure D.6: (a) Chrom Perfect interface as creating the "Calibration File." (b) A plain calibration file.

g) s and molar concentration of the calibration gas (Airgas, speciality gas) are hydrogen (35%), carbon monoxide (50%), carbon dioxide (2%), methane (5%), acetylene (2%), ethylene (4%), and ethane (2%). The chosen mixture concentration is somewhat arbitrary in that only serves as a known reference for the analysis. The important aspect is to ensure all anticipated species are included. This concentration was chosen as a guess of the actual composition based on the previous study (Kechagiopoulos 2007).

h) Enter the chemical species and its corresponding molar concentration in the column "component name" and "level 1 amount."

i) Return to the Chrom Perfect interface, select "Analysis." Open the GC trace file of the calibration gas.

j) Use the "Flip +" function in "Time Event". Flip the downward peaks to upward, and adjust the peak beginning and ending ticks to appropriate times (Figure D.7).

k) Right click on the mouse, and select "Peak Properties."

l) Left click on the peak of interest, and peak properties will be shown (Figure D.8).

m) Enter the peak properties "Retention Time," "Width," and "Area" to the calibration file (Figure D.9).

n) Save the file.

o) Return to the Chrom Perfect interface, and select "Analysis"; open the GC trace file of the product gas that you would like to analyze.

p) Use the "Flip +" function in "Time Event". Flip the downward peaks to upward, and adjust the peak beginning and ending ticks to appropriate times.

q) In the tool bar, go to "File" → "Select Calibration," and select the calibration file that was just created.

r) In the tool bar, under "Report," select "Long Report." Figure D.10 which shows the product gas species and its concentration shown under the column of "Amt %."

s) Repeat steps o) to r) for different GC traces sampled during the experiment. The molar fraction as a function of tube temperature can be generated. Fit molar fractions with trend lines (y_i).

D.5 Total Flow Rate and Molar Flow Rate

The previous sections outlined development of the calibration curves (section E.3) and the molar faction as a function of tube temperature (section E.4). This section discusses how to integrate these information to generate the volumetric and molar flow rates. The relationship between the total exhaust gas volumetric flow rate ($\dot{V}$, mL/min), and flow meter voltage output from the digital flow meters is

$$\dot{V} = \sum_{i=1}^{N} y_i \dot{S}_i \qquad \text{(E.6)}$$

The total molar flow rate ($\dot{N}$, mole/s) can be computed from the ideal gas law by using the total volumetric flow rate ($\dot{V}$, mL/min).

$$\dot{N} = \frac{P\dot{V}}{RT} \qquad \text{(E.7)}$$

Then, we can write the species molar flow rate ($\dot{n}$, mole/s) as

$$\dot{n}_i = y_i \dot{N} \qquad \text{(E.8)}$$

The species molar flow rate ($\dot{n}$, mole/s) is determined and can be plotted as a function of tube temperature. It provides the insights of the chemical conversion occurring within the vapor film.

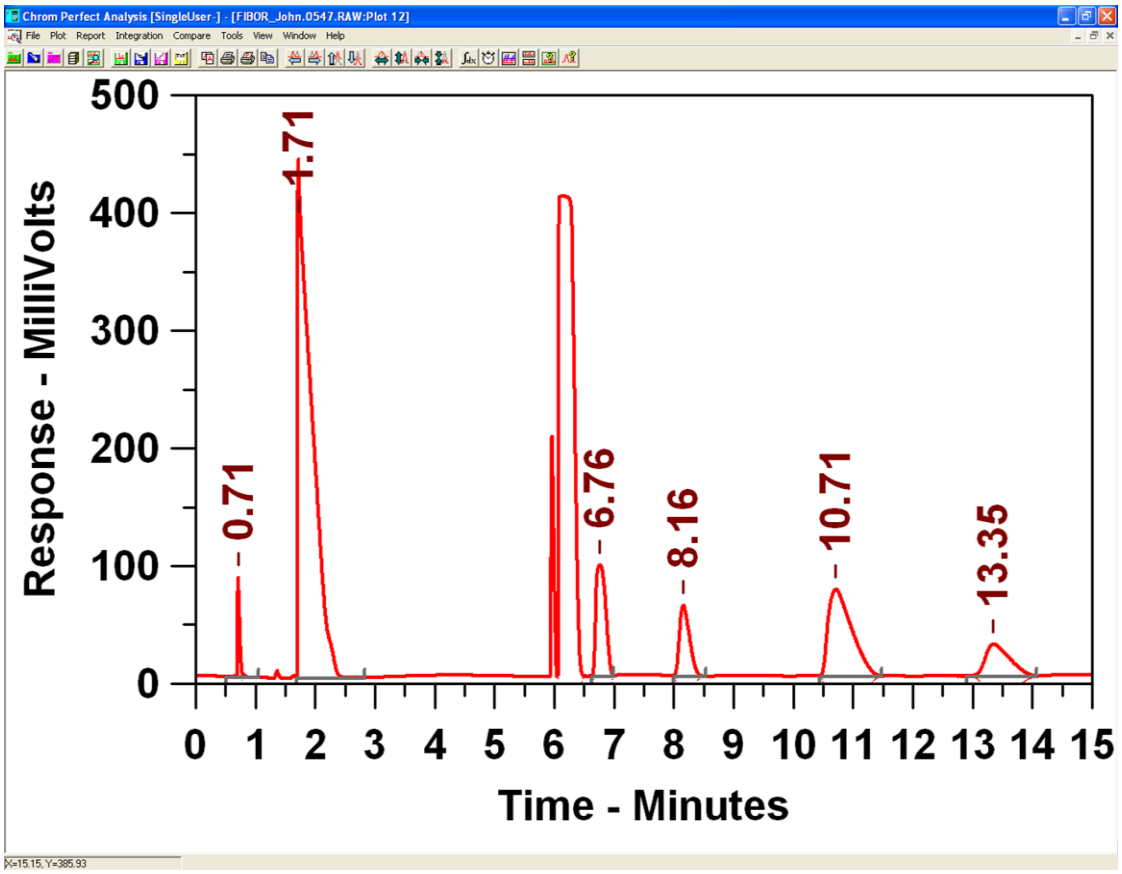

Figure D.7: GC trace of the calibration gas.

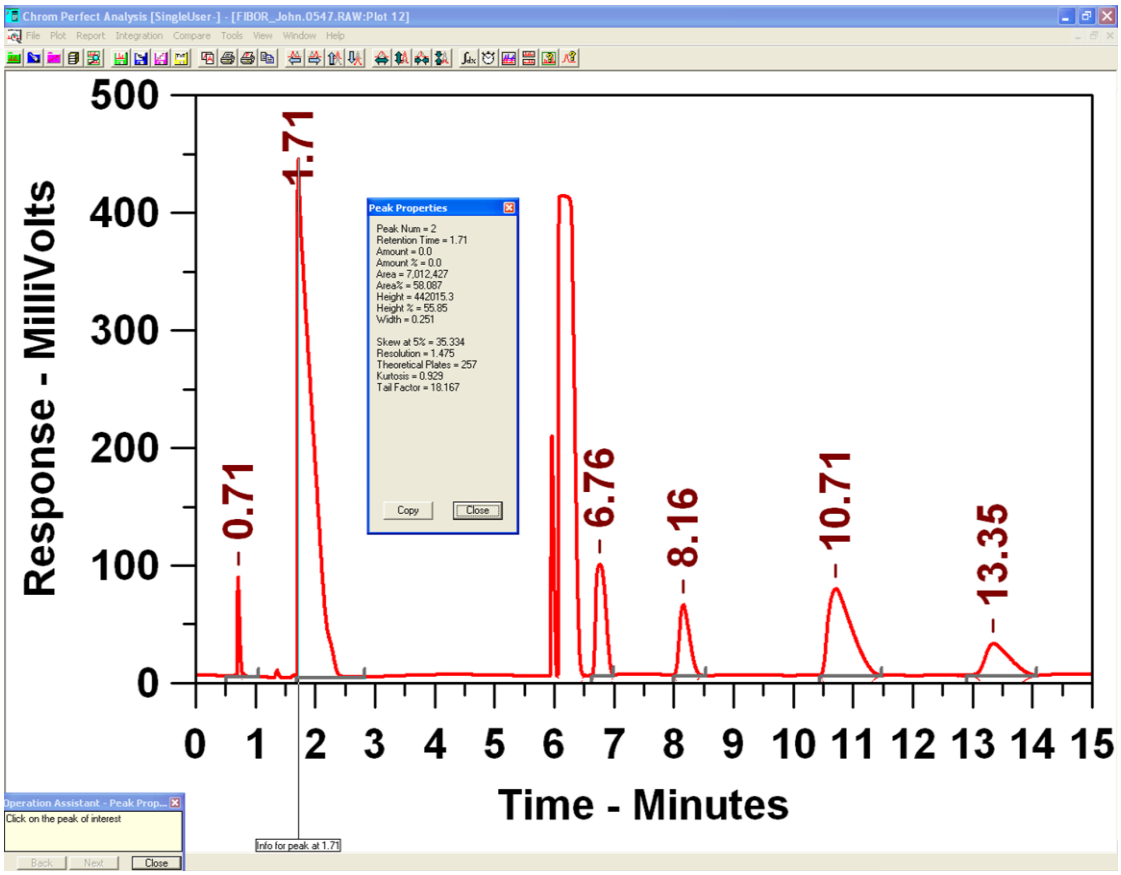

Figure D.8: Peak properties from the GC trace.

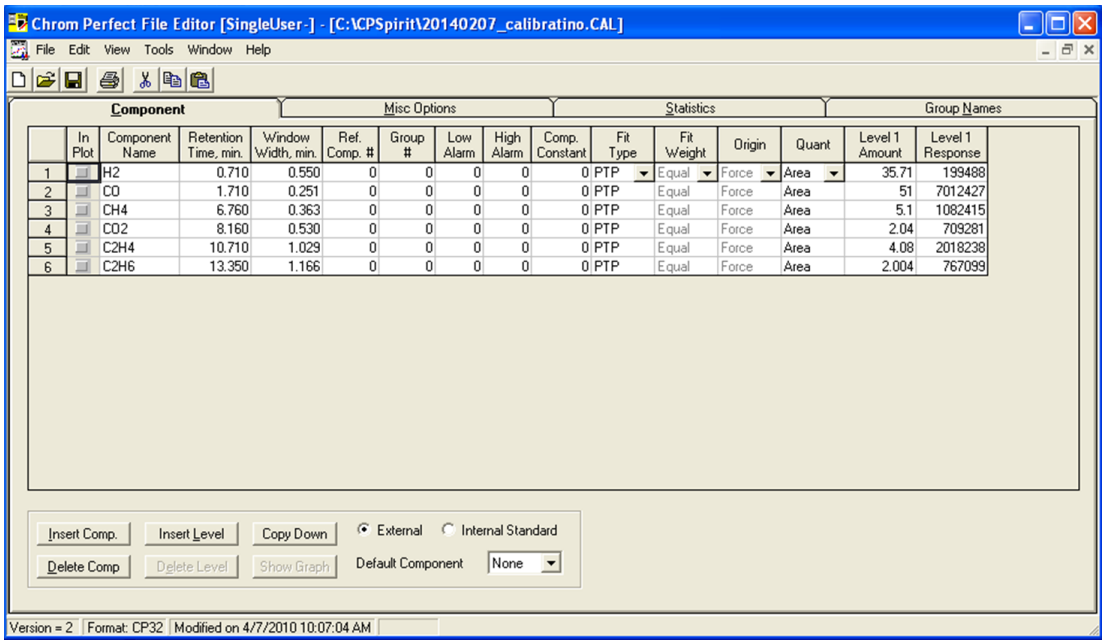

Figure D.9: The calibration file after entering all the required information.

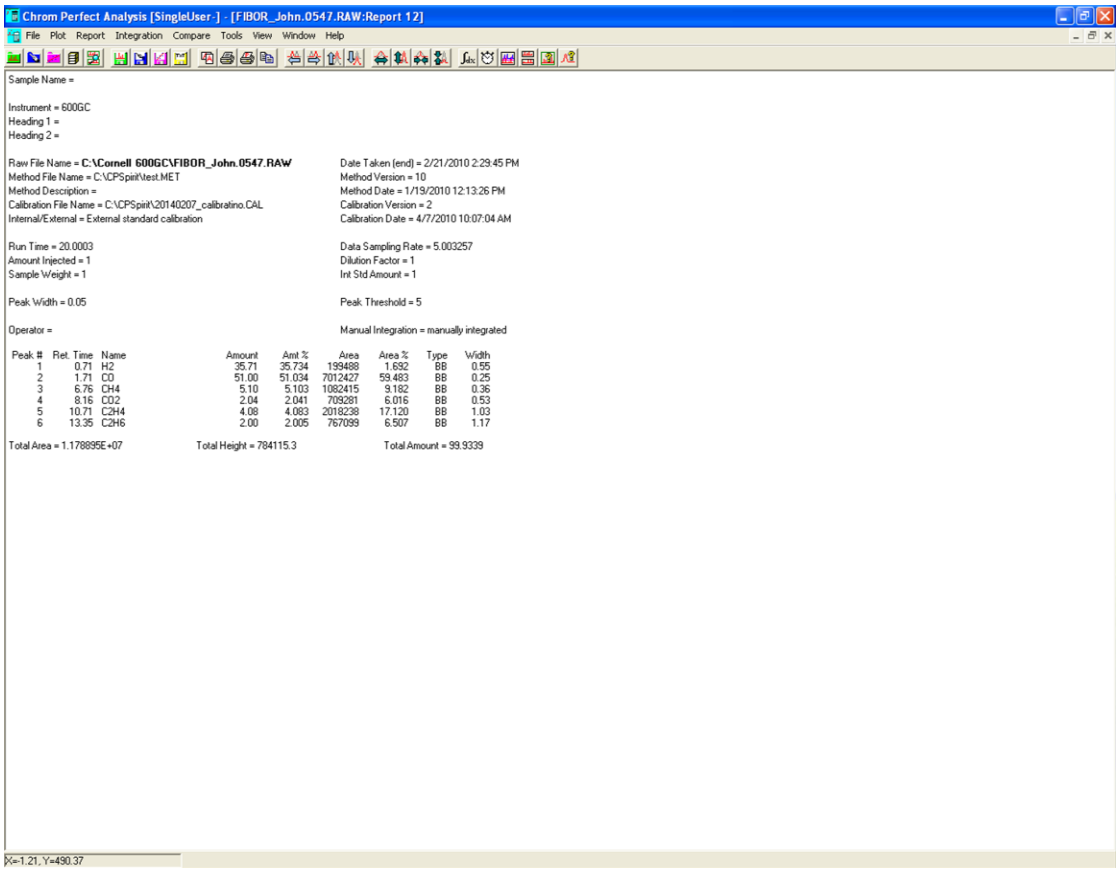

Figure D.10: The long report showing the product gas concentration.

D.6 Condensable Species Analysis

The bulk liquid was analyzed by gas chromatography-mass spectrum (Agilent, GC/MS 5890, DB-5 GC column) in view of condensable product species refluxing to the liquid chamber. Following are the steps to perform the GC/MS analysis.

a) Use pipettes to deliver liquid samples to the GC/MS vials, and prepare 20 mL of acetone.
b) Place the samples on the automatic sampling holder, and refill solvent #2 with prepared acetone.
c) Run the GC/MS analysis by using the recipe "WEI_SPL2.RES."
d) On the GC trace, right click the mouse on the peak of interest, and the mass spectrum corresponding to this peak will show up.
e) Double click the mass spectrum, the software will access the NIST (National Institute of Standards and Technology) mass spectrum library and show possible chemical species.
f) Use your own judgment to determine the chemical specie of each peak.
g) The area underneath each peak will be exported to an Excel file "RESULTS.CSV."
h) Prepare a calibration sample with known concentrations, and run the GC/MS analysis using identical steps b) to g).
i) Using the calibration sample peak area and known concentration to determine the unknown bulk liquid concentration.

APPENDIX E

EQUILIBRIUM CONSTANTS

As for the reactions listed in previous chapters, some reactions (e.g., Eq. (3.1)) include the forward reaction only while others (e.g., Eq. (3.2)) have both forward and backward reactions. It is determined by an equilibrium constant (K_C), which is the forward reaction rate divided by the backward reaction rate. The equilibrium constant of a reaction can be calculated from Eq. (2.66) and (4.41) of Turns (2012) as follows.

$$K_c = K_p \exp\left(P^o / \overline{R}T\right)^{\sum \nu'' - \sum \nu'} \quad \text{(E.1)}$$

$$K_p = \exp\left(-\Delta G_T^o / \overline{R}T\right) \quad \text{(E.2)}$$

To determine the equilibrium constant, the standard state Gibbs function needs to be determined for every chemical species in the reaction. The standard state Gibbs function of glycerine, ethyl acetate, acetic acid, diethyl carbonate, ethanol, acetaldehyde, and acetal are calculated from Reids et al (1977) while it can be looked up from NIST-JANAF thermochemical tables (NIST-JANAF) for rest of the chemical species in this study. Table E.1 and Table E.2 list the standard-pressure Gibbs function at different temperatures used to calculate equilibrium constants.

If the equilibrium constant of a chemical reaction is greater than unity for the temperature range investigated, only the forward reaction will be included in the reaction. However, if the equilibrium constant changes from less than unity to greater than unity (or vice versa), both forward and backward reactions are included.

Figure E.1, Figure E.2, Figure E.3, and Figure E.4 shows the equilibrium constants for the reactions in Chapter 3, Chapter 4, Chapter 5, and Chapter 6. The dominant reaction temperature range from Appendix A is labeled, and the reactions are listed below each figure.

Table E.1: Calculated standard pressure Gibbs function (Reids et al 1977).

Temperature	glycerine	EA	AA	DEC	EtOH	acetaldehyde	acetal
K	kJ/mole						
600	-276.215	-299.063	-364.877	-171.209	-92.634	-95.663	37.752
700	-226.685	-262.877	-348.189	-132.842	-66.442	-81.998	100.441
800	-177.155	-226.691	-331.500	-94.475	-40.250	-68.333	163.130
900	-127.625	-190.505	-314.811	-56.107	-14.058	-54.668	225.819
1000	-78.094	-154.318	-298.123	-17.740	12.134	-41.003	288.508
1100	-28.564	-118.132	-281.434	20.627	38.325	-27.338	351.197
1200	20.966	-81.946	-264.745	58.994	64.517	-13.673	413.885
1300	70.496	-45.760	-248.056	97.362	90.709	-0.008	476.574
1400	120.026	-9.574	-231.368	135.729	116.901	13.657	539.263
1500	169.557	26.612	-214.679	174.096	143.093	27.322	601.952

Table E.2: The standard pressure Gibbs function from JANAF Table.

Temperature	H_2	CO	CO_2	H_2O	CH_4	C_2H_4	C_2H_6	CH_2O
K	kJ/mole							
600	0	-164.486	-395.182	-214.007	-23.740	86.935	19.297	-101.917
700	0	-173.518	-395.398	-208.812	-12.878	94.835	39.681	-98.675
800	0	-182.497	-395.586	-203.496	-2.017	102.734	60.066	-95.259
900	0	-191.416	-395.748	-198.083	8.845	110.633	80.450	-91.712
1000	0	-200.275	-395.886	-192.590	19.707	118.533	100.834	-88.068
1100	0	-209.075	-396.001	-187.033	30.568	126.432	121.219	-84.351
1200	0	-217.819	-396.098	-181.425	41.430	134.332	141.603	-80.578
1300	0	-226.509	-396.177	-175.774	52.292	142.231	161.988	-76.763
1400	0	-235.149	-396.240	-170.089	63.153	150.130	182.372	-72.914
1500	0	-243.740	-396.288	-164.376	74.015	158.030	202.757	-69.039

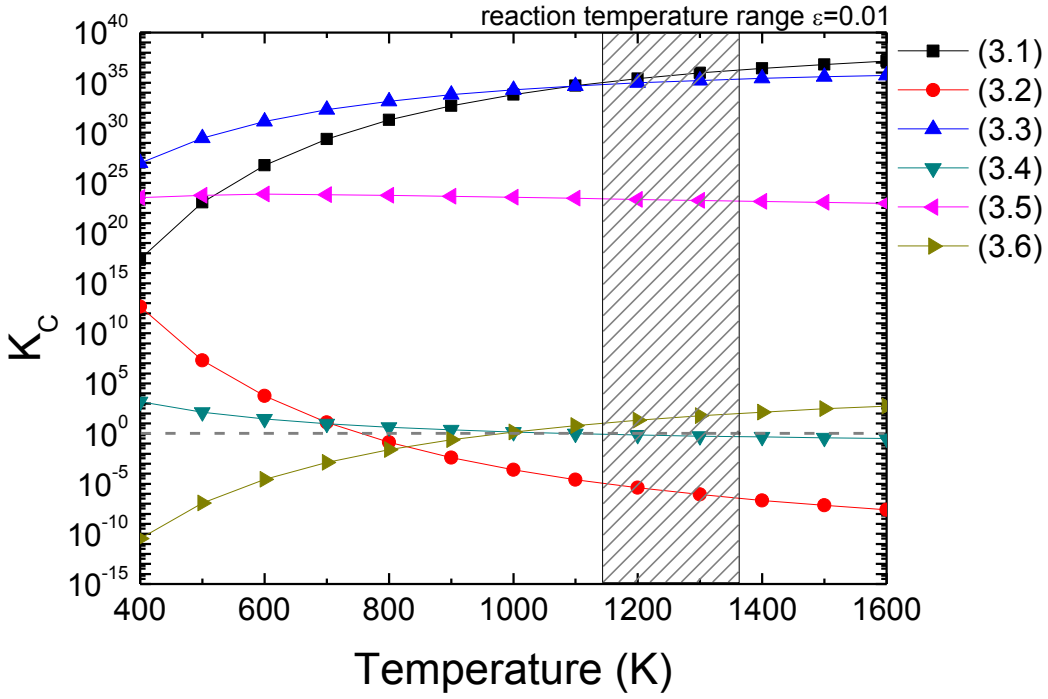

Figure E.1: Equilibrium constants for reactions (3.1) to (3.6).

$$C_3H_5(OH)_3 \rightarrow 4H_2 + 3CO \quad (3.1)$$

$$CO + 3H_2 \rightleftarrows CH_4 + \mathbf{H_2O} \quad (3.2)$$

$$C_3H_5(OH)_3 + 3H_2O \rightarrow 7H_2 + 3CO_2 \quad (3.3)$$

$$CO + \mathbf{H_2O} \rightleftarrows H_2 + CO_2 \quad (3.4)$$

$$C_3H_5(OH)_3 \rightarrow C_2H_4 + CO + 2\mathbf{H_2O} \quad (3.5)$$

$$C_2H_4 + H_2 \rightleftarrows C_2H_6 \quad (3.6)$$

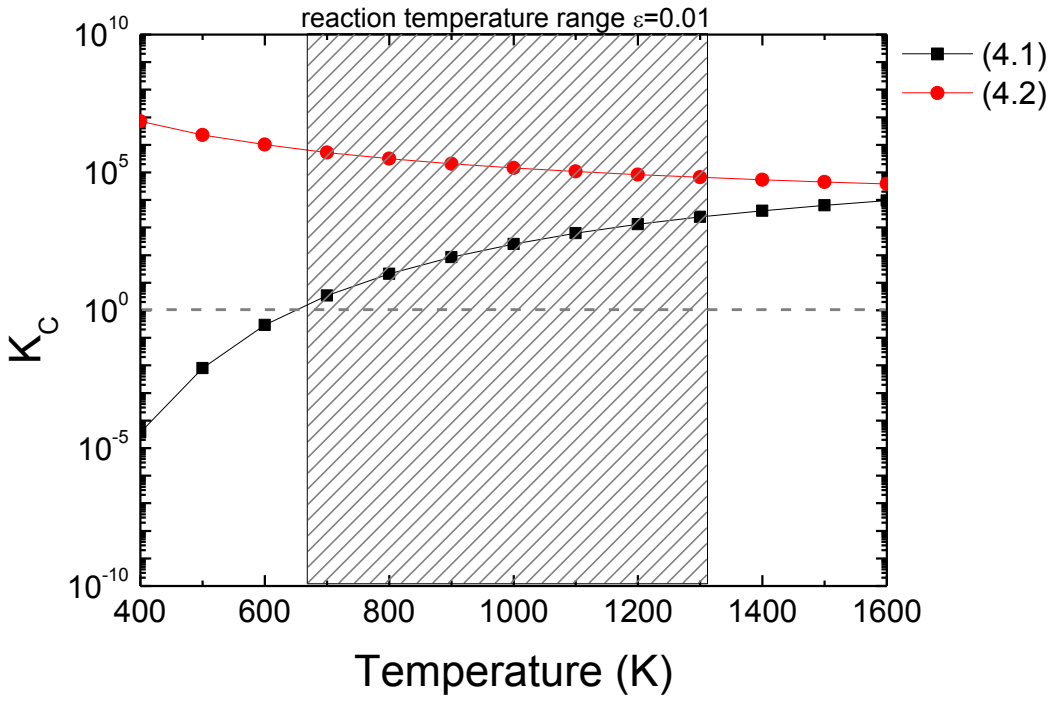

Figure E.2: Equilibrium constants for reactions (4.1) and (4.2).

$$CH_3COOC_2H_5 \rightarrow \mathbf{CH_3COOH} + C_2H_4 \qquad (4.1)$$

$$CH_3COOH \rightarrow CO_2 + CH_4 \qquad (4.2)$$

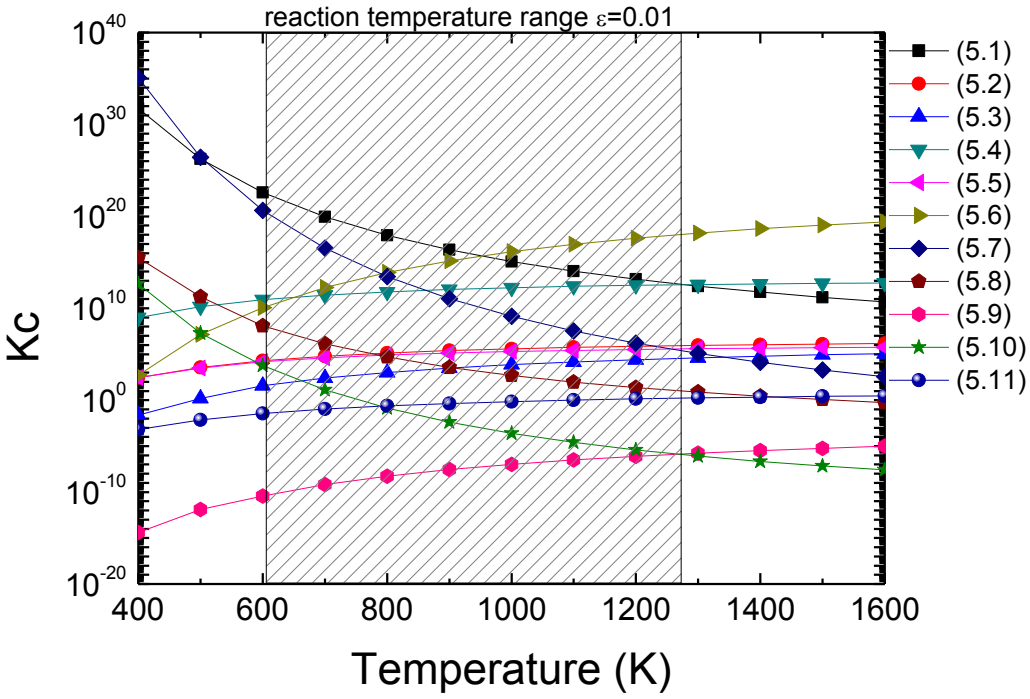

Figure E.3: Equilibrium constants for reactions (5.1) to (5.11).

$$(CH_3CH_2O)_2CO \rightarrow C_2H_4 + CO_2 + \mathbf{C_2H_5OH} \quad (5.1)$$

$$C_2H_5(OH) \rightarrow C_2H_4 + \mathbf{H_2O} \quad (5.2)$$

$$C_2H_5(OH) \rightarrow \mathbf{CH_3CHO} + H_2 \quad (5.3)$$

$$C_2H_5(OH) \rightarrow CH_4 + CO + H_2 \quad (5.4)$$

$$C_2H_5(OH) \rightarrow CH_4 + \mathbf{CH_2O} \quad (5.5)$$

$$C_2H_5(OH) + 3H_2O \rightarrow 2CO_2 + 6H_2 \quad (5.6)$$

$$3C_2H_4 \rightarrow 2C + 2C_2H_6 \quad (5.7)$$

$$2CH_3CHO \rightarrow \mathbf{CH_3COOC_2H_5} \quad (5.8)$$

$$CH_3CHO + 2C_2H_5OH \leftarrow \mathbf{H_2O} + \mathbf{CH_3CH(OC_2H_5)_2} \quad (5.9)$$

$$3H_2 + CO \rightleftarrows CH_4 + \mathbf{H_2O} \quad (5.10)$$

$$H_2 + CO_2 \rightleftarrows CO + \mathbf{H_2O} \quad (5.11)$$

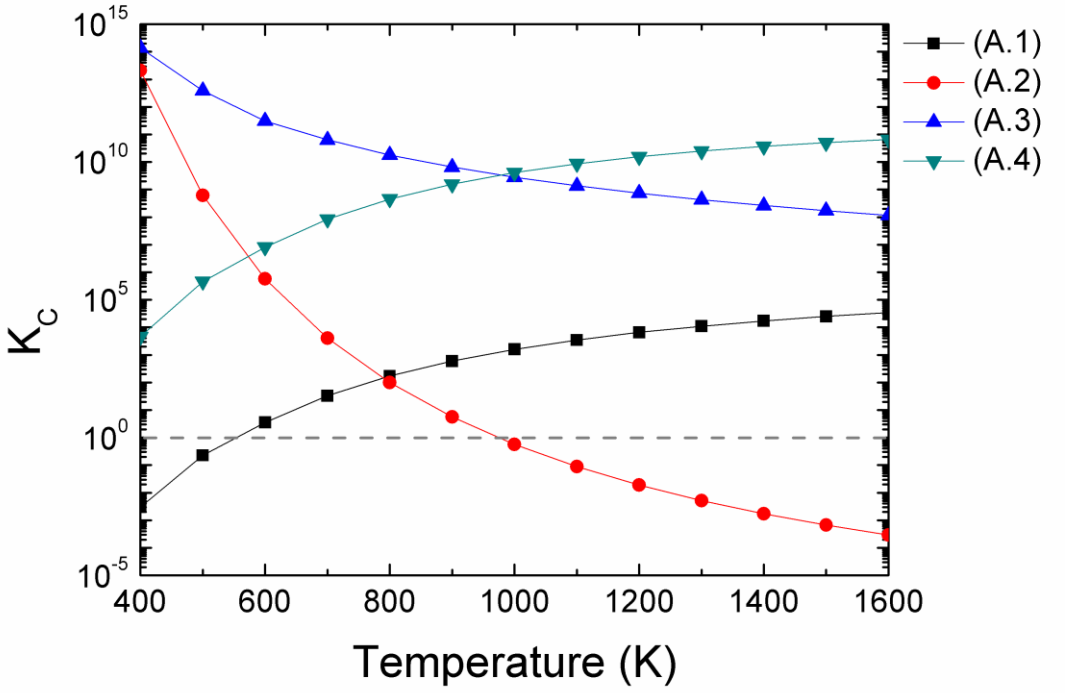

Figure E.4: Equilibrium constants for reactions (6.1) to (6.4).

$$CH_4 \rightarrow 2H_2 + C_{(s)} \quad (6.1)$$

$$2CO \rightleftarrows CO_2 + C_{(s)} \quad (6.2)$$

$$C_2H_4 \rightarrow 2H_2 + 2C_{(s)} \quad (6.3)$$

$$C_2H_6 \rightarrow 3H_2 + 2C_{(s)} \quad (6.4)$$

APPENDIX F

BOILING CURVE AND FLOW RATE DATA

This section includes the boiling curve and flow data presented in this study.

Aqueous glycerine mixtures (nucleate boiling regime)

Tube Temperature	Heat Flux	Tube Temperature	Heat Flux	Tube Temperature	Heat Flux	Tube Temperature	Heat Flux
K	kW/m^2	K	kW/m^2	K	kW/m^2	K	kW/m^2
97/3		94/6		90/10		80/20	
301.99	0.46	299.15	0.46	301.15	0.46	299.15	0.52
306.64	1.83	304.15	1.95	305.40	1.94	302.40	1.96
315.01	4.12	310.40	4.30	311.65	4.29	307.65	4.50
323.13	7.04	318.15	7.82	318.65	7.82	313.65	8.09
332.71	11.13	326.90	12.09	327.65	12.08	319.90	12.74
343.86	16.12	336.40	17.29	336.40	17.65	327.40	18.44
354.26	22.07	346.40	23.85	346.15	23.82	335.40	24.74
365.72	28.44	357.15	30.99	356.15	30.94	343.40	32.49
377.35	36.19	368.90	39.03	367.15	39.57	352.65	41.31
389.74	44.85	381.40	48.03	378.90	48.61	361.90	50.54
399.74	53.69	396.40	57.97	392.90	58.61	371.40	61.41
417.51	64.39	425.65	68.92	418.15	69.55	382.15	72.44
428.04	75.02	444.90	80.99	433.15	81.56	392.90	85.53
442.20	86.57	444.15	93.71	431.40	94.34	405.15	98.67
454.76	99.79	446.40	107.37	430.40	108.03	405.40	113.61
470.24	112.22	449.15	121.99	429.65	122.64	402.90	128.55
466.16	126.03	451.90	137.57	426.65	138.13	402.65	145.50
468.65	141.85	441.15	153.78	426.90	155.72	404.65	163.72
467.82	157.34	439.65	171.83	427.65	173.20	405.90	181.41
469.36	175.08	440.65	190.63	428.65	191.60	407.65	201.52
471.07	192.37	440.40	209.89	429.65	212.25	408.90	221.31
471.43	210.48	440.90	230.10	430.65	232.57	410.65	243.46
473.07	230.74	441.65	252.70	431.90	253.84	411.65	265.18
475.35	250.54	443.65	274.87	432.90	277.53	413.15	289.34
477.32	272.82	444.65	297.95	434.15	300.71	414.90	314.61
479.79	294.35	447.40	322.01	435.90	324.86	416.40	339.25
480.99	318.25	450.15	347.01	437.40	351.62	417.65	366.56
482.63	341.47	452.65	372.98	439.15	377.68	419.65	393.15
485.13	365.54	455.15	399.88	441.40	404.71	421.15	422.48

487.75	392.23	458.15	429.62	443.15	434.56	422.90	451.01
489.92	418.00	461.40	458.50	445.90	463.54	424.90	482.44
492.20	444.73	464.40	488.34	448.40	493.47	426.65	512.88
495.54	474.23	467.65	516.82	451.15	526.46	428.65	546.39
497.91	502.58	471.90	550.97	453.90	558.34	430.90	578.80
499.87	531.57	475.65	583.72	457.15	593.43	432.65	612.11
503.16	561.80	481.90	617.68	460.15	627.31	434.90	648.71
507.09	595.03	486.90	652.53	462.90	662.15	435.90	683.93
510.90	624.65	489.15	688.09	466.40	700.39	437.15	722.52
513.28	659.70	491.65	727.07	468.65	739.64	438.90	759.74
516.42	693.26	493.65	762.09	470.65	777.39	440.15	797.82
518.83	727.56	496.15	800.58	473.15	816.16	441.90	839.55
520.76	762.68	498.90	840.06	477.15	858.71	443.90	879.65
522.54	801.19	501.65	880.51	481.65	899.69	446.65	920.77
524.23	838.02	503.90	921.87	486.40	941.71	448.65	962.79
526.81	875.82	506.90	964.27	490.65	984.67		
529.39	917.37	510.40	1007.80	495.65	1031.67		
532.08	956.98	513.65	1052.24	500.65	1076.82		
534.07	1000.19	516.90	1097.71				
536.40	1041.47	520.40	1141.11				
539.23	1083.74	524.40	1188.66				
542.02	1126.86						
545.04	1170.91						
548.50	1216.13						
552.30	1262.12						
556.51	1309.14						
560.60	1353.67						

Ethyl acetate, diethyl carbonate, and ethanol (nucleate boiling regime)

Tube Temperature	Heat Flux	Tube Temperature	Heat Flux	Tube Temperature	Heat Flux	Tube Temperature	Heat Flux
K	kW/m^2	K	kW/m^2	K	kW/m^2	K	kW/m^2
EA		DEC		EtOH			
351.46	0.40	397.15	0.46	352.51	0.40	370.13	19.41
352.86	1.72	397.39	0.35	352.80	0.53	370.17	225.96
352.88	0.35	398.15	1.73	353.14	1.42	370.33	113.23
354.70	1.49	398.41	0.40	353.33	0.11	370.55	53.10
355.61	3.78	398.88	1.39	353.77	0.13	370.56	45.05
357.52	3.44	399.32	1.73	354.26	0.69	370.76	243.50
357.59	6.89	400.83	3.29	354.39	1.72	370.79	128.16

360.68	10.62	401.40	3.98	354.48	0.49	371.18	64.96
361.28	6.20	402.15	3.98	354.56	2.42	371.18	144.00
364.16	15.51	402.83	5.77	354.83	1.12	371.48	53.06
365.46	20.91	402.98	17.77	355.36	3.68	371.58	258.42
365.67	51.82	403.12	23.53	355.51	1.88	371.61	160.77
366.18	9.76	403.66	9.23	355.76	3.11	371.86	75.33
366.87	62.06	403.82	13.15	356.28	3.96	372.07	271.88
366.99	34.64	403.96	29.60	356.55	3.01	372.13	61.63
367.18	27.11	404.24	7.15	357.20	5.70	372.19	177.26
367.23	43.09	405.15	7.15	357.47	3.78	372.57	66.62
368.05	72.46	405.78	36.91	357.54	5.80	372.58	195.82
369.01	19.28	406.48	44.42	358.20	7.13	372.71	290.87
369.35	25.26	407.54	52.63	358.71	8.43	372.85	100.11
369.48	32.03	407.71	11.25	359.49	8.28	372.87	74.52
369.68	14.12	408.77	94.16	359.68	7.29	373.02	301.60
369.73	84.50	409.03	62.25	360.28	10.91	373.08	215.30
369.88	39.61	409.93	71.91	360.86	11.38	373.29	83.68
370.51	47.37	410.04	105.96	361.99	10.83	373.50	234.32
370.61	96.56	410.15	11.26	362.06	15.51	373.55	319.99
371.14	57.19	411.16	82.27	362.22	19.89	373.75	123.05
371.58	110.38	411.42	124.72	362.34	24.75	373.86	94.48
371.94	66.44	411.55	16.28	362.34	15.86	374.05	255.59
372.37	124.11	412.65	16.29	362.41	30.20	374.22	348.36
372.89	77.19	412.72	132.71	362.82	35.52	374.45	103.72
373.00	139.71	413.44	146.65	363.33	42.66	374.54	146.51
373.67	155.11	414.35	22.24	363.74	48.23	374.57	277.79
373.71	88.74	414.65	22.25	363.96	14.10	374.86	116.80
374.43	171.32	414.82	161.30	364.27	58.04	374.91	372.02
374.48	101.09	415.68	29.12	364.84	64.61	375.05	298.27
375.32	114.25	416.25	176.64	365.29	73.16	375.38	174.02
375.34	189.58	416.51	65.93	365.59	18.73	375.65	324.95
375.98	128.22	416.65	29.13	365.61	12.60	375.88	131.83
376.41	207.46	416.89	36.93	365.78	82.35	376.41	144.08
376.88	141.91	417.33	77.45	366.04	21.74	376.46	210.76
377.20	227.50	417.63	45.67	366.16	28.05	376.99	160.72
377.91	157.43	417.65	36.94	366.17	90.99	377.47	243.53
378.60	173.75	417.90	193.96	366.63	100.06	377.50	179.63
379.45	189.64	418.37	55.34	366.83	35.71	377.94	195.30
380.19	247.10	418.65	45.69	367.14	109.69	378.50	217.59
380.24	207.52	418.89	89.89	367.21	22.47	378.62	278.67

380.90	224.85	419.64	103.27	367.41	44.29	379.06	237.94
381.65	244.28	419.65	54.68	367.69	122.01	379.50	257.56
382.17	261.58	419.65	65.94	367.96	27.16	379.91	324.72
		419.65	77.46	368.04	53.80	380.00	279.66
		420.15	89.05	368.19	134.83	380.22	302.66
		420.15	102.36	368.23	153.59	380.77	326.58
		420.25	117.58	368.50	64.22	381.29	343.59
		421.13	131.76	368.56	173.42		
		421.15	116.60	368.86	33.38		
		422.05	148.97	369.02	29.35		
		422.23	210.81	369.06	74.79		
		422.52	164.88	369.29	187.25		
		422.65	131.78	369.50	87.00		
		423.15	147.88	369.70	204.70		
		423.24	182.84	369.71	35.99		
		423.65	164.90	369.87	40.36		
		423.65	182.84	369.88	100.14		
		423.65	201.71				
		423.88	201.72				
		424.52	221.53				

97/3 aqueous glycerine mixture (film boiling regime)

Tube Temperature	Heat Flux	Total Flow Rate	Species Molar flow rate					
K	kW/m^2	mL/min	mole/s					
97/3			H2	CO	CH4	CO2	C2H4	C2H6
1521.50	1417.83	721.65	2.04E-04	1.60E-04	8.75E-05	5.27E-06	3.14E-05	2.86E-06
1513.01	1364.94	663.53	1.87E-04	1.47E-04	8.04E-05	4.85E-06	2.89E-05	2.63E-06
1501.64	1302.65	673.81	1.90E-04	1.50E-04	8.17E-05	4.94E-06	2.95E-05	2.67E-06
1494.55	1265.04	618.99	1.74E-04	1.38E-04	7.50E-05	4.55E-06	2.72E-05	2.45E-06
1489.45	1254.08	591.74	1.66E-04	1.32E-04	7.17E-05	4.36E-06	2.61E-05	2.34E-06
1489.19	1231.24	619.89	1.74E-04	1.38E-04	7.52E-05	4.57E-06	2.73E-05	2.46E-06
1488.17	1271.02	594.19	1.67E-04	1.32E-04	7.20E-05	4.38E-06	2.62E-05	2.35E-06
1482.80	1173.53	611.75	1.72E-04	1.36E-04	7.42E-05	4.52E-06	2.70E-05	2.42E-06
1476.58	1172.47	605.33	1.70E-04	1.35E-04	7.34E-05	4.48E-06	2.68E-05	2.40E-06
1473.32	1136.63	626.95	1.75E-04	1.40E-04	7.60E-05	4.64E-06	2.78E-05	2.48E-06
1469.81	1141.06	563.14	1.58E-04	1.26E-04	6.83E-05	4.18E-06	2.50E-05	2.23E-06
1468.98	1114.06	579.14	1.62E-04	1.29E-04	7.02E-05	4.30E-06	2.58E-05	2.29E-06
1453.99	1078.75	563.60	1.57E-04	1.26E-04	6.84E-05	4.21E-06	2.53E-05	2.23E-06
1453.04	1068.03	525.97	1.47E-04	1.17E-04	6.38E-05	3.93E-06	2.36E-05	2.08E-06

1448.40	1046.82	519.99	1.45E-04	1.16E-04	6.31E-05	3.90E-06	2.34E-05	2.06E-06
1445.99	1024.90	492.44	1.37E-04	1.10E-04	5.97E-05	3.70E-06	2.22E-05	1.95E-06
1442.56	1000.66	505.89	1.41E-04	1.13E-04	6.14E-05	3.80E-06	2.29E-05	2.00E-06
1436.64	981.18	521.19	1.45E-04	1.17E-04	6.33E-05	3.93E-06	2.37E-05	2.07E-06
1432.78	981.92	474.29	1.32E-04	1.06E-04	5.76E-05	3.59E-06	2.16E-05	1.88E-06
1424.44	932.99	479.88	1.33E-04	1.07E-04	5.83E-05	3.65E-06	2.21E-05	1.90E-06
1414.53	920.12	434.91	1.20E-04	9.75E-05	5.29E-05	3.34E-06	2.02E-05	1.72E-06
1411.39	906.34	429.53	1.19E-04	9.63E-05	5.23E-05	3.30E-06	2.00E-05	1.70E-06
1408.17	909.35	458.66	1.27E-04	1.03E-04	5.58E-05	3.54E-06	2.15E-05	1.82E-06
1388.76	831.18	397.85	1.10E-04	8.94E-05	4.87E-05	3.13E-06	1.91E-05	1.58E-06
1386.32	837.45	389.09	1.07E-04	8.74E-05	4.77E-05	3.07E-06	1.87E-05	1.54E-06
1375.58	807.86	395.88	1.09E-04	8.90E-05	4.88E-05	3.17E-06	1.94E-05	1.57E-06
1372.18	802.10	386.59	1.06E-04	8.70E-05	4.78E-05	3.11E-06	1.90E-05	1.53E-06
1368.26	792.67	353.35	9.71E-05	7.95E-05	4.39E-05	2.85E-06	1.75E-05	1.40E-06
1366.58	784.06	334.44	9.19E-05	7.53E-05	4.16E-05	2.71E-06	1.66E-05	1.33E-06
1338.46	726.96	307.72	8.41E-05	6.94E-05	4.09E-05	2.62E-06	1.62E-05	1.22E-06
1319.40	685.81	259.14	7.06E-05	5.86E-05	3.86E-05	2.30E-06	1.44E-05	1.03E-06
1318.86	690.55	250.76	6.84E-05	5.67E-05	3.75E-05	2.23E-06	1.40E-05	9.94E-07

94/6 aqueous glycerine mixture (film boiling regime)

Tube Temperature	Heat Flux	Total Flow Rate	Species Molar flow rate					
K	kW/m^2	mL/min	mole/s					
94/6			H2	CO	CH4	CO2	C2H4	C2H6
1546.94	1613.95	358.90	1.30E-04	8.15E-05	1.48E-05	3.02E-06	1.60E-05	1.23E-06
1540.72	1537.72	346.20	1.25E-04	7.87E-05	1.43E-05	2.92E-06	1.54E-05	1.20E-06
1531.85	1436.65	333.09	1.20E-04	7.59E-05	1.38E-05	2.81E-06	1.49E-05	1.18E-06
1527.09	1374.84	331.07	1.19E-04	7.55E-05	1.37E-05	2.79E-06	1.48E-05	1.18E-06
1517.35	1336.97	338.33	1.22E-04	7.72E-05	1.40E-05	2.85E-06	1.51E-05	1.23E-06
1515.24	1331.99	324.47	1.17E-04	7.41E-05	1.34E-05	2.73E-06	1.45E-05	1.18E-06
1503.77	1293.17	287.67	1.03E-04	6.58E-05	1.19E-05	2.42E-06	1.28E-05	1.07E-06
1503.27	1232.40	300.02	1.07E-04	6.87E-05	1.24E-05	2.53E-06	1.34E-05	1.12E-06
1497.03	1344.86	293.84	1.05E-04	6.73E-05	1.21E-05	2.48E-06	1.31E-05	1.10E-06
1494.34	1233.34	312.26	1.12E-04	7.16E-05	1.29E-05	2.63E-06	1.39E-05	1.18E-06
1492.87	1201.61	303.46	1.08E-04	6.96E-05	1.25E-05	2.56E-06	1.35E-05	1.15E-06
1490.13	1178.65	302.99	1.08E-04	6.95E-05	1.25E-05	2.55E-06	1.35E-05	1.15E-06
1488.56	1256.65	304.57	1.09E-04	6.99E-05	1.26E-05	2.57E-06	1.36E-05	1.16E-06
1482.01	1124.93	250.13	8.91E-05	5.74E-05	1.03E-05	2.11E-06	1.12E-05	9.65E-07
1480.51	1103.50	279.97	9.96E-05	6.43E-05	1.16E-05	2.36E-06	1.25E-05	1.08E-06
1476.76	1173.27	238.08	8.46E-05	5.47E-05	9.84E-06	2.01E-06	1.06E-05	9.26E-07

1473.51	1129.12	235.72	8.37E-05	5.42E-05	9.74E-06	1.99E-06	1.05E-05	9.22E-07
1467.82	1090.40	271.92	9.65E-05	6.26E-05	1.12E-05	2.29E-06	1.21E-05	1.07E-06
1465.78	1052.57	277.51	9.84E-05	6.39E-05	1.15E-05	2.34E-06	1.24E-05	1.10E-06
1465.25	1108.00	272.12	9.65E-05	6.27E-05	1.12E-05	2.29E-06	1.21E-05	1.08E-06
1464.86	1061.45	256.34	9.09E-05	5.90E-05	1.06E-05	2.16E-06	1.14E-05	1.02E-06
1453.94	980.27	215.42	7.61E-05	4.97E-05	8.90E-06	1.81E-06	9.61E-06	8.70E-07
1448.00	1008.26	233.96	8.25E-05	5.40E-05	9.67E-06	1.97E-06	1.04E-05	9.53E-07
1444.70	948.29	187.66	6.62E-05	4.34E-05	7.75E-06	1.58E-06	8.37E-06	7.69E-07
1443.59	966.99	217.11	7.65E-05	5.02E-05	8.97E-06	1.83E-06	9.68E-06	8.91E-07
1442.05	948.61	190.34	6.71E-05	4.40E-05	7.86E-06	1.60E-06	8.49E-06	7.83E-07
1438.49	975.31	183.47	6.46E-05	4.24E-05	7.58E-06	1.55E-06	8.18E-06	7.59E-07
1434.60	1041.42	205.64	7.23E-05	4.76E-05	8.50E-06	1.73E-06	9.17E-06	8.56E-07
1434.03	924.94	226.27	7.95E-05	5.24E-05	9.35E-06	1.91E-06	1.01E-05	9.42E-07
1432.88	894.50	186.08	6.54E-05	4.31E-05	7.69E-06	1.57E-06	8.30E-06	7.76E-07
1424.25	953.51	192.19	6.74E-05	4.46E-05	7.94E-06	1.62E-06	8.57E-06	8.13E-07
1420.63	876.67	183.20	6.42E-05	4.25E-05	7.57E-06	1.54E-06	8.17E-06	7.79E-07
1412.46	855.74	183.54	6.41E-05	4.26E-05	7.58E-06	1.55E-06	8.19E-06	7.90E-07
1407.02	809.43	152.58	5.32E-05	3.55E-05	6.30E-06	1.29E-06	6.81E-06	6.62E-07
1401.84	895.11	174.23	6.07E-05	4.05E-05	7.20E-06	1.47E-06	7.77E-06	7.62E-07
1397.22	778.65	147.88	5.15E-05	3.44E-05	6.11E-06	1.25E-06	6.60E-06	6.51E-07
1395.22	830.90	133.27	4.64E-05	3.10E-05	5.51E-06	1.12E-06	5.94E-06	5.88E-07
1386.69	760.35	149.53	5.19E-05	3.49E-05	6.18E-06	1.26E-06	6.67E-06	6.68E-07
1382.98	842.20	175.84	6.10E-05	4.10E-05	7.27E-06	1.48E-06	7.84E-06	7.90E-07
1372.48	728.85	141.57	4.89E-05	3.31E-05	5.85E-06	1.19E-06	6.31E-06	6.46E-07
1367.10	709.52	122.47	4.23E-05	2.87E-05	5.06E-06	1.03E-06	5.46E-06	5.63E-07
1366.28	719.73	139.88	4.83E-05	3.27E-05	5.78E-06	1.18E-06	6.24E-06	6.44E-07
1352.69	668.07	112.70	3.88E-05	2.64E-05	4.66E-06	9.49E-07	5.03E-06	5.28E-07
1349.43	672.13	120.90	4.15E-05	2.84E-05	5.00E-06	1.02E-06	5.39E-06	5.69E-07
1342.22	709.63	85.24	2.92E-05	2.00E-05	3.52E-06	7.18E-07	3.80E-06	4.05E-07
1331.37	633.58	100.91	3.45E-05	2.37E-05	4.17E-06	8.50E-07	4.50E-06	4.87E-07
1330.60	621.85	101.78	3.48E-05	2.40E-05	4.21E-06	8.57E-07	4.54E-06	4.92E-07
1325.21	724.28	131.98	4.50E-05	3.11E-05	5.45E-06	1.11E-06	5.89E-06	6.42E-07
1325.04	631.58	97.90	3.34E-05	2.31E-05	4.05E-06	8.25E-07	4.37E-06	4.76E-07
1314.65	694.23	100.32	3.41E-05	2.37E-05	4.15E-06	8.45E-07	4.47E-06	4.95E-07
1314.37	598.67	91.09	3.10E-05	2.15E-05	3.76E-06	7.67E-07	4.06E-06	4.50E-07
1303.63	669.47	60.72	2.06E-05	1.44E-05	2.51E-06	5.11E-07	2.71E-06	3.04E-07
1291.95	558.82	72.89	2.46E-05	1.73E-05	3.01E-06	6.14E-07	3.25E-06	3.70E-07

90/10 aqueous glycerine mixture (film boiling regime)

Tube Temperature	Heat Flux	Total Flow Rate	Species Molar flow rate					
K	kW/m^2	mL/min	mole/s					
90/10			H2	CO	CH4	CO2	C2H4	C2H6
1534.50	1469.20	147.72	5.46E-05	3.15E-05	5.87E-06	1.18E-06	7.38E-06	8.49E-07
1532.74	1512.76	147.58	5.44E-05	3.14E-05	5.87E-06	1.18E-06	7.38E-06	8.49E-07
1528.64	1471.94	150.85	5.55E-05	3.22E-05	6.01E-06	1.21E-06	7.54E-06	8.67E-07
1520.01	1425.87	149.49	5.48E-05	3.20E-05	5.97E-06	1.19E-06	7.47E-06	8.60E-07
1516.86	1339.00	128.17	4.69E-05	2.74E-05	5.12E-06	1.02E-06	6.41E-06	7.37E-07
1508.69	1272.06	123.92	4.51E-05	2.66E-05	4.96E-06	9.87E-07	6.19E-06	7.12E-07
1499.46	1235.39	120.30	4.36E-05	2.59E-05	4.83E-06	9.56E-07	6.01E-06	6.92E-07
1498.49	1289.97	117.51	4.26E-05	2.53E-05	4.72E-06	9.33E-07	5.87E-06	6.76E-07
1497.76	1224.44	115.94	4.20E-05	2.49E-05	4.66E-06	9.21E-07	5.79E-06	6.67E-07
1494.55	1190.54	116.22	4.21E-05	2.50E-05	4.67E-06	9.22E-07	5.81E-06	6.68E-07
1490.74	1237.26	112.72	4.08E-05	2.43E-05	4.54E-06	8.94E-07	5.63E-06	6.48E-07
1481.34	1139.16	102.98	3.71E-05	2.23E-05	4.15E-06	8.15E-07	5.15E-06	5.92E-07
1477.92	1148.28	105.69	3.80E-05	2.29E-05	4.27E-06	8.36E-07	5.28E-06	6.08E-07
1468.64	1088.03	96.88	3.48E-05	2.10E-05	3.92E-06	7.65E-07	4.84E-06	5.57E-07
1467.81	1114.48	93.16	3.34E-05	2.02E-05	3.77E-06	7.35E-07	4.66E-06	5.36E-07
1463.76	1042.56	91.03	3.26E-05	1.98E-05	3.69E-06	7.18E-07	4.55E-06	5.23E-07
1461.29	1077.92	92.64	3.32E-05	2.01E-05	3.76E-06	7.30E-07	4.63E-06	5.33E-07
1446.75	979.03	94.81	3.40E-05	2.06E-05	3.85E-06	7.47E-07	4.74E-06	5.45E-07
1439.45	985.17	80.94	2.89E-05	1.77E-05	3.30E-06	6.36E-07	4.05E-06	4.65E-07
1436.55	924.15	75.52	2.69E-05	1.65E-05	3.08E-06	5.92E-07	3.77E-06	4.34E-07
1430.56	944.56	77.55	2.76E-05	1.70E-05	3.17E-06	6.08E-07	3.88E-06	4.46E-07
1420.74	887.08	75.01	2.67E-05	1.64E-05	3.07E-06	5.87E-07	3.75E-06	4.31E-07
1419.78	835.25	73.17	2.60E-05	1.61E-05	3.00E-06	5.71E-07	3.66E-06	4.21E-07
1418.41	858.53	78.60	2.79E-05	1.73E-05	3.23E-06	6.14E-07	3.93E-06	4.52E-07
1408.97	845.32	74.84	2.66E-05	1.65E-05	3.07E-06	5.84E-07	3.74E-06	4.31E-07
1408.89	843.91	75.61	2.68E-05	1.66E-05	3.10E-06	5.90E-07	3.78E-06	4.35E-07
1406.60	821.27	65.16	2.31E-05	1.44E-05	2.68E-06	5.07E-07	3.26E-06	3.75E-07
1405.59	857.91	55.96	1.98E-05	1.24E-05	2.31E-06	4.36E-07	2.80E-06	3.22E-07
1402.65	785.50	66.97	2.37E-05	1.48E-05	2.76E-06	5.21E-07	3.35E-06	3.85E-07
1397.00	769.11	72.40	2.56E-05	1.60E-05	2.99E-06	5.62E-07	3.62E-06	4.17E-07
1396.37	820.61	53.82	1.90E-05	1.19E-05	2.22E-06	4.18E-07	2.69E-06	3.10E-07
1387.68	768.02	60.24	2.13E-05	1.34E-05	2.49E-06	4.67E-07	3.01E-06	3.47E-07
1373.36	727.34	48.26	1.70E-05	1.07E-05	2.01E-06	3.73E-07	2.41E-06	2.78E-07
1372.10	739.99	44.71	1.58E-05	9.96E-06	1.86E-06	3.45E-07	2.23E-06	2.58E-07
1370.29	717.03	49.46	1.75E-05	1.10E-05	2.06E-06	3.82E-07	2.47E-06	2.85E-07
1369.13	752.93	37.67	1.33E-05	8.40E-06	1.57E-06	2.91E-07	1.88E-06	2.17E-07
1366.09	669.16	61.41	2.17E-05	1.37E-05	2.56E-06	4.74E-07	3.07E-06	3.55E-07

1359.48	718.69	40.01	1.41E-05	8.94E-06	1.67E-06	3.08E-07	2.00E-06	2.31E-07
1354.89	679.08	38.91	1.37E-05	8.71E-06	1.63E-06	2.99E-07	1.94E-06	2.25E-07
1350.31	665.15	42.28	1.49E-05	9.48E-06	1.77E-06	3.25E-07	2.11E-06	2.45E-07
1346.04	670.03	43.14	1.52E-05	9.68E-06	1.81E-06	3.31E-07	2.16E-06	2.51E-07
1341.38	625.67	37.57	1.32E-05	8.44E-06	1.57E-06	2.88E-07	1.88E-06	2.19E-07
1329.11	662.04	27.02	9.50E-06	6.09E-06	1.14E-06	2.07E-07	1.35E-06	1.59E-07
1328.06	616.77	30.15	1.06E-05	6.80E-06	1.27E-06	2.31E-07	1.51E-06	1.77E-07
1327.36	616.07	40.72	1.43E-05	9.18E-06	1.71E-06	3.11E-07	2.03E-06	2.40E-07
1325.37	642.37	37.63	1.32E-05	8.49E-06	1.58E-06	2.88E-07	1.88E-06	2.22E-07
1318.87	635.84	27.06	9.51E-06	6.12E-06	1.14E-06	2.07E-07	1.35E-06	1.61E-07
1310.50	585.50	39.66	1.39E-05	8.98E-06	1.68E-06	3.02E-07	1.98E-06	2.39E-07
1300.62	531.02	19.29	6.78E-06	4.38E-06	8.17E-07	1.47E-07	9.64E-07	1.19E-07
1284.90	589.74	18.28	6.42E-06	4.17E-06	7.78E-07	1.38E-07	9.14E-07	1.21E-07
1284.69	549.22	36.23	1.27E-05	8.26E-06	1.54E-06	2.74E-07	1.81E-06	2.40E-07
1280.98	567.90	26.23	9.21E-06	5.99E-06	1.12E-06	1.99E-07	1.31E-06	1.78E-07
1276.21	567.11	22.20	7.79E-06	5.07E-06	9.47E-07	1.68E-07	1.11E-06	1.56E-07

80/20 aqueous glycerine mixture (film boiling regime)

Tube Temperature	Heat Flux	Total Flow Rate	Species Molar flow rate					
K	kW/m^2	mL/min	mole/s					
80/20			H2	CO	CH4	CO2	C2H4	C2H6
1534.64	1434.99	24.67	1.05E-05	3.62E-06	1.33E-06	5.32E-07	1.03E-06	1.70E-07
1533.92	1431.60	30.50	1.29E-05	4.48E-06	1.63E-06	6.49E-07	1.27E-06	2.09E-07
1531.36	1419.42	27.18	1.15E-05	4.02E-06	1.42E-06	5.55E-07	1.12E-06	1.83E-07
1525.06	1307.90	24.59	1.04E-05	3.69E-06	1.23E-06	4.60E-07	9.77E-07	1.59E-07
1516.82	1320.04	20.77	8.80E-06	3.17E-06	9.83E-07	3.54E-07	7.92E-07	1.28E-07
1504.15	1236.02	20.85	8.83E-06	3.26E-06	9.26E-07	3.22E-07	7.53E-07	1.20E-07
1500.94	1179.52	19.72	8.35E-06	3.10E-06	8.64E-07	3.00E-07	7.03E-07	1.12E-07
1484.47	1080.02	12.50	5.29E-06	2.02E-06	5.19E-07	1.79E-07	4.21E-07	6.60E-08
1482.89	1128.07	13.02	5.50E-06	2.11E-06	5.38E-07	1.85E-07	4.36E-07	6.82E-08
1477.17	1044.66	12.47	5.27E-06	2.04E-06	5.09E-07	1.75E-07	4.11E-07	6.40E-08
1476.18	1097.47	19.67	8.31E-06	3.23E-06	8.00E-07	2.76E-07	6.46E-07	1.01E-07
1473.73	1069.58	18.44	7.79E-06	3.04E-06	7.47E-07	2.57E-07	6.02E-07	9.35E-08
1471.86	1001.34	21.46	9.06E-06	3.54E-06	8.66E-07	2.99E-07	6.97E-07	1.08E-07
1461.25	1025.39	18.12	7.64E-06	3.03E-06	7.18E-07	2.49E-07	5.73E-07	8.84E-08
1458.35	966.59	10.82	4.57E-06	1.82E-06	4.28E-07	1.48E-07	3.40E-07	5.24E-08
1455.92	956.29	16.74	7.06E-06	2.82E-06	6.59E-07	2.29E-07	5.24E-07	8.05E-08
1455.48	955.10	10.93	4.61E-06	1.84E-06	4.30E-07	1.50E-07	3.42E-07	5.25E-08
1449.10	970.89	11.41	4.81E-06	1.94E-06	4.46E-07	1.55E-07	3.52E-07	5.39E-08

1447.75	924.01	16.40	6.91E-06	2.79E-06	6.40E-07	2.23E-07	5.05E-07	7.73E-08
1443.44	868.08	12.66	5.33E-06	2.17E-06	4.92E-07	1.72E-07	3.86E-07	5.91E-08
1441.54	926.13	16.94	7.14E-06	2.91E-06	6.57E-07	2.30E-07	5.15E-07	7.88E-08
1426.68	840.14	9.10	3.83E-06	1.59E-06	3.50E-07	1.23E-07	2.71E-07	4.11E-08
1423.69	833.73	13.39	5.63E-06	2.34E-06	5.14E-07	1.81E-07	3.96E-07	6.02E-08
1420.94	870.79	17.09	7.18E-06	3.00E-06	6.55E-07	2.31E-07	5.04E-07	7.65E-08
1414.04	839.62	10.17	4.27E-06	1.80E-06	3.89E-07	1.37E-07	2.98E-07	4.51E-08
1407.34	751.15	13.68	5.74E-06	2.43E-06	5.21E-07	1.84E-07	3.97E-07	6.01E-08
1407.24	803.66	11.61	4.87E-06	2.06E-06	4.42E-07	1.57E-07	3.37E-07	5.10E-08
1406.67	785.24	9.29	3.90E-06	1.65E-06	3.54E-07	1.25E-07	2.70E-07	4.08E-08
1405.93	776.13	13.45	5.65E-06	2.39E-06	5.12E-07	1.81E-07	3.90E-07	5.90E-08
1391.70	733.05	8.44	3.54E-06	1.52E-06	3.21E-07	1.14E-07	2.42E-07	3.64E-08
1383.65	714.31	12.38	5.19E-06	2.24E-06	4.69E-07	1.67E-07	3.52E-07	5.31E-08
1383.36	722.51	10.97	4.60E-06	1.99E-06	4.16E-07	1.48E-07	3.12E-07	4.70E-08
1378.86	701.23	10.52	4.41E-06	1.91E-06	3.99E-07	1.42E-07	2.98E-07	4.49E-08
1378.23	734.92	7.81	3.27E-06	1.42E-06	2.96E-07	1.05E-07	2.21E-07	3.33E-08
1376.22	734.70	9.87	4.13E-06	1.80E-06	3.74E-07	1.33E-07	2.79E-07	4.20E-08
1364.11	663.77	7.74	3.24E-06	1.42E-06	2.93E-07	1.04E-07	2.17E-07	3.27E-08
1361.10	654.43	7.61	3.18E-06	1.40E-06	2.88E-07	1.02E-07	2.13E-07	3.21E-08
1355.77	645.05	8.58	3.58E-06	1.58E-06	3.24E-07	1.15E-07	2.40E-07	3.60E-08
1350.48	637.33	7.23	3.02E-06	1.34E-06	2.73E-07	9.73E-08	2.02E-07	3.03E-08
1338.13	642.98	3.74	1.56E-06	6.95E-07	1.41E-07	5.03E-08	1.04E-07	1.56E-08
1336.85	605.41	6.32	2.64E-06	1.18E-06	2.39E-07	8.51E-08	1.75E-07	2.63E-08
1332.56	604.76	7.19	3.00E-06	1.34E-06	2.71E-07	9.68E-08	1.99E-07	2.99E-08
1328.05	586.59	4.21	1.76E-06	7.88E-07	1.59E-07	5.67E-08	1.17E-07	1.75E-08
1318.30	570.42	8.82	3.68E-06	1.66E-06	3.33E-07	1.19E-07	2.43E-07	3.65E-08
1312.79	560.76	5.21	2.17E-06	9.82E-07	1.97E-07	7.02E-08	1.44E-07	2.15E-08
1299.09	538.29	4.03	1.68E-06	7.64E-07	1.52E-07	5.43E-08	1.11E-07	1.66E-08
1297.23	534.62	2.96	1.23E-06	5.62E-07	1.12E-07	3.99E-08	8.14E-08	1.22E-08
1290.45	519.62	5.80	2.41E-06	1.10E-06	2.19E-07	7.81E-08	1.59E-07	2.38E-08
1290.30	495.98	5.05	2.10E-06	9.61E-07	1.91E-07	6.80E-08	1.39E-07	2.08E-08
1282.12	510.98	2.98	1.24E-06	5.69E-07	1.13E-07	4.02E-08	8.17E-08	1.22E-08

Ethyl Acetate (film boiling regime)

Tube Temperature	Heat Flux	Total Flow Rate	Species Molar Flow Rate		
K	kW/m^2	mL/min	mole/s		
EA			C2H4	CO2	CH4
1469.88	1165.98	1460.13	8.80E-05	4.18E-05	7.23E-05
1443.34	969.86	1263.57	9.91E-05	2.88E-05	4.93E-05
1442.84	957.73	1230.52	9.69E-05	2.80E-05	4.78E-05

1420.50	879.71	1103.67	1.01E-04	2.08E-05	3.52E-05
1419.85	874.94	1114.74	1.02E-04	2.09E-05	3.54E-05
1412.99	863.32	1107.18	1.06E-04	1.95E-05	3.30E-05
1399.61	842.50	1083.32	1.10E-04	1.71E-05	2.88E-05
1398.52	805.72	1027.96	1.05E-04	1.61E-05	2.70E-05
1389.60	792.49	1060.14	1.13E-04	1.54E-05	2.58E-05
1379.80	772.66	994.76	1.10E-04	1.33E-05	2.22E-05
1376.88	744.38	970.89	1.08E-04	1.27E-05	2.12E-05
1372.46	746.23	945.76	1.07E-04	1.19E-05	1.98E-05
1361.93	736.23	946.41	1.11E-04	1.10E-05	1.81E-05
1360.05	722.14	956.64	1.13E-04	1.09E-05	1.80E-05
1347.16	685.62	866.13	1.06E-04	8.91E-06	1.46E-05
1345.90	692.14	889.72	1.09E-04	9.04E-06	1.48E-05
1341.67	670.75	897.60	1.12E-04	8.82E-06	1.44E-05
1337.26	679.05	869.25	1.10E-04	8.26E-06	1.35E-05
1332.38	639.24	835.29	1.07E-04	7.63E-06	1.24E-05
1320.68	632.37	786.26	1.03E-04	6.55E-06	1.06E-05
1318.17	622.23	851.00	1.12E-04	6.95E-06	1.12E-05
1313.48	625.35	793.34	1.06E-04	6.24E-06	1.01E-05
1310.04	624.81	792.13	1.06E-04	6.08E-06	9.79E-06
1294.49	582.17	748.52	1.03E-04	5.09E-06	8.12E-06
1289.81	585.97	641.23	8.96E-05	4.21E-06	6.71E-06
1288.84	561.42	709.81	9.94E-05	4.63E-06	7.37E-06
1280.63	572.28	710.84	1.01E-04	4.36E-06	6.91E-06
1279.91	569.33	696.99	9.89E-05	4.24E-06	6.72E-06
1278.67	569.88	767.40	1.09E-04	4.64E-06	7.34E-06
1277.70	553.86	752.25	1.07E-04	4.51E-06	7.14E-06
1271.76	553.21	750.92	1.08E-04	4.31E-06	6.80E-06
1271.33	545.58	736.27	1.06E-04	4.22E-06	6.64E-06
1268.75	556.17	732.71	1.06E-04	4.12E-06	6.48E-06
1265.40	550.49	675.87	9.85E-05	3.72E-06	5.84E-06
1259.25	538.53	603.99	8.89E-05	3.17E-06	4.95E-06
1251.94	519.00	612.84	9.11E-05	3.04E-06	4.74E-06
1249.22	498.02	587.00	8.78E-05	2.86E-06	4.45E-06
1247.21	527.95	596.08	8.94E-05	2.87E-06	4.45E-06
1244.90	522.31	597.34	8.97E-05	2.82E-06	4.37E-06
1238.90	499.99	614.36	9.33E-05	2.79E-06	4.31E-06
1226.37	495.23	504.71	7.79E-05	2.10E-06	3.22E-06
1224.79	486.13	611.15	9.47E-05	2.52E-06	3.85E-06
1215.70	489.43	521.33	8.17E-05	2.02E-06	3.07E-06
1214.77	470.12	492.75	7.72E-05	1.90E-06	2.88E-06
1209.64	452.21	440.28	6.95E-05	1.64E-06	2.48E-06
1203.58	454.60	505.75	8.05E-05	1.81E-06	2.73E-06
1198.30	499.18	474.23	7.59E-05	1.64E-06	2.47E-06
1183.78	452.12	441.84	7.20E-05	1.40E-06	2.08E-06
1181.42	427.61	356.22	5.82E-05	1.11E-06	1.65E-06
1180.87	441.51	470.47	7.70E-05	1.47E-06	2.17E-06
1179.23	443.03	397.41	6.51E-05	1.22E-06	1.81E-06
1171.52	463.99	382.97	6.33E-05	1.13E-06	1.66E-06
1169.23	417.74	400.82	6.64E-05	1.16E-06	1.71E-06
1160.96	422.45	324.19	5.41E-05	8.97E-07	1.31E-06
1148.80	409.18	301.99	5.13E-05	7.84E-07	1.13E-06
1142.93	429.94	292.40	5.00E-05	7.36E-07	1.06E-06

1142.64	408.68	370.97	6.33E-05	9.32E-07	1.34E-06
1139.19	385.67	306.70	5.24E-05	7.55E-07	1.08E-06
1129.93	390.59	230.88	3.96E-05	5.39E-07	7.68E-07
1123.03	391.94	278.00	4.83E-05	6.30E-07	8.93E-07
1116.32	378.41	205.05	3.61E-05	4.53E-07	6.38E-07
1114.02	380.29	278.79	4.89E-05	6.06E-07	8.53E-07
1112.18	396.82	208.37	3.68E-05	4.52E-07	6.34E-07
1110.40	356.49	225.00	3.94E-05	4.79E-07	6.72E-07
1098.72	366.90	166.12	2.96E-05	3.38E-07	4.69E-07
1090.15	355.85	176.51	3.18E-05	3.46E-07	4.78E-07
1083.48	329.47	156.43	2.83E-05	2.99E-07	4.10E-07
1083.40	361.06	180.07	3.26E-05	3.44E-07	4.72E-07
1082.45	350.21	144.10	2.65E-05	2.78E-07	3.81E-07
1081.95	368.10	141.87	2.61E-05	2.73E-07	3.75E-07
1066.16	329.30	104.56	1.94E-05	1.88E-07	2.55E-07
1058.70	339.70	95.15	1.78E-05	1.68E-07	2.26E-07
1054.62	305.69	100.86	1.89E-05	1.75E-07	2.35E-07
1050.97	336.14	116.17	2.18E-05	1.99E-07	2.66E-07
1049.54	339.46	85.73	1.61E-05	1.46E-07	1.96E-07
1042.73	323.97	83.03	1.57E-05	1.39E-07	1.85E-07
1024.90	283.14	63.14	1.24E-05	1.02E-07	1.34E-07
1016.47	270.68	33.28	6.89E-06	5.52E-08	7.22E-08
1015.78	312.68	46.65	8.90E-06	7.11E-08	9.29E-08
1011.19	314.34	54.07	1.09E-05	8.55E-08	1.11E-07
997.71	297.70	43.37	8.40E-06	6.34E-08	8.19E-08
994.37	261.60	57.60	1.17E-05	8.78E-08	1.13E-07
976.97	286.63	29.69	5.73E-06	4.08E-08	5.21E-08
970.19	288.54	27.82	6.17E-06	4.32E-08	5.49E-08
965.95	249.74	24.17	5.47E-06	3.79E-08	4.81E-08
961.99	240.92	22.45	5.16E-06	3.54E-08	4.48E-08
948.77	274.14	22.01	4.25E-06	2.83E-08	3.56E-08
935.60	260.30	23.96	4.74E-06	3.07E-08	3.85E-08
930.36	266.72	15.48	3.91E-06	2.51E-08	3.14E-08
927.81	229.43	15.94	4.35E-06	2.78E-08	3.47E-08
927.57	220.95	17.57	3.99E-06	2.55E-08	3.19E-08
903.97	248.21	15.84	3.06E-06	1.88E-08	2.33E-08
895.60	209.74	12.76	3.49E-06	2.12E-08	2.62E-08
894.36	227.37	15.98	3.13E-06	1.90E-08	2.34E-08
892.62	200.29	12.66	3.48E-06	2.10E-08	2.60E-08
886.88	243.90	11.25	3.20E-06	1.92E-08	2.36E-08
863.32	224.55	10.99	2.06E-06	1.20E-08	1.47E-08
854.64	182.89	13.17	3.75E-06	2.17E-08	2.65E-08
854.52	191.91	8.01	2.60E-06	1.50E-08	1.84E-08
852.50	213.16	11.58	2.22E-06	1.28E-08	1.57E-08
839.49	220.16	7.63	2.56E-06	1.46E-08	1.78E-08
820.52	201.68	7.61	1.32E-06	7.41E-09	8.99E-09
819.40	172.24	7.43	2.58E-06	1.45E-08	1.76E-08
813.73	163.55	11.06	3.44E-06	1.93E-08	2.34E-08
805.76	189.34	7.88	1.41E-06	7.85E-09	9.52E-09
788.27	154.72	6.56	2.47E-06	1.36E-08	1.64E-08
777.32	146.35	11.01	3.59E-06	1.97E-08	2.38E-08
767.96	179.45	4.73	6.37E-07	3.47E-09	4.19E-09
754.25	139.07	8.90	3.17E-06	1.72E-08	2.07E-08

743.60	131.17	11.40	3.86E-06	2.08E-08	2.51E-08
713.46	122.96	6.82	2.80E-06	1.49E-08	1.80E-08
709.28	158.06	3.96	4.68E-07	2.50E-09	3.00E-09

Diethyl Carbonate (film boiling regime)

Tube Temperature	Heat Flux	Total Flow Rate	Species Molar flow rate					
K	kW/m^2	mL/min	mole/s					
DEC			H2	CO	CH4	CO2	C2H4	C2H6
729.30	159.81	7.50	1.24E-08	1.76E-08	1.97E-08	2.50E-06	2.61E-06	5.46E-09
742.21	144.83	5.95	9.86E-09	1.39E-08	1.56E-08	1.98E-06	2.07E-06	4.33E-09
768.46	172.67	7.37	1.22E-08	1.73E-08	1.93E-08	2.46E-06	2.57E-06	5.36E-09
772.24	130.54	27.94	4.64E-08	6.54E-08	7.33E-08	9.32E-06	9.74E-06	2.03E-08
807.24	162.93	7.54	1.25E-08	1.77E-08	1.98E-08	2.52E-06	2.63E-06	5.49E-09
813.40	148.10	27.06	4.49E-08	6.34E-08	7.10E-08	9.03E-06	9.43E-06	1.97E-08
816.24	180.02	5.75	9.54E-09	1.35E-08	1.51E-08	1.92E-06	2.00E-06	4.19E-09
819.28	155.17	36.27	6.02E-08	8.50E-08	9.52E-08	1.21E-05	1.26E-05	2.64E-08
826.57	203.57	15.25	2.53E-08	3.57E-08	4.01E-08	5.09E-06	5.32E-06	1.11E-08
828.24	191.62	25.60	4.25E-08	6.00E-08	6.72E-08	8.54E-06	8.93E-06	1.86E-08
850.45	182.30	20.68	3.43E-08	4.85E-08	5.43E-08	6.89E-06	7.21E-06	1.51E-08
852.09	164.64	42.24	7.02E-08	9.90E-08	1.11E-07	1.41E-05	1.47E-05	3.08E-08
862.74	199.47	39.92	6.63E-08	9.36E-08	1.05E-07	1.33E-05	1.39E-05	2.91E-08
866.95	172.13	58.85	9.78E-08	1.38E-07	1.55E-07	1.96E-05	2.05E-05	4.29E-08
867.52	211.95	20.01	3.33E-08	4.69E-08	5.26E-08	6.67E-06	6.98E-06	1.46E-08
870.61	227.31	29.43	4.89E-08	6.90E-08	7.74E-08	9.81E-06	1.03E-05	2.14E-08
874.79	214.67	54.41	9.04E-08	1.28E-07	1.43E-07	1.81E-05	1.90E-05	3.96E-08
886.92	201.00	29.04	4.83E-08	6.81E-08	7.65E-08	9.68E-06	1.01E-05	2.11E-08
889.50	183.76	70.26	1.17E-07	1.65E-07	1.85E-07	2.34E-05	2.45E-05	5.12E-08
903.58	221.29	97.93	1.63E-07	2.30E-07	2.58E-07	3.26E-05	3.41E-05	7.13E-08
904.98	191.82	110.21	1.83E-07	2.59E-07	2.91E-07	3.67E-05	3.84E-05	8.03E-08
905.79	238.54	107.35	1.79E-07	2.52E-07	2.83E-07	3.58E-05	3.74E-05	7.82E-08
910.79	232.46	67.83	1.13E-07	1.59E-07	1.79E-07	2.26E-05	2.36E-05	4.94E-08
917.54	221.73	129.43	2.16E-07	3.04E-07	3.42E-07	4.31E-05	4.51E-05	9.43E-08
922.66	249.60	96.74	1.61E-07	2.27E-07	2.56E-07	3.22E-05	3.37E-05	7.05E-08
929.66	199.76	148.67	2.48E-07	3.50E-07	3.93E-07	4.95E-05	5.18E-05	1.08E-07
940.02	243.88	169.91	2.84E-07	4.00E-07	4.50E-07	5.66E-05	5.92E-05	1.24E-07
940.13	209.91	163.07	2.72E-07	3.84E-07	4.32E-07	5.43E-05	5.68E-05	1.19E-07
943.48	261.01	189.80	3.17E-07	4.47E-07	5.03E-07	6.32E-05	6.61E-05	1.38E-07
944.33	255.56	103.62	1.73E-07	2.44E-07	2.75E-07	3.45E-05	3.61E-05	7.55E-08
963.00	270.03	197.94	3.31E-07	4.67E-07	5.27E-07	6.58E-05	6.89E-05	1.44E-07
965.13	220.22	225.26	3.77E-07	5.31E-07	6.00E-07	7.49E-05	7.84E-05	1.64E-07
976.26	267.30	279.02	4.68E-07	6.59E-07	7.45E-07	9.28E-05	9.71E-05	2.03E-07
977.10	228.59	253.36	4.25E-07	5.99E-07	6.77E-07	8.42E-05	8.82E-05	1.85E-07
980.93	284.22	293.09	4.92E-07	6.93E-07	7.84E-07	9.74E-05	1.02E-04	2.13E-07
986.84	279.44	217.03	3.65E-07	5.14E-07	5.82E-07	7.21E-05	7.55E-05	1.58E-07
996.24	252.14	279.67	4.72E-07	6.63E-07	7.52E-07	9.29E-05	9.73E-05	2.04E-07
997.08	239.57	277.50	4.68E-07	6.58E-07	7.46E-07	9.22E-05	9.65E-05	2.02E-07
1007.74	289.57	359.57	6.09E-07	8.55E-07	9.72E-07	1.19E-04	1.25E-04	2.62E-07
1012.42	250.56	363.08	6.16E-07	8.65E-07	9.83E-07	1.21E-04	1.26E-04	2.64E-07
1012.84	274.98	333.88	5.66E-07	7.95E-07	9.05E-07	1.11E-04	1.16E-04	2.43E-07
1018.34	308.29	408.27	6.94E-07	9.74E-07	1.11E-06	1.35E-04	1.42E-04	2.97E-07

1024.73	302.16	377.21	6.43E-07	9.02E-07	1.03E-06	1.25E-04	1.31E-04	2.75E-07
1036.31	304.95	423.29	7.25E-07	1.02E-06	1.16E-06	1.40E-04	1.47E-04	3.08E-07
1043.23	298.83	492.83	8.48E-07	1.19E-06	1.36E-06	1.63E-04	1.71E-04	3.59E-07
1045.65	270.94	480.39	8.28E-07	1.16E-06	1.33E-06	1.59E-04	1.67E-04	3.50E-07
1048.97	312.77	496.16	8.57E-07	1.20E-06	1.38E-06	1.64E-04	1.72E-04	3.61E-07
1053.32	333.54	568.70	9.85E-07	1.38E-06	1.59E-06	1.88E-04	1.97E-04	4.14E-07
1063.71	326.02	509.96	8.90E-07	1.24E-06	1.44E-06	1.69E-04	1.77E-04	3.71E-07
1072.36	327.64	549.84	9.68E-07	1.35E-06	1.57E-06	1.82E-04	1.91E-04	4.00E-07
1074.09	324.31	587.34	1.04E-06	1.44E-06	1.68E-06	1.94E-04	2.04E-04	4.28E-07
1076.42	294.93	603.24	1.07E-06	1.49E-06	1.73E-06	1.99E-04	2.09E-04	4.39E-07
1088.34	337.48	638.25	1.14E-06	1.59E-06	1.86E-06	2.11E-04	2.21E-04	4.65E-07
1089.51	357.97	663.75	1.19E-06	1.66E-06	1.94E-06	2.19E-04	2.30E-04	4.83E-07
1101.85	353.67	626.25	1.14E-06	1.58E-06	1.87E-06	2.06E-04	2.17E-04	4.56E-07
1105.50	351.15	710.94	1.31E-06	1.81E-06	2.13E-06	2.34E-04	2.46E-04	5.18E-07
1105.51	318.20	725.21	1.33E-06	1.84E-06	2.18E-06	2.39E-04	2.51E-04	5.28E-07
1108.99	352.03	678.01	1.25E-06	1.73E-06	2.05E-06	2.23E-04	2.34E-04	4.94E-07
1125.75	384.13	767.37	1.47E-06	2.01E-06	2.41E-06	2.52E-04	2.65E-04	5.59E-07
1130.55	364.68	806.47	1.56E-06	2.14E-06	2.57E-06	2.65E-04	2.78E-04	5.87E-07
1135.06	380.06	794.98	1.55E-06	2.13E-06	2.57E-06	2.61E-04	2.74E-04	5.79E-07
1137.78	343.15	799.58	1.57E-06	2.15E-06	2.60E-06	2.62E-04	2.76E-04	5.82E-07
1142.45	382.12	768.74	1.53E-06	2.09E-06	2.54E-06	2.52E-04	2.65E-04	5.60E-07
1147.05	381.89	803.20	1.62E-06	2.21E-06	2.70E-06	2.63E-04	2.77E-04	5.85E-07
1161.15	413.54	902.93	1.91E-06	2.59E-06	3.20E-06	2.95E-04	3.10E-04	6.58E-07
1168.10	395.06	920.86	2.00E-06	2.70E-06	3.36E-06	3.00E-04	3.16E-04	6.71E-07
1169.12	412.32	899.38	1.97E-06	2.64E-06	3.30E-06	2.93E-04	3.09E-04	6.55E-07
1173.32	374.02	914.13	2.03E-06	2.73E-06	3.41E-06	2.98E-04	3.14E-04	6.66E-07
1180.91	414.69	864.15	1.99E-06	2.66E-06	3.35E-06	2.81E-04	2.96E-04	6.29E-07
1184.99	413.18	929.89	2.18E-06	2.91E-06	3.68E-06	3.02E-04	3.19E-04	6.77E-07
1194.41	443.06	970.65	2.40E-06	3.17E-06	4.05E-06	3.15E-04	3.32E-04	7.07E-07
1201.75	423.87	976.87	2.52E-06	3.31E-06	4.27E-06	3.16E-04	3.34E-04	7.11E-07
1208.21	453.40	1082.01	2.90E-06	3.80E-06	4.93E-06	3.49E-04	3.69E-04	7.88E-07
1211.70	410.06	1084.27	2.98E-06	3.89E-06	5.06E-06	3.50E-04	3.69E-04	7.90E-07
1218.60	449.49	1009.51	2.91E-06	3.78E-06	4.95E-06	3.25E-04	3.43E-04	7.35E-07
1223.64	446.56	1053.44	3.15E-06	4.08E-06	5.37E-06	3.38E-04	3.58E-04	7.67E-07
1230.36	478.62	1139.74	3.59E-06	4.62E-06	6.12E-06	3.65E-04	3.87E-04	8.30E-07
1247.28	498.96	1201.79	4.39E-06	5.57E-06	7.47E-06	3.82E-04	4.06E-04	8.75E-07
1254.31	455.19	1221.54	4.77E-06	6.02E-06	8.11E-06	3.87E-04	4.11E-04	8.90E-07
1255.64	493.90	1151.11	4.55E-06	5.74E-06	7.74E-06	3.65E-04	3.87E-04	8.38E-07
1262.12	494.25	1182.47	4.99E-06	6.26E-06	8.47E-06	3.73E-04	3.97E-04	8.61E-07
1265.90	520.69	1280.66	5.63E-06	7.04E-06	9.54E-06	4.04E-04	4.29E-04	9.33E-07
1270.19	489.64	1287.99	5.93E-06	7.39E-06	1.00E-05	4.05E-04	4.31E-04	9.38E-07
1285.35	557.67	1336.33	7.31E-06	9.01E-06	1.23E-05	4.17E-04	4.44E-04	9.73E-07
1297.21	511.48	1358.42	8.59E-06	1.05E-05	1.43E-05	4.20E-04	4.49E-04	9.89E-07
1299.04	570.52	1436.48	9.29E-06	1.14E-05	1.55E-05	4.44E-04	4.74E-04	1.05E-06
1299.74	544.39	1323.04	8.64E-06	1.06E-05	1.44E-05	4.08E-04	4.37E-04	9.63E-07
1300.08	551.61	1338.09	8.77E-06	1.07E-05	1.46E-05	4.13E-04	4.42E-04	9.74E-07
1320.42	631.03	1518.34	1.30E-05	1.58E-05	2.13E-05	4.61E-04	4.95E-04	1.11E-06
1328.78	631.64	1468.69	1.42E-05	1.71E-05	2.30E-05	4.42E-04	4.76E-04	1.07E-06
1330.94	629.02	1567.28	1.56E-05	1.88E-05	2.53E-05	4.71E-04	5.07E-04	1.14E-06
1336.72	602.79	1506.78	1.63E-05	1.96E-05	2.63E-05	4.50E-04	4.85E-04	1.10E-06
1337.22	576.69	1550.27	1.69E-05	2.03E-05	2.72E-05	4.63E-04	4.99E-04	1.13E-06
1349.16	707.91	1644.10	2.13E-05	2.55E-05	3.39E-05	4.84E-04	5.24E-04	1.20E-06
1357.53	688.70	1706.32	2.51E-05	2.99E-05	3.96E-05	4.98E-04	5.40E-04	1.24E-06

1370.61	675.28	1654.66	2.97E-05	3.54E-05	4.62E-05	4.74E-04	5.16E-04	1.20E-06
1378.83	670.25	1732.79	3.53E-05	4.20E-05	5.45E-05	4.90E-04	5.35E-04	1.26E-06
1381.75	759.33	1878.33	4.01E-05	4.77E-05	6.16E-05	5.29E-04	5.78E-04	1.37E-06
1389.66	829.45	1901.12	4.60E-05	5.46E-05	7.00E-05	5.28E-04	5.79E-04	1.38E-06
1401.14	753.98	1867.06	5.42E-05	6.44E-05	8.15E-05	5.07E-04	5.59E-04	1.36E-06
1407.00	842.49	2014.24	6.43E-05	7.63E-05	9.60E-05	5.40E-04	5.98E-04	1.47E-06
1421.82	793.06	2038.85	8.28E-05	9.83E-05	1.21E-04	5.28E-04	5.89E-04	1.48E-06
1426.56	948.77	2154.02	9.46E-05	1.12E-04	1.38E-04	5.51E-04	6.16E-04	1.57E-06
1428.02	840.46	2105.20	9.47E-05	1.12E-04	1.38E-04	5.36E-04	6.00E-04	1.53E-06
1433.80	977.27	2184.87	1.08E-04	1.28E-04	1.56E-04	5.47E-04	6.15E-04	1.59E-06
1454.77	930.48	2193.26	1.53E-04	1.82E-04	2.16E-04	5.12E-04	5.85E-04	1.60E-06
1462.04	955.60	2256.70	1.78E-04	2.12E-04	2.49E-04	5.11E-04	5.88E-04	1.64E-06

Ethanol (film boiling regime)

Tube Temperature	Heat Flux	Total Flow Rate	Species Molar flow rate					
K	kW/m^2	mL/min	mole/s					
EtOH			H2	CO	CH4	CO2	C2H4	C2H6
627.23	106.06	6.00	2.05E-06	5.91E-07	6.97E-07	1.97E-09	7.28E-07	4.43E-08
638.63	113.85	13.47	4.60E-06	1.33E-06	1.57E-06	4.43E-09	1.63E-06	9.96E-08
652.88	120.28	4.06	1.39E-06	4.04E-07	4.73E-07	1.34E-09	4.90E-07	3.00E-08
659.17	122.47	8.10	2.76E-06	8.08E-07	9.42E-07	2.66E-09	9.74E-07	5.98E-08
673.59	129.15	8.61	2.94E-06	8.64E-07	1.00E-06	2.83E-09	1.03E-06	6.37E-08
678.19	131.71	4.92	1.68E-06	4.95E-07	5.72E-07	1.62E-09	5.89E-07	3.64E-08
682.92	133.06	6.19	2.11E-06	6.23E-07	7.20E-07	2.04E-09	7.40E-07	4.57E-08
683.69	133.92	8.94	3.05E-06	9.01E-07	1.04E-06	2.94E-09	1.07E-06	6.61E-08
693.63	138.37	9.00	3.06E-06	9.10E-07	1.05E-06	2.96E-09	1.07E-06	6.65E-08
696.10	140.97	5.61	1.91E-06	5.68E-07	6.53E-07	1.85E-09	6.69E-07	4.15E-08
704.15	143.72	6.74	2.30E-06	6.84E-07	7.84E-07	2.22E-09	8.02E-07	4.98E-08
709.56	145.54	9.93	3.38E-06	1.01E-06	1.16E-06	3.27E-09	1.18E-06	7.34E-08
728.07	153.59	10.73	3.65E-06	1.10E-06	1.25E-06	3.53E-09	1.27E-06	7.93E-08
728.14	155.29	9.85	3.35E-06	1.01E-06	1.15E-06	3.24E-09	1.16E-06	7.28E-08
736.46	146.39	10.20	3.47E-06	1.05E-06	1.19E-06	3.36E-09	1.20E-06	7.54E-08
740.35	159.40	8.96	3.05E-06	9.22E-07	1.04E-06	2.95E-09	1.05E-06	6.62E-08
745.73	162.95	10.24	3.48E-06	1.06E-06	1.19E-06	3.37E-09	1.20E-06	7.57E-08
764.40	199.62	10.17	3.46E-06	1.06E-06	1.18E-06	3.35E-09	1.19E-06	7.52E-08
764.91	171.18	15.42	5.24E-06	1.60E-06	1.79E-06	5.08E-09	1.80E-06	1.14E-07
765.35	160.03	13.02	4.42E-06	1.35E-06	1.51E-06	4.29E-09	1.52E-06	9.62E-08
765.40	172.05	10.70	3.64E-06	1.11E-06	1.24E-06	3.52E-09	1.25E-06	7.91E-08
783.71	182.60	9.55	3.24E-06	9.99E-07	1.11E-06	3.14E-09	1.11E-06	7.06E-08
789.56	170.96	14.46	4.91E-06	1.52E-06	1.68E-06	4.76E-09	1.68E-06	1.07E-07
798.17	189.68	13.67	4.64E-06	1.44E-06	1.59E-06	4.50E-09	1.58E-06	1.01E-07
802.93	191.05	9.02	3.06E-06	9.51E-07	1.05E-06	2.97E-09	1.04E-06	6.67E-08
803.62	192.64	11.51	3.91E-06	1.21E-06	1.34E-06	3.79E-09	1.33E-06	8.51E-08
804.43	178.95	13.91	4.72E-06	1.47E-06	1.62E-06	4.58E-09	1.61E-06	1.03E-07
806.74	219.09	16.74	5.69E-06	1.77E-06	1.95E-06	5.51E-09	1.93E-06	1.24E-07
813.83	208.41	21.02	7.13E-06	2.22E-06	2.44E-06	6.92E-09	2.42E-06	1.55E-07
821.65	203.20	9.83	3.33E-06	1.04E-06	1.14E-06	3.24E-09	1.13E-06	7.26E-08
828.69	210.94	11.80	4.00E-06	1.25E-06	1.37E-06	3.88E-09	1.35E-06	8.72E-08
840.70	213.12	11.91	4.04E-06	1.27E-06	1.38E-06	3.92E-09	1.36E-06	8.80E-08
841.73	195.30	16.08	5.45E-06	1.72E-06	1.87E-06	5.29E-09	1.84E-06	1.19E-07

854.90	218.49	10.92	3.70E-06	1.17E-06	1.27E-06	3.60E-09	1.24E-06	8.07E-08
855.52	244.90	10.52	3.57E-06	1.13E-06	1.22E-06	3.47E-09	1.20E-06	7.78E-08
857.29	223.19	10.11	3.43E-06	1.09E-06	1.18E-06	3.33E-09	1.15E-06	7.47E-08
868.96	226.03	24.86	8.42E-06	2.68E-06	2.89E-06	8.19E-09	2.82E-06	1.84E-07
876.89	233.42	12.81	4.34E-06	1.39E-06	1.49E-06	4.22E-09	1.45E-06	9.47E-08
877.31	215.57	15.14	5.13E-06	1.64E-06	1.76E-06	4.99E-09	1.71E-06	1.12E-07
887.26	238.53	13.10	4.44E-06	1.42E-06	1.52E-06	4.32E-09	1.48E-06	9.69E-08
889.49	261.74	19.61	6.64E-06	2.13E-06	2.28E-06	6.46E-09	2.21E-06	1.45E-07
892.72	243.80	10.77	3.65E-06	1.17E-06	1.25E-06	3.55E-09	1.21E-06	7.96E-08
896.30	246.21	18.94	6.42E-06	2.06E-06	2.20E-06	6.24E-09	2.13E-06	1.40E-07
901.79	243.71	26.30	8.90E-06	2.87E-06	3.06E-06	8.67E-09	2.96E-06	1.94E-07
902.60	229.42	13.93	4.72E-06	1.52E-06	1.62E-06	4.59E-09	1.56E-06	1.03E-07
914.68	255.55	10.71	3.62E-06	1.17E-06	1.25E-06	3.53E-09	1.20E-06	7.92E-08
915.06	255.84	13.18	4.46E-06	1.45E-06	1.53E-06	4.34E-09	1.48E-06	9.74E-08
921.14	278.81	16.37	5.54E-06	1.80E-06	1.90E-06	5.40E-09	1.83E-06	1.21E-07
928.00	243.54	13.33	4.51E-06	1.47E-06	1.55E-06	4.40E-09	1.49E-06	9.86E-08
928.56	266.54	11.07	3.74E-06	1.22E-06	1.29E-06	3.65E-09	1.23E-06	8.18E-08
935.19	269.91	19.81	6.70E-06	2.19E-06	2.30E-06	6.53E-09	2.20E-06	1.46E-07
944.40	266.92	31.24	1.06E-05	3.46E-06	3.63E-06	1.03E-08	3.47E-06	2.31E-07
946.66	274.93	12.48	4.22E-06	1.38E-06	1.45E-06	4.11E-09	1.38E-06	9.22E-08
950.70	277.35	13.31	4.50E-06	1.48E-06	1.55E-06	4.39E-09	1.48E-06	9.84E-08
951.99	292.29	18.64	6.30E-06	2.07E-06	2.17E-06	6.15E-09	2.06E-06	1.38E-07
958.69	259.96	13.44	4.54E-06	1.50E-06	1.56E-06	4.43E-09	1.49E-06	9.94E-08
961.42	288.41	13.18	4.45E-06	1.47E-06	1.53E-06	4.35E-09	1.46E-06	9.74E-08
972.95	294.04	25.35	8.57E-06	2.84E-06	2.95E-06	8.37E-09	2.79E-06	1.87E-07
979.60	296.63	14.71	4.97E-06	1.65E-06	1.71E-06	4.86E-09	1.62E-06	1.09E-07
980.78	288.51	33.77	1.14E-05	3.79E-06	3.93E-06	1.11E-08	3.71E-06	2.50E-07
985.73	301.14	14.75	4.98E-06	1.66E-06	1.72E-06	4.87E-09	1.62E-06	1.09E-07
990.51	315.99	18.10	6.11E-06	2.04E-06	2.11E-06	5.98E-09	1.98E-06	1.34E-07
991.28	274.64	14.41	4.87E-06	1.62E-06	1.68E-06	4.76E-09	1.58E-06	1.07E-07
993.85	310.97	16.29	5.50E-06	1.84E-06	1.89E-06	5.38E-09	1.78E-06	1.20E-07
996.47	313.33	15.40	5.20E-06	1.74E-06	1.79E-06	5.09E-09	1.68E-06	1.14E-07
1005.74	313.43	24.34	8.22E-06	2.75E-06	2.83E-06	8.04E-09	2.65E-06	1.80E-07
1011.94	322.84	31.14	1.05E-05	3.53E-06	3.62E-06	1.03E-08	3.39E-06	2.30E-07
1013.10	310.52	32.72	1.10E-05	3.71E-06	3.81E-06	1.08E-08	3.56E-06	2.42E-07
1020.54	324.12	19.66	6.63E-06	2.24E-06	2.29E-06	6.50E-09	2.13E-06	1.45E-07
1021.50	293.80	16.58	5.59E-06	1.89E-06	1.93E-06	5.48E-09	1.80E-06	1.23E-07
1025.33	328.69	19.95	6.73E-06	2.27E-06	2.32E-06	6.59E-09	2.16E-06	1.47E-07
1030.62	340.56	20.78	7.01E-06	2.37E-06	2.42E-06	6.87E-09	2.25E-06	1.54E-07
1031.18	332.60	29.13	9.83E-06	3.33E-06	3.39E-06	9.63E-09	3.15E-06	2.15E-07
1031.72	333.54	24.10	8.13E-06	2.75E-06	2.80E-06	7.97E-09	2.61E-06	1.78E-07
1049.43	325.82	48.42	1.63E-05	5.56E-06	5.63E-06	1.60E-08	5.20E-06	3.58E-07
1050.44	333.44	35.12	1.18E-05	4.04E-06	4.09E-06	1.16E-08	3.77E-06	2.60E-07
1052.83	348.15	32.46	1.09E-05	3.73E-06	3.78E-06	1.07E-08	3.49E-06	2.40E-07
1052.86	344.34	43.35	1.46E-05	4.99E-06	5.04E-06	1.44E-08	4.66E-06	3.21E-07
1058.84	351.47	28.73	9.68E-06	3.31E-06	3.34E-06	9.52E-09	3.08E-06	2.12E-07
1058.96	362.08	63.26	2.13E-05	7.29E-06	7.36E-06	2.10E-08	6.78E-06	4.68E-07
1060.68	382.01	42.39	1.43E-05	4.89E-06	4.93E-06	1.40E-08	4.54E-06	3.13E-07
1062.24	350.28	42.60	1.44E-05	4.91E-06	4.95E-06	1.41E-08	4.56E-06	3.15E-07
1066.30	355.29	53.84	1.81E-05	6.22E-06	6.26E-06	1.78E-08	5.76E-06	3.98E-07
1076.14	362.66	53.06	1.79E-05	6.15E-06	6.17E-06	1.76E-08	5.66E-06	3.92E-07
1084.10	373.52	54.40	1.83E-05	6.32E-06	6.33E-06	1.81E-08	5.79E-06	4.02E-07
1089.72	376.49	38.47	1.30E-05	4.48E-06	4.48E-06	1.28E-08	4.08E-06	2.84E-07

1091.99	389.27	72.80	2.45E-05	8.48E-06	8.47E-06	2.42E-08	7.72E-06	5.38E-07
1093.15	361.31	49.77	1.68E-05	5.80E-06	5.79E-06	1.65E-08	5.28E-06	3.68E-07
1094.30	408.83	62.23	2.10E-05	7.26E-06	7.24E-06	2.07E-08	6.60E-06	4.60E-07
1101.18	386.35	78.95	2.66E-05	9.23E-06	9.18E-06	2.62E-08	8.35E-06	5.84E-07
1106.33	380.05	97.97	3.30E-05	1.15E-05	1.14E-05	3.26E-08	1.03E-05	7.24E-07
1113.65	400.57	87.03	2.93E-05	1.02E-05	1.01E-05	2.90E-08	9.17E-06	6.43E-07
1116.95	413.18	104.30	3.51E-05	1.23E-05	1.21E-05	3.47E-08	1.10E-05	7.71E-07
1118.08	380.72	68.73	2.31E-05	8.08E-06	7.99E-06	2.29E-08	7.23E-06	5.08E-07
1118.37	400.00	51.06	1.72E-05	6.00E-06	5.94E-06	1.70E-08	5.37E-06	3.77E-07
1125.82	437.19	103.58	3.48E-05	1.22E-05	1.20E-05	3.45E-08	1.09E-05	7.66E-07
1127.91	413.83	128.14	4.31E-05	1.51E-05	1.49E-05	4.27E-08	1.34E-05	9.47E-07
1140.47	401.67	94.57	3.18E-05	1.12E-05	1.10E-05	3.16E-08	9.88E-06	6.99E-07
1140.93	431.58	132.53	4.46E-05	1.57E-05	1.54E-05	4.43E-08	1.38E-05	9.80E-07
1142.99	436.52	122.18	4.11E-05	1.45E-05	1.42E-05	4.08E-08	1.28E-05	9.03E-07
1145.40	418.73	74.83	2.52E-05	8.87E-06	8.71E-06	2.50E-08	7.81E-06	5.53E-07
1151.86	443.17	188.42	6.33E-05	2.24E-05	2.19E-05	6.31E-08	1.96E-05	1.39E-06
1155.65	467.03	160.42	5.39E-05	1.91E-05	1.87E-05	5.37E-08	1.67E-05	1.19E-06
1166.33	402.35	72.50	2.44E-05	8.65E-06	8.43E-06	2.43E-08	7.51E-06	5.36E-07
1166.87	424.75	131.69	4.42E-05	1.57E-05	1.53E-05	4.42E-08	1.36E-05	9.74E-07
1168.19	465.33	197.39	6.63E-05	2.36E-05	2.30E-05	6.63E-08	2.04E-05	1.46E-06
1168.98	462.24	186.71	6.27E-05	2.23E-05	2.17E-05	6.27E-08	1.93E-05	1.38E-06
1169.83	445.68	111.41	3.74E-05	1.33E-05	1.30E-05	3.74E-08	1.15E-05	8.24E-07
1182.33	480.92	299.81	1.01E-04	3.60E-05	3.49E-05	1.01E-07	3.09E-05	2.22E-06
1184.25	499.35	238.74	8.02E-05	2.87E-05	2.78E-05	8.05E-08	2.46E-05	1.76E-06
1191.93	489.56	196.76	6.61E-05	2.37E-05	2.29E-05	6.64E-08	2.02E-05	1.45E-06
1193.38	471.45	160.97	5.40E-05	1.94E-05	1.87E-05	5.44E-08	1.65E-05	1.19E-06
1194.08	441.17	112.16	3.77E-05	1.35E-05	1.30E-05	3.79E-08	1.15E-05	8.29E-07
1195.32	502.54	279.78	9.39E-05	3.37E-05	3.25E-05	9.46E-08	2.87E-05	2.07E-06
1195.70	494.16	196.40	6.59E-05	2.37E-05	2.28E-05	6.64E-08	2.02E-05	1.45E-06
1209.68	536.82	325.01	1.09E-04	3.93E-05	3.78E-05	1.10E-07	3.32E-05	2.40E-06
1212.99	474.18	164.87	5.53E-05	2.00E-05	1.92E-05	5.60E-08	1.68E-05	1.22E-06
1213.60	519.49	284.16	9.54E-05	3.44E-05	3.31E-05	9.66E-08	2.90E-05	2.10E-06
1214.88	476.96	226.87	7.61E-05	2.75E-05	2.64E-05	7.71E-08	2.31E-05	1.68E-06
1215.36	495.78	264.06	8.86E-05	3.21E-05	3.07E-05	8.99E-08	2.69E-05	1.95E-06
1222.59	544.15	384.61	1.29E-04	4.67E-05	4.47E-05	1.31E-07	3.91E-05	2.84E-06
1228.72	536.77	295.20	9.90E-05	3.59E-05	3.43E-05	1.01E-07	3.00E-05	2.18E-06
1230.52	567.34	411.42	1.38E-04	5.01E-05	4.79E-05	1.41E-07	4.17E-05	3.04E-06
1235.00	507.55	245.69	8.24E-05	3.00E-05	2.86E-05	8.41E-08	2.49E-05	1.82E-06
1237.58	530.38	307.77	1.03E-04	3.76E-05	3.58E-05	1.05E-07	3.11E-05	2.28E-06
1250.13	593.81	509.87	1.71E-04	6.25E-05	5.93E-05	1.76E-07	5.14E-05	3.77E-06
1251.41	598.70	511.89	1.72E-04	6.28E-05	5.95E-05	1.77E-07	5.16E-05	3.78E-06
1253.97	582.29	374.62	1.26E-04	4.60E-05	4.36E-05	1.29E-07	3.77E-05	2.77E-06
1257.82	568.83	421.54	1.41E-04	5.18E-05	4.90E-05	1.46E-07	4.24E-05	3.12E-06
1259.98	568.94	410.53	1.38E-04	5.05E-05	4.78E-05	1.42E-07	4.12E-05	3.03E-06
1261.37	559.07	375.45	1.26E-04	4.62E-05	4.37E-05	1.30E-07	3.77E-05	2.78E-06
1279.77	649.77	656.24	2.20E-04	8.12E-05	7.63E-05	2.30E-07	6.55E-05	4.85E-06
1283.83	617.90	553.60	1.85E-04	6.86E-05	6.44E-05	1.94E-07	5.52E-05	4.09E-06
1285.19	638.46	510.54	1.71E-04	6.33E-05	5.94E-05	1.79E-07	5.09E-05	3.77E-06
1285.76	666.60	689.77	2.31E-04	8.55E-05	8.02E-05	2.42E-07	6.87E-05	5.10E-06
1286.56	616.48	539.40	1.81E-04	6.69E-05	6.27E-05	1.90E-07	5.37E-05	3.99E-06
1287.12	615.73	570.36	1.91E-04	7.07E-05	6.63E-05	2.01E-07	5.68E-05	4.22E-06
1308.27	713.60	828.52	2.77E-04	1.03E-04	9.64E-05	2.96E-07	8.19E-05	6.13E-06
1308.62	717.34	822.15	2.75E-04	1.03E-04	9.56E-05	2.94E-07	8.12E-05	6.08E-06

1312.96	700.08	746.09	2.50E-04	9.33E-05	8.68E-05	2.68E-07	7.36E-05	5.52E-06
1315.52	680.83	758.49	2.54E-04	9.49E-05	8.82E-05	2.73E-07	7.48E-05	5.61E-06
1316.71	682.77	757.42	2.53E-04	9.48E-05	8.81E-05	2.73E-07	7.46E-05	5.60E-06
1319.51	708.52	745.44	2.49E-04	9.34E-05	8.67E-05	2.69E-07	7.34E-05	5.51E-06
1327.40	732.81	854.01	2.86E-04	1.07E-04	9.93E-05	3.10E-07	8.38E-05	6.31E-06
1328.92	767.57	958.81	3.21E-04	1.20E-04	1.12E-04	3.49E-07	9.41E-05	7.09E-06
1336.92	793.13	1000.48	3.35E-04	1.26E-04	1.16E-04	3.67E-07	9.79E-05	7.40E-06
1338.55	770.86	957.38	3.20E-04	1.21E-04	1.11E-04	3.52E-07	9.36E-05	7.08E-06
1344.23	776.31	941.43	3.15E-04	1.19E-04	1.10E-04	3.48E-07	9.19E-05	6.96E-06
1344.30	752.45	1003.25	3.35E-04	1.27E-04	1.17E-04	3.71E-07	9.79E-05	7.42E-06
1347.89	825.85	1088.65	3.64E-04	1.38E-04	1.27E-04	4.05E-07	1.06E-04	8.05E-06
1349.60	765.97	1016.05	3.40E-04	1.28E-04	1.18E-04	3.78E-07	9.90E-05	7.51E-06
1354.30	825.67	1109.45	3.71E-04	1.40E-04	1.29E-04	4.16E-07	1.08E-04	8.20E-06
1366.18	883.50	1212.00	4.05E-04	1.54E-04	1.41E-04	4.61E-07	1.17E-04	8.96E-06
1367.26	886.20	1211.16	4.05E-04	1.54E-04	1.41E-04	4.61E-07	1.17E-04	8.95E-06
1369.37	855.88	1165.68	3.89E-04	1.48E-04	1.36E-04	4.45E-07	1.13E-04	8.62E-06
1378.66	859.29	1259.86	4.21E-04	1.61E-04	1.47E-04	4.88E-07	1.22E-04	9.31E-06
1382.27	944.09	1347.54	4.50E-04	1.72E-04	1.57E-04	5.25E-07	1.30E-04	9.96E-06
1387.01	884.96	1400.79	4.68E-04	1.79E-04	1.63E-04	5.50E-07	1.35E-04	1.04E-05
1392.75	983.32	1388.44	4.63E-04	1.78E-04	1.62E-04	5.51E-07	1.33E-04	1.03E-05
1394.34	960.09	1417.02	4.73E-04	1.82E-04	1.65E-04	5.63E-07	1.36E-04	1.05E-05
1394.38	938.26	1491.65	4.98E-04	1.91E-04	1.74E-04	5.93E-07	1.43E-04	1.10E-05
1403.08	946.55	1587.67	5.30E-04	2.04E-04	1.85E-04	6.42E-07	1.52E-04	1.17E-05
1407.27	964.24	1525.07	5.09E-04	1.96E-04	1.77E-04	6.21E-07	1.46E-04	1.13E-05
1416.13	1027.00	1734.30	5.79E-04	2.24E-04	2.02E-04	7.20E-07	1.65E-04	1.28E-05
1420.35	1024.27	1785.28	5.95E-04	2.31E-04	2.08E-04	7.47E-07	1.70E-04	1.32E-05
1420.81	1076.68	1694.96	5.65E-04	2.19E-04	1.97E-04	7.10E-07	1.61E-04	1.25E-05
1434.64	1031.55	1811.42	6.04E-04	2.35E-04	2.11E-04	7.84E-07	1.71E-04	1.34E-05
1435.82	1092.46	1948.98	6.50E-04	2.53E-04	2.27E-04	8.46E-07	1.84E-04	1.44E-05
1441.75	1168.75	2049.92	6.83E-04	2.67E-04	2.38E-04	9.03E-07	1.93E-04	1.52E-05
1445.08	1201.36	1972.68	6.57E-04	2.57E-04	2.29E-04	8.77E-07	1.86E-04	1.46E-05
1446.53	1158.65	2147.18	7.16E-04	2.80E-04	2.50E-04	9.58E-07	2.02E-04	1.59E-05
1455.98	1246.05	2297.15	7.65E-04	3.00E-04	2.67E-04	1.05E-06	2.16E-04	1.70E-05
1457.85	1223.70	2366.41	7.88E-04	3.09E-04	2.75E-04	1.09E-06	2.22E-04	1.75E-05
1460.01	1188.59	2174.53	7.24E-04	2.84E-04	2.53E-04	1.01E-06	2.04E-04	1.61E-05
1467.97	1350.79	2303.53	7.67E-04	3.02E-04	2.68E-04	1.09E-06	2.15E-04	1.70E-05

APPENDIX G

VENDOR LIST

Calibration and carrier gases

Model #: Customized calibration gas, Helium carrier gas (99.999%)

Company: Airgas

Address: 230 Cherry Street, Ithaca, New York 14850

Contact: Mike Norris, michael.norris@airgas.com, (607) 273-1972

Ceramic insulators

Model #: ORX-132116 (OD 1.59 mm, ID 0.79 mm)

Company: Omega Engineering, Inc.

Address: One Omega Drive Box 4047, Stamford, CT 06907-0047

Contact: www.omega.com, (800)-872-9436

Condensers and cold trap

Model #: Z517232, Z164038, Z422347 (condensers), and Z256870 (cold trap)

Company: Sigma-Aldrich

Address: 3050 Spruce St., St. Louis, MO 63103

Contact: www.sigmaaldrich.com, (800) 521-8956

Fittings and valves

Company: Swagelok

Address: 29500 Solon Road, Solon OH 44139

Contact: http://www.swagelok.com

Flow meter

Model #: FMA-A2309 and FMA-4310.

Company: Omega Engineering, Inc.

Address: One Omega Drive Box 4047, Stamford, CT 06907-0047

Contact: www.omega.com, (800)-872-9436

Flow meter for calibration

Model #: Drycal Definer 220

Company Mesa Labs

Address: 12100 W. 6th Avenue Lakewood, CO 80228

Contact: mesalabs.com, (303) 987-8000

Gas Chromatography

Model #: GC600P00012801

Company: Gow-Mac Instrument Company

Address: 277 Brodhead Road, Bethlehem, PA 18017

Contact: Dave Turner, repairs@gow-mac.com, (610) 954-9000 Ext-233

Glass chamber

Model #: Special Item: Glass Cross Pipe DN 150 L 250

Company: Goel Scientific Glass Works Pvt. Ltd.

Address: D-35, Sardar Estate, Ajwa Road, Sardar Estate, Vadodara, Gujarat 390019, India

Contact: Anshul Goel, anshul@goelscientific.com, 0091-265-2561595

Heater tube

Model #: 600F10093X010SL, OD 2.38 mm, ID 1.87 mm

Wall Annealed Inconel 600 tube

Company: MicroGroup Inc.

Address: 7 Industrial Park Road, Medway, MA 020553-1732

Contact: www.microgroup.com, Ms. Erin Bates,

Email: ebates@microgroup.com, Phone: (800) 255-8823

Machine shop

Company: Machine shop in Hollister Hall

Address: Hollister Hall B56 in Cornell University

Contact: Tim Brock, teb4@cornell.edu, (607) 255-4201

O-ring

Model #: Parker ARP36275V

Company: Sealing Devices, Inc.

Address: 4400 Walden Ave. Lancaster, NY 14086

Contact: Jim Poirier, jpoirier@sealingdevices.com, (315) 457-0800

Thermocouples

Model #: KMQXL-010G-18 (wall temperature), GKMQSS-040G-12 (bulk temperature)

Company: Omega Engineering, Inc.

Address: One Omega Drive Box 4047, Stamford, CT 06907-0047

Contact: www.omega.com, (800) 872-9436

REFERENCES

Adhikari, S.; Fernando, S.D.; To, S.D.F.; Bricka, R.M.; Steele, P.H.; Haryanto, A., Conversion of Glycerol to Hydrogen via a Steam Reforming Process over Nickel Catalysts, Energy & Fuels 2008, 22, 1220–1226

Aicher, T.; Griesser, L.J., Novel process to evaporate liquid fuels and its application to the catalytic partial oxidation of diesel, J. Power Source 165 (2007) 210–216.

Anderson, M.H.; Meekunnasombat, P.; Corradini, M.L., Experimental Behavior of Molten Sn_xLi_y When Impacted by a Vertical Column of Water, Fusion Technology., 39 (2001), 965-969.

ASTM D6584: Standard Test Method for Determination of Free and Total Glycerin in B-100 Biodiesel Methyl Esters By Gas Chromatography.

Aurbach, D.; Ein-Eli Y.; Markovsky, B.; Zaban, A.; Luski, S.; Carmeli, Y.; Yamin, H., The Study of Electrolyte Solutions Based on Ethylene and Diethyl Carbonates for Rechargeable Li Batteries, J. Electrochem. Soc., 142, 9 (1995), 2882-2889.

Avedisian, C.T.; Koplik, J., Leidenfrost boiling of methanol droplets on hot porous/ceramic surfacesJ., Int. J. Heat Mass Transfer, 30, 2 (1987), 379–393.

Avedisian, C.T.; Tsang, W.; Davidovits, T.; Allaben, T.J.R., Influence of radiation on product yields in a film boiling reactor, AIChE J., 54 (2008), 575–581.

Bamford, C.H.; Dewar, M.J.S., The thermal decomposition of acetic acid, J. Chem. Soc., (1949) 2877–2882.

Battin-Leclerc, F.; Simmie, J.M.; Blurock, E., Cleaner Combustion, Springer, 2013.

Beadle, P.C.; Golden, D.M.; Benson, S.W. "Very low-pressure pyrolysis: VI. The decomposition of ethyl acetate," International Journal of Chemical Kinetics, 4 (30 (1972), 265–271.

Bigley, D. B.; Wren, C. M., Pyrolysis of Carbonates. Part 1. The Gas-phase Pyrolysis of Some Symmetrical Primary Alkyl Carbonates, J. Chem. Soc., Perkin Trans. II, (1972), 927-928.

Blades, A.T., The kinetics of the pyrolysis of ethyl and isopropyl formats and acetates, Can. J. Chem., 32 (1954) 366–372.

Blades, A.T.; Gilderson, P.W., The secondary hydrogen isotope effects in the pyrolysis of the ethyl-d_5 acetate and ethyl acetate-d_3, Can. J. Chem., 38, 9 (1960), 1407-1411

Blake, P.G.; Jackson, G.E., The thermal decomposition of acetic acid, J. Chem. Soc. B, (1968) 1153–1155.

Blake, P.G.; Jackson, G.E., High- and low-temperature mechanisms in the thermal decomposition of acetic acid, J. Chem. Soc. B, (1969) 94–96.

Bohon, M.D.; Metzger, B.A.; Linak, W.P.; King, C.J.; Roberts, W.L., Glycerol combustion and emissions, Proceedings of the Combustion Institute 33 (2011) 2717–2724.

Bruneton, E.; Narch, B.; Oberlin, A., Carbon-carbon composites prepared by a rapid densification process I: Synthesis and physico-chemical data, Carbon, 35 (1997), 1593-1598.

Bruno, T.J.; Naydich, A.W.A.; Huber, M.L., Composition-explicit distillation curves for mixtures of diesel fuel with dimethyl carbonate and diethyl carbonate, Energy and Fuels, 23 (2009), 3989–3997.

Bühler, W.; Dinjus, E.; Ederer, H.J.; Kruse, A.; Mas, C., Ionic reactions and pyrolysis of glycerol as competing reaction pathways in near- and supercritical water, The Journal of Supercritical Fluids, 22, 1 (2002), 37–53

Buffoni, I.N.; Pompeo, F.; Santori, G.F.; Nichio, N.N., Nickel catalysts applied in steam reforming of glycerol for hydrogen production, Catalysis Communications 10, 13 (2009), 1656–1660

Chai, S.-H.; Wang, H.-P.; Liang Y., Xu, B.-Q., Sustainable production of acrolein: Gas-phase dehydration of glycerol over Nb_2O_5 catalyst, Journal of Catalysis, 250, 2 (2007), 342–349

Chandra, S.; Avedisian, C.T., On the Collision of a Droplet with a Solid Surface, Proc. R. Soc. A, 432 (1991), 13–41.

Chandra, S.; Avedisian, C.T., Observations of droplet impingement on a ceramic porous surface, Int. J. Heat Mass Transfer, 35 (1992), 2377–2388.

Chen, David H. T.; Thompson, A. Ralph, Isobaric vapor- liquid equilibriums for the systems glycerol-water and glycerol- water saturated with sodium chloride. J of Chemical and Engineering Data, 15, 4 (1970), 471-474.

Choi, S.R., Experimental study of chemical conversion of organic liquids by film boiling, Ph.D Thesis, Cornell University, 2010.

Choi, S.R.; Evangelista, J.W.; Avedisian, C.T.; Tsang, W, Experimental study of chemical conversion of methanol and ethylene glycol in a film boiling reactor, Int. J. Heat Mass Transfer, 54 (2011), 500–511.

Chou, X.S.; Witte, L.C., Subcooled Flow Film Boiling Across a Horizontal Cylinder: Part I—Analytical Model, J. Heat Transfer, 117 (1995 a), 167–174.

Chou, X.S.; Sankaran, S.; Witte, L.C., Subcooled Flow Film Boiling Across a Horizontal Cylinder: Part II—Comparison to Experimental Data, J. Heat Transfer, 117 (1995 b), 175–178.

Corma, A.; Huber, G.W.; Sauvanaud, L.; O'Connor, P., Biomass to chemicals: Catalytic conversion of glycerol/water mixtures into acrolein, reaction network, Journal of Catalysis, 257, 1 (2008), 163–171.

Corradini, M.L.; Jepson, D.W., Lithium alloy chemical reactivity with reactor materials: state of knowledge, Fusion Eng. Design, 14 (1991), 273-288

CRC Handbook of Chemistry and Physics. 92th ed. Taylor and Francis Group, LLC., 2011–2012. www.hbcpnetbase.com.

Crooks, RC; Hershall, PG; Sorgenti, HA; Lemmon, AW; Filbert, RB. Studies Relatingto the Reaction between Zirconium and Water at High Temperatures. Report BMI-1154. Columbus, OH: Batelle Memorial Institute; May 1962.

Cross, J. T. D.; Hunter, R.; Stimson, R., The Thermal Decomposition of Simple Carbonate Esters, Aust. J. Chem., 29 (1976), 1477-1481

David, H. T.; Chen, A.; Ralph, T., Isobaric vapor liquid equilibriums for the systems glycerol-water and glycerol-water saturated with sodium chloride, J. of Chem. and Eng. Data, 15, 4 (1970), 471-474.

Dagaut, P.; Gail,S.; Sahasrabudhe, M., Rapeseed oil methyl ester oxidation over extended ranges of pressure, temperature, and equivalence ratio: Experimental and modeling kinetic study, Proc. Combust. Inst. 31, (2007) 2955–2961.

Delhaes, P, Chemical vapor deposition and infiltration processes of carbon Materials," Carbon, 40 (2002), 641–657.

Delhae`s P.; Trinquecoste M.; Lines, J.-F.; Cosculluela, A.; Goyhe´ne`che, J.-M.; Couzi, M., Chemical vapor infiltration of C/C composites: Fast densification processes and matrix characterizations, Carbon, 43 (2005), 681-691.

Deluga, G.A.; Salge, J.R.; Schmidt, L.D.; Verykios X.E., Renewable Hydrogen from Ethanol by Autothermal Reforming, Science, 303 (2004), 993-996.

Duan, X.; Page, M., Theoretical Investigation of Competing Mechanisms in the Thermal Unimolecular Decomposition of Acetic Acid and the Hydration Reaction of Ketene, J. Am. Chem. Soc., 117 (1995), 5114-5119.

Dunn,B.C.; Guenneau, C.; Hilton,S.A.; Pahnke, J.; Eyring, E.M., Production of diethyl carbonate from ethanol and carbon monoxide over a heterogeneous catalyst, Energy and Fuels, 16 (2002), 177–181.

Eberhardt, J.E.; Knott, R.B.; Pryor, A., Master equation description of the multiphoton decomposition of ethyl acetate, Chemical Physics, 69 (1982), 45-59.

EN 14105: Fat and oil derivatives – Fatty Acid Methyl Esters (FAME) - Determination of free and total glycerol and mono-di-, tri-glyceride content.

Epstein, M.; Leung, JC.; Hauser, GM; Henry, RE. Film boiling on a reactive surface, Int. J. Heat Mass Transfer, 27 (1984), 1365-1378.

Evangelista, J.W.; Avedisian, C.T.; Tsang, W., Thermal and catalytic decomposition of aqueous ethylene glycol mixtures by film boiling, Int. J. Heat Mass Transfer, 55 (2012), 6425–6434.

Evangelista, J.W., An experimental demonstration of converting organic liquids and their aqueous solutions in a film boiling reactor, M.S. Thesis, Sibley School of Mechanical and Aerospace Engineering, Cornell, University, 2010

Fernández, Y.; Arenillas, A.; Díez, M.A.; Pis, J.J.; Menéndez; J.A., Pyrolysis of glycerol over activated carbons for syngas production, Journal of Analytical and Applied Pyrolysis, 84, 2 (2009), 145–150.

Galvita, V.V.; Semin, G.L.; Belyaev, V.D.; Semikolenov, V.A.; Tsiakaras, P.; Sobyanin, V.A., Synthesis gas production by steam reforming of ethanol, Applied Catalysis A: General, 220 (2001), 123–127.

Garner, F.H.; Ellis, S.R.M.; Pearce, C.J., Extraction of acetic acid from water: 3—Binary vapour-liquid equilibrium data, Chem. Eng. Sci., 3 (1954) 48–54.

Goetsch, D.A.; Schmidt, L.D., Microsecond catalytic partial oxidation of alkanes, Science, 271 (1996), 1560–1562

Gordon, A.S.; Norris, W.P., A Study of the Pyrolysis of Methyl Ethyl and Diethyl Carbonates in the Gas Phase, J. Phys. Chem., 69, (1965) 3013–3017.

Hagos, F.Y.; Aziz, R.A.; Sulaiman, S.A., Trends of Syngas as a Fuel in Internal Combustion Engines, Advances in Mechanical Engineering (2014), 401587.

Hemings, E.B.; Cavallotti, C.; Cuoci, A.; Faravelli, T.; Ranzi, E., A DETAILED KINETIC STUDY OF PYROLYSIS AND OXIDATION OF GLYCEROL (PROPANE-1,2,3-TRIOL), Chia Laguna, Cagliari, Sardinia, Italy, September 11-15, (2011)

Herzog, J.P.; Corradini, M.L.. Lithium-lead/water reaction experiments and analysis Fusion Technology, 15 (1989), 979-983.

Ghenai, C., Combustion of Syngas Fuel in Gas Turbine Can Combustor, Advances in Mechanical Engineering (2010), 342357.

Gutman, D.; Braun, W.; Tsang, W., Comparison of the thermal and infrared laser induced unimolecular decompositions of allylmethylether, ethylacetate, and isopropylbromide, J. Chem. Phys. 67 (1977), 4291-4296.

Herzler, J.; Manion, J. A.; Tsang, W., Single-Pulse Shock Tube Studies of the Decomposition of Ethoxy Compounds, J. Phys. Chem. A, 101 (1997), 5494-5499.

Hickman, D.A.; Schmidt, L.D., Production of syngas by direct catalytic oxidation of methane, Science, 259 (1993), 343–346.

Higgins, H.M., A Study of the Reaction of Metals and Water, AECD-3664, Richland, WA: Hanford Atomic Products Operation, (1955).

Kechagiopoulos, P.N.; Voutetakis, S.S.; Lemonidou, A.A.; Vasalos, I.A., Sustainable hydrogen production via reforming of ethylene glycol using a novel spouted bed reactor, Catalysis Today, 127, 30 (2007), 246-255.

Kirillov, V. A.; Ogarkov, B.L., Film Boiling with Chemical Reaction on a Vertical Catalyst Surface, Journal of engineering physics, 36, 3 (1979), 266-271.

Kranert, O.; Kottowski, H., Small scale lithium-lead/water-interaction studies, Fusion Eng. Design, 15 (1991), 137-154.

Krummenacher, J.J.; West, K.N.; Schmidt, L.D., Catalytic partial oxidation of higher hydrocarbons at millisecond contact times: decane, hexadecane, and diesel fuel, J. Catal., 215 (2003) 332–343.

Lee, C.; Mun, B.; Ross, P. N., The Chemical Reaction of Diethyl Carbonate with Lithium Intercalated Graphite Studied by X-Ray Photoelectron Spectroscopy, Journal of The Electrochemical Society, 149 (10) (2002), 1286-1292.

Lee, I.S.G., Refining Analysis of the FIBOR chemical reaction with subcooling and liquid motion, Master of Engineering Report, Sibley School of Mechanical and Aerospace Engineering, Cornell University (2010).

Li, J.; Kazakov, A.; and Dryer, F.L., Ethanol pyrolysis experiments in a variable pressure flow reactor, International Journal of Chemical Kinetics, 33, 12 (2001), 859–867.

Li, J.; Kazakov, A.; and Dryer, F.L., Experimental and Numerical Studies of Ethanol Decomposition Reactions, J. Phys. Chem. A, 108 (2004), 7671-7680.

Lienhard IV, J.H. and Lienhard V, J.H., A Heat Transfer Textbook, Fourth Edition, Phlogiston Press, 2012.

Liguras, D.K.; Kondarides, D.I.; Verykios, X.E., Production of hydrogen for fuel cells by steam reforming of ethanol over supported noble metal catalysts, Appl. Catal. B: Environ., 43 (2003), 345–354.

Llorca, J.; de la Piscina, P. R.; Sales, J.; Homs, N., Direct production of hydrogen from ethanolic aqueous solutions over oxide catalysts, Chem. Commun., 2001, 641–642.

Lustman, B., Zirconium–Water Reactions. Report WAPD-137. Pittsburgh, PA: Bettis Atomic Power Laboratory, December 1955.

Ma, F.; Hanna, M.A., Biodiesel production: a review, Bioresource Technology, 70, 1 (1999), 1–15

Mackie, J.C.; Doolan, K.R.; High-temperature kinetics of thermal decomposition of acetic acid and its products, Int. J. Chem. Kinet., 16, 5 (1984), 525–541.

Marinov, N.M., A detailed chemical kinetic model for high temperature ethanol oxidation, International Journal of Chemical Kinetics, 31, 3 (1999), 183–220.

Kanamur, K; Matsushita, T.; Dokko, K., In situ FT-IR measurement for electrochemical oxidation of electrolyte with ethylene carbonate and diethyl carbonate on cathode active material used in rechargeable lithium batteries, Journal of Power Sources, 146 (2005), 360–364.

McNeil, J.; Day, P.; Sirovski, F., Glycerine from biodiesel: The perfect diesel fuel., Process Safety and Environmental Protection, 90, 3 (2012), 180–188.

Metzger B., Glycerol Combustion, MSc. Thesis, Mechanical Engineering, North Carolina State University (2007)

Morris, H.E., Reactions of Ethyl Alcohol, Chem. Rev., 10, 3 (1932), 465–506.

Nilles, D., Combating the Glycerine Glut, Biodiesel Magazine, Spt., 2006.

NIST-JANAF Thermochemical Tables (http://kinetics.nist.gov/janaf/)

Nguyen, M.T.; Sengupta, D.; Raspoet, G.; Vanquickenborne, L.G., Theoretical Study of the Thermal Decomposition of Acetic Acid: Decarboxylation Versus Dehydration, J. Phys. Chem., 99 (1995), 11883-11888.

Notario, R.; Quijano, J.; Sa´nchez, C.; Ve´lez, E., Theoretical study of the mechanism of thermal decomposition of carbonate esters in the gas phase, J. Phys. Org. Chem., 18 (2005), 134–141.

Okuyama, K.; Iida, Y., Film-boiling heat transfer with a catalytic decomposition reaction, JSME International Journal B, 37 (1994), 123-131.

Oliveira, L.M.; Nascimento, M.A.R.; Menon, G.J., The Thermal Impact of Using Syngas as Fuel in the Regenerator of Regenerative Gas Turbine Engine, ASME Turbo Expo 2009: Power for Land, Sea, and Air, Orlando, Florida, USA, June 8–12, 2009.

Panuccio, G.J.; Dreyer, B.J.; Schmidt, L.D., A comparison of the catalytic partial oxidation of C1 to C16 normal paraffins, AIChE J., 53 (2007), 187–195.

"Physical Properties of Glycerine and Its Solutions," Glycerine Producers' Association (1963).

Pompeo, F.; Santori, G.; Nichio N.N., Hydrogen and/or syngas from steam reforming of glycerol. Study of platinum catalysts, International Journal of Hydrogen Energy, 35, (2010), 8912–8920.

Park, J.; Zhu, R.S.; Lin, M.C., Thermal decomposition of ethanol. I. Ab Initio molecular orbital/Rice–Ramsperger–Kassel–Marcus prediction of rate constant and product branching ratios, J. Chem. Phys., 117 (2002), 3224-3231

Queiro´s, P.; Costa, M.; Carvalho, R.H., Co-combustion of crude glycerin with natural gas and hydrogen, Proceedings of the Combustion Institute, 34 (2013), 2759–2767.

Quispe C.A.G..; Coronado, C.J.R.; Carvalho, J.A. Jr, Glycerol: Production, consumption, prices, characterization and new trends in combustion, Renewable and Sustainable Energy Reviews, 27 (2013), 475–493.

Okuno, H.; Trinquecoste, M.; Derre, A.; Monthioux, M.; Delhaes, P., Catalytic effects on carbon/carbon composites fabricated by a film boiling chemical vapor infiltration process, J. Mater. Res., 17 (2002), 1904-1913.

Rao, P.K.M., Andrews, D.G., "Post-nucleate Boiling and Critical Heat Flux from Horizontal Heated Surfaces," Sixth International Heat Transfer Conference (1978), 227-232.

Reid, R.C., Prausnitz, J.M., Poling, B.E., "The Properties of Gas & Liquids," 3rd Edition (1977), 278-285.

Rennard, D.C.; Kruger, J.S.; Schmidt, L.D., Autothermal catalytic partial oxidation of glycerol to syngas and to non-equilibrium products, ChemSusChem.,2, 1 (2009), 89-98.

Rodrı´guez, A.; Canosa, J.; Domı´nguez, A.; Tojo, J., Isobaric Phase Equilibria of Diethyl Carbonate with Five Alcohols at 101.3 kPa, J. Chem. Eng. Data, 48 (2003), 86-91.

Roh, N.S.; Dunn, B.C.; Eyring, E.M., Continuous Production of Diethyl Carbonate Over a Supported $CuCl_2/PdCl_2$/KOH Catalyst, Fuel Chemistry Division Preprints, 47, 1 (2002), 142-143.

Rovillain, D.; Trinquecoste, M.; Bruneton, E.; Derre, A.; David, P.; Delhaes, P., Film boiling chemical vapor infiltration. An experimental study on carbon/carbon composite materials," Carbon, 39 (2001),1355-1365.

Rotzoll, G., High-temperature pyrolysis of ethanol, Journal of Analytical and Applied Pyrolysis, 9, 1 (1985), 43–52.

Ruebsamen, W.C.; Shon, F.J.; Chrisney, J.B., Chemical Reaction between Water and Rapidly Heated Metals. Report NAA-SR-197. Los Angeles, CA: North American Aviation; October 1952.

Taylor, R., The Mechanism of Thermal Eliminations. Part 15.' Abnormal Rate Spread in Pyrolysis of Alkyl Methyl Carbonates and S-Alkyl 0-Methyl Carbonates due to Enhanced Nucleophilicity of the Carbonyl Group, J. Chem. Soc. Perkin Trans. II, 3 (1983), 291-236.

Sahoo, B.B.; Saha, U.K.; Sahoo, N., Effect of Load Level on the Performance of a Dual Fuel Compression Ignition Engine Operating on Syngas Fuels With Varying H2 /CO Content, J. Eng. Gas Turbines Power, 133, 12 (2011), 122802.

Sahoo, B.B.; Sahoo, N.; Saha, U.K., Effect of H2:CO ratio in syngas on the performance of a dual fuel diesel engine operation, Applied Thermal Engineering, 49 (2012), 139-146.

Saito, K.; Sasaki, T.; Yoshinobu, I.; Imamura, A., Thermal decomposition of ethyl acetate. Branching ratio of the competing paths in the pyrolysis of the produced acetic acid, Chemical Physics Letters, 170 (4) (1990), 385-388.

Salge, J.R.; Dryer, B.J.; Dauenhauer, P.J.; Schmidt, L.D., Renewable hydrogen from nonvolatile fuels by reactive flash volatilization, Science, 314 (2006), 801–804.

Satterfield, C.N.; Audibert, F.P., Nucleate and Film Boiling in Catalytic Decomposition of Hydrogen Peroxide, Ind. Eng. Chem. Fundamen., 2 (3) (1963), 200-202.

Sakurai,A.; Shiotsu, M.; Hata, K., A General Correlation for Pool Film Boiling Heat Transfer From a Horizontal Cylinder to Subcooled Liquid: Part 1—A Theoretical Pool Film Boiling Heat Transfer Model Including Radiation Contributions and Its Analytical Solution, J. Heat Transfer 112 (1990 a) 430–440.

Sakurai,A.; Shiotsu, M.; Hata, K., A General Correlation for Pool Film Boiling Heat Transfer From a Horizontal Cylinder to Subcooled Liquid: Part 1—A Theoretical Pool Film Boiling Heat Transfer Model Including Radiation Contributions and Its Analytical Solution, J. Heat Transfer 112 (1990 b) 441–450.

Scheer, J.C.; Kooyman, E.C.; Sixma, F.L.J., Gas phase pyrolysis of alkyl acetates, Recueil des Travaux Chimiques desPays-Bas, 82, 11 (1963), 1123–1154.

Seiser, R.; Truett, L.; Trees, D.; Seshadri, K., Structure and extinction of non-premixed n-heptane flames, Proc. Combust. Inst., 27 (1998), 649–657.

Seshadri, K.; Lu, T.; Herbinet,O.; Humer, S.; Niemann, U.; Pitz, W.J.; Seiser, R.; Law, C.K., Experimental and kinetic modeling study of extinction and ignition of methyl decanoate in laminar non-premixed flows, Proc. Combust. Inst., 32 (2009), 1067–1074.

Sivaramakrishnan, R.; Su, M.-C.; Michael, J.V.; Klippenstein, S.J.; Harding, L.B.; Ruscic, B., Rate Constants for the Thermal Decomposition of Ethanol and Its Bimolecular Reactions with OH and D: Reflected Shock Tube and Theoretical Studies, The Journal of Physical Chemistry A, 114 (2010), 9425-9439.

Skoulou, V.K.; Manara, P.; Zabaniotou, A.A., H_2 enriched fuels from co-pyrolysis of crude glycerol with biomass, Journal of Analytical and Applied Pyrolysis, 97 (2012), 198–204.

Special Metals Corp. Inconel Alloy 600. Publication Number SMC-027. (http:// www.specialmetals.com/documents/Inconel%20alloy%20600%20(Sept%202008).pdf) 2008

Srinivasan, N.K.; Michael, J.V., The thermal decomposition of water, International Journal of Chemical Kinetics, 38 (3) (2006), 211–219.

Stralen, S.V.; Cole, R., “Boiling Phenomena” Volume 2, McGraw-Hill (1979), p. 632.

Steinmetz, S.A.; Herrington, J.S.; Winterrowd, C.K.; Roberts, W.L.; Wendt, J.O.L.; Linak, W.P., Crude glycerol combustion: Particulate, acrolein, and other volatile organic emissions, Proceedings of the Combustion Institute, 34 (2013), 2749–2757.

Stein, Y.S.; Antal, M.J.Jr., A study of the gas-phase pyrolysis of glycerol, Journal of Analytical and Applied Pyrolysis, 4, 4 (1983), 283–296.

Subramanian, R.; Schmidt, L.D., Renewable Olefins from Biodiesel by Autothermal Reforming, Angew. Chem. Int. Ed. (2005) 302–305.

Tsnag, W, Energy transfer effects during the multichannel decomposition of ethanol, International Journal of Chemical Kinetics, 36, 8 (2004), 456–465.

Tsang, W.; Walker, J.A.; Braun, W.; Herron, J.T., Mechanisms of decomposition of mixtures of ethyl acetate and isopropyl bromide subjected to pulsed infrared laser irradiation, Chem. Phys. Lett., 59, 3 (1978), 487–491.

Turns, S.R., "An Introduction to Combustion," 3rd Edition, McGraw Hill, 2012.

Urban, B.J.; Avedisian, C.T.; Tsang, W., The film boiling reactor: A new environment for chemical processing, AIChE J. 52 (2006), 2582–2595.

Vaidya, P.D., Rodrigues, A.E., Insight into steam reforming of ethanol to produce hydrogen for fuel cells, Chemical Engineering Journal, 117 (2006), 39–49.

Varlamova, T M.; Yurina, E.S., Lithium perchlorate (tetrafluoroborate)-diethyl carbonate-propylene carbonate electrolyte systems, Russian Journal of Physical Chemistry, 80 (8) (2006), 1265-1268.

Valliyappan, T., Hydrogen or Syn Gas Production from Glycerol Using Pyrolysis and Steam Gasification Processes, Chemical Engineering, University of Saskatchewan, M.S. Thesis, 2004.

Valliyappan, T.; Bakhshi, N.N.; Dalai, A.K., Pyrolysis of glycerol for the production of hydrogen or syn gas, Bioresource Technology, 99, 10 (2008), 4476–4483

Van Bennekom, J.G.; Venderbosch, R.H.; Assink, D.; Heeres, H.J., Reforming of methanol and glycerol in supercritical water, J. of Supercritical Fluids, 58 (2011) 99–113.

Van Kasterena, J.M.N.; Nisworob, A.P., A process model to estimate the cost of industrial scale biodiesel production from waste cooking oil by supercritical transesterification, Resources, Conservation and Recycling, 50, 4 (2007), 442-458.

Varady, M.J., Fuel reformation and hydrogen generation in direct droplet impingement reactors, Ph.D. Thesis, School of Mechanical Engineering, Georgia Institute of Technology, December, 2010.

Wang, X.; Wang, N.; Li, M.; Li, S.; Wang, S., Ma, X., Hydrogen production by glycerol steam reforming with in situ hydrogen separation: A thermodynamic investigation, International Journal of Hydrogen Energy, 35, 19 (2010), 10252–10256.

Willams, F.A., Combustion Theory, Addison-Wesley, 1965. pp. 358–364.

Wu, C.-W.; Matsui, H.; Wang, N.-S.; Lin, M. C., Shock Tube Study on the Thermal Decomposition of Ethanol, J. Phys. Chem. A, 115 (28) (2011), 8086-8092.

Yang, C.; Lai, H.; Liu, Z.; Ma, P., Densities and Viscosities of Diethyl Carbonate + Toluene, + Methanol, and + 2-Propanol from (293.15 to 363.15) K, J. Chem. Eng. Data, 51 (2006), 584-589.

Zhang, Y.; Gamo, M.N.; Nakagawa, K.; Ando, T., Synthesis of aligned carbon nanotubes in organic liquids, J. Mat. Research, 17 (2002), 2457-2464.

Zhang, Y.F.; Gamo, M.N.; Xiao, C.Y.; Ando, T., Liquid phase synthesis of carbon nanotubes, Physica B, 323 (2002), 293-295.

Zhao, G.; Bi, S.; Li, X.; Wu, J., "Surface tension of diethyl carbonate, 1,2-dimethoxyethane and diethyl adipate," Fluid Phase Equilibria, 295 (2010), 46–49.

Zhao, L.-C.; Hou, Z.-Q.; Liu, C.-Z.; Wang, Y.-Y.; Dai, L.-Y., A catalyst-free novel synthesis of diethyl carbonate from ethyl carbamate in supercritical ethanol, Chinese Chemical Letters, in press.

Zhen, J.X.; Hua, S.Y.; Hua, C.S, Novel synthesis of diethyl carbonate over palladium/ MCM-41 catalysts, Catal. Lett., 69 (2000), 153–156.

Zhou, Y.Q.; Rose, J.W., Effect of two-dimensional conduction in the condensate film on laminar film condensation on a horizontal tube with variable wall temperature Int. J. Heat Mass Transfer, 39 (1996), 3187–3191.

Zukov, S.A.; Rafeev, V.A.; Afanas'ev, S. Yu.; Echmaev, S.B.; Korsunskii, B.L. Singularities of realization of film boiling on wire heaters. Organic liquids., High Temperature, 41, 2 (2003), 243-251.